Green Chemistry

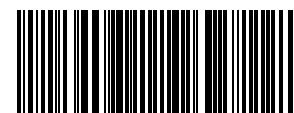**Cutting-edge research for a greener sustainable future**

Delhomme *et al*.
Succinic acid from renewable resources

Shirai *et al*.
Cyclic ether formation with high
pressure carbon dioxide

Hargreaves *et al*.
Making mud magnetic

Jessop *et al*.
Soybean oil extraction and
separation

Celebrating 5 years

High quality research

Enhanced html articles via RSC Prospect
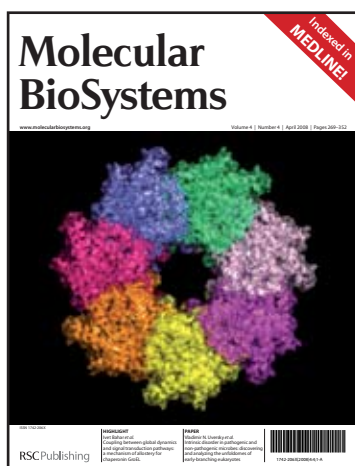
Indexed in MEDLINE

4.12

5 years of publishing

Molecular BioSystems...

Celebrating 5 years of publishing, *Molecular BioSystems* publishes cutting-edge research at the interface between chemistry, the –omic sciences and systems biology.

Fast publication and additional online features, added to the high visibility ensured by indexing in MEDLINE, makes *Molecular BioSystems* the perfect place for your research in subject areas including chemical biology, systems biology, proteomics and genomics, cellular processes and metabolism.

Impact Factor: 4.12 (2007 Thomson (ISI) Journal Citation Reports)

Submit your manuscript at **www.rsc.org/ReSourCe**, or contact the editorial team at **MolBioSyst@rsc.org**

Submit your work today!

RSCPublishing

www.molecularbiosystems.org

Registered Charity Number 207890

Green Chemistry

Cutting-edge research for a greener sustainable future

www.rsc.org/greenchem

RSC Publishing is a not-for-profit publisher and a division of the Royal Society of Chemistry. Any surplus made is used to support charitable activities aimed at advancing the chemical sciences. Full details are available from www.rsc.org

IN THIS ISSUE

Cover
See Shirai *et al.*, pp. 48–52.
Green acid using water and carbon dioxide.
Image reproduced with permission from Masayuki Shirai from *Green Chem.*, 2009, **1**, 48.

CHEMICAL TECHNOLOGY

T1

Drawing together research highlights and news from all RSC publications, *Chemical Technology* provides a 'snapshot' of the latest applications and technological aspects of research across the chemical sciences, showcasing newsworthy articles and significant scientific advances.

Chemical Technology

January 2009/Volume 6/Issue 1
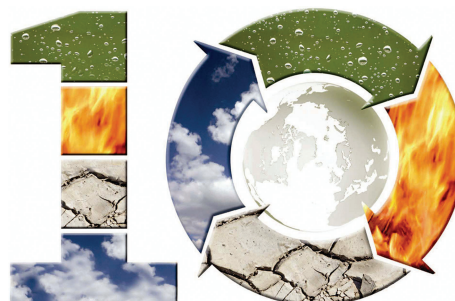
www.rsc.org/chemicaltechnology

EDITORIAL

11

Green Chemistry… **10 years on**

During 2008 *Green Chemistry* celebrated 10 years of publishing. The editors look at the celebrations last year and look forward to the year ahead.

Green Chemistry

Cutting-edge research for a greener sustainable future

www.rsc.org/greenchem

Green Chemistry focuses on cutting-edge research that attempts to reduce the environmental impact of the chemical enterprise by developing a technology base that is inherently non-toxic to living things and the environment.

INFORMATION FOR AUTHORS

Full details of how to submit material for publication in Green Chemistry are given in the Instructions for Authors (available from http://www.rsc.org/authors). Submissions should be sent *via* ReSourCe: http://www.rsc.org/resource.

Authors may reproduce/republish portions of their published contribution without seeking permission from the RSC, provided that any such republication is accompanied by an acknowledgement in the form: (Original citation) – Reproduced by permission of the Royal Society of Chemistry.

The Royal Society of Chemistry takes reasonable care in the preparation of this publication but does not accept liability for the consequences of any errors or omissions.

∞ The paper used in this publication meets the requirements of ANSI/NISO Z39.48-1992 (Permanence of Paper).

Royal Society of Chemistry: Registered Charity No. 207890

CRITICAL REVIEW

13

Succinic acid from renewable resources as a C$_4$ building-block chemical—a review of the catalytic possibilities in aqueous media

Clara Delhomme,* Dirk Weuster-Botz and Fritz E. Kühn

Aqueous hydrogenation of bio-based succinic acid has been reported with a variety of heterogeneous metallic catalysts. As for organometallic complexes, the research is thus far limited to solvent reactions.
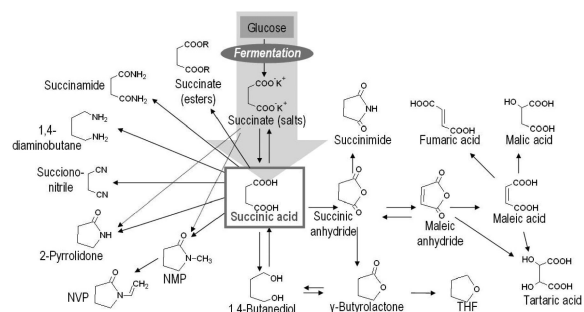
COMMUNICATIONS

27

Pretreatment of lignocellulosic biomass associated with the autoxidation of ethanol to acetal

Yoshiyuki Sasaki, Takashi Endo, Noriko Tanaka and Hiroyuki Inoue*

Lignocellulosic biomass was effectively delignified by aerobic oxidation in ethanol. During the process, ethanol was partially oxidized to acetal, a promising fuel additive. The resulting pulp could then be enzymatically converted into sugars in good yields.
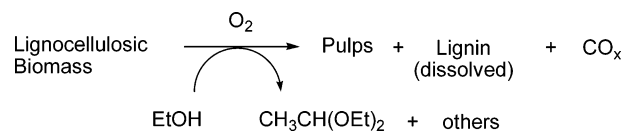
31

Study of technical CNSL and its main components as new green larvicides

D. Lomonaco,* G. M. Pinheiro Santiago, Y. S. Ferreira, Â. M. Campos Arriaga, S. E. Mazzetto, G. Mele and G. Vasapollo

Larvicidal activities against *Aedes aegypti* of technical cashew (*Anarcadium Occidentale* L.) nut shell liquid (CNSL) and its main constituents, cardanol, cardol and their products of hydrogenation were evaluated. In addition, the structure-activity relationship is also discussed.
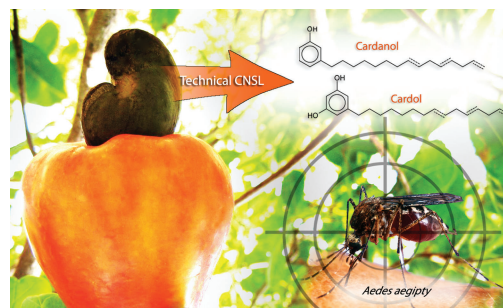
34

Chlorine borrowing: an efficient method for an easier use of alcohols as alkylation agents

Philippe Makowski, Regina Rothe, Arne Thomas, Markus Niederberger and Frédéric Goettmann*

Chlorine functionalised tin dioxide nanoparticles proved able to partially convert alcohols into the corresponding chlorides, which act as alkylation agents with an increased electrophilicity.
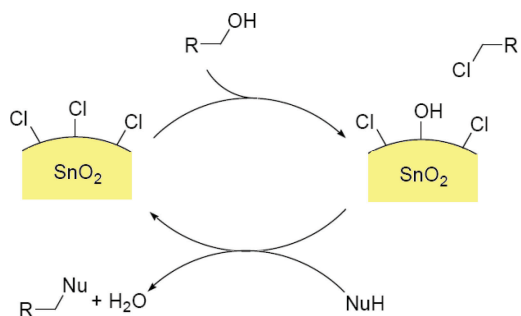
COMMUNICATIONS

38
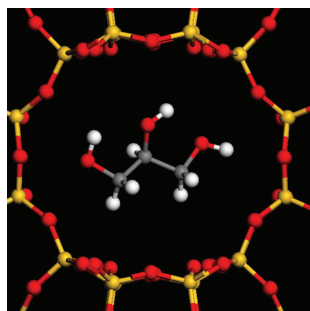
Water-tolerant zeolite catalyst for the acetalisation of glycerol

Carolina X. A. da Silva, Valter L. C. Gonçalves and Claudio J. A. Mota*

Acetalisation of glycerol with acetone or aqueous formaldehyde can be carried out in absence of solvents, using silicon-rich zeolite Beta.

42

Hydrogen production from methane in the presence of red mud – *making mud magnetic*

M. Balakrishnan, V. S. Batra, J. S. J. Hargreaves,*
A. Monaghan, I. D. Pulford, J. L. Rico and S. Sushil

A magnetic carbon containing material is the co-product, along with hydrogen, of the interaction of two by-products, methane and red mud.

PAPERS

48
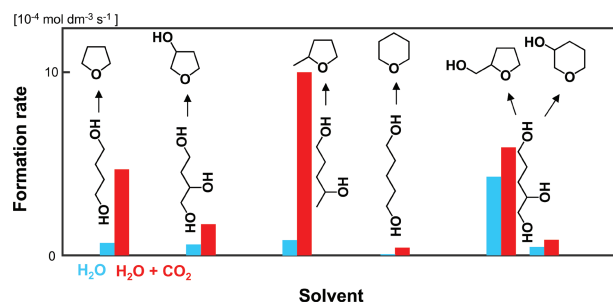
Enhancement of cyclic ether formation from polyalcohol compounds in high temperature liquid water by high pressure carbon dioxide

Aritomo Yamaguchi, Norihito Hiyoshi, Osamu Sato, Kyoko K. Bando and Masayuki Shirai*

High pressure carbon dioxide accelerated dehydration rates from polyalcohols to cyclic ether compounds in water at 573 K.

53

Soybean oil extraction and separation using switchable or expanded solvents

Lam Phan, Heather Brown, James White, Allan Hodgson and Philip G. Jessop*

Three possible alternative methods for oil extraction and subsequent separation of solvent, using switchable or CO_2-expanded solvents, are evaluated.

PAPERS

60

The mechanism of the oxidation of benzyl alcohol by iron(III)nitrate: conventional *versus* microwave heating

Mark H. C. L. Dressen, Jelle E. Stumpel, Bastiaan H. P. van de Kruijs, Jan Meuldijk, Jef A. J. M. Vekemans and Lumbertus A. Hulshof*

The mechanism and process scalability of the oxidation of benzyl alcohol with iron(III)nitrate nonahydrate under conventional and under microwave heating conditions have been investigated.
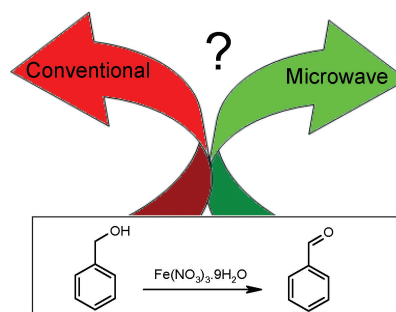
65

The green solvent ethyl lactate: an experimental and theoretical characterization

Santiago Aparicio* and Rafael Alcalde

Ethyl lactate is characterized both from micro and macroscopic viewpoints in wide pressure/temperature ranges using several experimental and theoretical approaches. Competing intra and intermolecular hydrogen bonding are characterized leading to the molecular level organization and macroscopic properties.
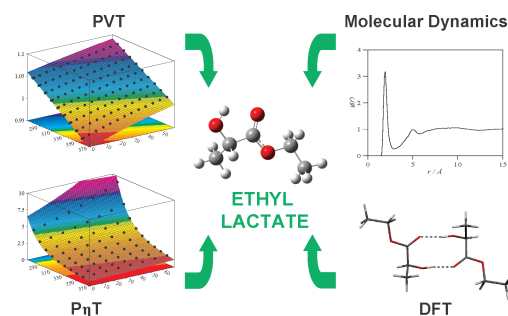
79

An environmentally benign solvent-free Tishchenko reaction

Daniel C. Waddell and James Mack*

Herein, we describe the solvent-free ball milling Tishchenko reaction. Using high speed ball milling and a sodium hydride catalyst, the Tishchenko reaction was performed for aryl aldehydes in high yields in 0.5 hours. The reaction is not affected by the type of ball bearing used and can be successful when conducted in a liquid nitrogen environment.
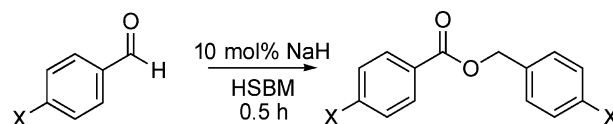
83

Biodegradable pyridinium ionic liquids: design, synthesis and evaluation

Jitendra R. Harjani, Robert D. Singer, M. Teresa Garcia and Peter J. Scammells*

A range of ionic liquids (ILs) with a pyridinium cation were synthesised and their biodegradability was evaluated using the CO_2 Headspace test (ISO 14593). The utility of a biodegradable IL as a reaction solvent for the Diels–Alder reaction was also investigated.
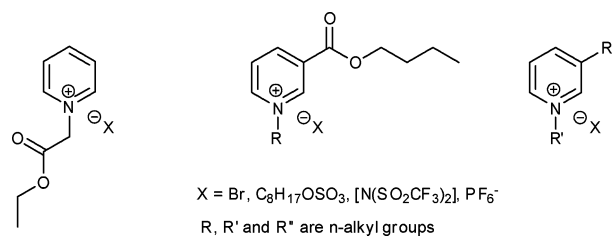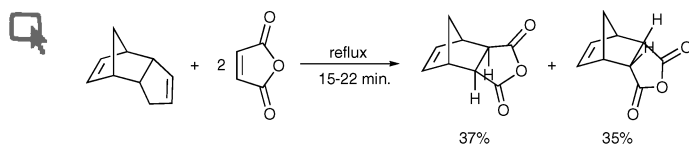
X = Br, $C_8H_{17}OSO_3$, $[N(SO_2CF_3)_2]$, PF_6^-

R, R' and R" are n-alkyl groups

PAPERS

91

37%   35%

Solvent-free Diels–Alder reactions of *in situ* generated cyclopentadiene

David Huertas, Melinda Florscher and Veljko Dragojlovic*

Dicyclopentadiene was used as a source of *in situ* generated cyclopentadiene for Diels–Alder reactions under solvent-free conditions.

96
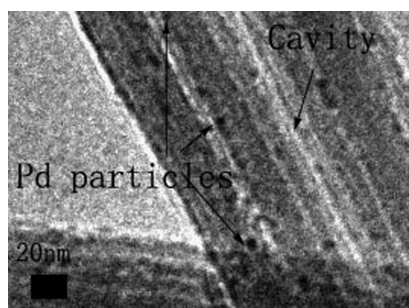
Pd nanoparticles immobilized on sepiolite by ionic liquids: efficient catalysts for hydrogenation of alkenes and Heck reactions

Ranting Tao, Shiding Miao, Zhimin Liu,* Yun Xie, Buxing Han, Guimin An and Kunlun Ding

Palladium nanoparticles were successfully immobilized on sepiolite mediated with guanidine cation-containing ILs, and the resultant Pd catalysts exhibited high efficiency for alkene hydrogenations and Heck reactions.

102
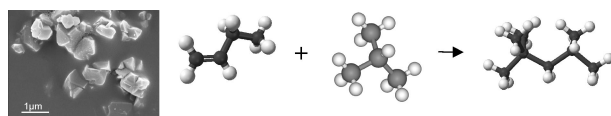
Isobutane/butene alkylation on microporous and mesoporous solid acid catalysts: probing the pore transport effects with liquid and near critical reaction media

V. R. Sarsani and Bala Subramaniam*

The title reaction is investigated on environmentally benign solid acid catalysts (β zeolite crystals shown) to probe the effects of media and pore size on catalyst stability to fouling.

109
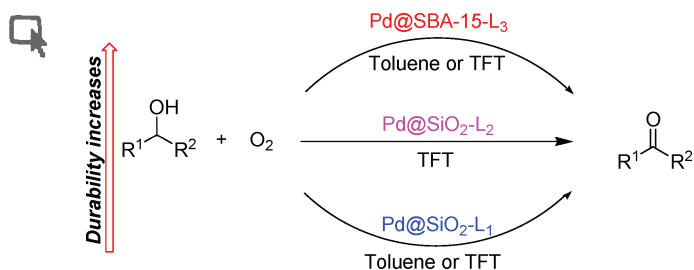
Aerobic oxidation of alcohols using various types of immobilized palladium catalyst: the synergistic role of functionalized ligands, morphology of support, and solvent in generating and stabilizing nanoparticles

Babak Karimi,* Asghar Zamani, Sedigheh Abedi and James H. Clark

For a number of immobilized palladium catalysts based on hybrid amorphous/mesoporous silica, the ligand, the structure of support, and the solvent could effectively lead to prevention of Pd nanoparticle agglomeration and generation of durable catalysts.

PAPERS

120

Selective aerobic oxidative dibromination of alkenes with aqueous HBr and sodium nitrite as a catalyst

Ajda Podgoršek, Marco Eissen, Jens Fleckenstein, Stojan Stavber, Marko Zupan and Jernej Iskra*

Various alkenes (internal, terminal, aryl and alkyl substituted) and 1,2-diphenylethyne were efficiently and selectively dibrominated using 2 equivalents of 48% aqueous hydrobromic acid, with air as an oxidant and sodium nitrite as a catalyst.
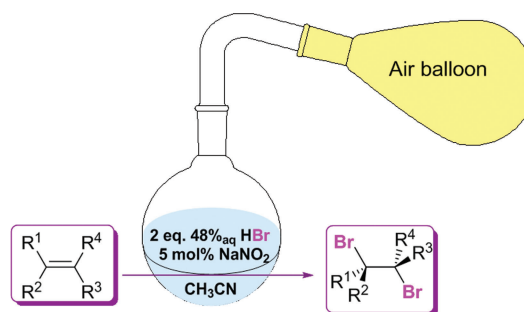
127

Nanoparticle-supported and magnetically recoverable nickel catalyst: a robust and economic hydrogenation and transfer hydrogenation protocol

Vivek Polshettiwar,* Babita Baruwati and Rajender S. Varma*

A magnetic nanoparticle-supported leach-proof Ni catalyst was readily prepared from inexpensive starting materials which catalyzes various hydrogenation and transfer hydrogenation reactions; high catalytic activity and ease of recovery are additional eco-friendly attributes of this catalytic system.
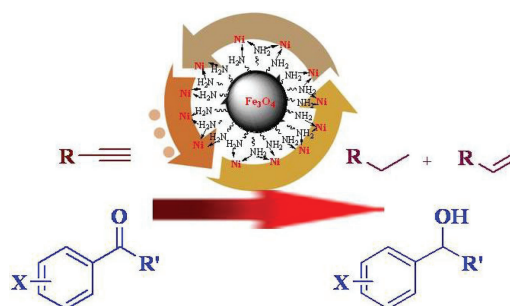
132

Direct analysis of cryptotanshinone and tanshinone IIA in biological samples and herbal medicinal preparations by a green technique of micellar liquid chromatography

Li Zhu, Li Ding, Qianli Zhang, Lin Wang, Fei Tang, Qian Liu and Shouzhuo Yao*

Instead of toxic acetonitrile or flammable methanol widely used in HPLC, a green mobile phase by micellar liquid chromatography gives a more sensitive and rapid separation for analysis of biological samples and herbal medicinal preparations.
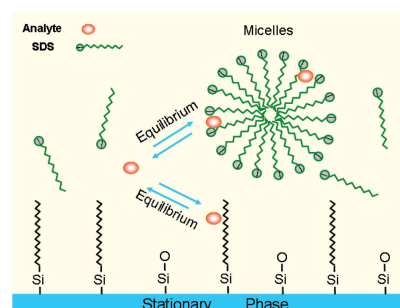
FREE E-MAIL ALERTS AND RSS FEEDS

Contents lists in advance of publication are available on the web *via* www.rsc.org/greenchem – or take advantage of our free e-mail alerting service (www.rsc.org/ej_alert) to receive notification each time a new list becomes available.

Try our RSS feeds for up-to-the-minute news of the latest research. By setting up RSS feeds, preferably using feed reader software, you can be alerted to the latest Advance Articles published on the RSC web site. Visit www.rsc.org/publishing/technology/rss.asp for details.

ADVANCE ARTICLES AND ELECTRONIC JOURNAL

Free site-wide access to Advance Articles and the electronic form of this journal is provided with a full-rate institutional subscription. See www.rsc.org/ejs for more information.

* Indicates the author for correspondence: see article for details.

Electronic supplementary information (ESI) is available *via* the online article (see http://www.rsc.org/esi for general information about ESI).

AUTHOR INDEX

Chemical Technology

New patterning method can guide the growth of nerve fibres

Lasers draw protein pictures

Scientists in Canada have recreated a famous painting on the microscale using a new protein patterning technique. The technique can also be used to mimic patterns of proteins found in cells and could lead to advances in neuroscience, they say.

Santiago Costantino, at the University of Montreal, and colleagues used laser-assisted protein adsorption by photobleaching to create the protein patterns. He used a laser to bind a fluorescent compound called biotin-4-fluorescein (B4F) to a protein-coated glass surface. By moving the laser around and varying the intensity of the beam, he created patterns of B4F with varying thickness. He then bound other proteins and antibodies to the surface to create fluorescent and biologically active protein surfaces.

Costantino showed that the protein patterns can be used to guide nerve fibres' direction of growth. He says he hopes this will be useful in neuroscience and immunology, for example to repair nerve damage. He also demonstrated the technique's

flexibility and precision by patterning a fluorescent microscale version of the 'Girl with a Pearl Earring' painting by Vermeer.

One of the advantages the method is its accessibility, says Costantino

More than just a pretty face: the precise protein patterning method could help to repair damaged nerves

– the technology uses equipment readily available in a typical neuroscience lab. 'We believe that our approach will lead to a major boost in the number of groups that can access new technologies for protein patterning,' he says.

'What impresses me is the dynamic range of protein adsorption that they are able to achieve, coupled to a versatile immobilisation scheme that allows for attaching just about anything to the surface,' says Albert Folch, an expert in bioengineering from University of Washington, Seattle, US. 'Something to be worked out is the long-term stability of the pattern, since cells produce enzymes which can break down proteins during growth and migration. It would be exciting to see if the technique allows patterns of competing signals to be shown to a nerve fibre in real time as the neuron's developmental clock is ticking.' *Sylvia Pegg*

Reference
J M Bélisle *et al, Lab Chip*, 2008, **8**, 2164 (DOI:10.1039/b813897d)

In this issue

Fingerprints show their dark side
Polymer reveals prints on almost any surface

Sensors go with the flow
Blind cave fish inspire scientists to develop a flow sensor

Interview: Discovering the Texas molecule
Jonathan Sessler reveals the motivation behind his drug research

Instant insight: Digging deep with microtools
Jaime Castillo and colleagues gain insight into disease with the help of micro and nano manipulation techniques
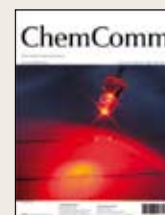
The latest applications and technological aspects of research across the chemical sciences

Application highlights

Photoresponsive surfactant disperses or separates oil and water mixtures

Shine a light for separation

UK scientists have used light to separate complex chemical mixtures. The method can be used to recover high value products and catalytic nanoparticles from reaction mixtures, they say.

Julian Eastoe, at the University of Bristol, and colleagues added light-sensitive surfactants to microemulsions. When they shone UV light on the mixtures, the surfactants caused the oil and water phases in the emulsions to separate.

Previously researchers have relied on heat, pH changes or salt addition to separate the phases in microemulsions. The new method does not change the chemical composition of the microemulsion or use as much energy as heat-induced separation.

'We are fascinated by the opportunities offered by light-activated particles, colloids and interfaces. It adds another dimension to the chemical engineering toolbox,' says Eastoe.
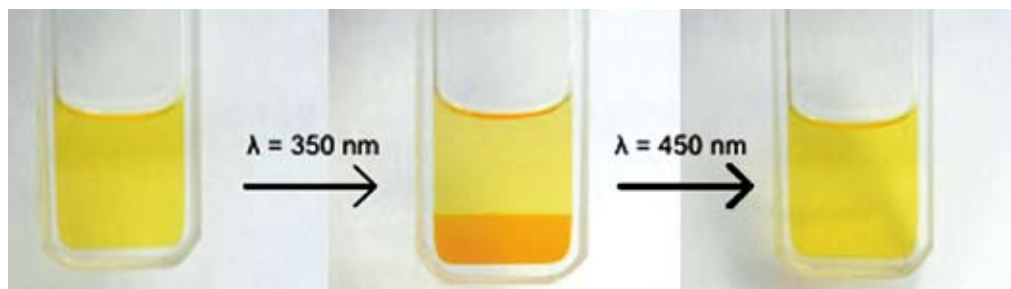
Importantly, adds Eastoe, these separations are reversible. A sample can be cycled between dispersed and separated states using only light. 'The research shows the dream of light-triggered colloids is becoming reality,' he says.

'What is particularly exciting about this work is that through the simple and elegant addition of a small amount of a photoresponsive surfactant, the team have transformed the

Flashes of light cycle the system between its dispersed and separated states

conventional microemulsion into a photoresponsive system,' says Ted Lee, an expert in responsive surfactant systems at the University of Southern California, Los Angeles, US.

The new method could be used in light-activated release and delivery systems for pharmaceuticals and agrochemicals, explains Eastoe. But he says their next challenge is to develop photosensitive surfactants that are cheap, safe and environmentally friendly.

Sarah Dixon

Reference

R F Tabor *et al*, *Soft Matter*, 2009, DOI: 10.1039/b813234h

Site-specific release of chemotherapeutics avoids damage to healthy cells

Drug delivery on target
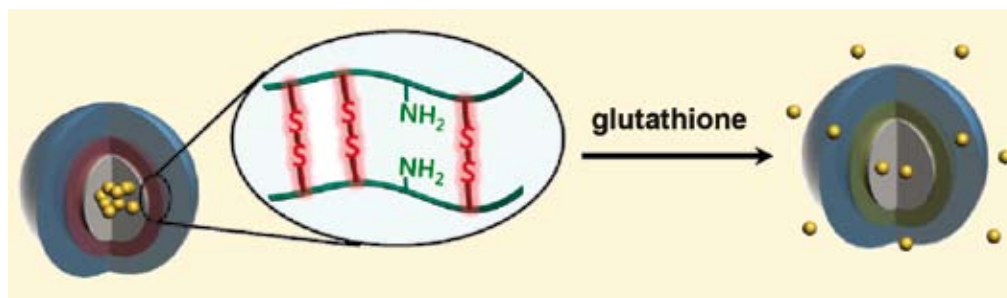
A peptide found in tumour cells can trigger the release of drugs from a novel nanocarrier, claim South Korean scientists. They say their drug delivery system could make anticancer drugs more effective and reduce their side effects.

Drug delivery systems transport drugs to diseased cells then release them, increasing their therapeutic action and preventing them from damaging healthy cells. Polymer micelles have been investigated as delivery systems but they lack stability and often release drugs at unwanted sites. Cross-linking the micelles makes them more stable but breaking the cross-links to release the drugs is problematic.

Sang Cheon Lee, at the Korea Institute of Ceramic Engineering and Technology, Seoul, and colleagues made polymer micelles linked by disulfide bonds. They loaded the micelles with methotrexate, an anticancer drug,

and tested the micelles' ability to deliver the drug in a cancer cell culture.

They found that the micelles were readily taken up by the cells and, once inside, a peptide called glutathione broke the disulfide bonds, releasing the drug. Since tumour cells often contain higher levels of glutathione than normal cells, Lee suggests that these micelles could be used to directly target tumour cells. He adds that the micelles would be broken down by the body into harmless products after drug delivery.

'Since the cleavable cross-links can be tailored for other cellular signals, this novel nanocarrier technology has the potential to treat many diseases,' says Lee. He adds that the team's next aim is to adapt the system for molecular imaging.

Harriet Brewerton

Glutathione breaks the disulfide cross-links, releasing the drug

Reference

A N Koo *et al*, *Chem. Comm.*, 2008, 6570 (DOI:10.1039/b815918a)

Polymer reveals prints on almost any surface
Fingerprints show their dark side

UK chemists have discovered a fascinating application for a polymer precursor, which could provide a new technique for the ancient forensic science of fingerprinting.

Paul Kelly and colleagues at Loughborough University were investigating the polymerisation of disulfur dinitride (S_2N_2) to form the conducting polymer $(SN)_x$ when they discovered that invisible (or latent) fingerprints on surfaces exposed to the S_2N_2 vapour turned black. They found that the darkening effect was due to the spontaneous formation of a layer of $(SN)_x$ polymer on the prints.

Forensic scientists normally detect latent prints using a soft brush and fine aluminum powder. Usually they only show up on hard surfaces such as glass, metal or polished wood. Kelly says his technique is unique because

it detects prints on almost any surface. 'It soon became apparent that S_2N_2 can "develop" prints from a vast range of media, from metal surfaces through to cotton and plastics. A one-covers-all versatile system like this has

S_2N_2 turns invisible fingerprints black

Reference
P F Kelly, *Chem. Commun.*, 2008, 6111 (DOI: 10.1039/b815742a)

obvious potential,' says Kelly.

Fingerprints appear to initiate the polymerisation process, claims Kelly, although traces of inkjet printer ink can also act as the initiator. The detection limit is so low that details of a printed letter previously contained inside an envelope could be read off the inside of the envelope after exposure to S_2N_2.

'This work has demonstrated that it is possible to obtain fingerprints from surfaces that hitherto have been considered extremely difficult, if not impossible, to obtain,' says Colin Lewis, scientific advisor at the UK Ministry of Defence. 'The method proposed has shown that this system could well provide capabilities which could significantly enhance the tools available to forensic scientists in the future.'

James Hodge

Scientists inspired by cave fish design potential tsunami detector
Sensors go with the flow

US scientists have created sensors that rival a fish's ability to detect underwater flow. The sensors could provide an alternative to sonar for underwater research, they claim.

Vladimir Tsukruk, at the Georgia Institute of Technology, Atlanta, and colleagues coated man-made flow sensors with a hydrogel to mimic the flow-sensing hair system on blind cave fish.

Cave fish rely on their natural flow sensors rather than eyesight for 'seeing' nearby obstacles. Their flow sensors consist of a variety of specialised structures, including long, bendy structures known as cupulae, that transmit flow information to bundles of hair cells. As the fish glide past objects, they can detect movement in the surrounding water and avoid collisions.

Tsukruk built up droplets of a polymer onto a man-made flow sensor. When the droplets dried,

they formed a tall hydrogel structure that mimicked the structure of a cupula. He compared the water flow sensitivity of bare sensors with the hydrogel-capped versions and found that the capped sensors were significantly better and rivalled the sensitivity of fish flow receptors.

Tsukruk explains that sonar detection of underwater objects can harm the surrounding environment. The hydrogel-capped sensor could provide an alternative to sonar in

The hydrogel-capped flow sensor

underwater applications, such as port security and tsunami detectors, as well as marine research, he claims. 'It's a simple but robust demonstration of the potential of bio-inspired design in solving difficult engineering problems,' he says.

Igor Luzinov, an expert in polymer films at Clemson University, US, was impressed with the approach. 'What's most amazing is that this man-made version is working pretty well,' he says.

Tsukruk says the challenge for the future is obtaining sufficient computing power to interpret the significant amount of information that an array of the sensors would produce.

Fay Riordan

Reference
M E McConney *et al*, *Soft Matter*, 2009, DOI: 10.1039/b808839j

Break-up of aggregates is breakthrough for nanomaterials

Magnetic solution for sticky problem

Belgian scientists have discovered a new method for stopping nanoparticles sticking together. The method will improve the use of nanoparticles in applications ranging from suncream to catalysis, say the scientists.

A nanoparticle's small size and large surface area give it improved properties over bulk solids in a number of applications. But nanoparticles have a tendency to aggregate, which reduces their surface area and makes them behave more like the bulk material. A magnetic field could solve the problem, claim Johan Martens and colleagues at the Catholic University of Leuven.

Martens suspended alumina and silica aggregates in a flowing solution within a stationary
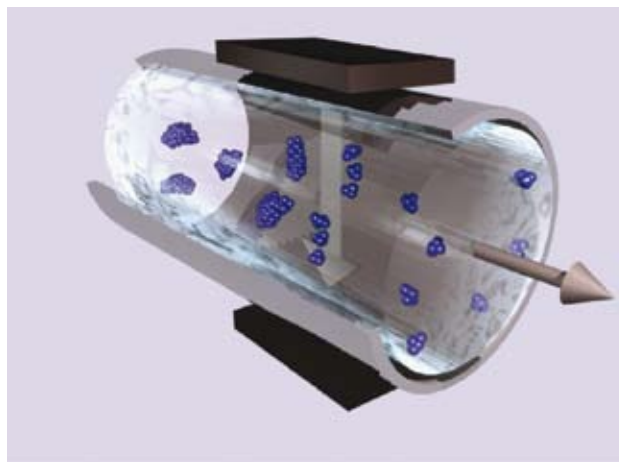
magnetic field. They found that the magnetic force broke up the aggregates, forming particles a fraction of the size.

Flowing past a magnet disperses the nanoparticles

According to Martens, the new dispersion method is simpler and more energy efficient than commonly used methods, such as ball milling and ultrasound.

'This is an important breakthrough for many of the real industrially relevant applications of nanomaterials,' says Luis Liz-Marzán, an expert in nanoparticles from the University of Vigo, Spain. 'It is a very elegant and efficient way to improve all these processes.'

Martens says the group plan to use the method to optimise particle dispersion in heterogeneous catalysis and pharmaceutical formulations.

Sophia Anderton

Reference

B Stuyven *et al, Chem. Commun.*, 2008, DOI: 10.1039/b816171b

Applying the golden touch to solder silver nanowires

Scaled-down soldering

A new a way of soldering metal wires together on the nanoscale will open the door to applications in nanocircuitry, say Japanese researchers.

The demand for ever-smaller electronics has generated a great deal of interest in electrical nanocircuits. The way nanowires are connected is of key importance when making stable nanocircuits, say Takaaki Toriyama and Tsutomu Ishiwatari of Shinshu

University, Ueda – simply laying nanowires across each other is mechanically unstable.

The previous method for joining silver nanowires involved chemically reducing chloroauric acid to produce metallic gold particles. When Toriyama and Ishiwatari tried this, they found that the silver wires corroded. By first treating the wires with excess thiol, which protects the surface of the silver, and then with chloroauric

Treat with thiol to protect your nanowire during soldering

Reference

T Toriyama and T Ishiwatari, *J. Mater. Chem.*, 2008, **18**, 5537 (DOI: 10.1039/b808588a)

acid, they avoided corrosion and created a permanent join between the nanowires.

Next, Toriyama and Ishiwatari converted the chloroauric acid in the join to metallic gold. They found that after chemical reduction some of the acid remained, but by simply heating the join, they achieved complete conversion.

Toriyama and Ishiwatari conclude that the newly developed method is 'superior to chemical reduction' and says that it holds promise as a way of soldering nanowires for electronics.

'Toriyama and Ishiwatari's method is simple and promises to be useful in device fabrication and other nanotechnology applications,' says C N R Rao, an expert in materials chemistry at the Jawaharlal Nehru Centre for Advanced Scientific Research, Bangalore, India.

David Barden

Interview

Discovering the Texas molecule

Jonathan Sessler talks to Michael Brown about what motivated him to discover texaphyrin and about the aims of the companies he co-founded
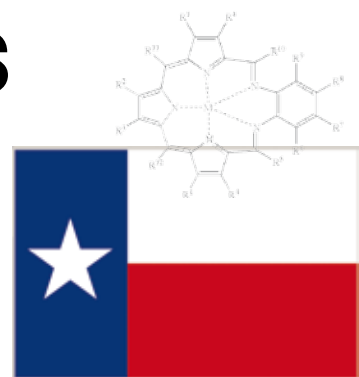
Jonathan Sessler

Jonathan Sessler is a professor at The University of Texas, US. He is co-founder of Pharmacyclics, a company developing biomedical applications of expanded porphyrins, and Anionics, a company that targets various commercial opportunities associated with anion recognition chemistry. He is an associate editor and a member of the editorial board for *Chemical Communications*.

What inspired you to become a chemist?

My love for chemistry started in the seventh grade at school when I had the chance to do some experiments as part of the curriculum. Also, my father was a physicist and we had a small laboratory in our house. I was able do experiments in there, such as making esters. These exploits finally came to an end when I successfully synthesised nitroglycerine and blew up half the lab!

What is the most significant aspect of your work?

Over the course of my career, it has been the use of new macrocycles for drug development. However, right now, it is the transition between supramolecular chemistry and polymer chemistry. We are particularly excited about a joint project with Chris Bielawski's group at The University of Texas. It combines the chemistry of various specific neutral anion receptors (these are more biocompatible than charged receptors) with polymeric materials. This is allowing us to couple the specificity of the receptors with the well controlled hydrophobic environment of polymers. We can extract ions into organic media using receptors that would never work by themselves.

How did you discover texaphyrins and what was your motivation?

The main focus of my effort over most of my career has been to develop anti-cancer drugs using compounds that we call 'expanded porphyrins'. In this context, we have put a particular emphasis on texaphyrins. This work was inspired, in part, by my own history. As a student, I underwent treatment for Hodgkin's lymphoma, and I went through radiation treatment as a senior at the University of California, Berkeley. I decided to do post graduate studies at Stanford University, as it was reputed for its chemistry and the particular treatment that I needed. Dr Henry Kaplan, at Stanford, had developed radiation treatment for soft tumours – radiation had been used for years for hard tumours – and he set up a school for the treatment of Hodgkin's disease. In my third year, I had a relapse and underwent chemotherapy in the

care of Dr Richard Miller. He suggested that as I was a chemist, I should be able to come up with a new cancer drug. My PhD and post doctoral work were in the area of porphyrins, which are pigments found in blood. Then, when I arrived in Texas, I realised that blood pigments only had four sub-units called pyrroles, and it would be interesting to investigate the chemistry of systems with five pyrroles. Texas, known as the 'Lone Star State', has a five point star as an emblem, so I was motivated to make a politically correct molecule with five nitrogens instead of four. We called the molecule 'texaphyrin'. It turned out that by expanding the core of the porphyrin, texaphyrin became attractive as an anti-cancer agent.

Could you tell us about the companies you co-founded?

When I was undergoing treatment, there were no drugs to prevent the nausea associated with the treatment so it was pretty tough. Dr Richard Miller suggested that we use our chemical talents to make better drugs; that motivated us to develop texaphyrin and set up Pharmacyclics. We are hoping to achieve our goal of commencing a definitive Phase III clinical trial for our drug motexafin gadolinium (MGd), a specific texaphyrin derivative, next year. MGd has been administered to about 1000 patients to date and the trials have been promising but not quite good enough for regulatory approval; we hope that the planned trial will allow this situation to be rectified.

The second company I co-founded is Anionics. We are working towards developing the polymeric materials that I mentioned earlier; we aim to use them to remove anions from renal patients and for water purification. This research is waiting for a real technological breakthrough to occur – we have the infrastructure in place.

What do you enjoy most about working on *Chemical Communications*?

The opportunity to interact with people has increased as a result of working for *Chemical Communications*. It is a joy to have friends all over the world and to be able to meet other researchers.

©The Royal Society of Chemistry 2009

Instant insight

Digging deep with microtools

Jaime Castillo, Maria Dimaki and Winnie E. Svendsen at the Technical University of Denmark explain how micro and nano manipulation techniques are helping researchers understand biological systems

Understanding the biochemical background of diseases at their deepest levels is a challenging task. It has motivated researchers from a range of disciplines – from biology to physics to robotics – to combine their efforts to improve patients' quality of life.

Much of this research is focused on developing techniques and tools to handle biological material without damaging it or altering its natural state. In this way, the study of biological systems will be as close to the real, in vivo situation that we can get in a research lab.

Several manipulation techniques have emerged in recent decades thanks to advances in micro- and nanofabrication. For instance, the atomic force microscope (AFM) uses a probe to image, push, pull, cut and indent biological material in air, liquid or vacuum.

Scanning electron microscopes offer improved magnification over AFMs but samples have to be fixed, dehydrated and coated with metal, which alters their size and shape. However, metal coating is not needed for environmental scanning electron microscopes, allowing scientists to image and manipulate samples in their natural state.

Using these techniques, scientists can make manipulation tools, such as microgrippers and nanotweezers, on the same length scale as the biological samples.
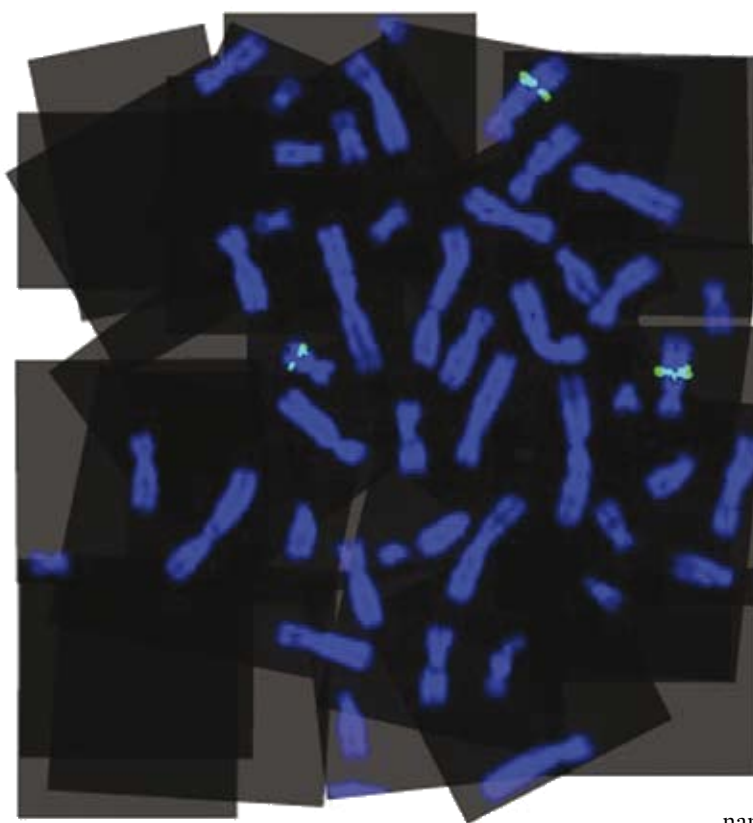
And so researchers can now move, position, image, stimulate and characterise biological samples, including cells, DNA and bacteria, in a controlled way. The choice of manipulation technique depends on the size and shape of the sample, in addition to the medium in which it is found.

Unfortunately, manipulation tools can affect the structure of biological samples. In these cases, techniques such as dielectrophoresis, acoustophoresis or microfluidics, which use physical phenomena rather than direct contact to manipulate the

Researchers can move, image and characterise chromosomes using micro and nano manipulation methods

samples, are good options. Combining these techniques increases the possibilities for handling samples. For example, scientists combine micromanipulators with precise fluidic and motion control in assisted in vitro fertilisation techniques.

Researchers need to consider the consequences of scaling down their studies. Effects that are dominant at the macroscale become negligible when moving to the micro- and nanoscale. For example, in a microfluidic microchannel, gravity no longer plays a role but surface tension, which is insignificant on the macroscale, is crucial. Understanding these scaling laws is critical for a successful transition from the macroscopic to the micro- and nanoscopic dimensions.

Although great progress has been made, challenges are still present. To understand the complex interactions between and inside biological samples, scientists will always have to manipulate, transport, sort and integrate samples in different environments. For this, we need to improve manipulation techniques and make new tools so we can continue to explore biological entities in their natural environments.

Read more in "Manipulation of biological samples using micro and nano techniques" in the first issue of Integrative Biology.

Reference
J Castillo, M Dimaki and W E Svendsen, *Integr. Biol.*, 2009, DOI: 10.1039/b814549k

Essential elements

Double debut

This month sees the debut of two highly interdisciplinary new journals from RSC Publishing: *Integrative Biology: Quantitative biosciences from nano to macro* and *Metallomics: Integrated biometal science*.

Integrative Biology is a unique journal focused on quantitative multiscale biology using enabling technologies and tools to exploit the convergence of biology with physics, chemistry, engineering, imaging and informatics. The first issue contains articles on human mammary progenitor cell fate decisions, the analysis of aptamer binding sequence–activity relationships using microarrays, and genome-wide transcriptome analysis of 150 cell samples and much more. Visit www.rsc.org/ibiology

Metallomics covers the research fields related to metals in biological, environmental and clinical systems and is expected to be the core publication for the emerging metallomics community. First issue articles include a look at the effect of vanadium(IV) in diabetic mice, cytotoxicity of chemical warfare degradation products, and identification and characterisation of metallodrug binding proteins. Visit www.rsc.org/metallomics

Authors from around the globe have submitted work of the highest quality, knowing that they can rely on RSC staff for overseeing a rigorous peer-review process, efficient manuscript handling and rapid publication.

The current issues of both new journals are freely available to all readers via the website. Free institutional online access to all 2009/2010 content will be available following a simple registration process.

And finally...

Materials science researchers joined RSC Publishing last month at a celebration reception at the Fall MRS 2008 meeting. Authors and readers were thanked for their continued support, while RSC journal *Soft Matter* announced its increase in frequency for 2009 and five years of successful publication.

Delegates were invited to pre-order the latest edition of the bestselling textbook, *Nanochemistry* by Geoff Ozin, and take part in a prize draw to win a solar powered charger in celebration of the 2008 launch of *Energy & Environmental Science*.
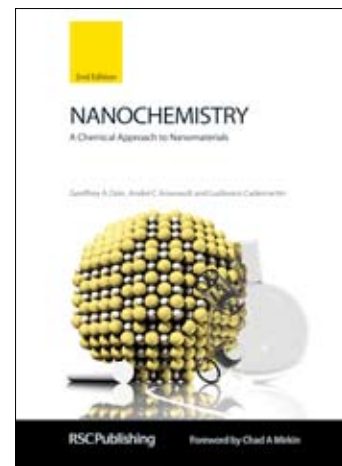
Looking ahead, preparations are underway for the Third International *ChemComm* Symposium, which is to be held in China next month. The subject will be organic chemistry and keynote speakers include Professors Peter Kundig, Keiji Maruoka and Susan Gibson.

To find out more visit: www.rsc.org/chemcommsymposia

InChI collaboration with ChemSpider

An InChI Resolver, a unique free service for scientists to share chemical structures and data, is to be developed via a collaboration between ChemZoo Inc., host of ChemSpider, and RSC Publishing.

Using the InChI – an IUPAC standard identifier for compounds – scientists can share, contribute and search molecular data from many web sources.

The InChI Resolver will give researchers the tools to create standard InChI data for their own compounds, create and use search engine-friendly InChIKeys to search for compounds, and deposit their data for others to use in the future.

'The wider adoption and unambiguous use of the InChI standard will be an important development for the future of chemistry publishing, and further development of the semantic web,' comments Robert Parker, managing director of RSC Publishing.

The InChI Resolver will be based on ChemSpider's existing database of over 21 million chemical compounds and will provide the first stable environment to promote the use and sharing of compound data. 'With the introduction of the InChI Resolver, we hope to expand the utility and value of both InChI and the ChemSpider service,' adds Antony Williams of Chemspider.

This collaboration sees RSC Publishing remain at the forefront of chemical information technology.

Editor: Joanne Thomson

Deputy editor: Michael Spencelayh

Associate editors: Celia Gitterman, Nina Notman

Interviews editor: Elinor Richards

Web editors: Nicola Convine, Michael Townsend, Debora Giovanelli

Essential elements: Daniel Bradnam and Christine Hartshorne

Publishing assistant: Jackie Cockrill

Publisher: Graham McCann

RSCPublishing

©The Royal Society of Chemistry 2009

Green Chemistry… 10 years on

DOI: 10.1039/b820904a

Celebrating the tenth year of *Green Chemistry*

During 2008 we celebrated the tenth year of *Green Chemistry* and to mark this occasion we had a number of activities. At the Green Chemistry & Engineering Conference in Washington in June we had a birthday cake for the Journal, with many of the readers and authors of *Green Chemistry* helping us celebrate. Professor Joan Brennecke, a member of the editorial board, had the honour of cutting the birthday cake for the Journal.

To mark the occasion we also published a number of reviews throughout the year, representing the broad range of subjects covered in the Journal and many hot topics. All of these reviews were accompanied by an editorial from a member of the *Green Chemistry* board, past or present. We would like to thank all of those authors who contributed a review during the 10th anniversary and to those Board Members who wrote introductions to the reviews, putting them in the context of the Journal. A complete list of the reviews and their accompanying editorials can be found on the Journal homepage (www.rsc.org/greenchem).

Green Chemistry was also proud to sponsor the opening lecture given by Istvan Horváth entitled 'Solvents from nature' at the 'Green Solvents–Progress in Science and Application' meeting in Friedrichshafen, Germany at the end of September.

We were also delighted that Istvan agreed to contribute a perspective to the Journal, based on his lecture, which was published in the October issue of *Green Chemistry* (I. T. Horváth, *Green Chem.*, 2008, **10**, 1024–1028, DOI: 10.1039/b812804a).

Increasing impact of *Green Chemistry*

As we look forward to 2009, RSC Publishing is working with more authors than ever before – 2008 saw the number of authors published in RSC Journals increase by 30%. Meanwhile titles from across the RSC collection recorded impressive rises in impact factors, and the latest immediacy indices confirm the relevance and topicality of research published by the RSC.

With the release of the 2007 Thomson ISI impact factors *Green Chemistry* saw a 15% rise in impact factor to 4.836, reaffirming its leading position as the number one green chemistry journal.
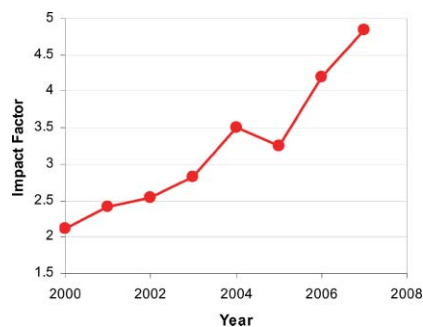
We would like to take this opportunity to thank our Authors and Referees for helping us to achieve this significant increase in impact factor for the Journal.

RSC Publishing is committed to providing a world-class publishing service and global visibility to its authors and with the number of citations increasing, immediacy and impact factors rising it is clear to see that *Green Chemistry* and RSC Publishing are recognised by researchers throughout the world as a key resource to publish and read the very best research.

Editorial Board

We would like to welcome Professor Shu Kobayashi, Tokyo University, onto the *Green Chemistry* Editorial Board from this year. Professor Kobayashi's long-standing and world-renowned experience in efficient synthetic methodologies including asymmetric catalysis, organic reactions in water, microencapsulated catalysts, and microreactors in organic synthesis will provide an additional regional link for *Green Chemistry* in Asia. Shu has been a stimulating plenary speaker at many green chemistry conferences and his research has been recognised with a long list of prestigious awards, including most recently the Arthur C. Cope Scholarship and Howard Memorial Lectureship. We look forward very much to his input and collaboration within the editorial board.

Improved ReSourCe

During 2009 we will release a new version of ReSourCe, our system for online manuscript submission and peer review (www.rsc.org/resource). Already popular with Authors and Referees, we've listened to your feedback and made further improvements to our service. We're keen to build on your experience of ReSourCe, so if you would you like to help us shape the next release by taking part in beta-testing or by supplying your comments and suggestions please contact resourcesupport@rsc.org

Your RSC subscriptions and free content

We know that it can be difficult to keep track of online resources that are available to you. So, we've introduced a special web page to help you to find out exactly what RSC content you can access. This new page is called Your RSC Subscriptions (www.rsc.org/Publishing/your_access.asp) and it lists all products for which your organisation has a current subscription, plus other content which may be available to you, such as the RSC Journals Archive and the RSC eBook collection.

You can also find out about RSC content that is available free, including: research articles that are free for a limited time; news articles in magazines; and free chapters from the RSC eBook Collection. Visit www.rsc.org/Publishing/freeRSCcontent.asp

Food: the RSC theme for 2009

In 2009, the theme for RSC public engagement activities will be food; looking at all aspects of the supply chain from field to fork and eventually to waste disposal and recycling. Planned activities include the launch of a major reports into securing a sustainable food supply; the publication of a new edition of the ground-breaking book *Kitchen Chemistry*; lectures and events at the new Chemistry Centre at Burlington House – the world's foremost venue for showcasing chemistry; and Chemistry Week 2009 (7th–15th November), when practicing scientists and science teachers will engage in a week-long festival for the chemical sciences. Please get in touch with us (food@rsc.org) if you would like to be involved.

New journals

Our journal portfolio has expanded with the launch of three new journals.

Energy & Environmental Science, launched in July 2008, publishes research from all aspects of the chemical sciences relating to energy conversion and storage, alternative fuel technologies and environmental science. www.rsc.org/ees

Metallomics: Integrated biometal science covers the research fields related to metals in biological, environmental and clinical systems. www.rsc.org/metallomics

Integrative Biology: Quantitative biosciences from nano to macro is a unique, interdisciplinary journal covering quantitative multi-scale biology using enabling technologies and tools to exploit the convergence of biology with physics, chemistry, engineering, imaging and informatics. www.rsc.org/ibiology

The current issue of all three journals is freely available online. Free online institutional access to all 2009 content is available for registered users – full details are on the web site.

The RSC eBook Collection

The RSC eBook Collection has become a world-class electronic resource with licenses being signed to leading institutions across the globe. New content continues to be uploaded regularly and this comprehensive resource now includes over 800 quality titles. Electronic book publications are uploaded within days of print publication, effortlessly disseminating extensive, high-quality, scientific content direct to scientists, libraries, students, teachers and researchers around the world. Please visit www.rsc.org/eBooks for further information or to visit the RSC eBook Collection.

Over 80 new print books will be published in 2009 as our list continues to grow in size and importance in the international market. Keep up-to-date with all the latest cutting edge titles being published by the RSC by visiting www.rsc.org/ej_alert and subscribing to our eAlerts. We send regular information on discount offers, print books and new electronic content throughout the year.

We wish you all a successful 2009, and thank you for your continued support of *Green Chemistry*.

Sarah Ruthven, Editor
Walter Leitner, Scientific Editor
Martyn Poliakoff, Chair of the Editorial Board

> *"I must say that the RSC has done a great job over the past few years of reinventing and reinvigorating its chemistry journals. In my opinion they are now the best in the world for publishing first rate topical modern chemistry in a rigorous yet appealing and accessible form"*
>
> **Professor Stephen Kent,** *University of Chicago*

Succinic acid from renewable resources as a C$_4$ building-block chemical—a review of the catalytic possibilities in aqueous media

Clara Delhomme,*[a] Dirk Weuster-Botz[a] and Fritz E. Kühn[b]

Aqueous hydrogenation of bio-based succinic acid has been reported for the production of value added chemicals, e.g. 1,4-butanediol, tetrahydrofuran, γ-butyrolactone, 2-pyrrolidone or N-methyl-2-pyrrolidone. A variety of heterogeneous metallic catalysts, active under quite severe conditions have previously been studied, whereas research into organometallic complexes is thus far limited to solvent reactions or to aqueous reactions producing succinic acid.

1.   Introduction

Prior to the end of the 18th century, the economy was largely based on agriculture; however, the industrial revolution changed this, establishing fossil fuels (petroleum, coal and natural gas) as the main resources. In continuation of this development, the chemical industry nowadays consumes more than 1 billion barrels of oil per year.[1] Considering this consumption and the limited nature of the fossil fuels, it is not astonishing that the economy faces several problems—a continuously rising price of oil, political and economic issues related to the unequal distribution of the remaining oil stocks and increasingly severe environmental impacts due to the use of these resources and the by-products generated during their consumption.

These problems have motivated the industry to find alternatives to fossil fuels. Considerable effort is being invested in biotechnology and "green chemistry" (among others) to develop a chemical industry based on renewable resources as at least (a partial) substitute for the dwindling fossil fuels. To that end, fermentation of biomass for the production of renewable building-block chemicals is currently being developed. The so-called "green chemistry" deals to a considerable extent with the optimization of chemical processes, reducing the negative environmental impact of the chemical industry, e.g. by lowering energy consumption, with more efficient catalysts and by enabling use of solvents with a lower environmental impact. Furthermore, bio-based feedstock (produced by fermentation) must be transformed into valuable chemicals. Since the output of fermentations consists usually of dilute aqueous solutions of organic products, new water-stable catalysts need to be designed for such applications.

Succinic acid is among the new bio-derived building-block chemicals that could replace the current maleic anhydride C$_4$ platform. The main interest in succinic acid lies in its derivatives,[1]

since it can be transformed into a lot of interesting products: 1,4-butanediol (BDO), γ-butyrolactone (GBL), tetrahydrofuran (THF), N-methyl-2-pyrrolidone (NMP), 2-pyrrolidone (2-Pyrr), succinimide, succinic esters, maleic acid (M.A.)/maleic anhydride (M.Anh.) and several others (cf. Fig. 1).

The optimization of the fermentation process for succinic acid production is currently underway. To that end, various natural succinate producing strains of bacteria (e.g. Anaerobiospirillum succiniciproducens, Actinobacillus succinogenes and Mannheimia succiniciproducens) and engineered Escherichia coli strains have been investigated.[3]

However, among the bottleneck problems of the industrial production of succinic acid from renewable resources remain the costs related to purification.[4] Because the fermentation must be done at neutral or low acidic pH, the fermentation broth must be acidified upon conclusion of the reaction to create the free acid. Furthermore, other organic acids produced as side products during the fermentation can unfavorably affect the recovery of succinic acid.[4] Therefore, the direct downstream catalysis of succinic acid in the filtered aqueous fermentation broth allows the production of valuable derivatives without the need to isolate pure succinic acid.

In the past century, the utilization of water as a reaction medium for organic synthesis was quite limited. The low water-solubility of most organics and the water-sensitivity of some reagents or intermediates[5] were serious disadvantages. However, the high waste production due to organic solvents, their volatility and the high energy consumption for gas phase reactions are two major environmental drawbacks for the chemical industry that must adapt to new environmental restrictions and to growing consumer awareness. Furthermore, the handling of flammable, explosive and carcinogenic organic solvents is a major safety problem. Water—an abundant and non-toxic solvent—could be a greener alternative as well as having other advantages: it favors ionic reactions, solvates cations and anions, is an ideal solvent for radical reactions, can facilitate the control of exothermic reaction due to its high phase change enthalpies and heat capacity[6,7] and, finally, water has been reported to suppress the coke and tar formation for the vapor hydrogenation of maleic acid with metal containing catalysts.[8]

[a]Institute of Biochemical Engineering, Technische Universität München, Boltzmannstr. 15, D-85748, Garching b. München, Germany. E-mail: C.Delhomme@lrz.tum.de
[b]Chair of Inorganic Chemistry and Molecular Catalysis, Faculty of Chemistry, Technische Universität München, Lichtenbergstr. 4, D-85747, Garching b. München, Germany. E-mail: fritz.kuehn@ch.tum.de.
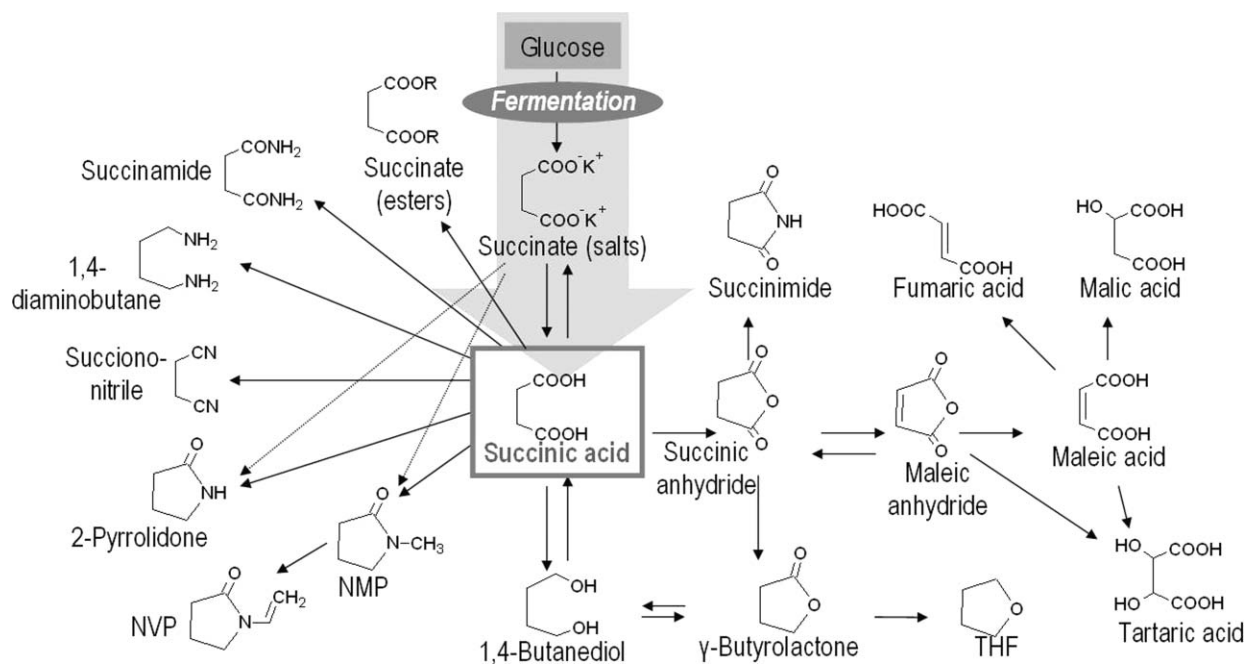
Fig. 1 Succinic acid derivatives.[2]

Furthermore, in opposition to liphophilic oil, coal or natural gas derived compounds, the chemicals produced from renewable resources are often hydrophilic. Hence, a new class of catalysts must be developed. These new catalysts must fulfill the following requirements: (1) water-stability, (2) high selectivity towards substrate and product, (3) no inhibition due to or degradation by fermentation side products, (4) immobilizability to enable easy recovery, (5) high activity at low pressure and temperature (ideally atmospheric pressure and room temperature so as to minimize energy requirements). Furthermore, the chemicals produced from the fossil fuels are mostly in a low oxidation state and must therefore be oxidized, whereas the compounds produced from renewable resources are often in a high oxidation state and must therefore be reduced. Current catalysts must therefore be substantially modified so that they are able to catalyze reductions of bio-based chemicals in aqueous media.

In the case of succinic acid, most derivatives presented in Fig. 1 are produced through hydrogenation or reductive amination (in the presence of hydrogen), hence, this review will focus on these types of reactions for production of succinic acid derivatives in presence of water. Additionally, some space is dedicated to the synthesis of succinic acid by the hydrogenation of maleic and fumaric acid with the help of aqueous organometallic catalysts. Although at first glance, this approach seems not to be relevant to succinic acid derived from renewable feedstock, it might nevertheless be helpful in the design of water-stable homogeneous or immobilized catalysts that are able to hydrogenate the renewable succinic acid in an aqueous environment. A summary of achievements in the area of organometallics for solvent hydrogenation of succinic anhydride has been added as further information and for comparative purposes.

2. Aqueous phase catalysis with metal containing heterogeneous catalysts

2.1. γ-Butyrolactone, tetrahydrofuran, 1,4-butanediol

Maleic anhydride is a petroleum derived C_4 starting material used for the production of many chemicals. One of the possible downstream treatments of this product is its hydrogenation for the manufacture of valuable chemicals such as GBL, BDO and THF. GBL is, for example, used as the starting material for the synthesis of NMP and other pyrrolidones, in particular *N*-vinylpyrrrolidone and its polymer which is widely used in medicine. It can also be utilized as a solvent. Its world wide production represents 250,000 t, approximately 20% of which originates from USA based production sites. BDO is an intermediate mainly for the synthesis of THF and polybutylene terephtalate. It is sold at 0.30–0.41 $/kg into a large global market of 1.3 million t/a (with the U.S. market being *ca.* 25% of this). Finally, THF is used as a monomer for the production of PTMEG, as solvent a in PVC cement, in pharmaceuticals and coatings, or as a reaction solvent. It is a high-value chemical (0.70–0.77 $/kg) and is produced worldwide at a level of 439,000 t/a (with 25% of that figure coming out of the USA alone).†

There has been much industrial research on the synthesis of these compounds and different research groups have tried to establish a hydrogenation approach starting from maleic anhydride or acid.[9–11] In Fig. 2, one possible reaction pathway starting from maleic acid—the hydrolyzed form of maleic
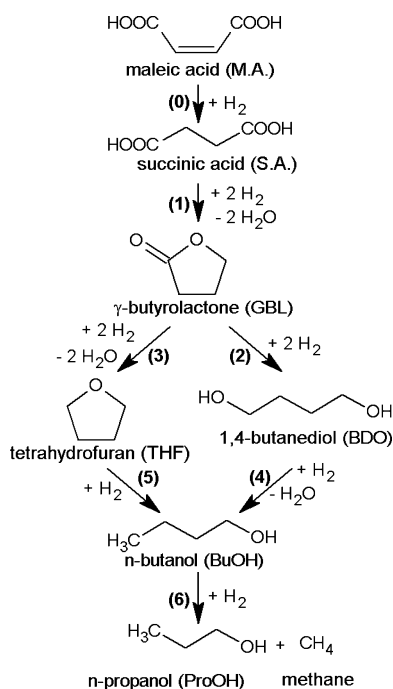
Fig. 2 Maleic acid hydrogenation pathway.[11]

Table 1 Metal containing heterogeneous catalysts for the aqueous hydrogenation of succinic acid into 1,4-butanediol, tetrahydrofurane or γ-butyrolactone

Company or Institute	Reaction	Optimal catalyst	T [°C]	P [MPa]	S [%]	Y [%]	Ref.	Year
E.I. Du Pont de Nemours	M.Ac. → THF +BDO	3%Pd–3%Re on C	190–200	17	90 (THF)	—	15–17	1985–1987
			180	17	79 (BDO)			
	S.Ac. → GBL + BDO	1%Pd–4%Re on TiO₂	200	3.5	90 (GBL)	90	18	1988
			200	6.9	90 (BDO)	89		
	S.Ac. → THF (+GBL)	1%Ru–4%Re on C	250	8.3	83 (THF)	82	19,20	1995
	M.Ac. → (GBL) → BDO	7%Ru–5%Sn on ZrO₂	225	14	96 (BDO)	94	21	1999
	M.Ac. → S.A. → BDO + THF	1) 1% Pd on C 2) 1%Ru–6%Re on C	1)120 2)175	20.7	— (BDO)	82	22	1999
		1.5%Ru–3%Re–0.6%Sn on C	250	13.8	— (THF)	67	23	2003
	M.Ac. → THF + GBL	1%Ru–6%Re on C	250	13.9	48–56 (GBL)	—		
			270	13.9	72 (THF)			
	M.Ac. → THF (+GBL)	1%Ru–6%Re on C	270	15	78 (THF)	—	24	2003
	M.Ac. → THF (+GBL)	1%Pt–6%Re–0.8%Sn on C	270	13.9	94 (THF)	—	25	2003
	M.Ac. → THF (+BDO)	4%Ru–1.4%Sn–1.3%Mo on TiO₂	250	13.9	89 (THF)	—	26	2004
	M.Ac. → THF +BDO	3%Pd–3%Re on C	175	9	80 (THF)	—	27	1995
Standard Oil Company	M.Ac. → BDO (+BuOH)	3.3%Pd–3.2%Ag–6.6%Re on C	175	9	74 (BDO)	—	28	1997
	M.Ac. → BDO (+THF + BuOH)	3%Pd–3%Ag–6%Re on oxidized C	140	17.2	93 (BDO)	—	29	1999
	M.Ac. → S.Ac. → BDO (+GBL + THF + BuOH)	Pd–Ag–Re–Al on oxidized C	152	17.2	91 (BDO)	—	30	2002
		Pd–Ag–Re on oxidized C	1)130 2)162	27.6	70 (BDO)	—		
ISP Investments	M.Ac. → S.Ac. → BDO (+GBL + THF + BuOH)	4%Pd–4%Ag–4%Re on C			—	—	31	2006
BP Inc.	M.Ac. → GBL	1%Pd–6%Ag–3%Re	230–260	5–8	98 (GBL)	—	32,33	1991–1992
	M.Ac. → S.Ac. → BDO (+GBL + THF + BuOH)	1) 0.5% Pd on Rutile TiO₂ 2) 5%Re on Rutile TiO₂	1)110ᵃ or 100ᵇ 2)165ᵃ or 177ᵇ	17.2–27.6	94 (BDO)ᵃ 89 (BDO)ᵇ	91ᵃ 90ᵇ	34–36	2006
Battelle Memorial Inst.	S.Ac. → GBL	5%Pd–5%Zr on C	225	17	92 (GBL)	90	14,37	2003

ᵃ First set of conditions. ᵇ Second set of conditions.

anhydride—is represented.[11] According to all published work, the first step of the hydrogenation is the hydrogen addition on the maleic anhydride/acid double bond for the formation of succinic anhydride/acid. Publications and patents discussing the hydrogenation of maleic acid in the aqueous phase could hence be easily adapted to the aqueous hydrogenation of succinic acid.

Some reviews summarize data on the hydrogenation of maleic or succinic anhydride/acid.[12,13] As the large majority of the published literature focuses on metal supported catalysts for vapor or solvent hydrogenation, not much information on aqueous phase reaction can be found. In the present review, attention will hence be brought to hydrogenation in aqueous media. Since water is a relatively reactive medium, ligand exchange or redox reactions would in many cases lead to rapid catalyst deactivation.[14] Accordingly, water stable derivatives of common organometallic or inorganic supported catalysts have been developed. An overview of the achievements in the domain of metal containing heterogeneous catalysts for the aqueous hydrogenation of maleic/succinic acid is presented in Table 1 and discussed in the following chapter.

2.1.1. Catalyst types. As shown in Table 1, various heterogeneous hydrogenation catalysts have been examined for the hydrogenation of succinic or maleic acid. The most active catalysts contain group VIII metals, combinations of them or combinations with other metals such as rhenium, tin, *etc*. Those metals are generally deposited on various inert supports.[21] The choice of the metal is indeed crucial for the nature, the yield and the selectivity towards the end product—many metal combinations have been studied so far. Since the literature on such reactions consists mainly of patents, little information can be found on promoting, synergetic and doping effects of various metals on the different hydrogenation reactions, and no kinetic data has been reported for aqueous hydrogenation of maleic/succinic acid. Furthermore, no systematic screening of

the performance of various metals or combination of metals has been performed. It is therefore difficult to draw a clear picture of the activity of the various metals under comparable conditions.

With regard to the nature of the metal used, different interpretations can be found in the literature. For example, Tooley and Black advocated the use of ruthenium—a group VIII metal—for its effectiveness towards carboxylic functional group reduction and as well as its acid resistance.[21] Campos and Strickland suggested replacing the expensive rhenium present in many catalysts by molybdenum—a lower cost and more available metal—particularly for bimetallic Ru-Re catalysts for the production of THF.[26]

The heterogeneous catalysts mentioned in the literature generally contain two or more metals. The reason for the presence of several metals is said to be the promoting and/or inhibition effect of the different metals and their synergetic interactions. In a complex set of reactions, such as the hydrogenation of succinic acid, metals can favor or inhibit different reactions and therefore increase the selectivity towards certain products.

The behavior of various metals for the hydrogenation of succinic acid in dioxane—a polar solvent—using a bimetallic ruthenium–cobalt catalyst was highlighted by Deshpande et al.[11] It was possible to show that ruthenium promotes the reactions 1, 3, 4, 6 presented in Fig. 2, whereas the activity for hydrogenation steps 2 and 5 were attributed to cobalt.[11]

The addition of a third metal can have an additional beneficial impact on the reactivity of the heterogeneous catalyst. For example, Budge et al. claimed that the addition of silver to a palladium–rhenium catalyst was increasing the BDO selectivity.[27] Certain patents[21,22,25] also reported that the incorporation of small amounts of tin into bimetallic catalysts improved the selectivity towards BDO, reducing the formation of side products such as n-butanol. Campos and Sisley made the assumption that tin moderated the high catalytic activity of the other two metals, limiting the over-hydrogenation of the products of interest. The selectivity is therefore favored at the expense of the overall hydrogenation rate and hence higher catalyst loading is necessary to compensate for this loss of activity.[25]

The nature of the metals is not the only parameter influencing the performance of the process. The dispersion and the repartitioning of the metals on and in the catalyst support are also considered to be of great importance. The formation of unwanted microstructures over time can lead to catalyst aging and activity losses. Schwartz highlighted the need for catalysts with a very high degree of metal dispersion that would remain constant throughout the many repetitive runs. In bimetallic catalysts, the high degree of dispersion of the metals can indeed prevent the formation of unwanted microstructures. Schwartz thus proposed a co-deposition/co-reduction procedure for the production of highly dispersed metal catalysts.[19,20] Later, Werpy et al. developed a new type of catalysts called "textured catalysts". These catalysts were prepared on high surface area carbon supports that can maintain their integrity under aqueous, acidic or basic conditions. The use of texturing agents during the metal deposition procedure led to a better distribution of the active metals on the catalyst's surface, particularly in the large pores that are more accessible to substrate. Such distribution enhanced the activity and the selectivity. Furthermore, less metal was used to achieve equivalent catalytic activity. Metal was deposited preferentially in the more accessible areas and little or no metal was "lost" to smaller inaccessible pores.[14]

Another important parameter in the design of metallic heterogeneous catalysts is the support itself. Carbon has generally been used as supporting material for heterogeneous hydrogenation catalysts, largely due to its inert behavior with respect to the hydrogenation reaction itself, its high surface area and its low cost. However, the main disadvantage of such a support is the formation of carbon fines during the reaction. These fines can plug void spaces in the catalyst and thereby cause a tremendous decrease in the catalyst activity. They can possibly be minimized but never completely avoided.[34] In some patents, investigations into the impact and the properties of the different supports were presented. For example, Perdersen et al. investigated on the impact of the support on the catalyst selectivity and activity. They noted that oxidized carbon supports could increase the selectivity and activity in comparison to normal carbon supports.[28,29] A procedure for the production of such catalysts that consists of the treatment of activated carbon with nitric acid at elevated temperature was developed.[28] However, this work did not focus on the catalyst aging and its stability in acidic media. To solve the previously mentioned problems, Tooley and Black suggested the use of refractory oxides as supports. TiO_2 and ZrO_2 were considered to more favourable candidates with respect to SiO_2 and Al_2O_3, which were too soluble in aqueous acidic media.[21] However, Bhattacharyya and Manila cautioned that TiO_2 in its normal form (anatase) was not resistant enough for such a process, due to its low crush strength, its tendency to disintegrate and to produce particles that can clog the catalyst pores thereby reducing the reaction efficiency. They proposed instead the use of the rutile form of TiO_2 to overcome the disadvantages of flaking, large pressure increases, and low crush strength found in the other catalyst supports. Moreover, they claimed that rutile as a support presented the advantage of being more stable at highly acidic conditions in contrast to the anatase form of TiO_2. Finally, they asserted that, using this particular support, the amount of some additionally added metals could be reduced or totally eliminated (e.g. silver).[34]

In conclusion, many different metals, supports and metal deposition procedures have been examined for the production of water-stable heterogeneous hydrogenation catalysts. However, no highly systematic testing procedure has been reported to date. It is therefore difficult to infer the impact of the different metals and supports.

Aside from the catalyst itself, the reaction parameters such as temperature, pressure, flow rates, etc. usually have a significant influence on the product selectivity and yield.

2.1.2. Reaction parameters. The optimization of the reaction conditions of a catalytic system is an important part in the development of an industrial process, especially when the process consists of a complex system of reactions. For example, the hydrogenation of maleic or succinic acid could be forced toward one product or another, depending on the reaction conditions (temperature, pressure, mass flow rate, etc.) and the metals used as catalysts.[15,16]

Various patents and articles describe the investigations into the influence of reaction parameters on the product distribution. In particular, Takar et al. performed a simulation of a

bubble–column–slurry reactor for the conversion of maleic acid into THF.[24] The results of this simulation gave useful information on the optimal reaction conditions. They showed for instance that maleic acid and succinic acid conversion increased with catalyst loading but decreased with the liquid velocity and that maleic acid and succinic acid displayed substrate inhibitory effects. It was also found that the selectivity towards the three useful products (GBL, THF and BDO) was much higher than the selectivity towards n-butanol and other unwanted end-products, except at high catalyst loadings and residence times, where the desirable products were further hydrogenated.[24]

A lot of patents focus on the production of THF as it is a high-value product that can be easily purified, due to its volatility. The studies on the effect of reactions parameters on THF selectivity revealed that selectivity towards it increases with catalyst loading, pressure and temperature[15,16,23] and is favored at lower liquid velocities or long liquid residence times.[24] Furthermore, continuous vapor removal of the product from the hydrogenation promotes the production of THF at the expense of BDO. Therefore, Campos and Sisley pointed out that slurry reactors or constantly stirred reactors are optimal for the production of THF.[25] Campos and Strickland optimized the THF formation by maintaining appropriate acidity in the reactor to favor ring closure and cyclic ether production at the expense of diol formation.[26]

In contrast, BDO formation is favored at lower temperature and with low temperature liquid removal. Campos and Sisley recommended therefore the use of a fixed bed catalyst reactor for the production for BDO.[25]

Finally, the hydrogenation of maleic acid or succinic acid to GBL is generally difficult to accomplish because GBL can be further hydrogenated. The metals must be carefully selected to decrease the rate of the unwanted reactions.[32]

Apart from the impact of the reaction parameters on the product distribution and the yield, optimization has also to concentrate on the safety and economics of the process. One major problem with the hydrogenation process of maleic acid is indeed the highly corrosive impact of this product on equipment at temperatures exceeding 140 °C[22,31,34] and especially in the temperature range required for the conversion of succinic acid into its valuable derivatives. Since succinic acid is much less corrosive at elevated temperature, a two-step process has been considered for the hydrogenation reaction starting from maleic acid. In the first step, maleic acid is converted to succinic acid at temperatures lower than 130 °C, because this reaction is much faster than the other hydrogenations. Then succinic acid is converted into THF, BDO or GBL at higher reaction temperatures. Accordingly, the corrosive impact of maleic acid is reduced. Since the hydrogenation of the double bond of maleic acid is exothermic, the heat of reaction can be used to preheat the feed to the second reactor,[22] thereby making better use of energy and prolonging reactor life, leading to an improvement in the overall process economics (capital, operating and maintenance costs).[31] Finally, the use of bio-derived (*i.e.* succinic acid), instead of oil derived building-block chemical (*i.e.* maleic acid) has the advantage of avoiding the hazardous handling of the latter.

In summary, optimizing the reaction conditions and using the optimal reactor type can have a crucial impact on the selectivity towards the desired products. However, considering the data presented in Table 1, the optimal reaction conditions reported are generally relatively severe (temperatures above 150 °C and pressures above 10 MPa). This has a major (negative) impact on the operating costs and the required equipment. Therefore, developing novel types of catalysts, which are active under milder conditions, is of great interest.

2.2. 2-pyrrolidone and *N*-methyl-2-pyrrolidone

1,4-Butanediol (BDO), γ-butyrolactone (GBL) and tetrahydrofuran (THF) are not the only products that can be produced by hydrogenation of succinic acid. Using amine, ammonium or ammonia and optionally alcohol, pyrrolidones and pyrrolidone derivatives can also be synthesized through reductive amination. Those products are C_5 lactams, *i.e.* cyclic amides.

2-Pyrrolidone (2-pyrr) is particularly useful, *e.g.* as an intermediate in the preparation of nylon-4 type polymers or in the synthesis of pharmaceuticals, medicines and agrochemicals.[41] *N*-methyl-2-pyrrolidone (NMP) is a solvent, used for instance for polyurethanes, polyacrylonitriles and heterocyclic polymers of high melting points.[52] It is also used as an extracting solvent for acetylene and butadiene. NMP can also be used as a replacement for chlorinated solvents as its low volatility results in lower VOC emissions.[53]

Pyrrolidones were produced originally by BASF and ISP from acetylene, using the Reppe process derived in the 1930s by W. Reppe and IG Farben. Because of the risks associated with the handling of acetylene under pressure, new routes were developed in the following decades. In the late 1970 s, Mitsubishi Chemical described a process starting from butadiene with 1,4-butanediol as intermediate. In 1990, ARCO Chemical transformed propylene oxide into pyrrolidone through the formation of 1,4-butanediol. However, these two processes were using old techniques for the downstream production of pyrrolidones. More recently developed technologies are based on butane or maleic anhydride with GBL as an intermediate. Maleic anhydride is indeed converted to GBL by the solvent hydrogenation process mentioned in the previous paragraph. GBL is then converted to pyrrolidones by conventional ammonolysis.[54] In recent decades, however, direct conversions of maleic anhydride/acid or succinic acid have also been reported. This reaction pathway in water will be the subject of paragraphs to come.

The direct aqueous reaction of maleic/succinic acid to pyrrolidones without producing GBL as intermediate is mainly described in patents. All these patents report different metallic heterogeneous catalysts using diverse reaction conditions. For better readability, all this information is presented in Table 2. As the information is mainly held in patents, no reliable kinetic data and only limited information concerning the reaction pathway can be found. Possible side products are often mentioned in the literature but only one patent tried to establish a reaction pathway for the synthesis of NMP with *N*-methyl-succinimide (NMS) as intermediate.[51] A reaction scheme for the production of NMP from diammonium succinate with addition of methanol is presented in Fig. 3. Side products mentioned in the literature are also integrated into the scheme. If 2-pyrrolidone is the desired product, no methanol is added to the reactor and the right hand side of the reaction diagram does not occur. As the reaction pathway from succinic/maleic acid to NMP or 2-pyrrolidone is

Table 2 Metal containing heterogeneous catalysts for the aqueous reductive amination of succinic acid into 2-pyrrolidone and *N*-methyl-2-pyrrolidone

Product	Company or Institute	Reaction	Other reactants/Solvent	Reactant ratios	Optimal catalyst	T [°C]	P [MPa]	S [%]	Y [%]	Ref.	Year
2-Pyrr	FMC Corp.	M.Anh./M.Ac.→ 2-Pyrr	H₂ + NH₃ (liq) + water	Am/Ac = 3.1:1	Raney Cobalt	238–258	9–11	—	61	38	1963
	Anilin- & Soda-Fabrik	DAS (or DAM) → 2-Pyrr	H₂ + water	Am/Ac = 2:1	Co	300	25	—	79	39	1965
	Sun R & D and Co.	M.Anh. → 2-Pyrr	H₂ + NH₄OH_aq	Am/Ac = 1.5:1	5% Ru on Al₂O₃	252	11.7	—	92	40	1975
	Standard Oil Company	M.Anh./M.Ac.→ 2-Pyrr	H₂ + NH₃ (liq) + water	Am/Ac = 2:1	RuFeNiOₓ	250	6.9	95	77	41	1981
	Phillips Petroleum Company	S.Anh → 2-Pyrr	H₂ + NH₃	Am/Ac = 4.4:1	5% Pd on Al₂O₃	270	17.2	—	77	42	1990
NMP	Huels Aktiengesellschaft	S.Anh./NMS → NMP	methylamine + H₂ + water	Am/Ac = 1.2:1	Ni, Ca, Mg, Fr, Cr, Si, Al oxides	200	30	—	88	43	1988
	BASF	DAM → NMP	methanol + H₂ + water	Am/Ac = 2:1; Al/Ac = 4.5:1	Co,Cu,Mn,Mo,P,Na, catalyst	230	20	—	89	44	1992
	BASF	M.Anh./M.Ac. → NMP	methylamine + H₂ + water	Am/Ac = 1.5:1	Co,Cu,Mn,Mo,P,Na, catalyst	250	20	—	91	45,46	1992, 1995
	Battelle Memorial Inst.	DAS → NMP	methanol + water + H₂	Am/Ac = 2:1; Al/Ac = 2:1	2.5%Rh–2.5%Re on C	265	13	68ᵇ	66	47–50	2003
	Battelle Memorial Inst.	DAS → NMS → NMP	1) methanol + water - 2) H₂	Am/Ac = 2:1	1) — 2) 2.5%Rh–2.5%Re on C	1) 300 2) 200	1) — 2) 13	1) 83ᵃ 2) 92ᵇ	1) 83 2) 88	51	2007
			1) methanol + water - 2) H₂	Al/Ac = 2:1; Am/Ac = 1.2:1; Al/Ac = 1.5:1	1) — 2) Rh cat.	1) 280 2) 220	1) — 2) 10.3	1) 75ᵃ 2) 95ᵇ	1) 70 2) 91		

ᵃ NMS yield. ᵇ NMP yield.
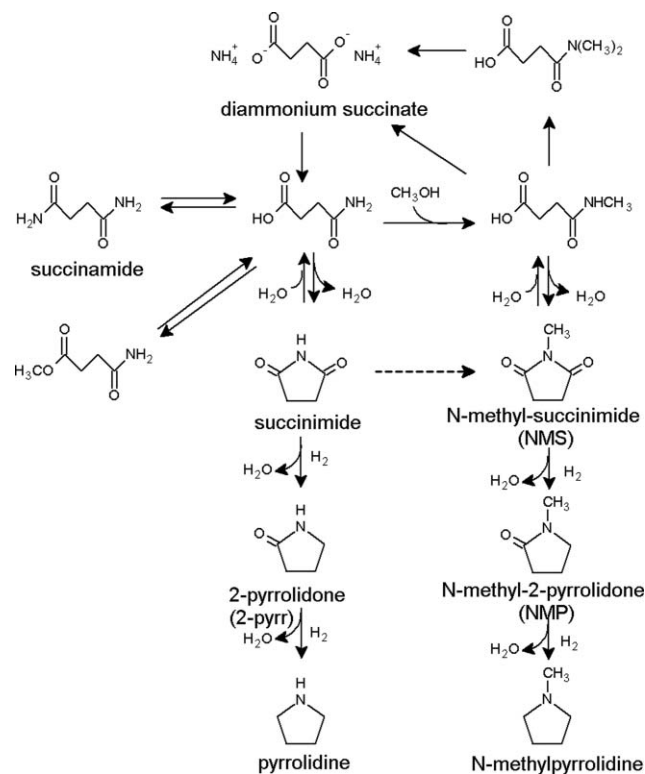
Fig. 3 Pyrrolidone synthesis pathway from succinic acid.[51]

relatively complex, forcing the reaction into a particular pathway seems to be a matter of carefully choosing the catalyst metals, the reaction conditions and especially the reactant ratios.[40,42]

2.2.1. Catalyst types. A lot of catalyst recipes are described in the literature; however, as was the case for the production of BDO, THF or GBL, no systematic study on the impact of the metal has been performed to date. It is therefore difficult to derive a general conclusion on the different synergetic and promoting effects of the various metals. A brief overview of the literature which relates to catalysts for the production of pyrrolidones will be presented in the next paragraph.

For the production of 2-pyrrolidone, Liao stated that suitable metals were cobalt, nickel, ruthenium and palladium.[38] He further claimed that Raney cobalt and nickel were the optimal catalysts for the formation of 2-pyrrolidone. However, two years later, Walldorf and von Kutepow asserted that the use of those catalysts was leading to the side formation of pyrrolidines and proposed a catalyst with cobalt, nickel, copper, iron and (optionally) manganese, silver and chromium.[39] As an alternative to cobalt catalysts, Hollstein and Butte highlighted the advantages of supported ruthenium catalysts, particularly because of their insensibility to catalyst poisons.[40] Pesa and Graham also studied ruthenium catalysts but with the addition of rhenium, iron and nickel.[41] Finally, palladium catalysts on alumina were also investigated for the production of 2-pyrrolidone by the Phillip Petroleum Company.[42]

For the production of NMP, mainly cobalt and rhenium catalysts were developed. The cobalt catalyst patented by BASF was doped by several other metals (copper, manganese, molybdenum, phosphate and sodium) to increase the NMP yield,[44,45] whereas the Battelle Memorial Institute focused on

simpler rhodium and rhenium catalysts. However, for these, lower yields were achieved when using a one-step process. Nickel catalysts with alkaline earth metal oxides in combination with iron and chromium oxides have also been reported earlier by zur Hausen and Otte for the reductive amination of succinic anhydride or the hydrogenation of NMS.[43]

In summary, various cobalt, ruthenium, palladium, rhenium or nickel catalysts have been studied for the synthesis of pyrrolidones. However, only very limited information can be found in the literature regarding the impact of the various metals on the activity and selectivity of the heterogeneous reductive amination of succinic acid.

2.2.2. Reaction parameters. The reaction pathway for the production of pyrrolidones consists also of a complex system of reactions; thus, the optimization of the reaction conditions must be executed carefully.

The formation of pyrrolidones from succinic/maleic acid is conducted in the presence of ammonia (in the gaseous or liquid phase), ammonium ions (from NH_4OH or diammonium salts of the acid)[39] or primary amine in the case of NMP and other pyrrolidones production.[43,45] If NMP is the desired product, ammonia/ammonium with ethanol is an alternative to primary amine. The reaction appears to be highly sensitive to the reactant ratios. It has been described in several patents that an excess both of alcohol and the nitrogen source is desirable.[38,41,47] The optimal ammonia/ammonium/amine to acid ratio seems to lie in a range from 1:1 to 3:1[44] but more specifically between 1:1 and 1.7:1.[43–47] The optimal methanol to acid ratio is approximately in the same range and according to Werpy *et al.* in the area of 1.5:1 to 2:1.[47] An excess of alcohol is necessary for the production of NMP because the 2-pyrrolidone production is a competing pathway that does not require alcohol.[47] In summary, choice of an appropriate reactant ratio is critical to achieve high yields, as a rapid decrease in yield is generally observed when deviating from the optimal ratios.[40]

For the pressure and temperature control, the data gathered in Table 2 show first of all that, like for the production of GBL, THF or BDO, severe reaction conditions (temperature above 200 °C, pressure above 10 MPa) are almost always necessary. In addition to this, Hollstein and Butte mentioned that the temperature control is an important parameter, particularly for the production of 2-pyrrolidone.[40] Indeed, they found that at low temperature ($T < 250$ °C), the reaction rate was too slow for industrial application, whereas at higher temperature ($T > 275$ °C), the reaction proceeds to give pyrrolidines and not the desired pyrrolidones.[40] In contrast, Matson observed that as the temperature increased (above 290 °C) the 2-pyrrolidone yield improved.[42] However, it is difficult to compare these two statements, as Hollstein and Butte used a ruthenium catalyst and Matson a palladium one and metals might have quite different effects on the reaction rates.

The current industrial process consists of the transformation of maleic acid/anhydride to GBL followed by its conversion into pyrrolidones. Werpy *et al.* proposed an alternative two-step process for the production of NMP with *N*-methyl-succinimide (NMS) as an intermediate, increasing the yield and selectivity of NMP.[47] They indicated that the yield of pyrrolidones diminishes at long reaction times in the presence of hydrogen and the

hydrogenation catalyst, most probably due the over-reduction of the products. They therefore designed a two-step process where the first step was performed without hydrogen and catalyst and was followed by a quench or flash cooling to avoid ring opening. This first step was then completed by the purification or solvent extraction of NMS. Werpy *et al.* claimed that the second step–the hydrogenation of NMS into NMP using the designed catalyst—was advantageously done with little or no water. By doing so, the authors affirmed that catalyst poisoning could be avoided in the second step.[47]

The possible application of a two-step process for the production of 2-pyrrolidone with improved selectivity and energy use was also reported by Weyer *et al.*[45] Unfortunately, no details of the reaction set-up or pathway are given.

In summary, the pyrrolidone synthesis has been less intensively studied than the hydrogenation of succinic acid to yield THF, BDO or GBL. The first attempts in aqueous phase were reported much earlier. However, the current process utilizing GBL as intermediate seems to remain the simplest pathway so far. One major problem of the direct pathway from succinic acid is the formation of many side products. A more selective process clearly needs to be developed. Accordingly, other types of catalysts have to be examined. Homogeneous organometallic catalysts are generally regarded as being more selective than classical heterogeneous catalysts. Furthermore, recent research has focused on developing water stable organometallic complexes. The use of such catalysts for the hydrogenation of succinic acid will be described in the next section.

3. Homogeneous aqueous phase catalysis utilizing organometallic catalysts

As mentioned above, the hydrogenation or the reductive amination of succinic or maleic acid has been mainly performed using heterogeneous catalysts. However, those catalysts have the drawback of being active only under high pressure and at elevated temperatures. Furthermore, the selectivity is not always optimal. Additionally, the presence of acidic aqueous solutions can degrade the catalyst rather quickly and thereby reduce its lifetime significantly. Organometallic complexes, being able to operate generally under milder conditions and being reputed for good selectivity, are therefore promising. However, so far this research field has been largely limited to reactions in organic solvents. As a matter of fact, the only available information in the literature on organometallic catalyzed aqueous reactions relating to the C_4 succinic or maleic platform concerns the hydrogenation of the double bonds of maleic and fumaric acid under formation of succinic acid. The hydrogenation of succinic acid itself has been studied solely in organic solvents. The information available from the literature is summarized in Tables 3 and 4. Given the similarities between the complexes reported in Tables 3 and 4, information on organometallic complexes for aqueous catalysis of maleic or fumaric acids and for solvent hydrogenation of succinic acid could be useful for the design of new organometallic catalysts for the aqueous hydrogenation of succinic acid, the reaction of interest. This is why the remainder of this review is dedicated to these two related subjects.

Table 3 Organometallic homogeneous catalysts for the aqueous hydrogenation of maleic and/or fumaric acid to succinic acid

Catalyst	T [°C]	P [MPa]	TOF [mol H_2/h mol metal]	Ref.	Year
[RhCl(TPPMS)$_3$]	60	0.08	M.Ac: 53 F.Ac.: 1270	55	1984
[RhCl(TPPMS)$_3$]	60	0.1	—	56	1993
[RhCl(TPPMS)$_3$]	60	0.1	M.Ac: ~60–370 F.Ac: ~300–1800	57	2001
trans-[IrCl(CO)(TPPMS)$_2$]	60	0.1	M.Ac: 11.3 F.Ac: 7.8	58	2000
[RhCl(PTA)$_3$]	37	?	M.Ac: 69 F.Ac: 342	59	1996
[RhI(CO)(MTPA$^+$I)$_3$]·4H$_2$O	20	0.1	M.Ac: 110 F.Ac: 210	60	1998
[Ru$_4$(η^6-C$_6$H$_6$)$_4$H$_6$]Cl$_2$	50	5.8	F.Ac: 38	61	1994

3.1. Aqueous catalysis with organometallic complexes

As mentioned above, the only aqueous hydrogenation involving succinic acid catalyzed by water-soluble organometallic complexes published so far is the hydrogenation of maleic or fumaric acid under formation of succinic acid. Two research groups—one at the Institute of Physical Chemistry of the University of Debrecen and the other at the Research Group of Homogeneous Catalysis of the Hungarian Academy of Sciences but both directed by F. Joo—were particularly active in this field and indeed, in the generally field of water-soluble organometallic complexes.

In this discipline, which was fairly new, novel water-soluble ligands had to be designed. The sulfonated versions of the triphenylphosphine (TPPMS or TPPTS) (*cf.* Fig. 4) are widely used ligands in this field. Joo *et al.* proposed a water-soluble analogue of Wilkinson's catalyst—[RhCl(TPPMS)$_3$]—for the hydrogenation of maleic and fumaric acids under formation of succinic acid.[55] This complex had been previously reported as catalyzing the hydrogenation of olefinic substrates under neutral or slightly acidic conditions. Later two other articles were published on this particular catalyst. These featured better characterization of the hydrogenation reaction and the behavior of this complex in aqueous solution.[56,57]
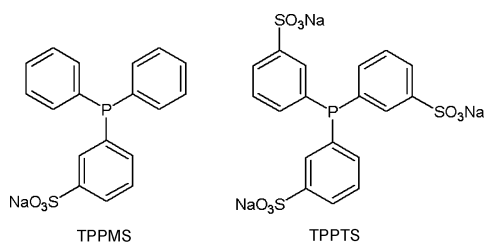
Fig. 4 TPPMS (*mono*-sulfonated triphenylphosphine) and TPPTS (*tri*-sulfonated triphenylphosphine), two water-soluble analogues of the widely used triphenylphosphine (PPh$_3$) ligand.

Utilizing sulfonated phosphine ligands, Joo's group also designed another catalyst for this reaction: the water soluble analogue of Vaska's complex—*trans*-IrCl(CO)(TPPMS).[58] Finally, as an alternative to [RhCl(TPPMS)$_3$], they suggested the use of [RhCl(PTA)$_3$], a complex with another water-soluble type of ligand.[59]

Other research groups came up with more complex propositions: Meister *et al.* synthesized [Ru$_4$(η^6-C$_6$H$_6$)$_4$H$_6$]Cl$_2$ for the hydrogenation of fumaric acid[61] and Pruchnik *et al.* (1998)

designed [RhI(CO)(MTPA$^+$I$^-$)$_3$]·4H$_2$O for the hydrogenation of fumaric and maleic acid.[60]

As already mentioned, the first article describing hydrogenation of maleic or fumaric acid under formation of succinic acid was published by Joo *et al.* in 1984.[55] The catalyst synthesized was derived from the non-water-soluble Wilkinson's catalyst [RhCl(PPh$_3$)] by modifying the polarity of the ligands through sulfonation. This technique is widely used in the aqueous organometallic catalysis. TPPTS ligands are used, for instance, in the two phase Ruhrchemie-Rhône Poulenc propene hydroformylation process, starting from 1999.[57]

Studying the [RhCl(TPPMS)$_3$] complex, Joo *et al.* concentrated at first on the influence of different parameters on the hydrogenation rate, namely the catalyst concentration, the partial pressure of hydrogen and the substrate concentration.[55] They concluded that the initial hydrogenation rate could be characterized by the following equation:

$$r_0 = \frac{k.K.[Rh]_0.[S]_0.[H_2]}{1 + K[S]_0}$$

with $[Rh]_0$ being the initial catalyst concentration, $[S]_0$ the initial substrate concentration, $[H_2]$ the hydrogen concentration and k and K the reaction constants in L. mol^{-1}. s^{-1} and L. mol^{-1} respectively.[55]

It was also observed, that at sufficiently high substrate concentrations, the influence of the ligand concentration was relatively small (no change in rate for maleic acid at 0.05 M). However, at lower substrate concentrations (0.02 M), the rate of maleic and fumaric acid dropped by as much as 75 and 78% respectively, for a [TPPMS]/[RhCl(TPPMS)$_3$] ratio ranging from 0 to 17.6.

Efforts were then made to characterize the reaction mechanism in water so as to see whether it depended on the solvent. The role of water in organometallic catalysis has been widely discussed and it has been concluded that, in many cases, it influences the reaction significantly and that it is not merely a spectator. Water can act, for example, as a hydride donor, as a base or an acid and easily solvates ions. The impact of water was highlighted by Kovacs *et al.*,[73] when they showed that [RhCl(TPPMS)$_3$] or [RhCl(PTA)$_3$] catalyzed the H–D exchange reaction, H$_2$ + D$_2$O $\rightleftarrows$ HD + HOD, in a pH range of 2–8, and 6–8 respectively. The deuteration of olefin hydrogenation

Table 4 Organometallic homogeneous catalysts for the solvent hydrogenation of succinic acid

Product	Reaction	Reactants/Solvent	Catalyst	T [°C]	P [MPa]	X [%]	S [%]	Y [%]	TOF[a]	Ref.	Year
Succinic anhydride	M.Anh. → S.Anh.	H₂ + DME	[RhCl(PPh₃)₃] + PPh₃	100	2	86	—	—	190.6	62	1999
GBL	S.Anh. → GBL	H₂ + toluene	RuCl₂(PPh₃)₃	100	1	100	50–58	50	2.4	63	1975
	S.Ac. (or Anh.) → GBL	H₂ + dioxane	H₄Ru₄(CO)₈(PBu₃)₄	180	13	100	100	100	1.7	64,65	1980, 2007
	S.Anh. (or Ac.) → GBL	H₂ + TGM	[Ru(acac)₃, P(octyl)₃] and p-TsOH	200	1–3	97	98	95	257.0	66–68	2000–2002
Asym GBL	Unsym S.Ac. → Unsym GBL	H₂ + toluene	H₂-[RuCl₂(PPh₃)₃] (or LiAlH₄ or Na-EtOH)	100	2.1	—	—	70–75	—	69	1976
	Unsym S.Ac. → Unsym GBL	H₂ + triethylamine	[RhCl₂(PPh₃)₃] or Ru₂Cl₄(DIOP)₃ or RuCl₂(TTP)	120	~1	—	—	52–62	1.3	70	1984
Asym Lactone	Unsym substrate → Unsym lactone	H₂ + toluene	RuCl₂(PPh₃)₃] or [RuH₂(PPh₃)₄] or [RhCl(PPh₃)₃]	180	1	—	—	56–99	—	71	1982
Alcohol	Carboxylic acid → Alcohol	Diphenylsilane + THF (solvent)	[RhCl(COD)]₂/4PPh₃	RT[b]	—	—	—	47–99	—	72	2008
			[RhCl(PPh₃)₃]	50	—	—	—	62–95	—		

[a] TOF (turn over frequency): in moles of H₂ or moles of product per hour and per mole of metal. [b] RT: room temperature.

products in heavy water had also been previously reported using the catalysts mentioned above.

Further studies of the behavior of the catalysts noted proton loss while dissolving [RhCl(TPPMS)₃] in water or while bubbling hydrogen through an aqueous solution of the complex. These observations were first explained by the following equilibria:[56]

$$[RhCl(TPPMS)_3] + H_2O \rightleftarrows [Rh(OH)(TPPMS)_3] + H^+ + Cl^-$$

$$[Rh(OH)(TPPMS)_3] + H_2 \rightleftarrows [RhH(TPPMS)_3] + H_2O$$

$$[RhCl(TPPMS)_3] + H_2 \rightleftarrows [RhH(TPPMS)_3] + Cl^- + H^+$$
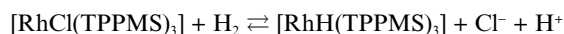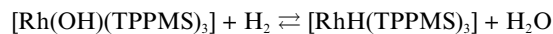
After a detailed examination with ¹H and ³¹P NMR spectroscopy, the following set of equations was suggested:[57]

$$[RhCl(TPPMS)_3] + H_2O \rightleftarrows [Rh(OH)(TPPMS)_3] + H^+ + Cl^-$$

$$[RhCl(TPPMS)_3] + H_2 \rightleftarrows [RhClH_2(TPPMS)_3]$$

$$[RhClH_2(TPPMS)_3] + H_2O \rightleftarrows [RhH(H_2O)(TPPMS)_3] + H^+ + Cl^-$$

$$[Rh(OH)(TPPMS)_3] + H_2 \rightleftarrows [RhH(H_2O)(TPPMS)_3]$$
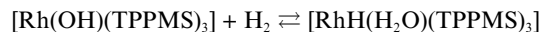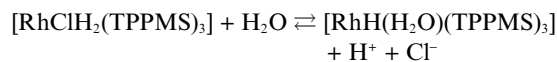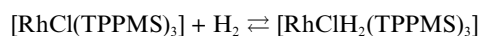
Reductive elimination of HCl from transition metal complexes is a well known process, achieved in organic solvents by the addition of bases. In water the equilibria are driven by the strong solvatation of ions.[57]

An NMR study of the complex at various pH levels gave the following information: in acidic media, the dihydridic *cis-mer*-[RhClH₂(TPPMS)₃] (23%) (**1a**) and *cis-fac*-[RhH₂X(TPPMS)] (**1b**) (77%, X = H₂O or Cl⁻) were observed, the ratio of **1a** to **1b** being reversed by addition of a ten-fold excess of NaCl. Under basic conditions [RhH(H₂O)(TPPMS)₃] monohydride (**2**) was observed. Phosphine oxides were also detected in strong basic solution, but never exceeding 10%.[57] This work claimed to have given the first evidence for the formation of rhodium(I)-monohydride in aqueous solution containing only monodentate phosphine ligands.[57] The acidity of the hydrido complexes was examined by determining a pseudo-pK_a (pK_a ~ 8.2), *i.e.* the pH at which complexes **1** and **2** concentrations are equal.

The hydrogenation of maleic and fumaric acids as a function of pH was also investigated. The reactivity of those two compounds has been shown to be directly linked to the ratio of dissociated/undissociated forms of the acids. It was found, for example, that the fumaric HA⁻ species was more reactive than the H₂A or A²⁻ forms (TOF of 1800 h⁻¹ for HA⁻ and ~200 h⁻¹ for H₂A or A²⁻). In contrast, the HA⁻ form of maleic acid led to the lowest activity (TOF of 60 h⁻¹ for HA⁻ and ~360 h⁻¹ for H₂A or A²⁻). The rate *vs.* pH curves of maleic and fumaric acids are in contrast to one another: while one goes through a minimum (maleic acid) at pH 3–5, the other reaches a maximum (fumaric acid) there. Therefore, at very low pH and at pH > 7, maleic acid is hydrogenated faster than fumaric acid, whereas from pH 1.5 to 7, fumaric acid is hydrogenated faster. Increasing the pH above 7 did not lead to a further change in reactivity. That is why the dihydride ⇌ monohydride equilibrium—with the pseudo-pK_a being above 7 (value: 8.2)—seems not to influence the reactivity of those two acids. Moreover, in solvents—where acids exist in their non-dissociated forms—Wilkinson's complex showed a

higher hydrogenation rate of maleic acid than that of its *trans*-isomer. This observation is in agreement with what has been reported in water for undissociated acids. Therefore, the aqueous phase reaction proceeds most likely in a very similar manner to that in organic solvents. Finally, the pH effects on the rates in aqueous solution can be ascribed to the changes of the ionisation state of the substrate due to the dissociation/protonation in water.[57]

Using the sulfonated phosphine ligands, Joo's group synthesized a water-soluble analogue of Vaska's complex.[58] The reactivity of this *trans*-[IrCl(CO)(TPPMS)$_2$] complex was studied, starting with its behavior in water. In this situation, upon dissolution of the complex in water followed by the bubbling of hydrogen through the obtained aqueous solution, a decreasing pH was observed. The following equations have been proposed for the description of this reaction:[58]

$$[IrCl(CO)(TPPMS)_2] + H_2O \rightleftarrows [Ir(OH)(CO)(TPPMS)_2] + Cl^- + H^+$$

$$[IrCl(CO)(TPPMS)_2] + H_2 + TPPMS \rightleftarrows [HIr(CO)(TPPMS)_3] + Cl^- + H^+$$

$$[IrCl(CO)(TPPMS)_2] + 2H_2 \rightleftarrows [H_3Ir(CO)(TPPMS)_2] + Cl^- + H^+$$
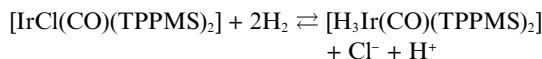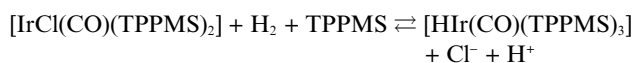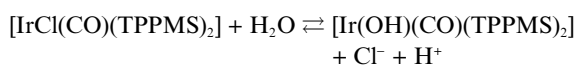
In the presence of excess ligand, the presence of the monohydride complex was deemed also to be likely. Furthermore, the pH dependence of the hydrogenation rate was found to be better explained by the presence of the monohydride species. In contrast to the observations made in the presence of the [RhCl(TPPMS)$_3$] catalyst, it was found that maleic acid was hydrogenated faster than fumaric acid at a pH of about 2.4–2.9; however, no further study of the impact of pH on the reactivity was performed and no further discussions of possible reaction mechanisms were reported.

Since sulfonated phosphine had been reported to readily link with activated olefinic bonds, leading to formation of the corresponding phosphonium salt, other ligands were investigated by Joo's group to improve understanding of the hydrogenation of maleic and fumaric acid in the absence of this side reaction;[59] thus, [RhCl(PTA)$_3$] was synthesized. PTA ligands are amino phosphane (*cf.* Fig. 5) displaying the following characteristics: resistance to oxidation, small size, strong binding abilities and water solubility.[74] In contrast to TPPMS, this basic ligand (pK_a ~ 6) does not react with olefins.[59]
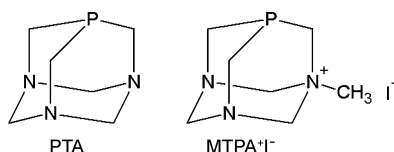
Fig. 5 PTA (1,3,5-triaza-7-phosphaadamantane) ligands and modified PTA ligands: MTPA$^+$I$^-$ (1-methyl-1-azonia-3,5-diaza-7-phospha-adamantane iodide.[60]

While studying the behavior of the catalyst in water, Joo's group recorded the same pH changes while dissolving the complex in water and then bubbling hydrogen through the solution as had been observed with [RhCl(TPPMS)$_3$]. This was explained by the reaction expressed by the following equation:[59]

$$[RhCl(PTA)_3] + H_2 \rightleftarrows [RhH(PTA)_3] + Cl^- + H^+$$
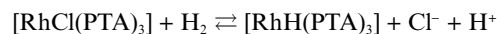
It was assumed that the main reaction pathway involved a monohydride complex because a strong pH dependence of the reaction rate of crotonic acid and allyl alcohol (maximum at pH 4.7) was been observed. However, the hydrogenation of maleic and fumaric acids with respect to pH was not investigated in detail. It was furthermore stated that fumaric acid is hydrogenated faster than its *cis*-isomer. This has been found using the rhodium sulfonated triphenylphosphine ligands at pH 1.5–7. Moreover, the hydrogenation rates recorded with this catalyst were lower than those obtained with the complex having a sulfonated ligand. Finally, it was observed that excess PTA decreases the hydrogenation rate but does not inhibit the reaction completely, probably due to the formation of other, less active catalyst complexes.

Deuteration experiments performed with the catalyst mentioned above led to partial deuteration of the products. However, the presence of undeuterated products indicated that a dihydridic mechanism is also at work.[59]

Modified PTA ligands—MTPA$^+$I$^-$ (*c.f.* Fig. 5)—were also evaluated for the hydrogenation of fumaric and maleic acid by Pruchnik *et al.*[60]

The complex with the MTPA$^+$I$^-$ ligands show very strong hydrophilic properties and therefore, Pruchnik *et al.* concluded that this would be an optimal catalyst for two phase reactions because a certain amount of the catalyst would not be lost in the organic phase. After characterizing the complex by NMR spectroscopy, its catalytic efficiency for the hydroformylation of 1-hexene, the hydrogenation of aldehyde and the one-phase hydrogenation of maleic and fumaric acids was studied. As for the catalyst with the unmodified PTA ligands, the hydrogenation of the *trans*-isomer was found to be faster than that of maleic acid. The maleic acid hydrogenation rate was observed to be in the same range as the rate found with the [RhCl(TPPMS)$_3$] catalyst, whereas the reaction rate on fumaric acid was noted to be lower than the ones recorded with the catalysts having sulfonated ligands and the [RhCl(PTA)$_3$] complex.[60]

Meister *et al.* studied an arene ruthenium catalyst for the hydrogenation of fumaric acid.[61] They mentioned that those ligands are particularly interesting for their unique structures, properties and their inherent catalytic potential.[61] In the last twenty years, a lot of arene ruthenium complexes have been synthesized and tested for many applications. Under pressure (5.8 MPa) and comparatively low temperature (55 °C), Meister's arene catalyst had shown the ability to hydrogenate the olefinic bond of fumaric acid by the cycle presented in Fig. 6.
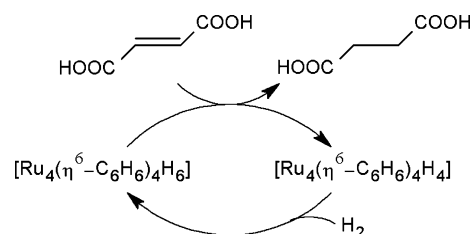
Fig. 6 Catalysis cycle of the hydrogenation of fumaric acid olefinic bond by the [Ru$_4$(η^6-C$_6$H$_6$)$_4$H$_6$]Cl$_2$.[61]

However, even at this high pressure (5.8 MPa), the turnover frequency (TOF) remained relatively low in comparison to the experiments performed with the catalysts described before.

3.2. Solvent catalysis with organometallic complexes

In contrast to aqueous phase catalysis, the use of organometallic catalysts for hydrogenations in organic solvents has been examined in far greater detail and a great variety of complexes have thus far been synthesized. For the hydrogenation of succinic anhydride, and more generally dicarboxylic acid anhydrides, mainly ruthenium and rhodium complexes with phosphine ligands have been reported (*cf.* Table 4). The hydrogenation product is generally the corresponding lactone—*i.e.* GBL for succinic anhydride. Apart from this, some studies of unsymmetrical anhydrides enabled a better understanding of the reaction mechanism as well as assessment of the enantioselectivity of the reaction.

In contrast to heterogeneous catalysts, the organometallic complexes do not seem to promote over-hydrogenation of GBL and therefore, their use could be quite interesting for the commercial production of this chemical. Furthermore, these organometallic catalysts are generally active at much lower pressures and temperatures.

The first article mentioning this reaction type was published in 1975 by Lyons.[63] He studied several complexes with PPh_3 ligands and different metal centers. Among $[IrCl(CO)(PPh_3)_2]$, $[RhCl(CO)(PPh_3)]$, $[Co_2(CO)_8]$ and $[RuCl_2(PPh_3)]$, the ruthenium complex was the only one active for the production of lactone under the conditions investigated in this article (1 MPa, 100 °C, toluene as solvent).[63] It was also found, as would be by other researchers later, that the water produced during the reaction had the unwanted effect of hydrolyzing succinic anhydride to the less active succinic acid.

Five years later, Bianchi *et al.* tested other ruthenium complexes in dioxane on different carboxylic acids—both aliphatic and aromatic ones and on dicarboxylic acids and their corresponding anhydrides.[64] The hydrogenations of succinic acid and anhydride were investigated in the presence of the complex $[H_4Ru_4(CO)_8(PBu_3)_4]$. The reaction rate (at 150 °C, 13 MPa) was disappointingly low but a yield and a selectivity of 100% was finally achieved within 48 h.[64]

More recently, Hara *et al.* from the Mitsubishi Chemical Corporation presented a more systematic development of an organometallic catalytic system for the hydrogenation of succinic anhydride to GBL.[66] Hara *et al.* described how the ruthenium catalysts reported by Lyons[63] and Bianchi *et al.*,[64] despite their ability to produce GBL and no other hydrogenation products, presented some technological drawbacks such as low activities or unfavorable halogen ligands that might corrode the reactor. In the case of the catalyst examined by Lyons,[63] Hara *et al.* also mentioned that the PPh_3 ligands were not stable at high temperatures (above 180 °C). Accordingly, there were attempts to develop a catalyst system consisting of a ruthenium salt, alkyl phosphines and an acid promoter in a particular solvent, with the aim of reinforcing the interaction between substrate and catalyst.[66]

Among the three types of organometallic complexes—anionic, neutral and cationic—a cationic complex was expected to make the carbonyl group of the substrate more accessible to the Ru metal and hence increase the activity. There were attempts to synthesize $[RuHX(PPh_3)_3]$ complexes, with X being more acidic than Cl. These complexes were formed through the reaction between the corresponding Brønsted acid of the anion and a Ru complex of the type $[H_2RuP_4]$, P being the phosphine ligand. Although the complex could not be isolated in the pure form, the authors assumed that the catalyst had the following structure:
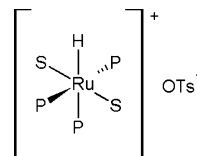
(S = solvent, P = phosphine ligand)[66]

Through screening of various catalysts, it was found that weakly coordinating anions, like OTs and PF_6, yielded higher activities. Additionally, Brønsted acids not only enhance the catalytic activity but also the selectivity toward GBL. A structural change in the Ru complexes was induced, leading to cationic complexes, with an increased stability. Among the acids studied, *p*-TsOH was found to be the best candidate because of its solubility, resistance to reduction and low price.

After determining the optimal Brønsted acid, the effect of the ligands on the catalytic properties was examined. Linear trialkyl phosphines, like PBu_3 or $P(octyl)_3$, gave the best recorded activity. The optimal ratio $P(octyl)_3$/Ru was found to be between 5 and 10 and trialkyl phosphines not only stabilize the ruthenium metal, but also act as a strong base. Hence, without the presence of the Brønsted acid, formation of spiro dilactone was monitored leading to a GBL selectivity of 50%. With the addition of *p*-TsOH, free $P(octyl)_3$ disappeared and was transformed into a phosphonium salt of $P(octyl)_3$ and *p*-TsOH.

Among the solvents studied, TGM (tetraglyme), dodecyl benzene, and sulfolane allowed high GBL yield. As succinic anhydride is not very soluble in the last two solvents, TGM was regarded as the optimal solvent.

The technology utilizing this novel homogeneous catalytic system to produce GBL was commercialized in 1997 by the Mitsubishi Chemical Corporation. A plant with a GBL capacity of 10,000 t/a was constructed initially but underwent subsequent enlargement to 15,000 t/a in 2002. This process is the first one to be used for the full-scale commercial production of GBL which employs a homogeneous catalyst. It represents also the first use of Ru complexes for the production of a chemical at a rate of over 10,000 t/a.[67] Hara *et al.* have also patented a similar homogeneous catalytic system for the production of BDO in 1991.[68]

A lot of effort has been put into betterment of the understanding of the reaction mechanism of the hydrogenation of dicarboxylic acid anhydrides to lactones. To that end, the hydrogenation of unsymmetrical anhydrides into unsymmetrical lactones has been studied. Two reaction pathways are possible (*cf.* Fig. 7). Morand and Kayser tried to achieve the regioselective reduction of the less hindered carbonyl group of the anhydride to yield the corresponding unsymmetrical lactones (**4**).[69] They found that the catalyst proposed by Lyons[63] was able
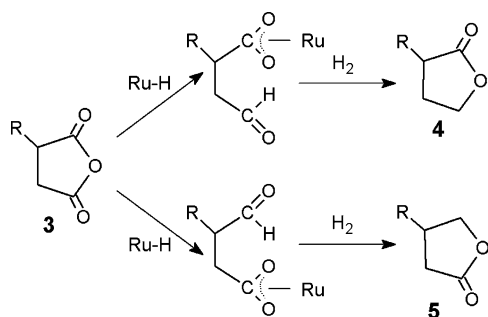
Fig. 7 Reaction mechanisms of the hydrogenation of asymmetrical anhydrides using ruthenium complexes, proposed by Ikariya *et al.*[64]

to catalyze such a reaction in toluene at 100 °C and 2.1 MPa, and that this was in contrast to LiAlH$_4$ or Na-EtOH, which preferentially catalyzed the reduction of the more hindered carbonyl group (**5**).

Ikariya *et al.* also investigated the catalytic reaction of unsymmetrical anhydrides with the four Ru catalysts RuCl$_2$(PPh$_3$)$_3$, Ru$_3$Cl$_4$(DIOP)$_3$, RuCl$_2$(TTP) and Ru$_2$Cl$_4$(DPPB)$_3$.[70] Like Morand and Kayer,[69] they obtained the hydrogenation product of the less hindered carbonyl group (**4**) as the major product.[70]

The first three catalysts gave maximum yields of 50–60% at 120 °C and 1 MPa. As shown in Fig. 7, they also assumed that the reaction occurred by an initial attack of ruthenium to the carbonyl group and successive C-O bond cleavage of one of the C–O bonds.[70]

Ikariya *et al.*[75] and then Osakada *et al.*[71] tried to explain more precisely the reaction mechanism of the transformation of succinic anhydride into GBL using [RuH$_2$(PPh$_3$)$_4$].

Osakada *et al.* isolated the intermediate complexes formed by the initial catalyst complex with the anhydride by C–O bond cleavage.[71] Then, upon contact with hydrogen at elevated temperatures (180 °C, 1.2 MPa), or with hydrogen chloride, or carbon monoxide at atmospheric pressure, these intermediate complexes release the lactones through reduction of formyl or acyl groups in the carboxylate ligands followed by intramolecular condensations. The two proposed mechanisms are shown in Fig. 8.
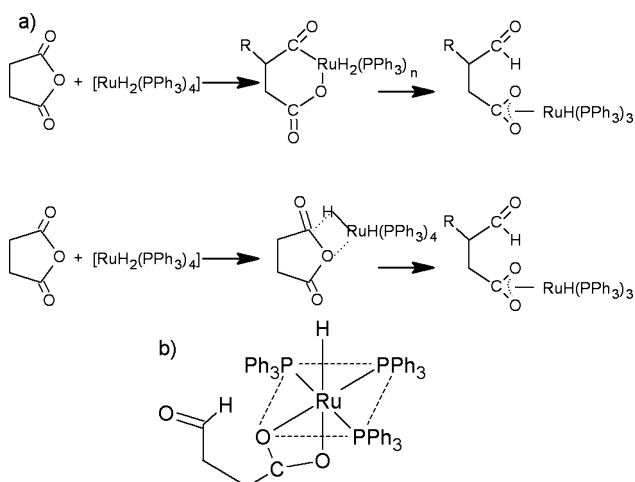
Fig. 8 (a) Reaction mechanism of the hydrogenation of succinic anhydride using [RuH$_2$(PPh$_3$)$_4$] as catalyst; (b) structure of the reaction intermediate.[71]

In the research field of water-stable organometallics, new catalysts have to be developed for the downstream transformations of bio-derived chemicals. For succinic acid, complexes for reactions in organic solvents have been reported. For those types of reactions, the reaction conditions mentioned in the literature are much less severe than those reported for heterogeneous metallic catalysts and could therefore lead to a reduction of the operating and equipment costs. However, systematic catalyst design and optimization of the reaction conditions must be performed in order to improve the catalyst activities that so far are relatively low.

4. Hydrogenation transfer

For hydrogenation reactions, a hydride donor is required. Hydrogen gas has the advantage of being a relatively cheap starting material that is available in large quantities. However, one major problem of using hydrogen gas is the requirement that the reaction be performed under pressure. If high pressure is necessary, special equipment is required and the operating and equipment costs increase. As mentioned before, Osakada *et al.*[71] tried, for example, to reduce the carbonyl group of an anhydride using HCl or CO. Similarly, various other articles discuss the possible reduction of dicarboxylic acids or anhydrides using hydrogen donors other than hydrogen gas.

Taking the work of Takahashi *et al.*[76] as an example, a vapor phase reduction of dicarboxylic anhydride or esters on hydrous zirconium oxide granules with 2-propanol as hydrid donor and dioxane as solvent was outlined. This reaction was executed at atmospheric pressure in a temperature range of 280–330 °C. The reaction of succinic anhydride gives rise to THF and GBL with selectivities of 62% and 20%, respectively. It was noted in this context that the reducibility of secondary alcohols is higher than that of primary alcohols. Depending on the anhydride to alcohol ratio, the main product can be either the lactone (ratio 1:130) or THF (ratio 1:260).[76] As for other reported heterogeneous reactions, the temperature seems to have a considerable impact on the selectivity: for temperatures between 280 and 300 °C, the main product is reported to be GBL whereas at temperature higher than 305 °C THF is produced as the major product.[76]

Another reduction method without hydrogen gas has been described by Ohta *et al.*[72] In this work diphenylsilane was used as a hydride donor for the reduction of carboxylic acid to alcohol, involving the use of an organometallic catalyst: [RhCl(COD)]$_2$/4PPh$_3$ in THF. The reaction is performed at low temperatures between 25 °C and 50 °C, but has the drawback of requiring diphenylsilane, a high cost, non-water-soluble hydride donor.

5. Conclusion

The downstream transformation of bio-derived chemicals is a fast growing sector. The production of bio-based organic acids as a (partial) replacement for oil-derived building-block chemicals is of particular interest and certainly requires further attention.[77] The currently limited market for succinic acid (16,000 t/a) is for instance predicted to increase to as much as 270,000 t/a within a couple of years.[77] Efforts must therefore be focused on the development of water-stable and highly active catalysts (metal

containing ones or organometallic complexes) for the direct aqueous treatment of this chemical with particular emphasis on environmental considerations.

List of symbols

2-pyrr, 2-pyrrolidone; BDO, 1,4-butanediol; COD, *cyclo*-octadiene; DAM, diammonium maleate; DAS, diammonium succinate; DIOP, 2*S*,3*S*-*O*-isopropylidene-2,3-dihydroxy-1,4-bis(diphenylphosphino)butane; DME, ethylene glycol-dimethylether; DPPB, 1,4-bis(diphenylphosphino)butane; F.Ac., fumaric acid; GBL, γ-butyrolactone; M.Ac., maleic acid; M.Anh., maleic anhydride; MTPA⁺I⁻, 1-methyl-1-azonia-3,5-diaza-7-phosphaadamantane iodide; NMP, *N*-methyl-2-pyrrolidone; NMS, *N*-methylsuccinimide; PTA, 1,3,5-triaza-7-phosphaadamantane; PTMEG, polytetramethylene ether glycol; S.Ac., succinic acid; S.Anh., succinic anhydride; TGM, tetraglyme; THF, tetrahydrofurane; TPPMS, sodium triphenylphosphine-3-monosulfonate; TPPTS, trisodium triphenylphosphine-3,3′,3″-trisulfonate; TTP, tetra-*p*-tolylporphyrinato dianion.

Acknowledgements

Notes and references

1 M. Paster, J. L. Pellegrino, and T. M. Carole, *Prospects for a Bio-based Industry*, U.S. Department, of Energy Report, 2003.
2 B. Kamm and M. Kamm, in *Advances in Biochemical Engineering/Biotechnology, White Biotechnology*, ed. R. Ulber and D. Sell, Springer, Heidelberg, 2007, vol. 105, ch. 4, pp. 175–203.
3 J. B. McKinlay, C. Vieille and J. G. Zeikus, *Appl. Microbiol. Biotechnol.*, 2007, **76**(4), 727.
4 Y. S. Huh, Y. S. Jun, Y. K. Hong, H. Song, S. Y. Lee and W. H. Hong, *Proc. Biochem.*, 2006, **41**, 1461.
5 A. Lubineau, J. Augé and M. C. Scherrmann, in *Aqueous Phase Organometallic Catalysis*, 2nd edition, ed. B. Cornils and W. A. Herrmann, Wiley-VCH, 2004, pp. 27–43.
6 W. A. Herrmann and F. E. Kühn, in *Aqueous Phase Organometallic Catalysis*, 2nd edition, ed. B. Cornils and W. A. Herrmann, Wiley-VCH, 2004, pp. 44–56.
7 H. C. Hails, *Org. Proc. Res. Dev.*, 2007, **11**, 114.
8 E. M. Miller, *US Pat.*, 4 001 282, 1977.
9 J. Kanetaka, T. Asano and S. Masamune, *Ind. Eng. Chem.*, 1970, **62**(4), 24.
10 Y.-L. Zhu, G.-W. Zhao, J. Chang, J. Yang, H.-Y. Zheng, H.-W. Xiang and Y.-W. Li, *Catal. Lett.*, 2004, **96**(3–4), 123.
11 R. M. Deshpande, V. V. Buwa, C. V. Rode, R. V. Chaudhari and P. L. Mills, *Catal. Commun.*, 2002, **3**, 269.
12 S. Varadarajan and D. J. Miller, *Biotechnol. Prog.*, 1999, **15**, 8451.
13 A. Corma, S. Iborra and A. Velty, *Chem. Rev.*, 2007, **107**(6), 2411.
14 T. Werpy, J. G. Frye, Jr., Y. Wang, and A. H. Zacher, *US Pat.*, 6 670 300, 2002.
15 M. A. Mabry, W. W. Prichard, and S. B. Ziemecki, *US Pat.*, 4 550 185, 1985.
16 M. A. Mabry, W. W. Prichard, and S. B. Ziemecki, *US Pat.*, 4 609 636, 1986.
17 B. W. Griffiths, and J. B. Michel, *US Pat.*, 4 659 686, 1987.
18 V. N. M. Rao, *US Pat.*, 4 782 197, 1988.
19 J.-A. T. Schwartz, *Int Pat.*, WO 96/27436, 1996.
20 J.-A. T. Schwartz, *US Pat.*, 5 478 952, 1995.
21 P. A. Tooley, and J. R. Black, *US Pat.*, 5 985 789, 1999.
22 R. E. Bockrath, D. Campos, J.-A. T. Schwartz, and R. T. Stimek, *US Pat.*, 6 008 384, 1999.
23 R. V. Chaudhari, C. V. Rode, R. M. Deshpande, R. Jaganathan, T. M. Leib and P. L. Mills, *Chem. Eng. Sci.*, 2003, **58**, 627.
24 N. N. Thakar, R. Jaganathan and R. V. Chaudhari, *AIChE J.*, 2003, **42**(12), 3199.
25 D. Campos, and G. M. Sisler, *US Pat.*, 6 670 490, 2003.
26 D. Campos, and F. D. Strickland, *Int Pat.*, WO 04/058397, 2004.
27 J. R. Budge, T. G. Attig, and S. E. Pedersen, *US Pat.*, 5 473 086, 1995.
28 S. E. Pedersen, J. G. Jr,. Frye, T. G. Attig, and J. R. Budge, *US Pat.*, 5 698 749, 1997.
29 J. R. Budge, T. G. Attig, and R. A. Dubbert, *US Pat.*, 5 969 164, 1999.
30 J. R. Budge, T. G. Attig, and R. A. Dubbert, *US Pat.*, 6 486 367, 2002.
31 R. P. Hepfer, C. T. Miller, G. A. Norenberg, T. G. Attig, and J. R. Budge, *US Pat.*, 6 989 455, 2006.
32 M. Kitson, and P. S. Williams, *US Pat.*, 4 985 572, 1991.
33 M. Kitson, and P. S. Williams, *US Pat.*, 5 149 680, 1992.
34 A. Bhattacharyya, and M. D. Maynard, *US Pat.*, 2006/0004212, 2006.
35 A. Bhattacharyya, and M. D. Maynard, *Int Pat.*, WO 06/007523, 2006.
36 A. Bhattacharyya, and M. D. Maynard, *Eur Pat.*, EP 1773746, 2007.
37 T. Werpy, J. G. Frye, Jr., Y. Wang and A. H. Zacher, *Int Pat.*, WO 02/102511, 2002.
38 H. P. Liao, *US Pat.*, 3 080 377, 1963.
39 W. H. Walldorf and N. von Kutepow, *US Pat.*, 3 198 808, 1965.
40 E. J. Hollstein and W. A. Butte, *US Pat.*, 3 812 148, 1975.
41 F. A. Pesa and A. M. Graham, *US Pat.*, 4 263 175, 1981.
42 M. S. Matson, *US Pat.*, 4 904 804, 1990.
43 H. zur Hausen and W. Otte, *US Pat.*, 4 780 547, 1988.
44 U. Koehler, and H. Siegel, *US Pat.*, 5 101 045, 1992.
45 H.-J. Weyer, R. Fischer, and W. Harder, *US Pat.*, 5 157 127, 1992.
46 H.-J. Weyer, and R. Fischer, US Pat., 5 434 273, 1995.
47 T. Werpy, J. G. Frye, Jr., Y. Wang, and A. H. Zacher, *US Pat.*, 6 632 951, 2003.
48 T. Werpy, J. G. Frye, Jr., Y. Wang and A. H. Zacher, *US Pat.*, 6 670 483, 2003.
49 T. Werpy, J. G. Frye, Jr., Y. Wang and A. H. Zacher, *Int Pat.*, WO 02/102772 A1, 2002.
50 T. Werpy, J. G. Frye, Jr., Y. Wang and A. H. Zacher, *US Pat.*, 6 706 893, 2004.
51 T. Werpy, J. G. Frye, Jr., J. F. White, J. E. Holladay, and A. H. Zacher, *US Pat.*, 2007/0173643, 2007.
52 G. Chichery, P. Benite, and P. Perras, *US Pat.*, 3 448 118, 1969.
53 Guide to Cleaner Technologies–Alternatives to Chlorinated Solvents for Cleaning and Degreasing, US Environmental Protection Agency Report, EPA/625/R-93/019, 1994.
54 Routes to Pyrrolidones, Nexan's ChemSystems PERP Report 94/95 S1, 1997.
55 F. Joo, L. Somsak and T. Beck, *J. Mol. Catal.*, 1984, **24**, 71.
56 F. Joo, P. Csiba and A. Benyei, *J. Chem. Soc. Chem. Commun.*, 1993, 1602.
57 F. Joo, J. Kovacs, A. Benyei, L. Nadasdi and G. Laurenczy, *Chem. Eur. J.*, 2001, **7**(1), 193.
58 J. Kovacs, T. J. Decuir, J. H. Reibenspies, F. Joo and D. J. Darensbourg, *Organometallics*, 2000, **19**, 3963.
59 F. Joo, L. Nadasdi, A. Benyei and D. J. Darensbourg, *J. Organomet. Chem.*, 1993, **512**, 45.
60 F. P. Pruchnik, P. Smolenski, E. Galdecka and Z. Galdecki, *New J. Chem.*, 1998, **22**(12), 1395.
61 G. Meister, G. Rheinwald, H. Stoeckli-Evans and G. Süss-Fink, *J. Chem. Soc. Dalton Trans.*, 1994, 3215.
62 L. Pu, L. Ye and Y. Yuanqi, *J. Mol. Catal. A: Chem.*, 1999, **138**, 129.
63 J. E. Lyons, *J. Chem. Soc. Chem. Commun.*, 1975, 412.
64 M. Bianchi, G. Menchi, F. Francalaci and F. Piacenti, *J. Organomet. Chem.*, 1980, **188**, 109.
65 P. Frediani, L. Rosi, M. Frediani, G. Bartolucci and M. Bambagiotti-Alberti, *J. Agri,. Food Chem.*, 5 101 045, 1992.
66 Y. Hara, H. Kusaka, H. Inagaki, K. Takahashi and K. Wada, *J. Catal.*, 2000, **194**, 188.
67 Y. Hara and K. Takaha, *Catal. Surv. Jpn.*, 2002, **6**(1/2), 73.
68 Y. Hara, and H. Inagaki, *US Pat.*, 5 077 442, 1991.
69 P. Morand and M. Kayser, *J. Chem. Soc. Chem. Commun.*, 1976, 314.

70 T. Ikariya, K. Osakada, Y. Ishii, S. Osawa, M. Saburi and S. Yoshikawa, *Bull. Chem. Soc. Jpn.*, 1984, **57**, 897.

71 K. Osakada, T. Ikariya and S. Yoshikawa, *J. Organomet. Chem.*, 1982, **231**, 79.

72 T. Ohta, M. Kamiya, M. Nobutomo, K. Kusui and I. Furukawa, *Bull. Chem. Soc. Jpn.*, 2005, **78**, 1856.

73 J. Kovacs, L. Nadasdi, G. Laurenczy and F. Joo, *Green Chem.*, 2003, **5**, 213.

74 B. J. Frost, C. M. Mebi and P. W. Gingrich, *Eur. J. Inorg. Chem.*, 2006, **6**, 1182.

75 T. Ikariya, K. Osakada and S. Yoshikawa, *Tetrahedron Lett.*, 1978, **39**, 3749.

76 K. Takahashi, M. Shibagaki and H. Matsushita, *Bull. Chem. Soc. Jpn.*, 1992, **65**, 262.

77 M. Sauer, D. Porro, D. Mattanovich and P. Branduardi, *Trends Biotechnol.*, 2008, **26**, 100.

Pretreatment of lignocellulosic biomass associated with the autoxidation of ethanol to acetal

Yoshiyuki Sasaki, Takashi Endo, Noriko Tanaka and Hiroyuki Inoue*

Lignocellulosic biomass was effectively delignified by aerobic oxidation in ethanol. During the process, ethanol was partially oxidized to acetal, a promising fuel additive, and other oxygenates. The resulting pulp could then be enzymatically converted into sugars in good yields for ethanol production.

The production of value-added chemicals from lignocellulosic biomass, which is the most abundant organic resource on the earth, can be effectively achieved by fractionating the biomass into its two main ingredients: carbohydrates and lignin. One of the most promising methods for separating these ingredients is the oxidative delignification of lignocellulosic biomass followed by the enzymatic saccharification of the resulting pulp. In particular, aerobic oxidation has the advantage of using a cheap oxidant such as oxygen or air. Wet oxidation is the most extensively investigated process; in this process, oxygen is used as the oxidant and water as the solvent. However, the saccharification of the residue obtained by this treatment gave a relatively low sugar yield (257 mg/g softwood), probably because of the poor solubility of oxygen in water (0.028 mL L^{-1}), resulting in insufficient delignification; the lignin content is still as high as 24–30% in the residue.[1] This problem may be solved to some extent by using oxidation catalysts such as polyoxometalates, as in the case of a pulp bleaching process.[2] However, the use of a metal-containing catalyst may lead to high cost and the possible contamination of the dissolved metals when the enzymatic saccharification of the resulting pulp is carried out.

During our investigations on the effective pretreatment methods for lignocellulosic biomass, we found that pulverized woody biomass could be effectively delignified by aerobic oxidation in ethanol, and the resulting pulp could be enzymatically hydrolyzed to monomeric sugars in good yields. During the pretreatment, ethanol was found to be partially oxidized to acetal (acetaldehyde diethyl acetal) and other oxygenates. On the other hand, the pretreatment under the same reaction conditions but in water resulted in the carbonization of the biomass.

Acetal is a stable and nontoxic oxygenate that has many uses, *e.g.*, as a solvent, fragrance producing liquor additive, an antioxidant for perfumes, and a fuel additive for maintaining or improving the cetane number of diesel oil and reducing particulate matter (PM, imperfect combustion products).[3] It

Biomass Technology Research Center, National Institute of Advanced Industrial Science and Technology (AIST), 2-2-2, Hiro-Suehiro, Kure, Hiroshima 737-0197, Japan. E-mail: inoue-h@aist.go.jp; Tel: +81 823 72 1935; Fax: +81 823 73 3284

can be produced either by the dehydrative condensation of acetaldehyde and ethanol,[4] or more preferably, by direct oxidation and acetalization of ethanol. A Wacker-type catalytic system has been employed for the latter reaction; in 1967, Lloyd first reported this type of catalytic system,[5] and more recently, Bueno *et al.* improved its catalytic performance by adding *p*-toluenesulfonic acid. The aerobic oxidation of ethanol was performed at 70 °C for 6 h to afford acetal in 28% yield.[6]

To our surprise, the aerobic oxidation of ethanol proceeded without any catalyst at 150 °C, but a significant amount of by-products such as acetic acid and methane was formed; it is usually difficult to control the rate and the course of radical reactions such as the abovementioned oxidation reaction. However, it has now been found that when lignin or lignocellulosic biomass is used as a kind of antioxidant in the aerobic oxidation of ethanol, acetal and acetaldehyde are predominantly formed from ethanol. Moreover, when lignocellulosic biomass is used in this reaction, its lignin fraction, except those partly oxidized to CO and CO_2, is effectively dissolved in the solution and its carbohydrate fraction can be separated as a cellulose-rich pulp (Scheme 1). These observations are a result of the carbohydrates contained in biomass being more resistant to oxidation than lignin.[7] The resulting pulp can be enzymatically hydrolyzed to monomeric sugars.
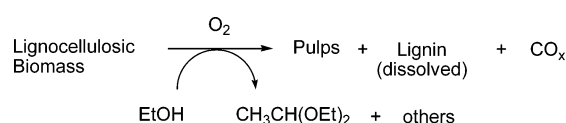
Scheme 1

Isolated lignin called organosolv lignin purchased from Sigma-Aldrich and two kinds of wood tips purchased from a paper mill were used as lignocellulosic biomass. The contents of cellulose, hemicellulose, and lignin in the tips of Douglas fir were determined to be 47%, 28%, and 25% and those in the tips of eucalyptus to be 43%, 34%, and 28% respectively. The wood tips were pulverized, sieved, dried *in vacuo*, and stored in a desiccator before use. Ethanol (99.5%) and all the other chemical reagents were used as purchased.

Aerobic oxidation was performed in a 50 mL autoclave made of stainless steel. A typical experimental procedure is as follows: Douglas fir samples pulverized to a particle size of 0.42–1 mm (1,000 mg) and 99.5% ethanol (6,900 mg) were placed in the autoclave, and oxygen (714 mg or 500 mL at ambient pressure and temperature) was introduced at 1.3 MP. The autoclave was heated at 150 °C for 19 h. After the reaction, the gas products were collected in a sampling bag through a flowmeter

and analyzed by GLC (GL Sciences GC 323 equipped with an MS-5A column for H_2, O_2, N_2, CH_4, and CO and Pora-Q column for CO_2). The gas phase was composed of unreacted O_2 (220 mL), CO_2 (36 mL), CO (11 mL), and H_2 (3 mL). The liquid products were analyzed by GLC (Shimadzu GC 14A equipped with a Restek Rtx-624 column) using 1,4-dioxane as the internal standard. The liquid phase was composed of unreacted EtOH (5,591 mg), acetal (536 mg), CH_3CHO (146 mg), HCO_2Et (137 mg), AcOEt (66 mg), and AcOH (49 mg). The lignin fraction dissolved in ethanol was isolated as a viscous liquid (422 mg) by evaporating the entire reaction solution *in vacuo*. Its number-average molecular weight (452) was determined using Gel Permeation Chromatography (GPC; Shimadzu), and it was found to be one-third of that of organosolv lignin (1,445). Since the weight of the dissolved lignin was greater than the lignin content in the original tip, it was considered that ethanol was contained in it. The solid residue was washed three times with diethyl ether and dried *in vacuo* to afford a pulp fraction (642 mg).

A part of the pulp (40 mg) was dispersed in 1 mL of 50 mM acetate buffer (pH 5.0) and the resulting buffer was hydrolyzed with an enzyme mixture consisting of 0.4 FPU (filter paper units) cellulase activity of Acremonium Cellulase (Meiji Seika), 0.05 mg of Cellulase Y-2NC (Yakult Pharmaceutical Industry), and 0.05 IU (international units) β-glucosidase activity of Novozyme 188 (Novozymes). Units of enzyme activities were determined according to the standard procedure recommended by the Commission on Biotechnology, IUPAC.[8] For cellulase, 1 FPU was defined as the amount of enzyme that releases 1 μmol reducing sugars/min under the assay condition using filter paper as substrate. For β-glucosidase, 1 IU was defined as the amount of enzyme that releases 1 μmol *p*-nitrophenol/min under the assay condition using *p*-nitrophenyl-β-D-glucoside as substrate.

The reaction mixture was incubated at 45 °C for 120 h. After the resultant solution was centrifuged, the hydrolysate in the supernatant was analyzed with LC (Jasco LC system equipped with a Bio-rad Aminex HPX-87H column). Glucose and mannose were formed in yields of 27 mg and 4 mg, respectively; the total sugar yield determined on the basis of the carbohydrate content of the original tip was 58%. The lignin content of the resulting pulp was determined as Klason lignin, and a part of the pulp (0.3 g) was hydrolyzed with 72% sulfuric acid to give a residue (13.2 mg, 4.36%).

Fig. 1 shows the time course of the aerobic oxidations of ethanol with and without biomass in terms of changes in the reaction pressure. In the latter case, the pressure began to decrease shortly after the reaction temperature reached 150 °C, while in the former case, only a gradual decrease was observed in the pressure up to a certain time. However, beyond that time, the pressure decreased fairly rapidly.

In order to determine the details of the oxidation process in the two cases, the gas, liquid, and solid products were analyzed for the reactions stopped at the points indicated by the arrows in Fig. 1. The numbers in the arrows representing the reactions are used as abscissae in Figs. 2–4. Fig. 2 shows the change in the yields of the gas products. The amounts of CO_2 and CO constantly increased up to point 4, while the formation of H_2 and CH_4 became significant after that point. Since only a small amount of CO_2 was detected in the reaction without biomass
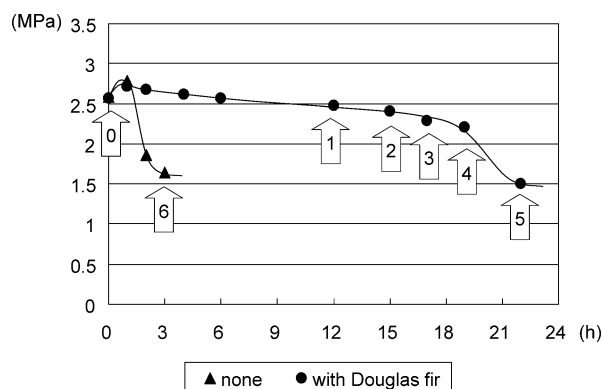
Fig. 1 Time course of the reaction with and without biomass in terms of the pressure change. Reaction conditions at 150 °C: ethanol 6.9 g, Douglas fir (0.42–1 mm), 1 g; O_2, 1.3 MPa (initial).
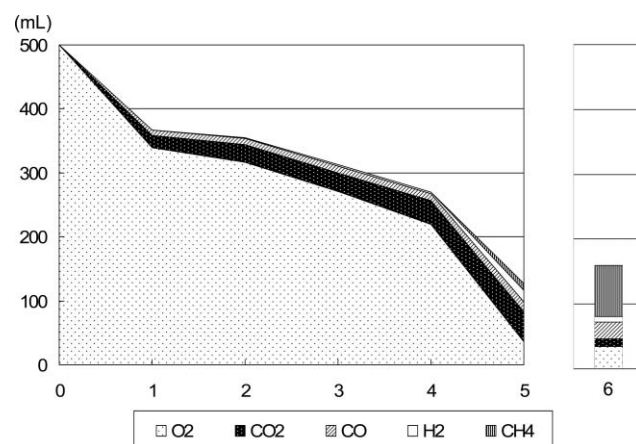
Fig. 2 Change in the yields of the gas products.
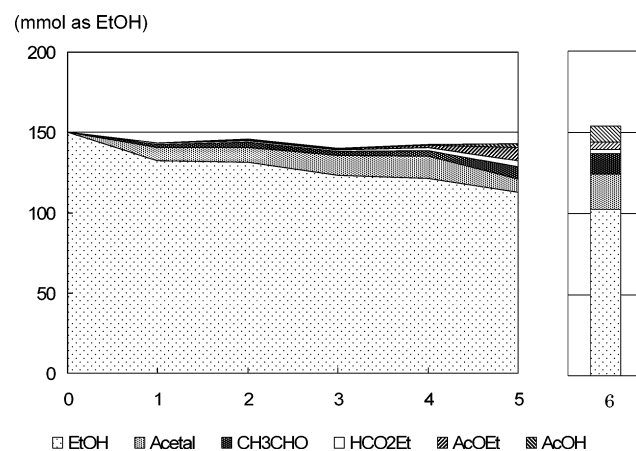
Fig. 3 Change in the yields of the liquid products.

(point 6), CO_2 formed during this stage is considered to be derived mainly from the biomass. Fig. 3 shows the change in the yields of the liquid products. While acetal and acetaldehyde were predominantly formed up to the vicinity of point 3, the formation of ethyl formate, ethyl acetate, and acetic acid became significant after that point, probably due to the degradation of the biomass. Fig. 4 shows the change in the yield of the pulp and yields of the sugars (glucose and mannose) obtained by the
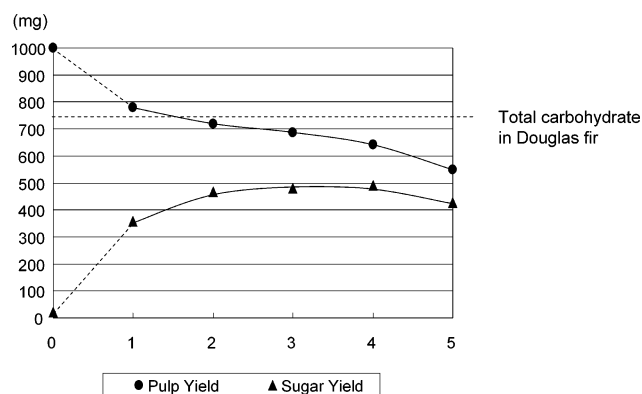
Fig. 4 Change in the yields of the pulp and those of the sugars obtained by the enzymatic saccharification of the pulp. Saccharification conditions at 45 °C for 120 h: 0.4 FPU cellulase mixture and 4% pulp loading.

enzymatic saccharification of the pulp. The sugar yields steadily increased with a decrease in the pulp yield up to the vicinity of point 3. Thereafter, it decreased even if the pulp yield decreased. This may be due to the degradation and partial acetylation of the pulp.

Table 1 shows the effects of various reaction conditions on the aerobic oxidation of ethanol. The aerobic oxidation reaction of ethanol without lignin or lignocellulosic biomass rapidly proceeded at 150 °C, as shown in Fig. 1, and significant amounts of ethyl acetate and acetic acid were formed together with acetal and acetaldehyde (entry 1). In the presence of organosolv lignin, the formation of these acetyl compounds was effectively suppressed without the yields of acetal and acetaldehyde being considerably affected; the total yield of acetal and acetaldehyde was 14% (entry 2). When the lignocellulosic biomass (Douglas fir) was used as an antioxidant, the result obtained was almost identical to that for lignin in terms of the liquid products; the total yield of acetal and acetaldehyde was 11% (entry 3). Some parts of the other products are considered to be derived from the lignocellulosic biomass, especially from hemicellulose that is more vulnerable to the oxidation and/or solvolysis than cellulose.[7]

The effect of the reaction temperature was then examined (entries 3–6). We attempted to regulate the reaction time so that the yield of the pulp was between 620 and 690 mg; this yield range gave the maximum yields of the sugars in the enzymatic saccharification process, as shown in Fig. 4. As expected, high reaction temperatures required short reaction times. However, the pulps obtained at high reaction temperatures contained high amounts of lignin; subsequently, the saccharification of the pulps resulted in low sugar yields.

In entries 7–10, the total sugar amounts recovered from Douglas fir were estimated as 452–492 mg/g wood, and were not significantly affected by the size of the wood particles. The results indicate that these reaction conditions were comparable to other pretreatments to improve the enzyme hydrolysis of woody biomass.[9] Significant amounts of ethyl acetate and acetic acid were formed with Douglas fir samples with the particle size of 2–4 mm (entry 10) which was also the case in the reaction without any lignin (entry 1). These results indicate that the lignin contained in the large-sized particles does not effectively

Table 1 Effects of the reaction conditions[a]

Entry	Woody biomass	Size/mm	Loading/mg	Temp./°C	Time/h	Pulp/mg	Lignin[b]/%	Sugar[c]/mg	Sugar recovery/%	Acetal/%[d]	CH_3CHO/%[d]	HCO_2Et %[d]	AcOEt/%[d]	AcOH/%[d]
1	none	—	—	150	3	—	—	—	—	14.6	8.7	1.7	2.9	6.5
2	Organosolv lignin	—	250	150	8	—	—	—	—	10.9	3.3	0.2	0.5	0.2
3	Douglas fir	0.42–1	1,000	150	19	642	4.4	484	58	9.1	2.2	1.2	1.0	0.5
4	Douglas fir	0.42–1	1,000	160	10	639	6.0	472	57	7.5	3.2	0.9	0.6	0.4
5	Douglas fir	0.42–1	1,000	170	6	629	6.8	403	49	5.9	3.7	0.9	0.4	0.3
6	Douglas fir	0.42–1	1,000	180	5	634	10.7	321	39	4.5	2.8	0.6	0.3	0.1
7	Douglas fir	0.25–0.42	1,000	150	16	653	3.9	492	59	6.9	3.1	1.0	0.6	0.3
8	Douglas fir	0.42–1	1,000	150	17	681	2.8	479	58	8.2	1.5	0.7	0.5	0.2
9	Douglas fir	1–2	1,000	150	17	688	5.8	452	54	7.0	2.7	0.9	0.8	0.4
10	Douglas fir	2–4	1,000	150	16	690	5.8	456	55	7.2	3.7	2.0	4.3	1.9
11	Douglas fir	0.42–1	1,500	150	19	1,027	6.4	720	58	6.4	3.0	1.3	0.8	0.2
12	Douglas fir	0.42–1	2,000	150	23	1,390	10.4	821	49	6.0	3.5	1.6	1.2	0.2
13	Eucalyptus	0.25–0.42	1,000	150	16	672	21.0	495	61	4.7	1.8	0.6	0.3	0.1
14	Douglas fir[e]	0.42–1	1,000	150	16	655	5.5	480	58	6.4	3.3	1.0	0.7	0.4

[a] Reaction conditions: Ethanol 6.9 g, O_2 1.3 MPa (initial). [b] Klason lignin of the resulting pulp. [c] Saccharification conditions: cellulase mixture 0.4 FPU mL^{-1}, pulp loading 4%, at 45 °C for 120 h. [d] Expressed as conversions from the original ethanol. [e] Air 6.5 MPa (initial).

function as an antioxidant, probably because of the limited diffusion rate of the oxidant; it is desirable to use biomass that is pulverized to a particle size less than 2 mm.

The effect of biomass loading was also examined. The yield of the sugars was constant up to 1,500 mg (entry 11), but the loading of 2,000 mg of biomass resulted in a relatively low yield of the sugars, even when a longer reaction time was employed (entry 12). Eucalyptus gave a slightly better yield of sugars (glucose and xylose) than the Douglas fir, despite the fact that its delignification rate was as low as 50% (entry 13); on the other hand, in the case of Douglas fir, the delignification rates were 70–90%. The pretreatment of biomass with air instead of oxygen (entry 14) gave almost the same result as the corresponding pretreatment with oxygen (entry 3), but a considerably higher reaction pressure was needed for a sufficient amount of oxygen to be present. This is because the reactor is a batch system and no additional supply of air is possible during the reaction; otherwise, such a high pressure would not be necessary because the solubility of oxygen in ethanol (unlike the solubility in water) is sufficiently high ($0.222 \ mL \ L^{-1}$) so as to not cause any diffusion problem.

Fig. 5 shows the estimated overall reaction mechanism. The first step of the oxidation process is considered to be the attack of O_2 on the C-1 atom of ethanol that gives a kind of peroxide intermediate; this intermediate may be unstable and readily decomposed to acetaldehyde, thereby releasing the active oxidizing species such as hydrogen peroxide. This active species is probably consumed either for the further oxidation of acetaldehyde to acetic acid or for the oxidation of lignin to CO and CO_2 if it is available. Meanwhile, acetaldehyde may undergo decarbonylation to give CH_4 and CO in the absence of the antioxidant.

In conclusion, the pretreatment of lignocellulosic biomass for enzymatic saccharification and fermentation was successfully
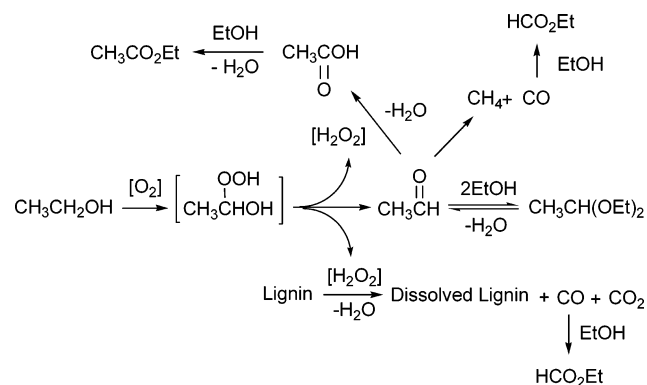
Fig. 5 Estimated overall reaction mechanism.

associated with the oxidation of ethanol to acetal, a promising fuel additive. We believe that these results will contribute to the realization of a "Biomass to Bioacetal" process.

References

1 H. Palonen, A. B. Thomsen, M. Tenkanen, A. S. Schmidt and L. Viikari, *Appl. Biochem. Biotechnol.*, 2004, **117**, 1.
2 A. R. Gaspar, J. A. F Gamelas, D. V. Evtuguin and C. P. Neto, *Green Chem.*, 2007, **9**, 717.
3 M. R. Capeletti, L. Balzano, G. de la Puente, M. Laborde and U. Sedran, *Appl. Catal.*, 2000, **198**, L1.
4 V. M. T. M. Silva and E. Rodrigues, *AIChE J.*, 2002, **48**, 625.
5 W. G. Lloyd, *J. Org. Chem.*, 1967, **32**, 2817.
6 A. C. Bueno, J. A. Gonçalves and E. V. Gusevskaya, *Appl. Catal. A*, 2007, **326**, 1.
7 H. B. Klinke, A. B. Thomsen and B. K. Ahring, *Appl. Microbiol. Biotechnol.*, 2004, **66**, 10.
8 T. M. Wood and K. M. Bhat, *Methods Enzymol.*, 1988, **160**, 87.
9 Y. Sun and J. Cheng, *Bioresour. Technol.*, 2002, **83**, 1.

www.rsc.org/greenchem | Green Chemistry

Study of technical CNSL and its main components as new green larvicides

Diego Lomonaco,*[a] Gilvandete Maria Pinheiro Santiago,[a,b] Yana Silva Ferreira,[b] Ângela Martha Campos Arriaga,[a] Selma Elaine Mazzetto,[a] Giuseppe Mele[c] and Giuseppe Vasapollo[c]

Larvicidal activities against *Aedes aegypti* of technical cashew (*Anarcadium Occidentale* L.) nut shell liquid (CNSL) and its main constituents, cardanol, cardol and their products of hydrogenation were evaluated. In addition, the structure-activity relationship is also discussed.

Introduction

Mosquitoes are vectors responsible for spreading serious human diseases like dengue, yellow fever and malaria. *Aedes aegypti* is one of the mosquito species responsible for the transmission of both dengue and yellow fever, which are endemic to Africa, Asia and South America. In the world, current estimates suggest that up to 50 million dengue cases occur annually, including 500,000 cases of the more serious related illness, dengue hemorrhagic fever (DHF).[1]

In the absence of an effective drug or vaccine, the ideal method for controlling mosquito infestation would be prevention of the mosquito breeding through the use of larvicides. Control the mosquito population in the larval stage is much easier compared to adult stage.[2]

The use of organophosphates, like temephos and fention, for control of mosquito larvae and insect growth regulators, like diflubenzuron and methoprene, has disrupted natural biological control systems and led to outbreaks of insect species showing pesticide resistance. Other undesirable effects include toxicity to nontarget organisms, and this has fostered environmental and human concerns.[3] Based on these problems, new strategies for selective mosquito larval control are needed.

Natural occurring larvicides are receiving considerable attention because they constitute a rich source of bioactive compounds that are biodegradable into nontoxic products and are potentially suitable for use in integral pest management programs.[4]

Despite the immense resource presented by the natural flora of Brazil, control of *Aedes aegypti* still depends basically on the use of synthetic pesticides.

Cashew (*Anacardium Occidentale* L.) is one of the well-know species of the *Anacardiaceae* family. The cashew nut shell liquid

[a] *Departamento de Química Orgânica e Inorgânica, Centro de Ciências, Universidade Federal do Ceará, 60451-970, Fortaleza, CE, Brazil. E-mail: lomonaco@gmail.com; Tel: +55 85 3366 9976*
[b] *Departamento de Farmácia, Universidade Federal do Ceará, Rua Capitão Francisco Pedro 1210, 60430-370, Fortaleza, CE, Brazil. E-mail: gil@ufc.br*
[c] *Dipartimento di Ingegneria dell'Innovazione, Università del Salento, Via Arnesano, 73100, Lecce, Italy*

(CNSL) is a unique natural source of unsaturated long-chain phenols obtained as a byproduct of the cashew industry.

On the basis of the mode of extraction from cashew nut shell, CNSL is classified into two types, solvent-extracted CNSL and technical CNSL. Commercially available technical CNSL is obtained by roasting shells, and contains mainly cardanol (Fig 1, Ia–d) and cardol (Fig 1, IIa–d), both having degrees of saturation of the C15 alkyl side chain varying from complete saturation to partial unsaturation, as shown in Fig. 1.[5] Worldwide CNSL production is estimated to be 300,000–360,000 tons per annum, and as the production of cashew nuts is rising every year the availability of up to 600,000 tons per annum of CNSL should be reached in the near future.[6]

(Z)-pentadec-8-enyl

(8Z,11Z)-pentadeca-8,11-dienyl

(8Z,11Z)-pentadeca-8,11,14-trienyl

structures of C15 chains
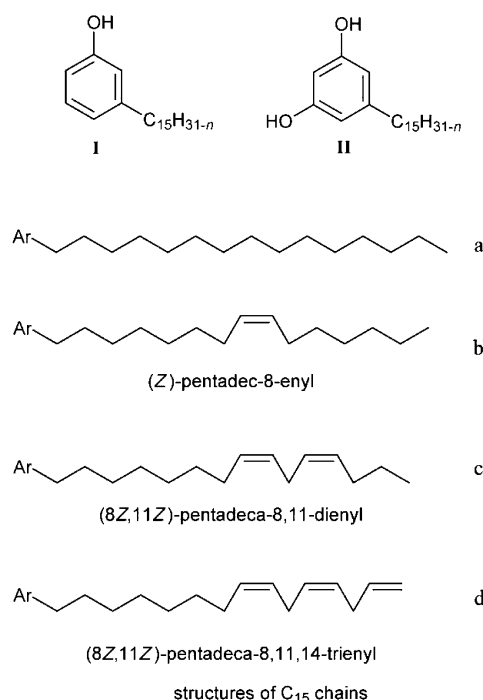
Fig. 1 Main constituents of technical CNSL.

Cashew nut shell liquid is also reported to be used in protecting wood against termites and is especially used in making insecticidal formulations.[7]

Since the international price of CNSL is about \$300/ton,[8] the use of an abundant and cheap source of natural compounds with larvicidal activity would be of great value not only for many emerging countries, but also for other countries looking for naturally occurring larvicides.

The aim of this work is to study the larvicidal activities of technical CNSL and its isolated main constituents against *Aedes aegypti*, and also discuss the structure-activity relationship of the products of hydrogenation of cardanol and cardol. Since Brazil, Vietnam and India are the largest producers and exporters of cashew kernel in the world and as Africa, Asia and South America presents the highest numbers of dengue cases annually,[1] the use of plants cultivated near the endemic areas could be of great interest and economically feasible for controlling mosquito infestation in developing countries.

Materials and methods

General

The samples obtained were analyzed by GC-MS on a Hewlett–Packard Model 5971 using a (5%-phenyl)-methylpolysiloxane DB-5 capillary column (30 m × 0.25 mm) with film thickness 0.1 μm; carrier gas helium, flow rate 1 mL/min with split mode. The injector temperature and detector temperature were 250 and 200 °C, respectively. NMR spectra were recorded on a Bruker Avance DRX-500 (500 MHz) using $CDCl_3$ as solvent for cardanol and $(CD_3)_2CO$ for cardol. Column chromatography was run using silica gel 60 (70–230 mesh, Vetec), while TLC was conducted on precoated silica gel polyester sheets (Kieselgel 60 F254, 0.20 mm, Merck). Compounds were detected by spraying with vanillin–perchloric acid–EtOH solution, followed by heating at 120 °C.

Cardanol and cardol

Cardanol (11.8 g) and cardol (2.1 g) were isolated from technical CNSL (20.0 g) using a silica gel column (Silica Gel 60) eluted with a stepwise gradient of *n*-hexane–ethyl acetate (from 9:1 to 7:3 by volume). The fractions obtained in the column chromatography were analyzed through thin layer chromatography (TLC) and then reunited according their retention factors.

Cardanol. brownish oil, ^{1}H RMN ($CDCl_3$, δ): 1.03 (t, 3H); 1.08; 1.36; 1.45; 1.50; 1.71; 2.19 (t, 2H); 2.65; 2.95; 5.13; 5.21; 5.53; 5.92; 6.79 (m, 1H); 6.82 (m, 1H); 6.86 (s, 1H); 7.22 (t, 1H).

Cardol. brownish oil, ^{1}H RMN (acetone-d6, δ): 1.08 (t, 3H); 1.46; 1.51; 1.58; 1.75; 2.25; 2.62; 2.96; 5.38; 6.22 (s, 2H); 6.65; 6.74; 7.08; 7.27 (s, 1H).

Hydrogenation of cardanol and cardol

Cardanol (3.0 g) was dissolved in 10 mL of ethanol, and 10% Pd/C (0.3 g) was added. The mixture was hydrogenated under pressure (2 bar) for 72 h. After removal of the catalyst and recrystallisation in ethyl ether, 2.56 g (85.3%) of a solid material was obtained (Fig. 1. Ia). Cardol (2.0 g) was hydrogenated with the same procedure described above, using 10% Pd/C (0.2 g); after removal of catalyst and solvent evaporation, 1.44 g (72%) of a solid material was obtained (Fig. 1. Ia).

Hydrogenated cardanol. white solid (m.p.: 51.5–52 °C), ^{1}H RMN ($CDCl_3$, δ): 0.90 (t, 3H); 1.04; 1.27; 1.32; 1.56; 1.63; 2.56 (t, 2H); 6.64 (m, 1H); 6.67 (m, 1H); 6.78 (d, 1H); 7.17 (s, 1H).

Table 1 LC_{50} values for larval mortality caused by technical CNSL, cardanol, cardol, cardanol hydrogenated and cardol hydrogenated

	LC_{50} (μg/mL)
Technical CNSL	51.04 ± 0.62
Cardanol (Fig 1, Ia–d)	32.89 ± 0.25
Cardol (Fig 1, IIa–d)	14.20 ± 0.62
Cardanol hydrogenated (Fig 1, Ia)	68.18 ± 0.50
Cardol hydrogenated (Fig 1, IIa)	>500

Hydrogenated cardol. white solid (m.p.: 94.5–95 °C), ^{1}H RMN (acetone-d6, δ): RMN [1]H (δ): 0.88 (t, 3H); 1.28; 1.56; 2.43 (t, 2H); 3.09; 6.18 (s, 2H); 8.09 (s, 1H).

Larvicidal bioassay

Portions of technical CNSL, its constituents cardanol and cardol and their derivatives (12.5 to 500 μg/mL) were placed in a beaker (50 ml) and dissolved in $DMSO/H_2O$ 1.5% (20 ml). 50 instar III larvae of *Aedes aegypti* were delivered to each beaker. After 24 hours, at room temperature, the number of dead larvae was counted and the lethal percentage calculated. A control using $DMSO/H_2O$ 1.5% was carried out in parallel. For each sample, three independent experiments were run.[9]

Results and discussion

The results obtained from the biological assay are shown in Table 1. Significant differences in larvicidal activity against *Aedes aegypti* between technical CNSL and its main constituents were observed. Technical CNSL presented a LC_{50} value of 51.04 ± 0.62 μg/mL, whereas cardol and cardanol showed LC_{50} values of 14.20 ± 0.62 and 32.90 ± 0.25 μg/mL, respectively. This way, cardol proved to be the main constituent responsible for the activity demonstrated by technical CNSL.

The differences in the LC_{50} values between cardanol and cardol can be justified by the degree of unsaturation of those molecules. After hydrogenation, cardol completely lost its larvicidal activity, while cardanol's activity was lowered to 68.18 ± 0.50 μg/mL. A plausible explanation for these results is based in the literature,[10] which describes that a large number of hydroxyl groups prevents the substance penetrating the insect cuticle and reaching their targets; in this case the hydrogenation of the side chain unsaturation diminished the lipophilic character of the molecules, restricting their passage through the larvae membrane. Gas chromatography-mass spectrometry analysis showed that cardanol mixture contains about 65% of the mo-nounsaturated cardanol, 11% of diunsaturated cardanol and 3% of saturated cardanol. The cardol mixture contains aproximately 55% of triunsaturated cardol and 44% of diunsaturated cardol.

The larvicidal activity showed by technical CNSL, which is lower than its main constituents, may be explained as an effect of the polymers and other subproducts present in it, produced in the process of roasting shells, that employs high temperatures, by which technical CNSL is obtained.

Conclusions

The present work demonstrated that technical CNSL has a good larvicidal activity against *Aedes aegypti*. This result is mostly due

the excellent effect exhibited by cardol, which demonstrates the importance of the unsaturation on the alkyl side chain, that increases its liposolubility facilitating passage through the cell membrane.

Since a previous work reported the low toxicity of cardol, which was orally tolerated up to a concentration of 5 g/kg body weight rats,[11] studies involving modification of the main constituents of CNSL are being executed in our laboratories searching for a more detailed structure-activity relationship and also to improve the larvicidal effect demonstrated by cardol and cardanol.

All those results suggests that the utilization of technical CNSL component cardol as a new green larvicidal may be considered as a new alternative to combat spreading of dengue.

Acknowledgements

References

1 E. Callaway, *Nature*, 2007, **448**, 734.
2 V. S. S. Dharmagadda, S. N. Naik, P. K. Mittal and P. Vasudevam, *Bioresour. Technol.*, 2005, **96**, 1235.
3 Y. C. Yang, S. G. Lee, H. K. Lee, M. K. Kim, S. H. Lee and H. S. Lee, *J. Agric. Food Chem.*, 2002, **50**, 3765.
4 S. S. Cheng, C. G. Huang, W. J. Chen, Y. H. Kuo and S. T. Chang, *Bioresour. Technol.*, 2008, **99**, 3617.
5 P. P. Kumar, R. Paramashivappa, P. J. Vithayathil, P. V. S. Rao and A. S. Rao, *J. Agric. Food Chem.*, 2002, **50**, 4705.
6 O. A. Attanasi, S. Berretta, C. Fiani, P. Filippone, G. Mele and R. Saladino, *Tetrahedron*, 2006, **62**, 6113.
7 E. S. Lepage and A. T. de Lelis, *For. Prod. J.*, 1980, **30**, 35.
8 D. Bastos-Netto, H. S. Couto and J. B. F. Duarte, *Proceedings of the 7th APISCEU*, 2004, 1–5.
9 M. F. Oliveira, M. C. Mattos, T. L. G. Lemos, T. A. Segundo, G. M. P. Santiago and R. Braz- Filho, *Ann. Acad. Bras. Cienc.*, 2002, **74**, 211.
10 O. López, J. G. Fernández-Bolaños and M. V. Gil, *Green Chem.*, 2005, **7**, 431.
11 M. Suresh and R. K. Raj, *Curr. Sci.*, 1990, **59**, 477.

Chlorine borrowing: an efficient method for an easier use of alcohols as alkylation agents†

Philippe Makowski,[a] Regina Rothe,[a] Arne Thomas,[a] Markus Niederberger[b] and Frédéric Goettmann*[a,c]

Chlorine functionalised tin dioxide nanoparticles proved able to partially convert alcohols into the corresponding chlorides, which act as alkylation agents with an increased electrophilicity, as evidenced on ether formation and Friedel–Crafts reactions.

In the first issue of this Journal, J. H. Clark exposed his vision of green chemistry in the article "Green chemistry: challenges and opportunities".[1] Therein, he selected Friedel–Crafts acylations as an archetypical example of industrially relevant, but immensely wasteful reactions. Indeed, the use of both an acyl chloride as electrophile and a homogeneous Lewis acid as promoter resulted in large amounts of, partly harmful, waste products. The same considerations are true for Friedel–Crafts alkylations. Nevertheless, due to their importance in synthetic chemistry, a lot of work has been devoted to finding true heterogenous catalysts for these reactions, such as zeolites, polyoxometalates or mesoporous oxides.[2–6] Another goal of these works was to enable the use of electrophiles greener than halogenoalkanes. In that respect, alcohols, which have already been largely used as alkylating agents for ketones, malonates or nitriles,[7–10] were thought to be ideal candidates. Indeed, they are easily accessible from biomass or hydroformylation products and produce only water as a by product. Many successes were recorded in the use of alcohols for Friedel–Crafts alkylations. Yadav *et al.*, for example, reported on the use of super acids to alkylate functional aromatics with alcohols.[11,12] Alternatively, Roy and co-workers described the use of a bifunctionnal Ir-Sn catalyst for this reaction. In this approach the tin centre was reported to act as a Lewis acid to activate the alcohol, while the iridium centre activated the electrophile.[13,14] The use of mesoporous carbon nitride as a catalyst for such reactions was also recently described.[15] Most of these approaches, however, suffered either from a lack of versatility or too harsh reaction conditions.

In order to allow for a more general use of alcohols as alkylating agents for, for example, Friedel–Crafts reactions or other C–C bond forming reactions, but also for ether or

amine syntheses, new activation paths are required. In that respect, recent progresses in understanding nonaqueous sol-gel chemistry are a great source of inspiration.[16] Indeed, this chemistry deals with the controlled synthesis of metal oxides under water free conditions and rely on the organic chemistry of alcohols, carboxylic acids or ketones as an oxygen source. The reactions providing the needed oxygen were mainly found to be based on the formation of alkyl chlorides, esters, ethers or C–C coupling products and were recently reviewed.[17] Our attention was attracted by the fact that during the nonaqueous synthesis of SnO_2 nanoparticles (SnO_2 NPs), starting with $SnCl_4$, in benzyl alcohol as a solvent, almost all the alcohol was converted into the corresponding ether.[18] This pointed to a possible catalytic activity of these particles, which will be investigated herein.

The employed SnO_2 nanoparticles were synthesised as previously described, by heating $SnCl_4$ in benzyl alcohol at 100 °C for 24 h.[18] The resulting particles are crystalline and feature a mean size of about 4 nm as described in the initial publication.† For reference experiments, chlorine free SnO_2 nanoparticles were also synthesised by using tin tert-butoxide as a precursor.†[19] A preliminary test to convert benzyl alcohol (300 mg) in dibenzyl ether in the presence of a catalytic amount of SnO_2 NPs (25 mg) under mild conditions (100 °C for 20 h), indeed showed the formation of ether but also of a small amount of benzyl chloride.† The needed chlorine atoms had to be provided by the nanoparticle itself, as it was previously evidenced that these SnO_2 NPs were decorated with chloride ligands.[18] We thus assumed that the formed chloro-alkanes were not only by-products of the reaction, but also acted as intermediates in the formation of the ether, as depicted in Scheme 1. Interestingly, the exchange of halogeno- and hydroxy-moieties between metal halides and alcohols to yield the corresponding metal oxide and halogeno-alkanes has early been identified as a major process in non-hydrolytic sol-gel chemistry.[20]
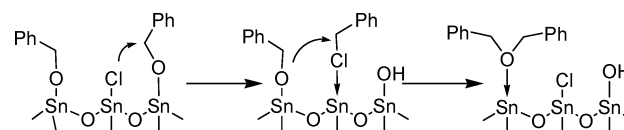
Scheme 1 Proposed mechanism for the SnO_2 NPs catalysed condensation of benzyl alcohol.

These observations are of great synthetic importance. Indeed, as halogenoalkanes are much better electrophiles than alcohols they open the possibility of a generalised use of alcohols as alkylating agent *via* a kind of chlorine borrowing mechanism, as depicted in Scheme 2.

[a]Max-Planck Institute of Colloids and Interfaces, Scientific Campus Golm, 14476, Potsdam, Germany
[b]Department of Materials, ETH Zürich, Wolfgang-Pauli-Str. 10, 8093, Zürich, Switzerland; Fax: +41 44 632 11 01; Tel: +41 44 633 63 90
[c]Institut de Chimie Séparative de Marcoule, UMR 5257, Site de Marcoule, BP 17171, 30207, Bagnols sur Cèze, France. E-mail: frederic.goettmann@cea.fr; Fax: (+33) 466 797 611; Tel: (+33) 466 905 758

† Electronic supplementary information (ESI) available: Synthetic procedure for the used nanoparticles. See DOI: 10.1039/b807230b
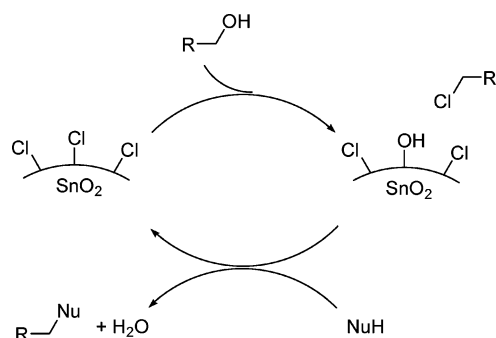
Scheme 2 Proposed mechanism for a general SnO_2NPs catalysed enhancement of the electrophilicity of alcohols.

In order to test this hypothesis, we attempted to catalyse the conversion of alcohols into ethers and their further use in Friedel–Crafts alkylations with SnO_2NPs. In a first set of experiments pure alcohols or mixtures of alcohols were heated between 120 and 150 °C with an oil bath in screw capped glass tubes in the presence of SnO_2NPs. During the reaction, a liquid condensed on the upper cool glass tube surface, which was attributed to water formation. Due to the temperature of the reaction mixtures, no formation of a second phase was observed. Table 1 displays some of the results we obtained. As can be seen, the wanted ethers were obtained in good yields with high selectivities as soon as benzyl alcohol derivatives were used (Table 1, entries 1, 3, 4), while other alcohols proved to be more difficult to convert. However, this result is particularly advantageous for the preparation of dissymmetric ethers, as evidenced by the condensation of benzyl alcohol with hexanol and cyclohexanol. These results are consistent with those recently obtained by Corma and Renz with tin supported on micro- and mesoporous oxides, although we had to employ harsher reaction conditions.[21] But it is, to the best of our knowledge, the first time a system containing mainly tin oxide is used for this purpose. Interestingly, particles prepared using $Sn({}^tBuO)_4$ as a tin source did not exhibit the same catalytic activity (Table 1, entry 2), thus supporting our assumption that chlorine was playing a major role in this reaction.

In order to be able to determine an accurate turnover number, we further investigated the chemical composition of the employed SnO_2 nanoparticles. Inductively coupled plasma-atomic emission spectroscopy (ICP-AES) was used to quantify the tin content and ion chromatography to quantify the chlorine in solutions resulting from the dissolution of SnO_2NPs in nitric acid. This enabled us to evaluate that 25 mg of catalyst corresponded to 0.14 mmol of tin and 0.06 mmol of chlorine. As a consequence, the turnover number (TON, determined as the number of mol of substrate converted at the end of the reaction per mol of catalyst) in the case of benzyl acohol (Table 1, entry 1) would be 20 calculated on the basis of tin and 46 calculated on the basis of chlorine. These are relatively modest TONs but they, at least, evidence that the process is really catalytic.

A series of tests was done on benzyl alcohol, in order to test the recyclability of our catalyst. For this purpose, the nanoparticles were separated by centrifugation after each reaction and reused with new batches of fresh benzyl alcohol at 150 °C for 80 h. As can be seen in Fig. 1, the first recyclings proved effective even if moderate activity and selectivity losses are observed. This indicates that the surface of our catalyst is still covered with active chlorinated sites after a few recyclings. The fourth test however evidenced strong activity and selectivity losses. The composition of the resulting reaction mixture could not be completely analysed, but GC-MS analysis showed the formation of benzaldehyde, benzoic acid benzyl ester and some higher mass compounds.
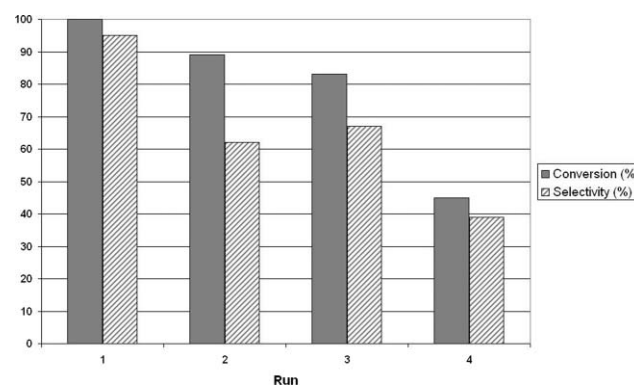
Fig. 1 Recycling of the SnO_2NPs. The test reaction was the conversion of benzyl alcohol into dibenzylether, at 150 °C for 80 h. The conversion was determined by GC-MS as the benzyl alcohol consumption. The selectivity is expressed as the ratio between formed dibenzyl ether and the benzyl alcohol consumption.

Table 1 SnO_2NPs catalysed etherification of various alcohols[a]

Entry	Substrate[a]	Temp./°C	Time/h	Conv. (%)[b]	Products[c]
1	Benzyl alcohol	150	80	100	Dibenzyl ether 95%
2	Benzyl alcohol[d]	150	80	1	Dibenzyl ether 100%
3	4-Methylbenzyl alcohol	120	48	44	Di(4-methyl)benzyl ether 100%
4	4-Chlorobenzyl alcohol	130	20	64	Di(4-chloro)benzyl ether 100%
5	Hexanol	150	120	3	Dihexyl ether 100%
6	Cyclohexanol	120	120	2	Dicyclohexylether 100%
7	Benzyl alcohol Hexanol[e]	150	96	11	Dibenzyl ether 10% Hexyl benzyl ether 90%
8	Benzyl alcohol Cyclohexanol[e]	150	96	20	Dibenzyl ether 10% Cyclohexyl benzyl ether 90%

[a] In a typical procedure 300 mg of the pure alcohol were heated in presence of 25 mg of NPs. [b] Conversion rates determined by GC on the basis of the initial substrate amount. [c] The indicated percentages correspond to the amount of the corresponding product relative to the overall amount of formed products. [d] Reference test with chlorine free nanoparticles. [e] For these tests 200 mg of benzyl alcohol were heated in 2 g of the other alcohol as a solvent with 25 mg of particles.

Table 2 SnO$_2$NPs catalysed Friedel–Crafts alkylation of various aromatic compounds with alcohols[a]

Entry	Aromatic compound Electrophile	Benzene Yield (%)[b]	Toluene Yield (%)	p/o[c]	Anisole Yield (%)	p/o
1	Benzyl alcohol	93	100	0.9:1	97	1:1
2	Benzyl alcohol[d]	0	0	—	0	—
3	Benzyl alcohol[e]	n.a.	n.a.	—	50	1:1
4	4-Methylbenzyl alcohol	90	100	0.5:1	100	1.4:1
5	Cinnamyl alcohol	100	100	1:0.55	100	1:0.26
6	Isopropanol	0	5	1:1	9	0.7:1
7	Cyclohexanol	0	0	—	10	1:1

[a] In a typical reaction 25 mg of catalyst, 100 mg of alcohol and 5 ml of aromatic compound were heated to 150 °C for 120 h. [b] The yields were determined by GC-FID with mesitylene as a reference and correspond to the molar ratio between the obtained alkylation product and the initial amount of alcohol. [c] p/o corresponds to the molar ratio between *para* and *ortho* substituted alkylation products. [d] Reference test with chlorine free SnO$_2$NPs. [e] Reference test with chlorine free SnO$_2$NPs but in presence of 20 mg of benzyl chloride, this test was only undertaken with anisole.

In a second study, we investigated whether the intermediate chloride species could also act as electrophiles for Friedel–Crafts reactions, as depicted in Scheme 3. Even if pure tin oxide does not seem to be a common catalyst for Friedel–Crafts reactions, the fact that tin complexes proved Lewis acidic enough to promote such reactions[22] encouraged us to proceed to our tests without an additional Friedel–Crafts catalyst. In a typical catalytic experiment 25 mg of catalyst, 100 mg of alcohol and 5 ml of aromatic compound were heated to 150 °C in 23 ml acid digestion bombs (Parr Instrument) for 120 h. Table 2 displays some of the obtained results.
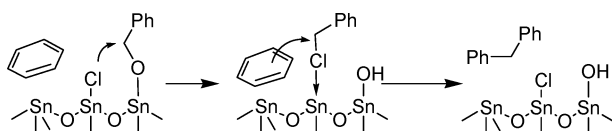
Scheme 3 Proposed mechanism for the SnO$_2$NPs catalysed benzylation of bezene with benzyl alcohol.

Here again, the Friedel–Crafts alkylation products are obtained in high yields as long as very active alcohols are used (Table 2, entries 1, 4, 5). This observation is consistent with other reports on the use of benzyl alcohol derivatives.[23–25] In the case of the reaction of benzyl alcohol with benzene the TON was calculated to be 6 on the basis of tin and 14 on the basis of chlorine. It is also worth noticing here, that, contrary to previous studies, the use of an electron rich aromatic derivative is not required. Indeed, benzene reacts nearly as well as toluene or anisole with active alcohols. In addition, toluene and anisole also give small amounts of alkylation products with less active secondary alcohols, which seems to be a novelty in the field.

As for the ether formation reaction, chlorine free SnO$_2$NPs show no catalytic activity. On the contrary the same SnO$_2$NPs yielded the desired benzyl alcohol alkylation product on anisole when 20 mg of benzyl chloride were added to the reaction mixture (Table 2, entry 3). Interestingly, the amount of obtained alkylation product is three time higher than the amount of added benzyl chloride, which clearly proves that chlorine transfer is possible and further supports our chlorine borrowing mechanism.

In conclusion, we have shown here that tin oxide nanoparticles with surface-adsorbed chloride ions could promote the electrophilicity of alcohols *via* a new chlorine borrowing mechanism.

As compared to other approaches to use alcohols as an alkylating agent, the reaction conditions we had to employ remained harsh, but we are confident in that this inconvenience can be overcome. Indeed, tin dioxide is not known to be a good Friedel–Crafts catalyst and we think that our results can be enhanced by designing bifunctional systems featuring both chlorinated tin sites and stronger Lewis acidic sites. In addition, the possibility of avoiding the use of noble metals[13,14] can possibly balance the requirement of harsher reaction conditions. Moreover, we are convinced that this mechanism could be much more general and allow alcohols to react more easily with a large variety of nucleophiles, such as ketones, nitriles or amines.

Notes and references

1 J. H. Clark, *Green Chem.*, 1999, **1**, 1.
2 C. Anand, P. Srinivasu, S. Alam, V. V. Balasubramanian, D. P. Sawant, M. Palanichamy, V. Murugesan and A. Vinu, *Microporous Mesoporous Mater.*, 2008, **111**, 72.
3 A. Corma, *Chem. Rev.*, 1997, **97**, 2373.
4 H. Firouzabadi and A. A. Jafari, *Curr. Org. Chem.*, 2008, **12**, 233.
5 G. Sartori and R. Maggi, *Chem. Rev.*, 2006, **106**, 1077.
6 A. Taguchi and F. Schüth, *Microporous Mesoporous Mater.*, 2005, **77**, 1.
7 A. Fischer, P. Makowski, J. O. Mueller, M. Antonietti, A. Thomas and F. Goettmann, *ChemSusChem*, 2008, **1**, 444.
8 M. S. Kwon, N. Khn, S. H. Seo, I. S. Park, R. K. Cheedrala and J. Park, *Angew. Chem., Int. Ed.*, 2005, **44**, 6913.
9 P. A. Slatford, M. K. Whittlesey and J. M. J. Williams, *Tetrahedron Lett.*, 2006, **47**, 6787.
10 M. Yasuda, T. Somyo and A. Baba, *Angew. Chem., Int. Ed.*, 2006, **45**, 793.
11 G. D. Yadav and G. S. Pathre, *Microporous Mesoporous Mater.*, 2006, **89**, 16.
12 G. D. Yadav and G. S. Pathre, *Appl. Catal., A*, 2006, **297**, 237.
13 J. Choudhury and S. Roy, *J. Mol. Catal. A: Chem.*, 2008, **279**, 37.
14 S. Podder, J. Choudhury and S. Roy, *J. Org. Chem.*, 2007, **72**, 3129.
15 F. Goettmann, A. Fischer, M. Antonietti and A. Thomas, *Chem. Commun.*, 2006, 4530.
16 A. Vioux, *Chem. Mater.*, 1997, **9**, 2292.

17 M. Niederberger and G. Garnweitner, *Chem.–Eur. J.*, 2006, **12**, 7282.
18 J. H. Ba, J. Polleux, M. Antonietti and M. Niederberger, *Adv. Mater.*, 2005, **17**, 2509.
19 N. Pinna, G. Neri, M. Antonietti and M. Niederberger, *Angew. Chem., Int. Ed.*, 2004, **43**, 4345.
20 V. Lafond, P. H. Mutin and A. Vioux, *J. Mol. Catal. A: Chem.*, 2002, **182–183**, 81.
21 A. Corma and M. Renz, *Angew. Chem., Int. Ed.*, 2007, **46**, 298.

22 R. P. Singh, R. M. Kamble, K. L. Chandra, P. Saravanan and V. K. Singh, *Tetrahedron*, 2001, **57**, 241.
23 M. H. C. de la Cruz, M. A. Abdel-Rehim, A. S. Rocha, J. F. C. da Silva, A. da Costa Faro Jr and E. R. Lachter, *Catal. Commun.*, 2007, **8**, 1650.
24 J. Le, Bras and J. Muzart, *Tetrahedron*, 2007, **63**, 7942.
25 J. S. Yadav, D. C. Bhunia, K. Vamshi, Krishna and P. Srihari, *Tetrahedron Lett.*, 2007, **48**, 8306.

Water-tolerant zeolite catalyst for the acetalisation of glycerol

Carolina X. A. da Silva, Valter L. C. Gonçalves and Claudio J. A. Mota*

We studied the acid-catalysed reaction of glycerol with aqueous formaldehyde and acetone in absence of solvents and using heterogeneous catalysts. The reactivity of acetone was usually higher than formaldehyde and the glycerol conversion was over 90% within 40 min of reaction time for all the heterogeneous acid catalysts studied. With aqueous formaldehyde solution, the glycerol conversion was within 60 to 80%, depending upon the acid catalyst used (Amberlyst-15, K-10 montmorillonite, *p*-toluene-sulfonic acid), due to the high amount of water in the reaction medium, which shifts the equilibrium and weakens the acid sites. However, the use of zeolite Beta, with Si/Al ratio of 16, leads to a conversion of over 95% within 60 min of reaction time. The hydrophobic character of the zeolite, due to the high silicon content, prevents the diffusion of the water to the interior of the pore, preserving the strength of the acid sites. In addition, the water formed during the acetalisation is expelled off from the pore environment, impairing the reverse reaction, and avoiding the use of hazard solvents, commonly employed to distil off the water formed.

Glycerol is formed as a byproduct in the biodiesel production from vegetable oils and animal fat.[1] The forecast for 2010 points out[2] to a global production of 1.2 million tons of glycerol, mostly coming from biodiesel production. Therefore, it is imperative to develop new uses for glycerol to prevent environmental problems and to add value to the biodiesel production chain.

The chemistry of glycerol has attracted the interest of the scientific community and several reviews have appeared in the literature.[2,3] Most of the studies are concentrated on etherification,[4] hydrogenation,[5] oxidation,[6] and dehydration.[7] On the other hand, glycerol acetals and ketals have received considerably less attention. They can find applications as fuel additives,[8] surfactants[9] and flavours.[10] The glycerol formal, produced upon the reaction of glycerol with formaldehyde, finds applications as a disinfectant and solvent for cosmetics and medical usage.[11] A drawback in the glycerol acetalisation is the formation of water, which weakens the acid strength of the catalyst and favors the reversibility of the reaction. The use of solvents to distil off the water formed has been employed[12] to increase the yield of the glycerol ketals and acetals, but this practice is not environmentally recommended, since most of these solvents, such as benzene, toluene, chloroform and dichloromethane, are hazards to humans. In this communication, we wish to present the results of glycerol

acetalisation with acetone and aqueous formaldehyde solution, under acid catalysis conditions, showing that the proper choice of a heterogeneous acid catalyst might prevent the use of hazard solvents.

The reactions were carried out under batch conditions. Typically, 5 g (54.3 mmol) of glycerol was stirred with 4.8 ml (65.5 mmol) of acetone or 5.3 ml (65.5 mmol) of aqueous formaldehyde solution (37%) and a specific mass of the catalyst, at 70 °C (Fig. 1,2). The weight of the catalyst varied to maintain 1.5 mmol of acid sites in every reaction. Table 1 shows some characterization data, as well as the pre-treatment temperature used to activate the catalysts. The molar ratio of glycerol to acetone or formaldehyde was 1 : 1.2. The kinetics of glycerol conversion was estimated by withdrawing samples at specific time intervals, followed by gas chromatography coupled with mass spectrometry analysis. In all experiments, 1,4-dioxane was used as an internal standard.

Fig. 1 Kinetics of the glycerol reaction with acetone at 70 °C over various acid catalysts. (■) Amberlyst-15, (□) zeolite Beta, (●) K-10, (○) PTSA, (▼) HUSY, (▲) zeolite ZSM-5.

The reactions with acetone afforded only one ketal (Scheme 1), with a five-membered ring, as already reported in the literature.[2] Amberlyst-15 acid resin showed the best performance among the catalysts tested, achieving over 95% of glycerol conversion within 15 min of reaction time. Zeolite Beta and K-10 montmorillonite behaved similarly in this reaction, showing a glycerol conversion of about 90% after 40 min. All these heterogeneous catalysts showed a better performance than *p*-toluene-sulfonic acid (PTSA), a model for homogeneous catalysis. The ZSM-5 zeolite showed a glycerol conversion of about 20% after 40 min of reaction time, whereas USY converted approximately 60% of the glycerol within the same period of

Universidade Federal do Rio de Janeiro, Instituto de Química, Av Athos da Silveira Ramos 149, CT Bloco A, 21941-909, Rio de Janeiro, Brazil

Table 1 Characterization data and pre-treatment temperature of the catalysts

Catalyst	Pre-treatment temperature (°C)[a]	Acidity (mmol/g)[b]	Area (m²/g)
Amberlyst-15	120	4.2[c]	50
K-10 Montmorillonite	150	0.5	240
Zeolite Beta (16)[d]	300	1.6	633
Zeolite ZSM-5 (14)	300	1.2	374
Zeolite USY (2.8)[e]	300	1.9	566

[a] Rate = 10 °C/min. Time in activation temperature = 2 h. [b] Measured by *n*-butylamine adsorption at 150 °C.[15] [c] Informed by the producer (Rohm and Haas). [d] Brackets stand for the Si/Al ratio. [e] Total Si/Al ratio = 2.8; framework Si/Al ratio = 4.5.
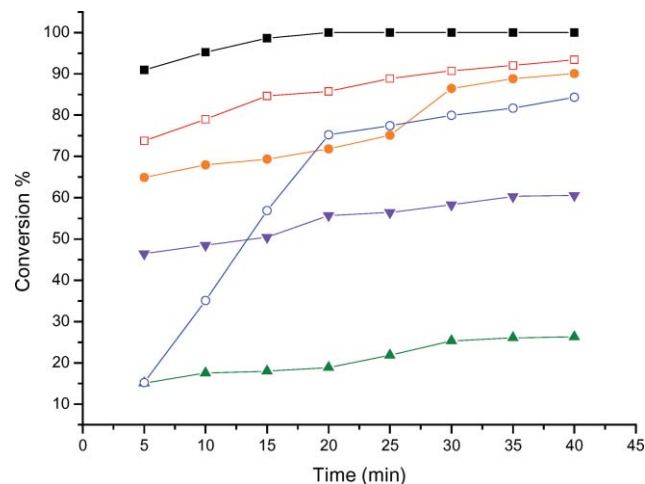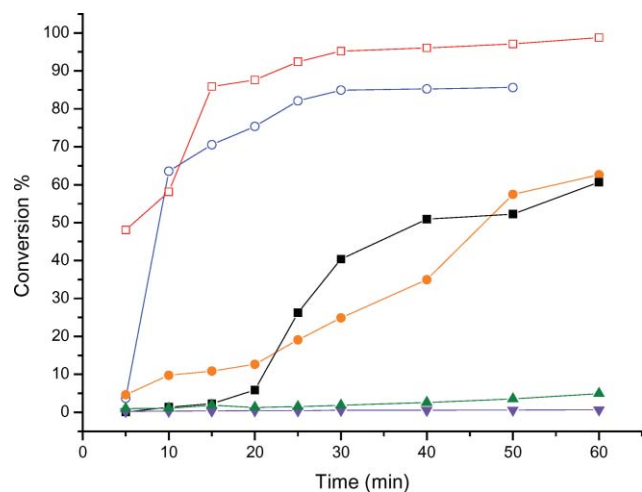

Fig. 2 Kinetics of the glycerol reaction with aqueous formaldehyde at 70 °C over various acid catalysts. (■) Amberlyst-15, (□) zeolite Beta, (●) K-10, (○) PTSA, (▼) HUSY, (▲) zeolite ZSM-5.
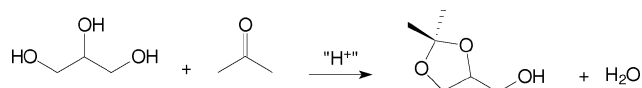
Scheme 1 Acid-catalysed acetalisation of glycerol with acetone.

time. The poor catalytic activity of the ZSM-5 zeolite can be explained in terms of the narrow pore structure, which probably does not permit the acetalisation to occur inside the pores. Thus, the reaction takes place at the external surface or at the pore entrance, leading to a poor yield of the ketal. USY is an aluminium-rich zeolite, having a hydrophilic character. Thus, the water formed during the reaction might remain inside the pores, weakening the acid sites and explaining its worse performance, compared with zeolite Beta, Amberlyst-15 and K-10 Montmorillonite.

The reactions with formaldehyde solution afforded two acetals (Scheme 2), one with a five-membered ring and another
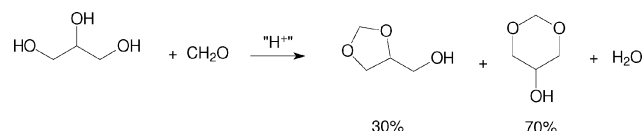
Scheme 2 Acid-catalysed acetalisation of glycerol with aqueous formaldehyde.

with a six-membered ring. The reaction proceeded slower than with acetone, when a same catalytic system was considered. For instance, in the reaction with acetone catalysed by Amberlyst-15, the glycerol conversion was over 95% after 15 min. Nevertheless, after the same period of time, the glycerol conversion was about 5% in the reaction with formaldehyde solution, using the same catalyst and conditions.

Contrarily to what was found in the reactions with acetone, Amberlyst-15 acid resin and K-10 Montmorillonite showed a worse performance than PTSA. They showed a glycerol conversion around 60% after 60 min of reaction time, whereas PTSA converted about 80% of the glycerol in 50 min of reaction. The best catalyst studied for the reaction of glycerol with formaldehyde solution was zeolite Beta, affording over 95% conversion after 60 min. This result might be explained in terms of the water-tolerance of this zeolite. Due to its high siliceous composition, the zeolite environment is hydrophobic and prevents the diffusion of the water molecules to the interior of the pores, where most of the acid sites are located. In the same way, the water formed upon the acetalisation is expelled off from the pores, thus preserving the integrity and strength of the acid sites and minimizing the reverse reaction. This behavior is typical of high-silica zeolites and has already been observed in other water-sensitive reactions, such as esterification and olefin hydration.[13] In opposition to this behavior, USY showed almost no conversion after 60 min of reaction. Although the pore aperture of USY is as wide as zeolite Beta, its Si/Al ratio is much lower, leading to a hydrophilic character for this zeolite. Hence, the water molecules might diffuse and remain adsorbed inside the pores, weakening the acid sites and explaining the low conversion observed in the experiments. The behavior of ZSM-5 might be understood in terms of its pore structure. Although this zeolite has a high Si/Al ratio, and should be considered hydrophobic, its pore structure, with a diameter in the range of 5.6 Å, is too narrow to allow the formation of the glycerol acetals and ketals. This property is known as shape selectivity,[14] and is typical of medium-pore zeolites. As observed in the reaction with acetone, ZSM-5 presented a low conversion for the acetalisation of glycerol with aqueous formaldehyde. This reinforces the hypothesis that the reaction takes place at the external surface of this zeolite, and therefore, the acid sites are weakened by the presence of the water molecules, explaining the low conversion observed.

We also tested the effect of catalyst loading. For the reactions with acetone, an increase of the catalyst loading did not significantly affect the performance, because the conversions were high enough, especially with Amberlyst-15. However, in reactions with formaldehyde solution the loading has an impact in the conversion. After 60 min, the conversion was 65% and 72% for 100% and 150% increase in the Amberlyst-15 loading, respectively, whereas with the standard loading the conversion was 61%. Notwithstanding, this increase in the number of active sites was not sufficient to level the catalytic activity of Amberlyst-15 and zeolite Beta. The conversion, using about one third of zeolite Beta loading, was significantly higher than that observed with Amberlyst-15. This is another additional proof of the importance of choosing a proper zeolite catalyst, with hydrophobic character, to perform this reaction.

Glycerol/acetone system

Glycerol/formaldehyde system
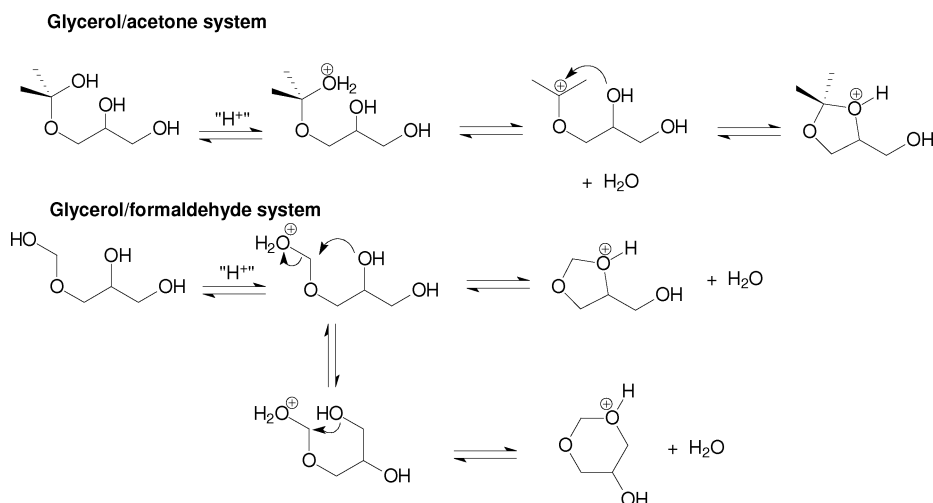
Scheme 3 Possible mechanistic scheme to explain the product selectivity in the acetalisation of glycerol with formaldehyde and acetone.

The distribution of the two acetals formed in the reactions of glycerol with aqueous formaldehyde did not change very much with the catalyst used, being around 70% for the six-membered ring and 30% for the five-membered ring acetal. We did not find in the literature a more systematic study to account for the difference in selectivity between acetone and formaldehyde in the acetalisation of glycerol. A possible explanation is shown in Scheme 3. Upon the formation of the hemiacetal or hemiketal, there could be two different pathways for the two systems. For acetone/glycerol hemiketal, dehydration yields a tertiary carbenium ion, also stabilized by resonance with the non-bonded electron pairs of the adjacent oxygen atom. Then, there occurs a rapid nucleophilic attack of the secondary hydroxyl group to form the five-membered ring ketal. As the lifetime of the carbenium ion in the reaction medium is supposed to be short compared with the lifetime of the hemiketal, the product distribution is governed by kinetics, which favors the formation of the less thermodynamically stable five-membered ring transition state, as already observed in other cyclisation reactions.[16] For the formaldehyde/glycerol hemiacetal, dehydration occurs simultaneously with the nucleophilic attack of the hydroxyl groups, as formation of a primary carbenium ion is not expected due to the high energy barrier. Thus, the system follows an S_N2-like mechanism that might proceed with the nucleophilic attack of the primary hydroxyl group, leading to the six-membered ring acetal, or attack of the secondary hydroxyl group, which yields the five-membered ring acetal. As the lifetime of the protonated hemiacetal might be long in the reaction medium, there is enough time for molecular reorientation, so both products, of thermodynamic (six-membered acetal) and kinetic (five-membered acetal) control could be formed. We are now investigating in further details the difference in reaction mechanism of the two systems, but we believe this difference is more related with the structure of the carbonyl compound (aldehyde or ketone) rather than with the structure of the catalyst, since other studies,[12] using different aldehydes and ketones, reported the same typical distribution.

The results of glycerol acetalisation with acetone and formaldehyde solution shows that the choice of the proper heterogeneous catalyst might prevent the use of hazardous solvents, such as benzene and chloroform, normally used to distil off the water formed and shift the equilibrium. This procedure might be employed in other reactions, where water is present in the reaction medium or is formed during the reaction and affects the catalyst activity.

Acknowledgements

References

1 A. C. Pinto, L. N. Guarieiro, M. J. C. Resende, N. M. Ribeiro, E. A. Torres, W. A. Lopes, P. A. D. Pereira and J. B. Andrade, *J. Braz. Chem. Soc.*, 2005, **16**, 1313–1330.

2 C. H. Zhou, J. N. Beltramini, Y. X. Fan and G. Q. Lu, *Chem. Soc. Rev.*, 2008, **37**, 527–549.

3 (a) A. Behr, J. Eilting, K. Irawadi, J. Leschinski and F. Lindner, *Green Chem.*, 2008, **10**, 13–30; (b) M. Pagliaro, R. Ciriminna, H. Kimura, M. Rossi and C. D. Pina, *Angew. Chem., Int. Ed.*, 2007, **46**, 4434–4440.

4 (a) R. S. Karinen and A. O. I. Krause, *Appl. Catal. A*, 2003, **306**, 128–133; (b) K. Klepacova, D. Mravec and M. Bajus, *Appl. Catal., A*, 2005, **294**, 141–147; (c) Y. Gu, A. Azzouzi, Y. Pouilloux, F. Jerome and J. Barrault, *Green Chem.*, 2008, **10**, 164–167.

5 (a) M. A. Dasari, P. P. Kiatsimkul, W. R. Sutterlin and G. J. Suppes, *Appl. Catal., A*, 2005, **281**, 225–231; (b) Y. Kusunoki, T. Miyazawa, K. Kunimori and K. Tomishige, *Catal. Commun.*, 2005, **6**, 645–649; (c) T. Miyazawa, Y. Kusunoki, K. Kunimori and K. Tomishige, *J. Catal.*, 2006, **240**, 213–221; (d) I. Furikado, T. Miyazawa, S. Koso, A. Shimao, K. Kunimori and K. Tomishige, *Green Chem*, 2007, **9**, 582–588.

6 (a) R. R. Soares, D. A. Simonetti and J. Dumesic, *Angew. Chem., Int. Ed.*, 2006, **45**, 3982–3985; (b) P. McMorn, G. Roberts and G. J. Hutchings, *Catal. Lett.*, 1999, **63**, 193–197.

7 (a) S. H. Chai, H. P. Wang, Y. Liang and B. Q. Xu, *J. Catal.*, 2007, **250**, 342–349; (b) E. Tsukuda, S. Sato, R. Takahashi and T. Sodesawa, *Catal. Commun.*, 2007, **8**, 1349–1353.

8 (a) *Fr Pat*, 2 833 607 A1, 2003; (b) *Int Pat*, 2005/093 015 A1, 2005.

9 A. Piasecki, A. Sokolowski, B. Burczyk and U. Kotlewska, *J. Am. Oil Chem. Soc.*, 1997, **74**, 33–37.

10 (*a*) M. J. Climent, A. Veltry and A. Corma, *Green Chem.*, 2002, **4**, 565–569; (*b*) M. J. Climent, A. Corma and A. Veltry, *Appl. Catal. A*, 2004, **263**, 155–161.

11 P. Sari, M. Razzak and I. G. Tucker, *Pharm. Dev. Technol*, 2004, **9**, 97–106.

12 J. Deutsch, A. Martin and H. Lieske, *J. Catal.*, 2007, **245**, 428–435.

13 T. Okuhara, *Chem. Rev*, 2002, **102**, 3641–3666.

14 B. Smit and T. L. M. Maessen, *Nature*, 2008, **451**, 671–678.

15 V. L. C. Gonçalves, B. P. Pinto, J. C. da Silva and C. J. A. Mota, *Catal. Today*, 2008, **133–135**, 673–677.

16 S. Chandrasekhar, *Chem. Soc. Rev.*, 1987, **16**, 313–338.

Hydrogen production from methane in the presence of red mud – *making mud magnetic*

M. Balakrishnan,[a] V. S. Batra,[a] J. S. J. Hargreaves,*[b] A. Monaghan,[b] I. D. Pulford,[b] J. L. Rico[c] and S. Sushil[a]

Red mud, a waste product of the aluminium industry, has been shown to possess significant activity for the decomposition of methane, a by-product of oil refining and landfill, generating hydrogen and a carbon containing magnetic material. It is envisaged that the latter material could be of interest in terms of downstream purification processes and that its magnetic properties may facilitate separation/handling. In this way, two valuable end products can be generated from two waste products.

Introduction

Red mud is a waste by-product of bauxite processing using the Bayer process. It is a highly alkaline material of variable composition dependent upon source. However, irrespective of its source, the principal components of red mud are iron oxides/oxyhydroxides/hydroxide, aluminium oxide/oxyhydroxide/hydroxide, silica, titania and a range of alkali and alkaline earth metal compounds such as sodium oxide and calcium oxide. Of these, the iron compounds are generally the major phase constituents. The world-wide production of red mud is currently *ca.* 70 Mtonnes per annum[1] and the exploitation of it, as an alternative to landfill or dumping at sea, is an area of current interest as reviewed recently elsewhere.[2,3] Potential applications which have attracted attention are its use in construction materials,[4] ceramics,[1] as a sorbent and coagulant for gas and water purification[3,5–7] and as a catalyst.[2,8–15] In the latter respect, investigations of catalytic activity of various red muds, and their pre-treated forms, have been made for hydrogenation,[13–15] hydrodechlorination[8–11] and hydrocarbon oxidation. In terms of oxidation, interest has centred upon the catalytic combustion of methane.[12] This area is topical since methane is known to be about 23 times more potent as a greenhouse gas than CO_2,[16] and it is often the undesirable by-product of landfill dumping and refinery operations where, in the latter case, it is flared. Anthropogenic sources are estimated to contribute 0.2–0.3 Gt CH_4 to the atmosphere every year. There has also been significant interest in the valorisation of methane,

the principal component of natural gas, by catalytic conversion routes both in the presence or the absence of gas-phase co-fed oxidants and a number of reviews in these areas are available, *e.g.* ref. 17–20. One potential route for methane utilisation is catalytic decomposition where interest centres on both the production of carbon and hydrogen.[21] Although it does not display the highest efficacy, iron is known to be an active catalyst for this reaction, *e.g.* ref. 22,23. In addition, some of the other components of the red mud may be anticipated to exhibit methane decomposition activity. Accordingly, we thought it worthwhile to investigate red mud for methane decomposition. In this manuscript, we show that various non-modified red mud samples exhibit significant hydrogen production rates, generating carbon containing materials in which graphite, Fe and Fe_3C are the predominant phases identified by powder X-ray diffraction. The presence of metallic iron and iron carbide imparts magnetic behaviour to the material, which may facilitate its separation/handling in various envisaged downstream applications, such as water and gas pre-treatment.

Results and discussion

The elemental composition of the three red mud samples, determined by ICP, are presented in Table 1. As has been common in the literature, *e.g.* ref. 3, the data are reported in terms of the weight percentage of the various elements assuming that they are present as the pure oxides. This is, of course, a simplification, and it is notable that the total weight percentages for each sample fall short of 100% and that there is mass loss upon ignition which is indicative of the presence of components such as oxyhydroxides and/or carbonates. However, the differences in composition are evident from these data. In all cases, iron, aluminium and silicon compounds are major constituents. However, the composition of RM4 and RM7, both obtained from the same site but with a two year gap, can be seen to differ fairly significantly. Pronounced differences, particularly in titanium content, can be seen for RM6, which was obtained from a different site. The variation of composition is likely to be a reflection of that for the bauxite ore used in the Bayer process at each particular time or site. Powder X-ray diffraction has been performed upon the three samples and the results are presented in Fig. 1. As expected, complex multi-component patterns are produced. With such complex patterns, it is possible to fit a number of different combinations of phases. Accordingly, we have indicated the positions of goethite, haematite, silica and gibbsite, which are known to be major components of red mud.[3] It can be seen that most of the major

[a]*Centre for Energy and Environment, TERI University, Darbari Seth Block, Habitat Place, Lodhi Road, New Delhi, 110003, India*
[b]*WestCHEM, Department of Chemistry, Joseph Black Building, University of Glasgow, Glasgow, G12 8QQ, UK. E-mail: justinh@chem.gla.ac.uk; Fax: +44-141-330-4888*
[c]*Laboratorio de Catalisis, Facultad de Ingeniería Química, Universidad Michoacana, Edificio E, CU, Morelia Mich, C.P., 58060, México*

Table 1 Elemental composition of red mud samples (wt%)

Sample code	Major elements										
	SiO_2	Al_2O_3	Fe_2O_3	TiO_2	CaO	MgO	Na_2O	K_2O	P_2O_5	MnO	LOI
RM4	16.40	10.44	42.70	6.44	2.85	1.56	3.72	0.05	0.02	—	15.30
RM6	12.40	10.12	36.40	18.70	2.65	2.52	3.85	0.09	0.02	—	12.80
RM7	14.60	23.51	36.79	0.74	1.18	0.07	6.08	0.02	0.15	0.12	16.47
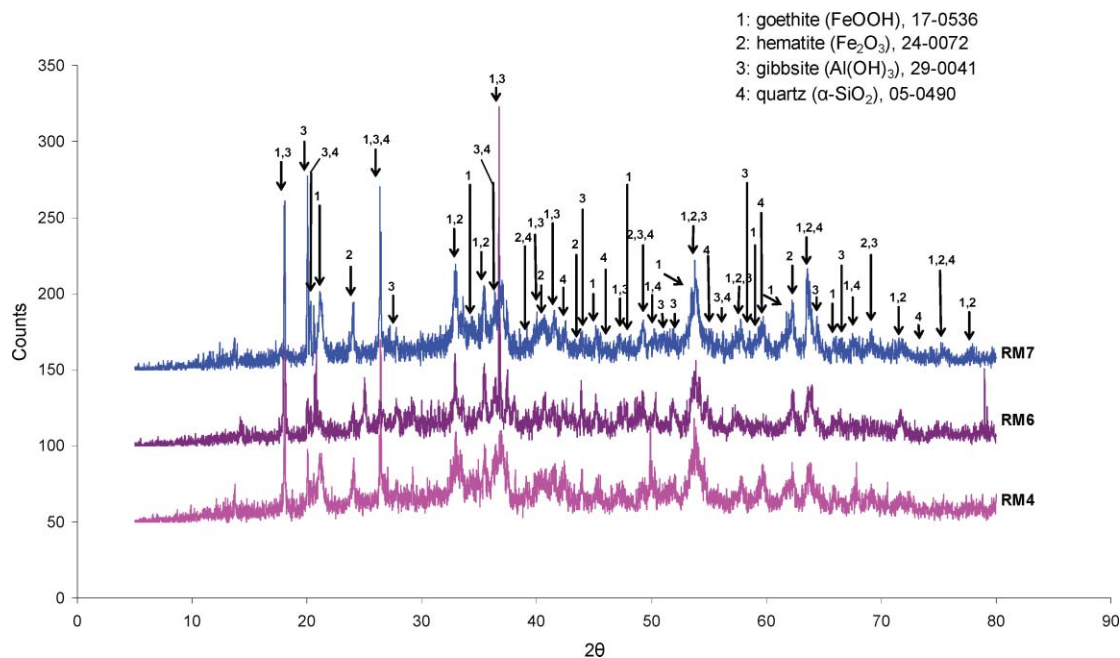
Fig. 1 Powder X-ray diffraction patterns of the RM4, RM6 and RM7 red mud samples as received (Cu Kα radiation).

reflections can be accounted for by the presence of these phases. In the case of RM6, the significant reflections which cannot be attributed to these phases can be matched to the anatase polymorph of TiO_2 (JCPDS 21–1272).

Methane decomposition experiments have been performed on the samples. The samples have been used as obtained, without further modification, and no pre-reduction procedure was performed. It is notable that pre-reduction to generate highly active metallic catalysts is often employed in methane decomposition, although frequently no quantification of the offset of hydrogen employed in this procedure *versus* hydrogen formed in the subsequent catalytic step has been made. Methane itself is a reductant and in view of the aim of our study, which is to valorise two waste resources, we have applied it directly. Therefore, all the hydrogen observed represents net production. It is notable that Otsuka and co-workers[23] and Muradov[24] have also employed this approach in their investigation of supported Fe_2O_3 systems. The results of hydrogen production at 800 °C for all three red mud samples are presented in Fig. 2. The data is presented in terms of mass normalised rates, and the activity is generally high. For example, rates of *ca.* 10×10^{-7} and 50×10^{-7} mol H_2 g^{-1} s^{-1} have been determined for methane conversion at 700 °C in the presence of 3 wt% MoO_3/H-ZSM-5 and 3 wt% Pd/H-ZSM-5 respectively, using the same grade of methane in the same microreactor.[25] It is hard to find comparative data for hydrogen formation rates in the presence of methane, but rates of
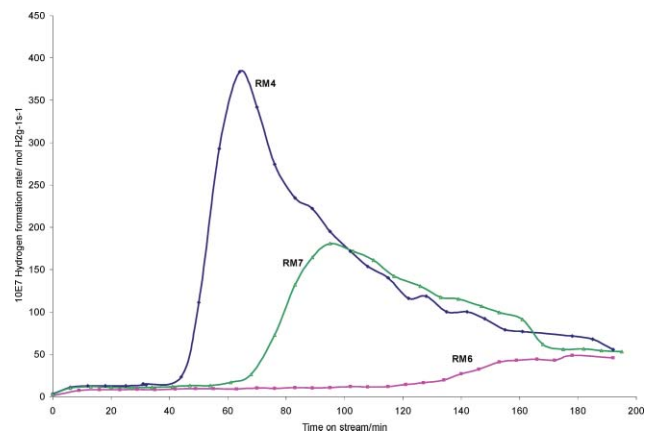
Fig. 2 Mass normalised hydrogen formation rates at 800 °C as a function of time on stream for the RM4 (BET surface area 15 m² g⁻¹), RM6 (BET surface area 8 m² g⁻¹) and RM7 (BET surface area 14 m² g⁻¹) red mud samples. Lines joining experimental points are guides for the eye. Peak CH_4 conversion rates of 18.0×10^{-6}, 7.7×10^{-6} and 3.5×10^{-6} mol CH_4 g^{-1} s^{-1} were measured for RM4, RM7 and RM6, respectively.

4.17×10^{-5}, 4.58×10^{-4} and 2.08×10^{-4} mol H_2 g^{-1} s^{-1} at 800 °C have been reported for 14, 38 and 77 wt% Fe_2O_3/Al_2O_3 respectively.[23] It is notable that there is variation of performance between the three red mud samples, which is not surprising given the differences in their composition. RM4 is by far the most active

sample, followed by RM7. The peak CH_4 conversion for RM4 is 19.8%. The profiles of RM4 and RM7 are similar in that after an induction period, hydrogen productivity rapidly increases, followed by a deactivation period, although the activation times and peak hydrogen production rates are markedly different. We are currently investigating the reaction pathways associated with these profiles by employing *in-situ* TGA with evolved gas-analysis. Similar profiles have been reported by both Otsuka and co-workers and Muradov in their studies of supported Fe_2O_3 systems. Indeed in the latter case, four periods of activity were identified. The activation period was stated to correspond to the reduction of iron oxide to iron metal, the peak hydrogen production period to iron catalysed decomposition of methane, the rapid deactivation to depletion of the catalytically active metal and carbide phase which is followed by a steady state methane decomposition period. CO_x formation was reported to occur during activation. Otsuka and co-workers directly followed CO_x formation which was observed to die off as activity peaked, resulting in CO_x-free H_2 production beyond this point. In comparing RM4 and RM7, it is notable that there is a higher concentration of iron and a lower concentration of alkali metal in the former sample, which can explain its higher efficacy both in terms of the greater peak production of H_2 and the shorter lag period. Elsewhere, alkali metals have been reported to be very effective poisons for the methane decomposition reaction.[22] In view of the very high activity of the RM4 sample, it was of interest to see if significant activity could be observed at a lower reaction temperature. A temperature programmed reaction was performed in which the temperature was increased from 600 °C using the regime summarised in Fig. 3. It can be seen that at 600 °C low levels of hydrogen are produced, which increase with temperature increments. At 700 °C, the system slowly activates in a manner similar to that observed for the sample at 800 °C, with comparable rates of hydrogen production. However, beyond 440 minutes on stream, pressure drop effects due to carbon deposition became severe and the experiment was terminated.

From Fig. 2, it is apparent that despite having a similar iron content to RM7 and alkali metal content to RM4, RM6 is much less active at 800 °C, although its activity is still reasonable. It is also apparent that the activation process is much less marked. In order to assess whether this was simply due to a more delayed activation, the reaction time with this sample was extended to 9 hrs. However, during this period the hydrogen production rate remained relatively steady at a value of *ca.* 40×10^{-7} mol H_2 g^{-1} s^{-1} (results not shown). There are two apparent major differences between this sample and the others in Table 1. It possesses both a higher titanium content and a lower loss on ignition. The former is reflected in the additional reflections noticeable in Fig. 1 and the latter may relate to a lower hydroxide, oxyhydroxide and/or carbonate content. At present, the exact origin of the different activity pattern for this sample with respect to the other two is unclear. However, in the context of the present observations, it is interesting to note that TiO_2 is reducible and one explanation of the so-called strong metal-support interaction effect (SMSI) is the mobility of its reduced phase decorating active metal particles.[26,27]

Post-reaction X-ray diffraction patterns are presented in Fig. 4. The positions of reflections corresponding to Fe and Fe_3C, in addition to graphite, quartz and alumina have been
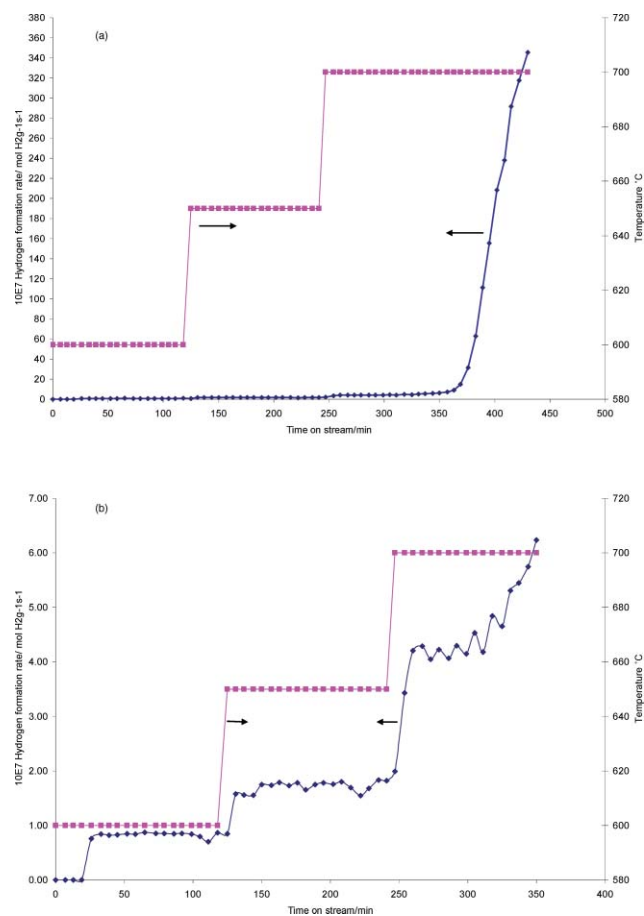
Fig. 3 Mass normalised hydrogen formation rates for red mud RM4 during temperature programmed reaction (a) entire profile, (b) profile before "light off" showing the changes occurring. Lines joining experimental points are guides for the eye.

marked on the patterns, which can be satisfactorily fitted with these phases. The presence of Fe_3C, in addition to Fe, has been widely reported in the literature related to hydrocarbon decomposition over iron based systems, *e.g.* ref. 28. CHN analysis indicated that the RM4, RM6 and RM7 post-reaction samples contained 47.71, 43.49 and 38.06 wt% carbon, respectively. Only traces of hydrogen were determined, and are therefore not reported. It is worth mentioning that the relatively high percentage of carbon present in RM6 resulted as a consequence of exposing this sample to methane for a longer time than the others. TEM analysis of all samples did not show any evidence of tubular forms of carbon as seen in other iron based systems, *e.g.* ref. 22. Instead, amorphous type structures were apparent and these are the subject of continuing investigation. TGA oxidation studies were performed and these are shown, along with the corresponding first derivative profiles, in Fig. 5. It is interesting to note the general differences between the samples. RM4 and RM7, both of which passed through activity maxima during testing, show an initial mass increase followed by a decrease which extends beyond 800 °C. The temperature at which mass increase occurs is equivalent for both samples and presumably corresponds to oxidation of the Fe_3C and/or Fe phases. The mass decrease can be attributed to oxidation of carbon, in agreement with the CHN analysis, and the breadth of this feature

a: Graphite (C) 23-0064
b: Iron (Fe) 03-1050
c: Iron carbide (Fe$_3$C) 03-0989
d: Aluminium oxide (Al$_2$O$_3$) 26-0031
e: Quartz (α-SiO$_2$), 05-0490
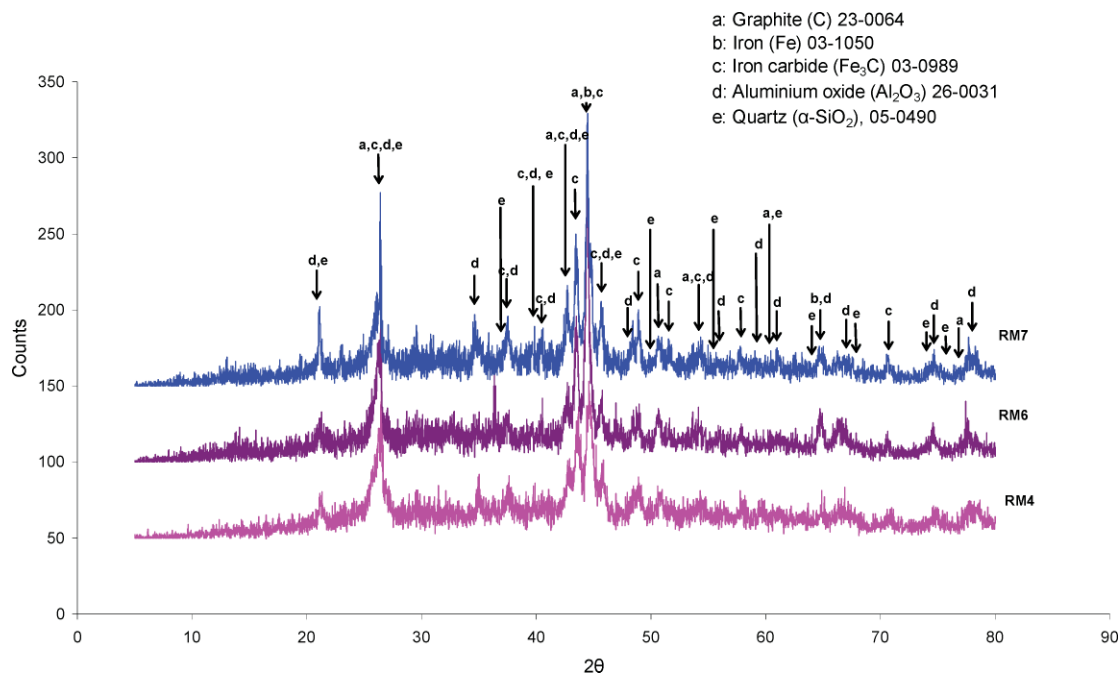
Fig. 4 Post-reaction (800 °C) powder X-ray diffraction patterns for red mud samples: RM4, RM6 and RM7. (Cu Kα radiation). RM4 and RM7 were run for *ca.* 200 min on stream whereas RM6 was run for 540 min on stream.
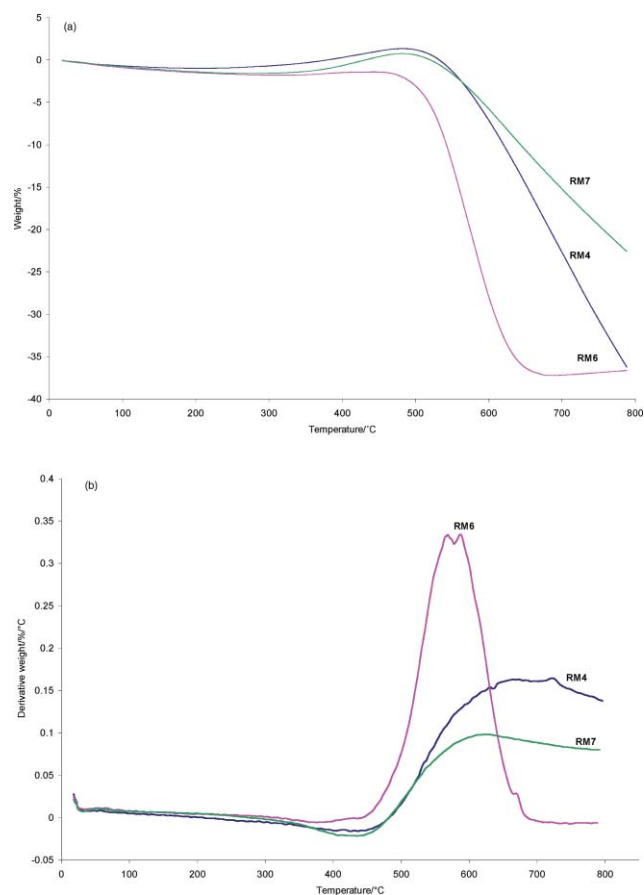
Fig. 5 (a) TGA oxidation profiles of RM4, RM6 and RM7 samples following reaction at 800 °C, and (b) corresponding first derivative patterns.

indicates a wide distribution in the nature of the species present. This aspect is also under investigation. In the case of RM6, there is no initial mass increase and the sharp mass decrease occurs over a narrower temperature range, at about 450–700 °C. It is suggested that these features are related to the absence of the reduced and re-oxidisable phases present in RM4 and RM7, which is consistent with the absence of a pronounced activity maximum in Fig. 2. The relative sharpness of the loss feature in this sample indicates a narrower distribution of carbon species. In relation to the latter point, it is notable that there are several maxima apparent on the derivative profile for this sample and these appear to be related to carbon species of differing reactivity. On comparing RM4 with RM7 more closely, inspection of Fig. 5 shows that the overall increase in mass is greater for RM4 than that observed for RM7. This is consistent with the different levels of iron phase(s) present in each sample. Differences in the gradient of the mass loss are evident in RM4 and RM7 and this may indicate differing reactivity of the carbon itself, although the difference in phase composition may be significant in this respect.

An interesting ramification of the presence of both Fe and Fe$_3$C (which is ferromagnetic)[29] in the post-reaction samples is that magnetism is imparted. In a series of experiments we have observed that the post-reaction samples are attracted by magnetic fields. Careful observations have shown that the sample is drawn to the applied magnetic field in its entirety (*i.e.* there are no portions of the sample which are not attracted.) In fact, it is possible to suspend a sample vial containing the post-reaction samples from the pole of a permanent magnet (a photograph of this effect has been used as the graphical abstract to this paper.) This effect is seen for all three red mud samples. This property has important consequences in terms of potential downstream utilisation, and hence further valorisation, of

post-reaction samples. It is our intention to investigate them for their water treatment potential and it is envisaged that magnetic separation will be employed.

Conclusion

The utility of red mud samples for methane decomposition to generate hydrogen has been demonstrated. A magnetic carbon containing material, of possible interest for a variety of potential further applications such as water treatment, is the co-product. The efficacy of the red mud samples is variable, which is related to differences in their composition which in turn reflects the purity of the bauxite ores from which they are produced. Iron, a major component of red mud, is the active phase. On the basis of previous literature, it can be anticipated that the activity is a strong function of alkali metal content, since alkali metals are known to be highly effective poisons of the decomposition reaction. In the present study, a sample which contains a relatively high content of titanium phase(s) seems to have reduced activity compared to a sample containing a comparable proportion of iron phase(s). The maximum hydrogen formation rate we have observed, 3.80×10^{-5} mol H_2 g^{-1} s^{-1}, is associated with a sample containing the highest proportion of iron. Studies into this system, concentrating upon the transformation pathways, the influence of phase fractions within the red mud samples and their interactions with one another, the form and nature of the deposited carbon, and potential downstream uses of the magnetic carbon containing product are currently in progress.

Experimental

Three red mud samples collected in India and designated RM4, RM6 and RM7 were used without modification in the present study. RM4 was collected from a site in Southern India in 2006, RM6 was collected from a site in Eastern India in 2006 and RM7 was collected from the same place as RM4 but after a two year interval.

Samples were analysed by inductively coupled plasma analysis (ICP), powder X-ray diffraction (XRD), BET surface area analysis, CHN analysis and thermogravimetric analysis (TGA). ICP was performed using a Varian ICP Vista MPX model ICPAES radial. Samples were investigated as known masses of fine powders dissolved in mixed acids, with any insoluble portions having been given fusion treatment. Simultaneous analysis against known standards was performed. Mass loss on ignition (LOI) studies were also performed to determine the content of decomposable species. Powder X-ray diffraction measurements were performed using a Siemens D5000 diffractometer with Cu Kα radiation. A 2θ range between 5 and 80° was scanned using a counting rate of 1 s per step with a step size of 0.02°. Samples were prepared by compaction into a Si sample holder. BET surface areas were determined where appropriate from N_2 physisorption isotherms measured at 77 K following out-gassing, using a Micromeritics Gemini. CHN analysis was performed by combustion using a CE 440 elemental analyzer. TGA was performed on a TA Instruments SDT Q600 instrument. Post-reaction samples were investigated using a 2% O_2/Ar mixture (BOC gases), and a temperature ramp rate of 10 °C min⁻¹ from ambient temperature up to 800 °C was applied.

Microreactor testing has been described in detail elsewhere.[25] In summary, catalysts were used in the form of powders held centrally within the heated zone of a quartz microreactor between quartz wool plugs. The feed gas composition applied was 80% CH_4 (BOC, 99.5%) and 20% N_2 (BOC, 99.98%) which were flowed at a total rate of 60 ml min⁻¹ over a *ca.* 0.4 g catalyst charge, typically resulting in a GHSV of 7200 h⁻¹. Product analysis was performed by on-line GC for H_2 quantification, Hewlett Packard 5980A, provided with a TCD and a mol sieve 3X packed column of 12′ long and 1/8″ O.D. GC analyses were performed approximately every six minutes. Background experiments, performed using an empty reactor tube containing quartz wool plugs only, confirmed that at temperatures reported here, H_2 production only occurred in the presence of the catalysts studied.

References

1 Y. Pontikes, C. Rathossi, P. Nikolopulos, G. N. Angelopoulos, D. D. Jayaseelan and W. E. Lee, *Ceram. Int.*, 2008, DOI: 10.1016/jceramint.2007.11.013.
2 S. Sushil and V. S. Batra, *Appl. Catal. B: Env.*, 2008, **81**, 64–77.
3 S. Wang, H. M. Ang and M. O. Tade, *Chemosphere*, 2008, **72**, 1621–1635.
4 A. Pappu, M. Saxena and S. R. Asolekar, *Building and Env.*, 2007, **42**, 2311–2320.
5 E. Poulin, J.-F. Blais and G. Mercier, *Hydrometallurgy*, 2008, **92**, 16–25.
6 Y. Li, C. Liu, Z. Luan, X. Peng, C. Zhu, Z. Chen, Z. Zhang, J. Fan and Z. Jia, *J. Hazard Mater.*, 2006, **137**, 374–383.
7 J. Pradhan, S. N. Das and R. S. Thakur, *J. Colloids Interf. Sci.*, 1999, **217**, 137–141.
8 S. Ordonez, H. Sastre and F. V. Diez, *Stud. Surf. Sci. and Catal.*, 1999, **126**, 443–446.
9 S. Ordonez, H. Sastre and F. V. Diez, *J. Hazard. Mater.*, 2001, **81**, 103–114.
10 S. Ordonez, H. Sastre and F. V. Diez, *Appl. Catal. B: Env.*, 2001, **29**, 263–273.
11 S. Ordonez, H. Sastre and F. V. Diez, *Appl. Catal. B: Env.*, 2001, **34**, 213–226.
12 J. R. Paredes, S. Ordonez, A. Vega and F. V. Diez, *Appl. Catal. B: Env.*, 2004, **47**, 37–45.
13 J. Alvarez, S. Ordonez, R. Rosal, H. Sastre and F. V. Diez, *Appl. Catal. A: Gen.*, 1999, **180**, 399–409.
14 J. Alvarez, R. Rosal, H. Sastre and F. V. Diez, *Appl. Catal. A: Gen.*, 1995, **128**, 259–273.
15 J. Alvarez, R. Rosal, H. Sastre and F. V. Diez, *Appl. Catal. A: Gen.*, 1998, **167**, 215–223.
16 I. Pulford and H. Flowers, *Environmental Chemistry at a Glance*, Blackwell Publishing, Oxford, 2006, ISBN 1405135328, 9781405135320.
17 G. J. Hutchings, M. S. Scurrell and J. R. Woodhouse, *Chem. Soc. Rev.*, 1989, **18**, 251–283.
18 T. J. Hall, J. S. J. Hargreaves, G. J. Hutchings, R. W. Joyner and S. H. Taylor, *Fuel Proc. Technol.*, 1995, **42**, 151–178.

19 T. V. Choudhary, E. Aksoylu and D. W. Goodman, *Catal. Rev. Sci. Eng.*, 2003, **45**, 151–203.
20 Y. Xu, X. Bao and L. Lin, *J. Catal.*, 2003, **216**, 386–395.
21 T. V. Choudhary and D. W. Goodman, *Catalysis*, 2006, **19**, 164–183.
22 M. A. Ermakova, D. Y. Ermakov, A. L. Chuvilin and G. G. Kuvshinov, *J. Catal.*, 2001, **201**, 183–197.
23 S. Takenaka, M. Serizawa and K. Otsuka, *J. Catal.*, 2004, **222**, 520–531.
24 N. Z. Muradov, *Energy Fuels*, 1998, **12**, 41–48.
25 S. Burns, J. G. Gallagher, J. S. J. Hargreaves and P. J. F. Harris, *Catal. Lett.*, 2007, **116**, 122–127.
26 G. L. Haller and D. E. Resasco, *Adv. Catal.*, 1989, **36**, 173.
27 T. Uchijima, *Catal. Today*, 1996, **28**, 105–117.
28 B. J. Cooper and D. L. Trimm, *J. Catal.*, 1980, **62**, 35–43.
29 B. David, O. Schneeweiss, M. Mashlan, E. Santava and I. Morjan, *J. Mag. Mag. Mater.*, 2007, **316**, 422–425.

Enhancement of cyclic ether formation from polyalcohol compounds in high temperature liquid water by high pressure carbon dioxide

Aritomo Yamaguchi, Norihito Hiyoshi, Osamu Sato, Kyoko K. Bando and Masayuki Shirai*

Cyclic ethers were produced by a dehydration reaction of polyalcohol compounds in high temperature liquid water, which was accelerated by the presence of carbon dioxide dissolved in the water. 3-hydroxytetrahydrofuran was produced by the dehydration of 1,2,4-butanetriol. Both tetrahydrofurfuryl alcohol and 3-hydroxytetrahydropyran were produced by the dehydration of 1,2,5-pentanetriol. Five-membered cyclic ethers were formed faster than six-membered cyclic ethers and the formation rates of the cyclic ethers depended strongly on the structure of the polyalcohol compounds. The position of the hydroxyl groups is crucial for the efficient intramolecular dehydration.

Introduction

Biomass has a large amount of oxygen atoms because plants combine carbon dioxide with water using solar energy to store oxygen as sugar building blocks, $(CH_2O)_n$. The selective removal of oxygen atoms from biomass-derived carbohydrates, which are polyalcohol compounds like fructose, sorbitol, and glycerol in most cases, by dehydration or hydrogenolysis is important to obtain valuable products with desired boiling points, water solubilities, octane numbers and viscosities.[1] The chemistry of intramolecular dehydration of polyalcohol compounds provides a key technology for developing an efficient conversion process of biomass derivatives to useful materials;[2] however, biomass-derived carbohydrates, such as fructose and sorbitol, have five or six hydroxyl groups in a molecule and their intramolecular dehydration mechanisms are complicated.

High temperature liquid water has attracted much attention as an alternative to harmful organic solvents because of its high proton concentration, which enhances the rates of acid-catalyzed reactions, such as dehydration in water, without adding any hazardous acid.[3,4] Cyclic ethers are essential materials for the chemical industry and they are produced from diols by intramolecular dehydration over strong mineral acids, aluminium silicates, and ion-exchange resins.[5] Savage's group reported that the addition of carbon dioxide to water (473–623 K) enhanced the production of tetrahydrofuran (THF) from 1,4-butanediol (1,4-BDO).[6–8] The added carbon dioxide was dissolved in water to form carbonic acid, accelerating the acid catalysis of high temperature water. An acid solvent composed of water and carbon dioxide is environmentally-benign not only because both water and carbon dioxide are non-toxic, but also separation and recycling of these two components are easily performed by depressurization after reaction. In this manuscript, we investigated the dehydration mechanism of polyalcohol compounds having two or three hydroxyl groups, as simple model compounds of biomass-derived carbohydrates, to corresponding five- or six-membered cyclic ethers in water under high pressure carbon dioxide at 573 K.

Experimental

1,2,4-Butanetriol (1,2,4-BTO, Wako Pure Chemical Industries), 1,2,5-pentanetriol (1,2,5-PTO, Tokyo Chemical Industry), 1,4-butanediol (1,4-BDO, Wako Pure Chemical Industries), 1,4-pentanediol (1,4-PDO, Aldrich) and 1,5-pentanediol (1,5-PDO, Wako Pure Chemical Industries) were purchased and used without any further purification.

The dehydration of polyalcohol compounds was carried out in a batch reactor (inner volume: 6 cm³) made of a SUS316 tube.[9] After 3 cm³ of polyalcohol aqueous solution (1.0 and 0.3 mol dm⁻³) was loaded in the reactor, the gas phase was purged with argon gas to remove air. Carbon dioxide (10 and 15 MPa) was then loaded in the reactor at 323 K.[10] The reactor was submerged into a molten-salt bath at 573 K for a given reaction time and then submerged into a water bath for cooling to ambient temperature quickly after the reaction. The water in the reactor maintained vapor-liquid equilibrium at 573 K under 8.6 MPa of partial pressure. The partial pressure of carbon dioxide at 573 K was estimated to be 17.7 and 26.6 MPa, based on the equation of Charles's law, corresponding to the initial pressure of 10 and 15 MPa at 323 K, respectively. A mixture of a reactant and liquid products was taken out from the reactor with distilled water.

The quantitative analysis of liquid products was conducted by gas chromatography with a flame ionization detector (GC-FID) equipped with a DB-WAX capillary column (Agilent Technologies) using 1-propanol (Wako Pure Chemical Industries) as an internal standard material. The products were identified by their retention times of the GC-FID analysis, compared with those for known materials; 3-hydroxytetrahydrofuran (3-HTHF, Wako Pure Chemical Industries), tetrahydrofur-

Research Center for Compact Chemical Process, National Institute of Advanced Industrial Science and Technology (AIST), 4-2-1 Nigatake, Miyagino, Sendai, 983-8551, Japan. E-mail: m.shirai@aist.go.jp; Fax: +81 22 237 5224; Tel: +81 22 237 5219

furyl alcohol (THFA, Sigma-Aldrich), tetrahydrofuran (THF, Wako Pure Chemical Industries), 2-methyltetrahydrofuran (2-MTHF, Sigma-Aldrich) and tetrahydropyran (THP, Wako Pure Chemical Industries). 4-hydroxytetrahydropyran (Aldrich) was used for the quantitative analysis for 3-hydroxytetrahydropyran (3-HTHP). The material balance of all reactions was more than 95%. Initial formation rates of cyclic ethers were estimated from initial slopes of the fitting curves of their profiles.

Results and discussion

Dehydration of 1,2,4-butanetriol (1,2,4-BTO) and 1,2,5-pentanetriol (1,2,5-PTO) in high temperature liquid water at 573 K

Dehydration of 1.0 mol dm^{-3} of 1,2,4-butanetriol (1,2,4-BTO) proceeded in water at 573 K (Fig. 1). 3-Hydroxytetrahydrofuran (3-HTHF) was the only product of this reaction (Scheme 1). The 3-HTHF yield for 10 minutes in liquid water at 573 K was 2.9% (as 1,2,4-BTO conversion) and increased to 10.7 and 22.4% by the addition of 17.7 and 26.6 MPa of carbon dioxide, respectively. On the other hand, the final yield of 3-HTHF after 3 hours of reaction was almost the same (70%) for the three conditions (under 0, 17.7 and 26.6 MPa of carbon dioxide), indicating that the added carbon dioxide enhanced the 3-HTHF formation rates to reach the equilibrium yield (70%).

Fig. 1 Yields of 3-hydroxytetrahydrofuran (3-HTHF, closed symbols) and 1,2,4-butanetriol (1,2,4-BTO, open symbols) as a function of elapsed time for the 1,2,4-BTO dehydration reaction at 573 K in water (initial 1,2,4-BTO concentration: 1.0 mol dm^{-3}, carbon dioxide partial pressure: 0 (circles), 17.7 (triangles) and 26.6 MPa (squares)).
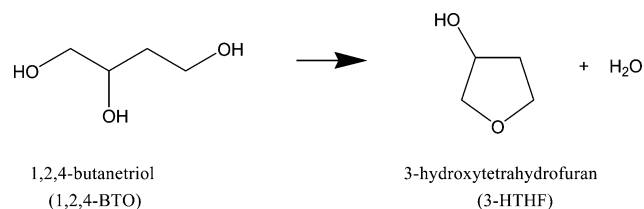
Scheme 1 Dehydration reaction of 1,2,4-butanetriol.

The dehydration of 1.0 mol dm^{-3} of 1,2,5-pentanetriol (1,2,5-PTO) also proceeded in water at 573 K and provided two products; tetrahydrofurfuryl alcohol (THFA) and

3-hydroxytetrahydropyran (3-HTHP) (Scheme 2, Fig. 2). The yields of THFA (25.6, 35.7, and 45.6%) were about 6 times larger than those of 3-HTHP (3.9, 5.2 and 7.6%) for 10 minutes of reaction (under 0, 17.7, and 26.6 MPa of carbon dioxide, respectively). The final yields of THFA and 3-HTHP for the dehydration of 1,2,5-PTO were 70% and 10%, respectively, and here again the pressure of carbon dioxide did not affect the equilibrium yields of the products.

Scheme 2 Dehydration reaction of 1,2,5-pentanetriol.

Fig. 2 Yields of tetrahydrofurfuryl alcohol (THFA, closed symbols), 3-hydroxytetrahydropyran (3-HTHP, checked symbols), and 1,2,5-pentanetriol (1,2,5-PTO, open symbols) as a function of elapsed time for the 1,2,5-PTO dehydration reaction at 573 K in water (initial 1,2,5-PTO concentration: 1.0 mol dm^{-3}, carbon dioxide partial pressure: 0 (circles), 17.7 (triangles) and 26.6 MPa (squares)).

Dehydration of 0.3 mol dm^{-3} 1,2,4-BTO and 0.3 mol dm^{-3} 1,2,5-PTO also proceeded in water at 573 K (Fig. 3). 3-HTHF was produced from 1,2,4-BTO and the 3-HTHF yield increased by the addition of 17.7 MPa of carbon dioxide (Fig. 3 (a)). THFA and 3-HTHP were produced from 1,2,5-PTO and the yield of THFA and 3-HTHP increased by the addition of carbon dioxide (Fig. 3 (b)). The product yields from different initial reactant concentrations (0.3 and 1.0 mol dm^{-3}) were quite similar to each other in both cases of 1,2,4-BTO and 1,2,5-PTO. The initial formation rates of cyclic ethers are summarized in Table 1. Formation rates of 3-HTHF, THFA and 3-HTHP increased with increasing carbon dioxide pressure or the initial concentrations of 1,2,4-BTO and 1,2,5-PTO. On the other hand, the formation rates divided by the initial reactant concentrations were unaffected by the initial reactant concentrations between

Table 1 Initial formation rates of cyclic ethers for dehydration reactions of 1,2,4-butanetriol (1,2,4-BTO) and 1,2,5-pentanetriol (1,2,5-PTO) in water at 573 K

Reactant	Product	CO_2 pressure/MPa	$C_i{}^a$/mol dm^{-3}	$r_i{}^{b,c}$/10^{-4} mol dm^{-3} s^{-1}	$r_i/C_i{}^c$/10^{-4} s^{-1}
1,2,4-BTO	3-HTHF	0	0.3	0.21	0.69
			1.0	0.61	0.61
		17.7	0.3	0.61	2.0
			1.0	1.7	1.7
1,2,5-PTO	THFA	0	0.3	1.4	4.7
			1.0	4.3	4.3
		17.7	0.3	1.9	6.3
			1.0	5.9	5.9
	3-HTHP	0	0.3	0.12	0.41
			1.0	0.47	0.47
		17.7	0.3	0.24	0.81
			1.0	0.87	0.87

^{a} Initial reactant concentration. ^{b} Initial formation rate. ^{c} The experimental errors were within 5%.
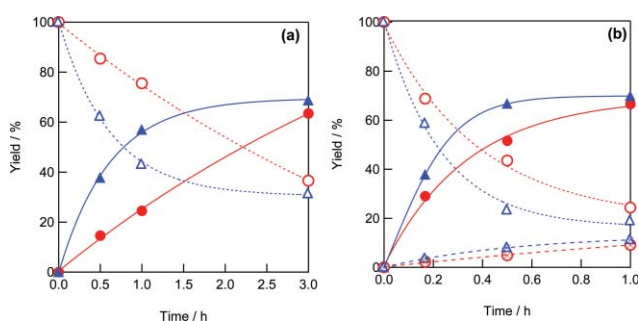
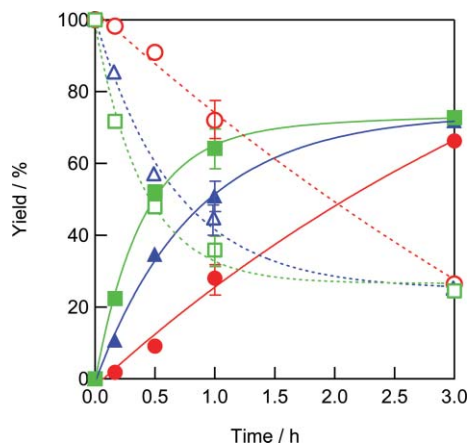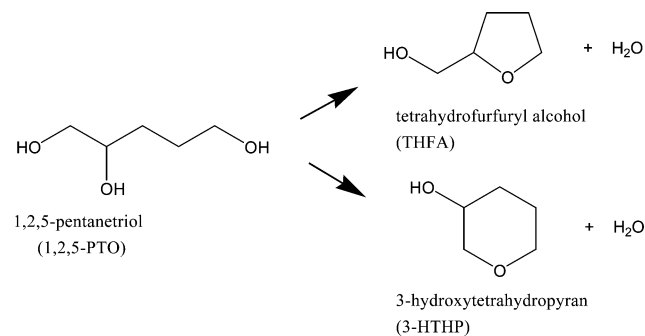**Fig. 3** (a) Yields of 3-hydroxytetrahydrofuran (3-HTHF, closed symbols) and 1,2,4-butanetriol (1,2,4-BTO, open symbols) as a function of elapsed time for the 1,2,4-BTO dehydration reaction at 573 K in water (initial 1,2,4-BTO concentration: 0.3 mol dm^{-3}, carbon di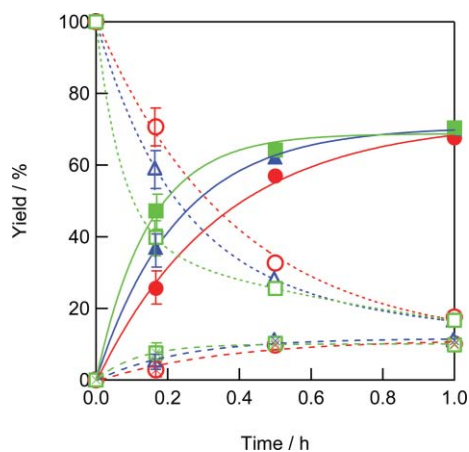oxide partial pressure: 0 (circles) and 17.7 MPa (triangles)). (b) Yields of tetrahydrofurfuryl alcohol (THFA, closed symbols), 3-hydroxytetrahydropyran (3-HTHP, checked symbols), and 1,2,5-pentanetriol (1,2,5-PTO, open symbols) as a function of elapsed time for the 1,2,5-PTO dehydration reaction at 573 K in water (initial 1,2,5-PTO concentration: 0.3 mol dm^{-3}, carbon dioxide partial pressure: 0 (circles) and 17.7 MPa (triangles)).

0.3 and 1.0 mol dm^{-3} (Table 1). This result indicates that the dehydration of 1,2,4-BTO and 1,2,5-PTO to the cyclic ether compounds has a first-order dependence on polyalcohol concentrations.

Effect of carbon dioxide on cyclic ethers formation from triol compounds in high temperature liquid water

The intramolecular dehydration reaction of 1,4-butanediol (1,4-BDO) to tetrahydrofuran (THF) is reported to be catalyzed by acid agents, such as ion exchange resins,[11] zeolites[12,13] and heteropolyacids.[14,15] The intramolecular dehydration reactions of triols to the cyclic ether compounds would be an acid-catalyzed reaction.

The increase of the proton concentration by the addition of carbon dioxide could be explained by the dissolution of carbon dioxide in high temperature liquid water, as shown below.

$$H_2O + CO_2 \rightleftarrows H_2CO_3 \rightleftarrows H^+ + HCO_3^- \rightleftarrows 2H^+ + CO_3^{2-} \quad (1)$$
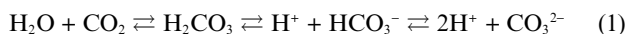
Hunter and Savage estimated the proton concentration of high temperature liquid water with an addition of carbon dioxide (Equation (2)).[6–8]

$$\left[H^+\right] = \frac{K_W}{\left[H^+\right]} + \left(\frac{K_{a1}}{\left[H^+\right]}\right)\left[CO_2\left(aq\right)\right] \quad (2)$$

where $[H^+]$, $[CO_2(aq)]$, K_W, and K_{a1} represent the concentrations of proton and dissolved carbon dioxide, ionization constant of water, and the first ionization constant of carbonic acid, respectively. They claimed that proton concentration depends approximately on the first dissociation of carbonic acid essentially because its second dissociation is negligible. Equation (2) can be written as,

$$\left[H^+\right] = \left(K_W + K_{a1}\left[CO_2\left(aq\right)\right]\right)^{1/2} = \left(K_W + \frac{K_{a1}}{K_H}P_{CO2}\right)^{1/2} \quad (3)$$

where K_H and P_{CO2} represent the Henry's law constant of carbon dioxide dissolved in water and the pressure of carbon dioxide, respectively.

The formation of cyclic ethers has a first-order dependence on polyalcohol concentrations and is an acid-catalyzed reaction. The formation rates could be represented as follows,

$$r = k[\text{triol}][H^+]^\alpha \quad (4)$$

where r, k, [triol], $[H^+]$, α represent a formation rate of the cyclic ether, an apparent reaction constant, a concentration of triol and proton, and an apparent reaction order of proton, respectively. We fitted Equation (4) to the formation rates of the cyclic ethers from 1,2,4-BTO and 1,2,5-PTO *versus* proton concentrations at 573 K with 0, 17.7 and 26.6 MPa carbon dioxide. The apparent reaction orders of proton (α) are 0.6, 0.2 and 0.3 for 3-HTHF from 1,2,4-BTO and THFA and 3-HTHP from 1,2,5-PTO, respectively. The dehydration of 1,2,4-BTO was enhanced strongly by proton concentration, compared with the dehydration of 1,2,5-PTO because α of 1,2,4-BTO dehydration (0.6) was larger than those of 1,2,5-PTO dehydration (0.2 and 0.3). It should be noted that the apparent reaction orders of proton for the dehydration reactions are not unity, indicating that the dehydration of 1,2,4-BTO and 1,2,5-PTO to the cyclic ether compounds does not have a first-order dependence on proton concentration and the reaction is not simply initiated by a collision between the triol molecule and proton. We will discuss

Table 2 Initial formation rates of cyclic ethers for dehydration reactions in water at 573 K

Reactant[a]	Product	CO_2 pressure/MPa	$r_i^{b,c}$/10^{-4} mol dm^{-3} s^{-1}
1,4-BDO	THF	0	0.68
		17.7	4.7
1,2,4-BTO[d]	3-HTHF	0	0.61
		17.7	1.7
1,4-PDO	2-MTHF	0	0.86
		17.7	10.0
1,5-PDO	THP	0	0.063
		17.7	0.42
1,2,5-PTO[c]	THFA	0	4.3
		17.7	5.9
	3-HTHP	0	0.47
		17.7	0.87

[a] Initial reactant concentration: 1.0 mol dm^{-3}. [b] Initial formation rate. [c] The experimental errors were within 5%. [d] The same data as shown in Table 1.

the promotion effect by carbon dioxide in terms of basicities of the hydroxyl groups and intramolecular hydrogen bond in triol compounds along with the dehydration results of various polyalcohol compounds in the following section.

Formation rates of cyclic ethers from various polyalcohol compounds

We investigated initial dehydration rates concerning three more polyalcohol compounds to understand the dehydration mechanism of polyalcohol compounds to five- or six-membered cyclic ethers, and the results are summarized in Table 2. The dehydration of 1,4-pentanediol (1,4-PDO) and 1,5-pentanediol (1,5-PDO) proceeded to produce a five-membered ether, 2-methyltetrahydrofuran (2-MTHF) and a six-membered ether, tetrahydropyran (THP), respectively (Scheme 3).
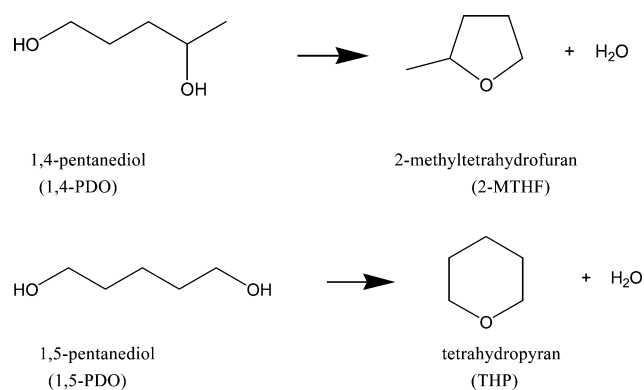
Scheme 3 Dehydration reactions of 1,4-pentanediol and 1,5-pentanediol.

The formation rate of 2-MTHF in 1,4-PDO dehydration was higher than that of THP in 1,5-PDO dehydration at 573 K (Table 2). Both formation rates were also accelerated by the addition of 17.7 MPa of carbon dioxide. These results could explain the higher THFA formation rate in 1,2,5-PTO dehydration than the 3-HTHP formation rate (Table 2). The difference between the dehydration rates of 1,4-PDO and 1,5-PDO indicates, (1) the formation rates of five-membered cyclic ethers are higher than six-membered cyclic ethers, as revealed by

the results that the dehydration rate of 1,4-BDO to THF (0.68×10^{-4} mol dm^{-3} s^{-1}) was larger than that of 1,5-PDO to THP (0.063×10^{-4} mol dm^{-3} s^{-1}); and, (2) the dehydration of 1,4-PDO proceeds through the formation of a secondary carbocation, and/or the basicity of the secondary hydroxyl group in the 4-position in 1,4-PDO is higher than that of the primary hydroxyl group, as shown by the result that the dehydration rate of 1,4-PDO to 2-MTHF (0.86×10^{-4} mol dm^{-3} s^{-1}) was higher than that of 1,4-BDO to THF (0.68×10^{-4} mol dm^{-3} s^{-1}). Therefore, in the case of the dehydration of 1,2,5-PTO, the formation rate of THFA, which is a five membered heterocyclic ether and formed by dehydration between primary and secondary hydroxyl groups, is much faster than that of 3-HTHP (a six membered heterocyclic ether and formed by dehydration between two primary hydroxyl groups). Table 2 also shows that the promotion effect by carbon dioxide on the dehydration rates of alkanediols (1,4-BDO and 1,5-PDO) was larger than that of corresponding alkanetriols (1,2,4-BTO and 1,2,5-PTO). These results may be explained by the intramolecular hydrogen bond between the two hydroxyl groups in the 1- and 2-position in triols, which was investigated by density functional theory (DFT) methods.[16–18] The DFT studies show that the hydroxyl group in the 2-position was preferentially protonated by the intramolecular hydrogen bond. The intramolecular interaction between the two hydroxyl groups in the 1- and 2-position of triols would make the effect of protons from external molecules smaller, which results in less promotion effect of carbon dioxide for triols.

Conclusions

Cyclic ethers were produced by the dehydration reactions of polyalcohol compounds in high temperature liquid water, which was accelerated by the presence of carbon dioxide dissolved in the water. Five-membered cyclic ethers were formed faster than six-membered cyclic ethers and the formation rates of the cyclic ethers depended strongly on the structure of the polyalcohol compounds. The position of the hydroxyl groups is crucial for the efficient intramolecular dehydration, which leads to a new technology for conversion of biomass derivatives to useful materials.

Notes and references

1 Y. Roman-Leshkov, C. J. Barrett, Z. Y. Liu and J. A. Dumesic, *Nature*, 2007, **447**, 982–985.
2 Pacific Northwest National Laboratory (PNNL) and National Renewable Energy Laboratory (NREL), *Top value added chemicals from biomass*, Report, 2004.
3 P. E. Savage, *Chem. Rev.*, 1999, **99**, 603–622.
4 N. Akiya and P. E. Savage, *Chem. Rev.*, 2002, **102**, 2725–2750.
5 U. Limbeck, C. Altwicker, U. Kunz and U. Hoffmann, *Chem. Eng. Sci.*, 2001, **56**, 2171–2178.
6 S. E. Hunter and P. E. Savage, *AIChE Journal*, 2008, **54**, 516–528.
7 S. E. Hunter, C. E. Ehrenberger and P. E. Savage, *J. Org. Chem.*, 2006, **71**, 6229–6239.
8 S. E. Hunter and P. E. Savage, *Ind. Eng. Chem. Res.*, 2003, **42**, 290–294.
9 A. Yamaguchi, N. Hiyoshi, O. Sato, M. Osada and M. Shirai, *Catal. Lett.*, 2008, **122**, 188–195.

10 A. Yamaguchi, N. Hiyoshi, O. Sato, C. V. Rode and M. Shirai, *Chem. Lett.*, 2008, **37**, 926–927.
11 S. H. Vaidya, V. M. Bhandari and R. V. Chaudhari, *Appl. Catal., A*, 2003, **242**, 321–328.
12 Y. V. S. Rao, S. J. Kulkarni, M. Subrahmanyam and A. V. R. Rao, *J. Org. Chem.*, 1994, **59**, 3998–4000.
13 M. Aghaziarati, M. Kazemeini, M. Soltanieh and S. Sahebdelfar, *Ind. Eng. Chem. Res.*, 2007, **46**, 726–733.

14 T. Baba and Y. Ono, *J. Mol. Catal.*, 1986, **37**, 317–326.
15 H. Li, H. Yin, T. Jiang, T. Hu, J. Wu and Y. Wada, *Catal. Commun.*, 2006, **7**, 778–782.
16 R. A. Klein, *J. Comput. Chem.*, 2002, **23**, 585–599.
17 R. A. Klein, *J. Comput. Chem.*, 2003, **24**, 1120–1131.
18 M. M. Deshmukh, N. V. Sastry and S. R. Gadre, *J. Chem. Phys.*, 2004, **121**, 12402–12410.

This journal is © The Royal Society of Chemistry 2009

Soybean oil extraction and separation using switchable or expanded solvents

Lam Phan,[a] Heather Brown,[b] James White,[b] Allan Hodgson[c] and Philip G. Jessop*[a]

The extraction of soy oil from soybean flakes in industry requires large amounts of hexane solvent and results in significant losses and energy consumption during the distillative removal of the solvent. Hexanes and related hydrocarbon extractants are also becoming an environmental and health concern. A new method for extraction of the oil is sought, that would require neither hexane nor distillative removal of solvent. This article presents a preliminary assessment of several new methods for soy oil extraction and subsequent solvent removal from the oil. The most promising are (a) extraction by an amidine switchable solvent that can then be removed from the soy oil by carbonated water and (b) extraction by a moderately hydrophilic solvent that can then be removed from the oil by water.

Introduction

A new method for extraction of soy oil from crushed soybeans is needed because of environmental considerations and legislative pressures against the current method of extraction with hexane. The existing approach, introduced in the United States in 1930,[1] involves a counter-current flow of hexane and soybean flakes, giving a saturated solution of oil in hexane. The best continuous soybean extraction has a solvent:bean mass ratio of 1, which is equivalent to a solvent:oil mass ratio of 5. Hexane losses are 1 kg per ton of beans processed.[1]

Replacement of hexane with a solvent less prone to losses is becoming a priority for the industry. Supercritical CO_2 (scCO_2) could be used but requires 500 bar for the most energy-efficient extraction of soy oil from soybeans (i.e. minimum energy cost per kg of extracted oil).[2,3] Soybean oil is miscible with many other low polarity organic solvents, especially those having a Hildebrand solubility parameter less than or equal to 22 MPa$^{1/2}$ (Table 1). The problem with the use of low polarity solvents is that miscibility with oil is only desired during the extraction of the oil from the flakes; after extraction is complete, the separation of the oil from the solvent is desired, and thus the miscibility becomes a hindrance. We therefore suggest three alternative strategies for surmounting this problem:

Strategy 1: Use a switchable-polarity solvent in its low polarity form to extract the soybean oil from the flakes, and then switch the solvent to its high polarity form to induce immiscibility with the oil, so that the solvent can be decanted from the oil. A switchable-polarity solvent (SPS) is a solvent that can

Table 1 Solvent and soy oil miscibility at room temperature

Solvent	δ,[a] MPa$^{1/2}$	ε[b]	Miscible[c]
DBU	—	—	yes
Triethylamine	15.1	2.4[10]	yes
Tripropylamine	18.0	2.4[10]	yes
THF	18.6	7.5[11]	yes
2-Propylamine	—	5.1	yes
Acetone	20.2	20.7	yes[d]
Dioxane	20.5	2.2[11]	yes
Acetic acid	20.7	6.2	no
Pyridine	21.9	12.9	yes
2-Propanol	23.5	18.3	no[d]
1-Propanol	24.3	20.1	yes[d]
Acetonitrile	24.3	37.5	no
DMSO	24.5	46.6	no
DMF	24.8	36.7	no
Ethanol	26.0	22.4	no[d]
Methanol	29.6	32.6	no[d]
Water	47.9	79.7	no[d]

[a] Hildebrand parameter, from Allen.[12] [b] Dielectric constant, from Smallwood[13] except where noted. [c] "yes" indicates a 2:1 v/v solvent and oil mixture forms a single liquid phase at room temperature. "no" indicates two liquid phases are present. [d] Miscibility or immiscibility also reported by Erickson et al.[14]

switch back and forth between low polarity and high polarity forms.[4–8]

Strategy 2: Use a switchable-hydrophilicity solvent[9] in its hydrophobic/lipophilic form to extract the soybean oil from the flakes, and then switch the solvent to its hydrophilic form and extract it from the oil with water. Remove the solvent from the water by switching the solvent back to its hydrophobic form. A switchable-hydrophilicity solvent (SHS) is a solvent that can switch back and forth between hydrophilic and hydrophobic forms.

Strategy 3: Use a normal (non-switchable) solvent of moderate polarity to extract the soybean oil from the flakes, and then extract the solvent from the oil with water. Remove the solvent from the water by dissolving CO_2 in the solvent/water mixture to induce a phase split.

[a]Department of Chemistry, Queen's University, Kingston, Ontario, Canada. E-mail: jessop@chem.queensu.ca; Fax: +1 613-533-6669; Tel: +1 613-5333-3212
[b]Battelle PNWD, 902 Battelle Blvd., PO Box 999, Mail Code: MSIN: P8-60, Richland, WA, USA 99352. E-mail: jim.white@pnl.gov; Fax: +1 509-372-4732
[c]Bunge, 725 North Kinzie Avenue, Bradley, Illinois, 60915, USA. E-mail: allan.hodgson@bunge.com; Fax: +1 815 523 8114; Tel: +1 815 523 8083

Experimental methods

Soy oil and flaked soybeans were used as received from Bunge. DBU (Aldrich, 98% grade) was dried *via* distillation. Supercritical grade CO_2 (99.999%, $H_2O < 0.5$ ppm), nitrogen (99.998%, $H_2O < 3$ ppm) and argon (99.998%, $H_2O < 5$ ppm) were used as received from Praxair. NMR spectra were acquired at 400 MHz and referenced to TMS at 0 ppm unless specified otherwise. All other solvents were used as received from Aldrich or Fisher.

Miscibility tests

A vial containing 4.0 ml of solvent and 2.0 ml of soybean oil was stirred for 10 minutes and left to settle for 20 min, then the miscibility of the soy oil and solvent was visually observed.

Quantitative analysis of solvent/soy oil mixtures by ¹H NMR spectroscopy

A calibration curve was prepared in the following manner. Different masses of oil and solvents were charged into sealed vials. The contents of each vial were stirred and then allowed to settle. If required, the contents were heated to an appropriate temperature to achieve miscibility. The ¹H NMR spectrum of a portion of the mixture in $CDCl_3$ was acquired and selected peaks from 4.1 to 4.2 ppm associated with the oil were compared to selected peaks of the solvent that did not have any overlap. The integration ratio was plotted against the mass% of solvent in the solvent/oil mixture (mass percentages ranged from 1 to 10%). Such calibration curves were prepared for mixtures of soy oil with: n-PrOH, i-PrOH, EtOH, DBU, 1,4-dioxane and benzylmethylamine.

The scan time for ¹H NMR analysis was 4 s, with a delay time of 1 s. The detection limit is typically 0.1 wt.% of the solvent. When an unknown mixture of soy oil and solvent is analyzed, its peak integration ratio can be used to calculate the amount of solvent in the soy oil.

Extraction of oil from soybean flakes

Flaked soybeans (4 g) were added to a 50 mL ace tube, equipped with a stir-bar, fritted dip-tube, pressure gauge, pressure release valve (set to 100 psi), and vent (Fig. 1). The system was heated to the desired extraction temperature *via* oil bath. A separate 25 mL Swagelok sample vessel, equipped with needle values at both ends, was charged with extraction solvent (20 g). The valves were closed and the sample vessel weighed. The entire vessel was then immersed in a hot water bath set to the desired extraction temperature. Once both vessels were at the desired temperature, the sample vessel was removed from the hot water bath and connected to the outlet of the fritted dip tube. The contents were then forced into the ace tube with sweeping nitrogen. The ace tube was then sealed and the sample vessel removed. The actual weight of solvent added was determined by subtracting the starting weight from the final weight of the sample vessel. This technique was employed to minimize error due to heat-up times.

During the extraction, aliquots were removed for HPLC analysis using a luer-lock syringe to pull solvent through the
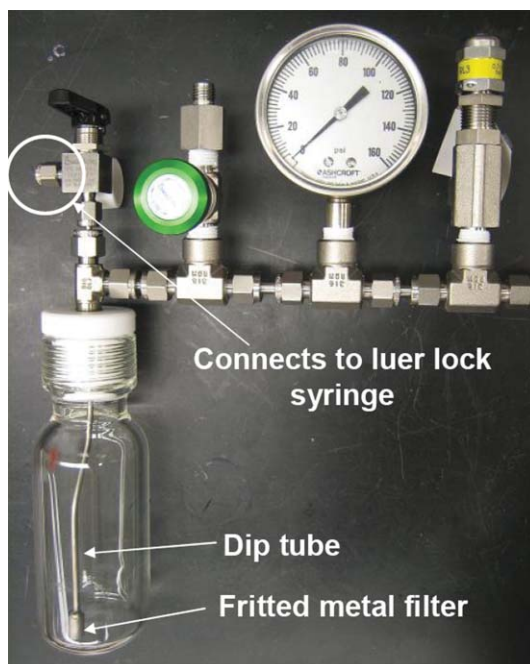
Fig. 1 Apparatus for the evaluation of solvents for extraction of oil from soybean flakes.

Table 2 HPLC Gradient

Time (min)	Acetonitrile (vol%)	Dichloromethane (vol%)
0	77	23
5	77	23
25	70	30
30	77	23

fritted dip-tube. The dip tube was rinsed several times with the bulk solution to ensure that representative samples were taken.

A Shimadzu 10A *vp* system, equipped with an Alltech Altima HP C18 HL 3 μm 150 mm × 3.0 mm column and an Alltech 2000 ELSD, was used to analyze samples from each extraction trial. The method utilized a gradient of acetonitrile and dichloromethane shown in Table 2. All sample dilutions were performed using dichloromethane.

The HPLC method was an external standard method. To obtain an accurate calibration curve, five dilutions (1, 0.5, 0.2, 0.1, and 0.05 wt%) of soy oil were prepared. Each of the dilutions was injected once. The calibration obtained from this five point curve had an R^2 value that fell between 0.995 and 0.999. External standards at high and low total oil concentrations were analyzed as spot checks, while running samples. The column was recalibrated when necessary as indicated by the performance of the external standards.

Separation of soy oil from switchable polarity solvents

For experiments with DBU/ROH SPS: CO_2 was bubbled through a mixture of 3.0 ml of DBU, 1.6 ml of EtOH, and 4 ml of soy oil in a septum-capped vial for 1 h with stirring. The contents were left to settle over night. The oil layer was analyzed as described above. Similar procedures were done using different amounts of EtOH, MeOH, and water.

For experiments with secondary amine SPS : CO_2 was bubbled through a mixture of 4.0 ml of benzylmethylamine and 2.0 ml soy oil in a stirred and septum-capped vial for at least 1 h or until the heat from the reaction subsided. The contents were left to settle over night. The oil layer was analyzed as described above.

Extraction of dioxane from soy oil

To a septum-sealed vial containing 4 mL dioxane and 2 mL soy oil, 4, 6, 8, or 10 mL of distilled water was added. The contents were shaken and then left standing for 1 week at room temperature. The contents separated into two-phases, with the top being the soy oil, and the bottom as the aqueous-dioxane mixture. The oil phase was analyzed by ^{1}H NMR spectroscopy and the dioxane content of that phase was determined with the use of a calibration curve (see supplementary material).

Results and discussion

Strategy 1: Extraction of oil with switchable-polarity solvents

A switchable solvent is a solvent that can be reversibly "switched" from one form to another, where the two forms differ significantly in one or more properties. Most important for the present discussion is a switch in polarity. The first switchable polarity solvent (SPS) was reported in 2005 by the Jessop group[4,15] and related designs have been published since.[5–7] That first SPS consisted of an equimolar mixture of an alcohol and an amidine such as DBU (1,8-diazabicyclo-[5.4.0]-undec-7-ene). The mixture has a dramatically greater polarity in the presence of an atmosphere of CO_2 than it has with no CO_2, because CO_2 reacts with the liquid mixture to create an ionic liquid (equation 1). Because the reaction is reversible, any action taken on the ionic liquid that removes the CO_2, such as heating the liquid or bubbling N_2 through it, causes the polar ionic liquid to revert to the original low-polarity non-ionic liquid. Secondary amines constitute another type of SPS; liquid secondary amines such as N-butyl-N-ethylamine and N-benzyl-N-methylamine are converted by CO_2 into more polar liquids (mixtures of carbamate salt and carbamic acid, equation 2).[5]

$$(1)$$

$$(2)$$

A switchable-polarity solvent (SPS) could be used in its low-polarity form as a solvent for the extraction of soy oil from soy flakes and then could be switched into its high-polarity form which would be immiscible with the soy oil (Fig. 2). Preferably, the high-polarity form would be so immiscible with the oil that the level of contamination of the oil with solvent would be extremely low. Further purification of the oil might be necessary to remove traces of the solvent. This strategy was evaluated with

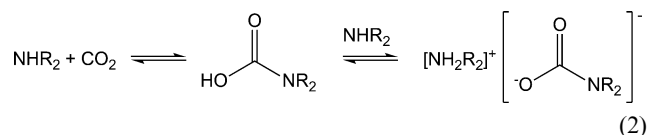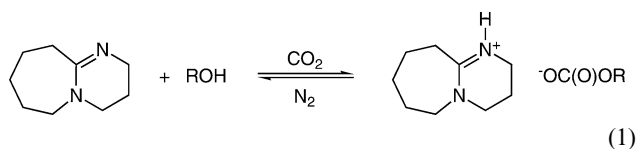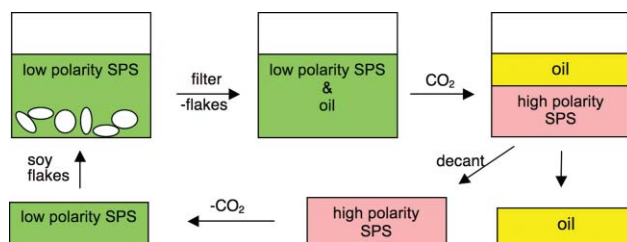**Fig. 2** Schematic for oil separation using switchable-polarity solvents. Pink represents the solvent in its high-polarity form, while green represents its low-polarity form.

two kinds of switchable solvents, secondary amines and mixtures of DBU and alcohol.

The DBU/alcohol mixtures are miscible with soy oil as long as CO_2 is absent, but their ionic liquid forms are immiscible with soy oil. Although the ionic liquids that form from DBU and short chain alcohols (methanol and ethanol) have melting points above room temperature,[6] these ionic liquids are in fact liquid at room temperature when they contain small amounts of soy oil. They can therefore be used at room temperature.

In each separation trial, soy oil (4 ml), DBU (3 ml) and water or an alcohol (at an amount equimolar to DBU) were mixed together. CO_2 was bubbled through the liquid for 1 h, after which the liquid mixture was allowed to settle overnight. The soy oil rose while the ionic liquid formed the lower layer. The soy oil layer was then analyzed for contamination with DBU. The separation of the ionic liquid layer from the oil layer was quite poor with methanol, so work with methanol was abandoned. The data (Table 3) showed that better results were obtained with ethanol than water. Because the oil still contained small amounts of both solvent components (ethanol and DBU), we speculated that additional CO_2 treatment could precipitate more ionic liquid. Bubbling extra CO_2 for 30 min at room temperature did indeed cause the precipitation of more ionic liquid and halved the level of contamination.

Using a higher than equimolar amount of ethanol only slightly decreases the amount of DBU contaminating the oil, but significantly increases the amount of ethanol contaminating the oil (using 5 ml ethanol: 2 ml DBU: 2 ml oil gave, after CO_2 treatment, oil containing 1.3 wt% DBU and 7.1 wt% ethanol).

If needed, any trace amounts of remaining DBU could be easily removed by treatment of the oil with acidic or carbonated water or by passing the oil through silica.

These promising results showed that investigation of the extraction of oil from soybean flakes by DBU/ethanol SPS and related solvents was warranted. Extractions with an equimolar mixture of DBU and anhydrous ethanol were run at both 25 °C and 70 °C (Figs. 3 and 4). Flaked soybeans (4 g) obtained from the industrial process were added to a sealed reaction vessel. Pre-heated solvent (20 g) was then added to the vessel. The vessel contents were only stirred slowly to simulate the industrial process, in which there is no stirring but rather flow of liquid over the flakes. Samples were taken by drawing up small aliquots through a 0.45 μm filter and analyzing for total oil by HPLC. The performance of hexane at 60 °C (as currently used in the industry) is shown for comparison. Given the gentle agitation, it is likely that mass transfer limitations are, at least in part, influencing the rate of extraction.
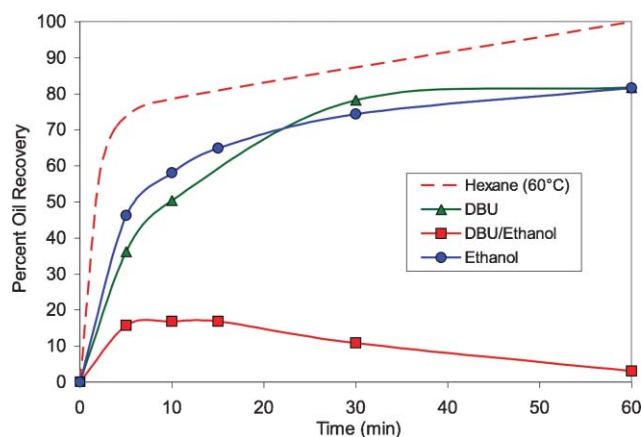
Fig. 3 Extraction of soybean oil from flakes at 70 °C using DBU, DBU/ethanol, and ethanol. Percent oil recovery based upon 23.35% total oil in the flakes. Hexane control experiment was performed at 60 °C.
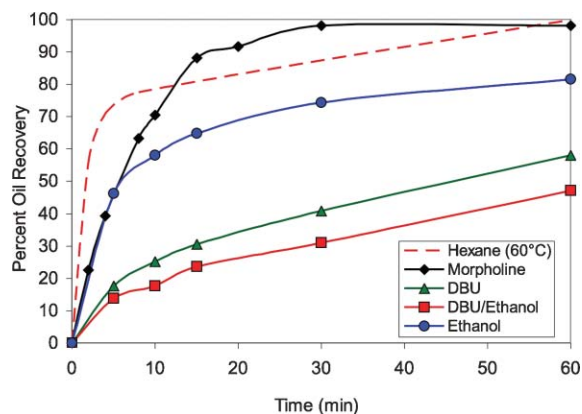
Fig. 4 Extraction of soybean oil from flakes at 25 °C using morpholine, DBU, DBU/ethanol, and ethanol. Percent oil recovery based upon 23.35% total oil in the flakes. Hexane control experiment was performed at 60 °C.

At 25 °C, DBU/ethanol extracted oil more slowly than ethanol or DBU alone, and much more slowly than the hexane control (at 60 °C). Only 45% of the oil was recovered after 60 min using the DBU/ethanol solution. In fact, the addition of DBU to anhydrous ethanol reduces ethanol's extracting power by nearly half. Increasing the extraction temperature to 70 °C gave marked improvement of 20% in DBU's extracting ability and no change in ethanol's extracting ability. Unfortunately, the soy oil proved highly unstable in the DBU/ethanol solution at 70 °C. Qualitative HPLC analysis showed that transesterification occurred under these conditions, resulting in the formation of mainly ethyl linoleate. For this reason, plus the possibility that water in the soybean flakes may interfere with the DBU/ethanol switchable solvent, this strategy has been rejected. A modification of the strategy shown in Fig. 2, using DBU as the sole extraction solvent and only adding the alcohol after the extraction is complete, would eliminate this transesterification problem for the first use of the solvent, but any attempt to recycle the DBU/ROH mixture for another extraction would result in transesterification.

A process for separating soy oil from the extraction solvent using secondary amine switchable solvents would be similar to one using amidine/alcohol switchable solvents except for the greater operational simplicity of using a single liquid component solvent rather than a mixture. Also, the transesterification observed with the DBU/ethanol system will not occur with the secondary amines.

Morpholine was chosen as a representative solvent to determine if secondary amines in general are capable of extracting soy oil from flakes. In the experiment, flaked soybeans (4 g) and solvent (20 g) were added to a sealed reaction vessel. Samples were taken by drawing up small aliquots through a 0.45 μm filter and analyzing for total oil by HPLC. An extraction of soybean flakes with hexane at 60 °C was used as a control. Morpholine at 25 °C is comparable to hexane at 60 °C for extracting soybean oil from flaked soybeans (Fig. 3). The extraction occurs slightly more slowly when using morpholine, but this could easily be due to the difference in extraction temperatures.

Dialkylamine/soy oil mixtures behave in different ways upon exposure to CO_2. NHBuEt is miscible with soy oil before and after CO_2 treatment. Morpholine precipitates as a white paste from soy oil upon treatment with CO_2, but the paste can not be easily filtered from the oil. Benzylmethylamine has, in its ionic form, sufficient polarity to be immiscible with soybean oil. The nonionic form of benzylmethylamine is miscible with soy oil at room temperature, but after the amine/oil mixture has been exposed to CO_2 and allowed to settle, two liquid phases slowly separate. Analysis of the oil layer showed that it contains 12 wt.% of the amine. Although removal of the remaining amine should presumably be possible by washing the oil in acidic water, the high level of contamination after the CO_2 treatment makes this strategy undesirable.

Another concern with benzylmethylamine is the cancer risk. Although benzylmethylamine occurs naturally in carrots and green salad, tests in rats show that the amine can be a precursor for N-nitroso-N-benzylmethylamine, a cause of esophageal cancer.[16]

Because of the high level of contamination of the oil and the health concerns, work with benzylmethylamine was discontinued.

Strategy 2: Extraction of oil with switchable-hydrophilicity solvents followed by water wash

The second strategy to be evaluated employs a solvent that can switch from hydrophobic/lipophilic to hydrophilic and back again. In this strategy (Fig. 5), a switchable solvent would be identified that is sufficiently lipophilic to extract the oil from the soybean flakes. After filtration to remove the flakes, the oil/solvent mixture would be exposed to water and the solvent would be switched by CO_2 to a state that is so hydrophilic that it partitions preferentially into the aqueous phase from the oil. If the hydrophilicity is sufficient, the amount of solvent remaining in the oil will be very low. The solvent would then have to be recovered from the water, either by distillation or by switching the solvent back to its hydrophobic form.

DBU was chosen as the first test solvent for this process for several reasons. Extraction data on actual flaked soybeans (detailed above, and shown in Fig. 3) showed 80% oil recovery
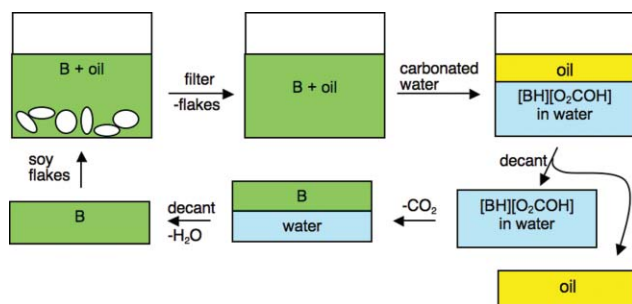
Fig. 5 A process utilizing a switchable-hydrophilicity solvent (hydrophobic state labelled "B") to extract soybean oil followed by switching of the solvent to a hydrophilic state ([BH][O$_2$COH]) so that it is easily extracted by water.

Table 3 Levels of contamination of soy oil after contact with ionic liquids prepared from CO$_2$ and equimolar mixtures of DBU and water or an alcohol[a]

ROH	ROH volume, ml	Contamination after first separation,%	Contamination after second separation,%
Water	0.4	6.2% DBU	1.8% DBU
MeOH	0.6	Poor separation	—
EtOH	1.6	2.1% DBU 0.52% EtOH	0.75% DBU 0.26% EtOH

[a] 4 ml of soy oil, 3.0 ml of DBU, 1 h of CO$_2$ bubbling at room temperature.

after 60 minutes of extraction with pure DBU at 70 °C. Also, we have found, during our work on switchable solvents,[4,17] that the hydrophilicity of DBU is switchable, in the sense that the partitioning of DBU into an organic solvent from water is greater in the presence of CO$_2$ than in its absence.[9] However, it was not clear how well DBU can be removed from the oil by water. While the 1.8% remaining contamination reported in Table 3 is promising, it was hoped that using a significant excess of water might reduce the level of DBU found in the separated oil.

In each of five identical trials, soy oil, DBU, and water (2 ml of each) were mixed together, CO$_2$ was bubbled through the mixture for 1 h, and the liquid was allowed to settle overnight. The soy oil layer was found to have an average of 0.5% DBU, with the highest being 1.2% and two of the five trials showing no detectable DBU (i.e. below the 0.1% detection limit of the analytical method). Thus, the use of excess water does decrease the amount of DBU in the soy oil compared to the 6.2% that was found when only an equimolar amount of water was used (as in Table 3).

The hardest part of the process in Fig. 5 is the separation of the solvent from the water. Removal of the CO$_2$ causes DBU to become much less hydrophilic, but not to the extent that it separates from water. The only successful method found in our tests was to distill all of the water from the DBU. The addition of salt to the water does not force the DBU to separate. We are currently searching for amidines that are sufficiently hydrophobic that removal of CO$_2$ from the water/amidine mixture would cause a phase separation. Such an amidine, were it to be found, would have the greatest potential for solving the soybean oil problem.

Strategy 3: Extraction of oil with moderate-polarity solvent followed by water wash

Extraction of oil from soybean flakes using a moderate-polarity solvent would give a mixture of soybean oil and the solvent, from which the solvent would be extracted by water (Fig. 6). Recycling of the solvent and the water would only be possible if the solvent could be separated from the water. Distillation is possible, but we are restricting ourselves to processes at or near ambient temperature. An alternative method for separating organic solvents from water is solvent expansion by CO$_2$. Dissolution of pressurized CO$_2$ gas into an organic liquid causes the liquid to expand volumetrically and to become less polar.[18] The polarity drop can cause the liquid to become immiscible with water. Thus dissolution of CO$_2$ into the solvent/water mixture could be the basis for a non-distillative method of separating the solvent from the water and allowing the recycling of both. Note that this strategy differs from the first two strategies in requiring the use of elevated pressures of CO$_2$, likely between 50 and 75 bar.
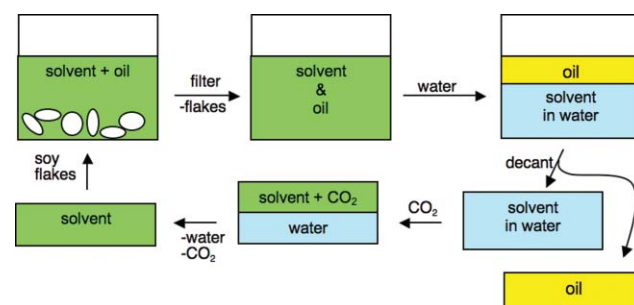
Fig. 6 A process utilizing a moderate polarity solvent to extract soybean oil followed by extraction of the solvent by water and CO$_2$ expansion to separate the solvent from water.

In order for this process to work, the solvent must be a) miscible with soy oil, b) extractable from oil by water, and c) separable from water by CO$_2$ pressure. A comparison of several potential solvents, all of which are miscible with soy oil, is shown in Table 4. Extractability of a solvent by water from a nonpolar organic liquid is usually quantified as the logP of the solvent, where P is the partition coefficient for the solvent molecule partitioning between 1-octanol and water. A positive logP value indicates a molecule that partitions preferentially into octanol rather than water. Those solvents with positive logP values can be rejected because they will be too difficult to extract from the oil with water. Finally, there is some limited data on the CO$_2$ pressure required for the separation of solvents from water,[19–23] summarized in a recent review paper.[18] The remaining two solvents in Table 4, acetone and 1,4-dioxane, are the most likely candidates.

Three solvents were tested in a preliminary experiment: THF, dioxane and acetone. Mixtures of soy oil (2 ml), water (1 ml) and solvent (4 ml) were prepared in glass vials. After thorough mixing, the contents of the vials were allowed to settle. In the case of THF, the water formed a thin layer at the bottom (Fig. 7, left), showing that the THF did not partition significantly into the water, as expected given the fact that the logP of THF is greater than zero. In the case of dioxane, the water formed a thick layer at the bottom (Fig. 7, centre), indicating that the

Table 4 A comparison of solvents potentially suitable for the process in Fig. 6

Solvent	logP	P_{CO_2} for separation from water, bar	Reference for separation from water
Hexane	3.5	—	—
THF	0.5	<10	22
n-PrOH	0.28	68	21
Acetone	−0.23	26	20
1,4-Dioxane	−0.27	<28	23

Fig. 7 Mixtures of soy oil (2 ml), water (1 ml) and solvent (4 ml), where the solvent is THF (left), dioxane (centre), or acetone (right).

dioxane partitioned largely into the water rather than the oil. This is the desired situation for the proposed process. In the case of acetone, the separation was not clear (Fig. 7, right) until many hours had passed. This preliminary experiment shows that dioxane is a viable candidate.

To determine the amount of dioxane remaining in the soy oil after extraction of the bulk of the dioxane by water, the experiment was repeated with different amounts of water. After shaking and then a week of settling time (to ensure that equilibrium conditions were obtained), the amount of dioxane remaining in the soy oil was determined by ^{1}H NMR spectroscopy (Fig. 8). Even using 15 mL of water was insufficient to bring the dioxane content of the oil down to a few percent. Using several smaller amounts of water or using continuous countercurrent washing with water would greatly decrease the amount of dioxane remaining in the oil and decrease the amount of water required to remove the dioxane. For example, two washes of 2 ml each results in the oil containing only 7.7 wt% dioxane, compared to 28% remaining after one wash of 4 ml
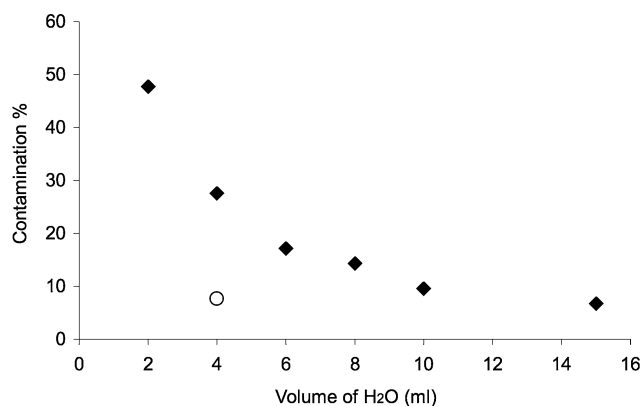
Fig. 8 The amount of dioxane remaining in soy oil after extraction of most of the dioxane with a single wash with water. The hollow circle represents the result after two washes with water totalling 4 ml.

(Fig. 8). Two washes, one of 10 ml and a second of 5 ml, brought the dioxane content of the oil to 2.7 wt%, which is 2.5 times lower than the amount after a single wash of 15 ml water.

It is known from the literature that application of CO_2 pressure to a water/dioxane mixture can cause the mixture to separate into two phases: a water-rich phase and a dioxane-rich phase. Application of a minimum of 28 bar of CO_2 at 40 °C causes water and dioxane to split in this manner,[23] but application of higher pressures gives much better separation. From Fig. 9, one can determine the minimum pressure required to induce a phase split; draw a horizontal line at the composition of the mixture – the pressure at which that line crosses a curve is the minimum pressure required. Mixtures having compositions below 2 wt% or above 80 wt% water will not phase-split. For example, a 70/30 water/dioxane mixture would start to split into two liquid phases at 44 bar. Increasing the pressure to 57 bar would improve the separation, giving an aqueous phase containing 19.7% dioxane and a dioxane phase containing 2.2% water (neglecting the CO_2 content of the liquid phases).
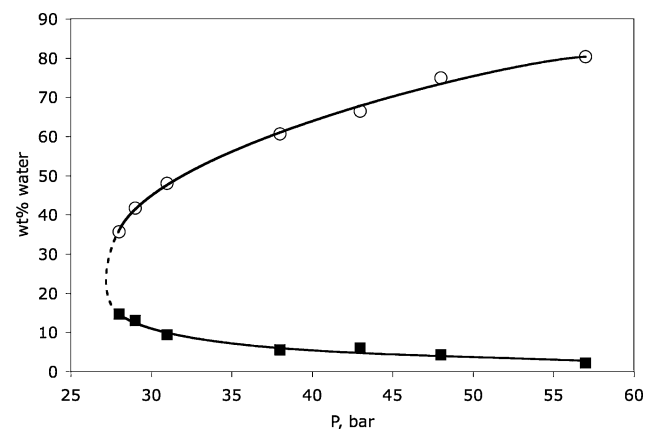
Fig. 9 The composition of the two liquid phases present in a dioxane/water mixture under CO_2 pressure, neglecting the CO_2 content of the phases, as a function of the CO_2 pressure at 40 °C. Dioxane/water mixtures having an overall composition between the two curves would split into two liquid phases when subjected to the indicated pressure of CO_2. The upper curve gives the composition of the water-rich phase while the lower curve represents the dioxane-rich phase. Calculated from the data of Lazzaroni et al.[23]

The water/dioxane mixture resulting from the washing of dioxane from the soy oil could be separated into a water-rich phase and a dioxane-rich phase by the application of gaseous CO_2 pressure. For this to be effective, the amount of water used to wash the dioxane from the oil must be kept at a minimum, because CO_2 pressure will not induce the phase separation of small amounts of dioxane from water. Counter-current extraction of dioxane from the oil should help minimize the amount of water needed. It is reasonable to anticipate that the wash water from an optimized process would contain 30% dioxane by volume. As shown in Fig. 9, the application of a CO_2 pressure of 57 bar to such a mixture would create a phase split. The dioxane phase, which would contain very little water, could be re-used immediately for the extraction of more soy oil from flakes. The aqueous phase would still contain a significant amount of dioxane (about 20%). It seems unlikely that this aqueous phase could be re-used without removal of more of

the dioxane. Further experimentation is necessary to determine methods for improving the separation of the dioxane from water; potential methods might include using different temperatures or pressures, the use of liquid or supercritical CO_2 instead of gaseous CO_2, additives in the water, or replacing dioxane with a different solvent.

Conclusions

Several hexane-free alternatives for the extraction of soybean oil from flakes have been evaluated.

a) Strategy 1, using an amidine/alcohol switchable solvent, gave excellent separation but was rejected because transesterification occurs during the extraction and because water from the soybean flakes may interfere with the DBU/ethanol solvent switching process.

b) Strategy 1, using a secondary amine switchable solvent, was rejected because the only secondary amine that worked successfully has serious health implications, because the contamination levels were too high, and because the separation was too slow.

c) Strategy 2, the combination of an amidine and excess water gave superior solvent/oil separation, adequate oil extraction, and was insensitive to adventitious water. The contamination levels of residual amidine in the soy oil are very low. This method takes advantage of the fact that amidines can be made to switch their hydrophilicity by application or removal of CO_2 in the system. While the separation of the amidine from water remains difficult, the results show that the identification of a switchable hydrophilicity solvent, especially one that in the absence of CO_2 is sufficiently hydrophobic to readily separate from water, is greatly needed. Work in that direction is underway.

d) Strategy 3, the use of dioxane to extract soy oil from flakes, followed by removal of the dioxane from the oil by water, results in soy oil that contains 2 to 8% dioxane after batch extraction. Use of counter-current extraction should give much better results. The water phase contains up to 30 vol% dioxane. Partial separation of the dioxane from the water can be achieved by CO_2 pressurization, giving a fairly pure dioxane phase and an aqueous phase that still contains a significant amount of dioxane. Extraction of dioxane from water using higher pressures of CO_2 or especially liquid CO_2 would require slightly higher pressure but give much more complete separation of dioxane from water.

Acknowledgements

Notes and references

1 D. R. Erikson, *Practical Handbook of Soybean Processing and Utilization*, AOCS Press and United Soybean Board, St. Louis, 1995.
2 U. Sievers, *Chem. Eng. Process.*, 1998, **37**, 451–460.
3 N. T. Dunford, in *Nutritionally Enhanced Edible Oil and Oilseed Processing*, eds. N. T. Dunford and H. B. Dunford, AOCS Press, Editon edn., 2004, pp. 100–116.
4 P. G. Jessop, D. J. Heldebrant, L. Xiaowang, C. A. Eckert and C. L. Liotta, *Nature*, 2005, **436**, 1102.
5 L. Phan, J. R. Andreatta, L. K. Horvey, C. F. Edie, A.-L. Luco, A. Mirchandi, D. J. Darensbourg and P. G. Jessop, *J. Org. Chem.*, 2008, **73**, 127–132.
6 L. Phan, X. Li, D. J. Heldebrant, R. Wang, D. Chiu, E. John, H. Huttenhower, P. Pollet, C. A. Eckert, C. L. Liotta and P. G. Jessop, *Ind. Eng. Chem. Res.*, 2008, **47**, 539–545.
7 T. Yamada, P. J. Lukac, M. George and R. G. Weiss, *Chem. Mater.*, 2007, **19**, 967–969.
8 T. Yamada, P. J. Lukac, T. Yu and R. G. Weiss, *Chem. Mater.*, 2007, **19**, 4761–4768.
9 P. G. Jessop and L. Phan, 2008, manuscript in preparation.
10 F. Ratkovics and L. Domonkos, *Acta Chim. Acad. Sci. Hung.*, 1976, **89**, 325–330.
11 D. R. Lide, ed., *CRC Handbook of Chemistry and Physics*, 84th edn., CRC Press, Boca Raton, Florida, 2003.
12 A. F. M. Barton, *Handbook of Solubility Parameters and Other Cohesion Parameters*, 2nd edn., CRC Press, Boca Raton, 1991.
13 I. M. Smallwood, *Handbook of organic solvent properties*, Halsted, New York, 1996.
14 D. R. Erickson, E. H. Pryde, O. L. Brekke, T. L. Mounts and R. A. Falb, *Handbook of Soy Oil Processing and Utilization*, American Soybean Association, St. Louis, 1980.
15 P. G. Jessop, C. A. Eckert, C. L. Liotta, "Switchable Solvents and Methods of Use Thereof," U.S. Patent, Application 60/781,336, filed 13 March 2006. Canadian Patent Application No. 2,539,418, filed 13 March 2006.
16 C. C. Hsia, T. T. Sun, Y. Y. Wang, L. M. Anderson, D. Armstrong and R. A. Good, *Proc. Nat. Acad. Sci. USA*, 1981, **78**, 1878–1881.
17 D. J. Heldebrant, P. G. Jessop, C. A. Thomas, C. A. Eckert and C. L. Liotta, *J. Org. Chem.*, 2005, **70**, 5335–5338.
18 P. G. Jessop and B. Subramaniam, *Chem. Rev.*, 2007, **107**, 2666–2694.
19 M. Wendland, H. Hasse and G. Maurer, *J. Supercrit. Fluids*, 1993, **6**, 211–222.
20 M. Wendland, H. Hasse and G. Maurer, *J. Supercrit. Fluids*, 1994, **7**, 245–250.
21 T. Adrian and G. Maurer, in *High Pressure Chemical Engineering: Proceedings of the 3rd International Symposium on High Pressure Chemical Engineering, Zurich, Switzerland, 7–9 October, 1996*, eds. P. R. von Rohr and C. Trepp, Elsevier, Amsterdam, Editon edn., 1996, pp. 241–246.
22 J. Lu, M. J. Lazzaroni, J. P. Hallett, A. S. Bommarius, C. L. Liotta and C. A. Eckert, *Ind. Eng. Chem. Res.*, 2004, **43**, 1586–1590.
23 M. J. Lazzaroni, D. Bush, R. Jones, J. P. Hallett, C. L. Liotta and C. A. Eckert, *Fluid Phase Equilib.*, 2004, **224**, 143–154.

The mechanism of the oxidation of benzyl alcohol by iron(III)nitrate: conventional *versus* microwave heating

Mark H. C. L. Dressen,[a] Jelle E. Stumpel,[a] Bastiaan H. P. van de Kruijs,[a] Jan Meuldijk,[b]
Jef A. J. M. Vekemans[a] and Lumbertus A. Hulshof*[a,c]

The mechanism of the oxidation of benzyl alcohol with iron(III)nitrate nonahydrate under conventional and under microwave heating conditions has been investigated and the reaction conditions have been optimized. A series of redox reactions leads to the formation of benzaldehyde and other products. Direct comparison between conventional and microwave heating revealed identical conversions profiles. Mastering the microwave induced heat, absence of a real microwave effect and byproduct formation are the major factors to advise a traditional batch-wise way of process development to a larger scale.

Introduction

In recent years much effort has been expended in an increasingly competitive world to meet the requirements of the fine chemical and pharmaceutical industry focusing on "first-time-right" performance, a short-time-to-market and avoiding surprises during process scale-up. A demand for larger quantities is not just rewriting a recipe by replacing "mg" with "kg" during chemical process research, which is largely based on changes of physical dimensions and other economic, technological and ecological factors including quality and safety aspects. Intensifications in process architecture, such as microreactor technology and microwave enhanced processing, as relatively novel tools in the field of organic chemistry, are actively pursued to achieve a better position in the industrial scene. The emersion of these promising techniques in the field of organic chemistry expands the toolbox of today's chemists.

The increase of reaction rates and improved selectivity, combined with the automation of repetitive procedures, demonstrate the advantageous application of these enabling techniques and are considered to be suitable for the job. One of the major drawbacks of microwave-assisted chemistry is the difficulty associated with process scale-up. Since the penetration depth of microwaves is limited, the best opportunities for increased production volumes lie in continuous-flow processing equipment, albeit that this is somewhat uncommon in the fine chemical industry.[1,2]

Although this combined technological concept of flow chemistry and microwave heating has demonstrated positive results,[2] the fundamental aspects of the rate enhancements remain unclear, and thermal as well as non-thermal effects are invoked to rationalize it.[3–6] Limited insight into the so called microwave

effects has been gained. These effects are defined as a rate enhancement or change of selectivity of chemical processes under microwave heating that cannot be reproduced under conventional heating. A thorough investigation of all techniques separately by accurate temperature measurements from inside either by fiber optics or by a gas-pressure sensor will strongly contribute to the reliability of the claims regarding microwave effects and will provide a real understanding of these rate enhancements.

The main focus of our research is aimed at a systematic investigation of the influence of microwave heating on chemical processes and assessing the technique for application on an industrial scale. We have demonstrated positive effects in terms of reaction rate enhancements of microwave heating compared to conventional heating in three cases of heterogeneous reactions.[7] These effects vanished completely or partly when either the heterogeneity of the system was diminished or when the metal surface was cleaned with an initiator in the case of metal mediated reactions. The observations suggested that these favorable microwave-induced rate enhancements might not appear when homogeneous systems are carefully scrutinized under entirely comparable conditions for microwave and conventional heating. The absence of microwave effects under homogeneous conditions in combination with the low energy ($\sim 10^{-5}$ eV) of a microwave photon make a direct influence of microwaves on the reaction mechanism highly unlikely.

The oxidation of benzyl alcohol with iron(III)nitrate nonahydrate has been amply reported. Good selectivity under mild reaction conditions and convenient isolation of the products were achieved employing various inorganic supports, such as silica gel,[8] K10-clay,[9] HZSM-5 zeolite,[10] kieselguhr[11] and graphite.[12] The K10 clay-supported version gave reaction rate enhancements under microwave irradiation conditions in the absence of solvents.[13] The oxidation rate of benzyl alcohol has been reported to be positively influenced by a combination of microwave heating and microreactor technology (Scheme 1).[4]

To our surprise these rate enhancements were reported for a homogeneous system. The paper prompted us to gain more insight in the microwave effect in this particular case. We

[a]Laboratory of Macromolecular and Organic Chemistry, Applied Organic Chemistry, Eindhoven University of Technology, Den Dolech 2, 5612 AZ, Eindhoven, The Netherlands. E-mail: L.A.Hulshof@tue.nl.
[b]Process Development Group, Eindhoven University of Technology, Den Dolech 2, 5612 AZ, Eindhoven, The Netherlands
[c]DSM Research, PO Box 18, 6160 MD, Geleen, The Netherlands
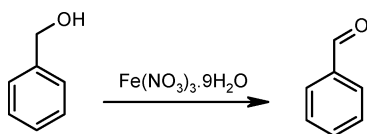
Scheme 1 Oxidation of benzyl alcohol with iron(III)nitrate nonahydrate.

investigated in detail the mechanism of this oxidation under conventional heating conditions. Subsequently, microwave heating has been applied to this homogeneous reaction aimed at witnessing any beneficial effect in a batch-wise setup with accurate temperature control. Furthermore, the process scalability has been assessed predominantly based on chemical aspects.

Results of conventional heating

In contrast to the reactions in a flow-reactor described by Jachuck *et al.*,[14] the oxidation of benzyl alcohol with $Fe(NO_3)_3 \cdot 9H_2O$ has been performed neat under aerobic conditions in an open vessel at various elevated temperatures reached by conventional heating.

Overview of operational reactions

In the first place it was found that the oxidation of benzyl alcohol with $Fe(NO_3)_3 \cdot 9H_2O$ includes a series of possible redox reactions. These reactions may occur with the oxidant and benzyl alcohol in the presence of water from the nonahydrate. This water is released upon dissolution of the iron(III) salt in benzyl alcohol. The rather complex reaction network may give rise to uncertainty in the exact stoichiometry. In general this oxidation is based on the hydrolysis of iron(III)nitrate,[15] see Scheme 2.

$$2\,Fe(NO_3)_3 + 3\,H_2O \rightleftharpoons Fe_2O_3 + 6\,HNO_3$$
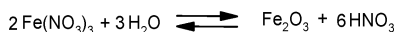
Scheme 2 The oxidation is based on the hydrolysis of iron(III)nitrate.

During the reaction also brown fumes were observed referring to the presence of NO_2, which led to a volume expansion of 42 mL gas per mL benzyl alcohol (molar ratio of benzyl alcohol : $Fe(NO_3)_3 \cdot 9H_2O$ is 4 : 1). The evolution of brown fumes was not observed when the reaction was performed in an argon or nitrogen atmosphere, indicating a direct oxidation of NO to NO_2 under aerobic conditions. However, working under anaerobic conditions lowered the conversion of benzyl alcohol by 15% as compared to aerobic conditions for the optimized reactions (Fig. 3). This result demonstrates that the absence or presence of oxygen has a profound effect on the stoichiometry of the reaction and also that a flow system leads to inferior conversions.

It was expected that iron(III) either acts as a catalyst for the oxidation under aerobic conditions or is consumed by the oxidation. Therefore, the amount of iron(III) was determined by a titration with EDTA before and after the reaction.[16] After the reaction was completed the amount of iron(III) in the reaction mixture was found to be unchanged within experimental error. However, by autodecomposition of iron(II)nitrate as an *in-situ* process, iron(II) may be formed, but this does not remain in this oxidative state in the reaction mixture by a redox reaction (see Scheme 3).[17]

Fig. 1 Time–molar composition plot of the oxidation of benzyl alcohol at a molar ratio of benzyl alcohol and $Fe(NO_3)_3 \cdot 9H_2O$ of 100 : 1 at 50 °C under conventional heating and aerobic conditions.
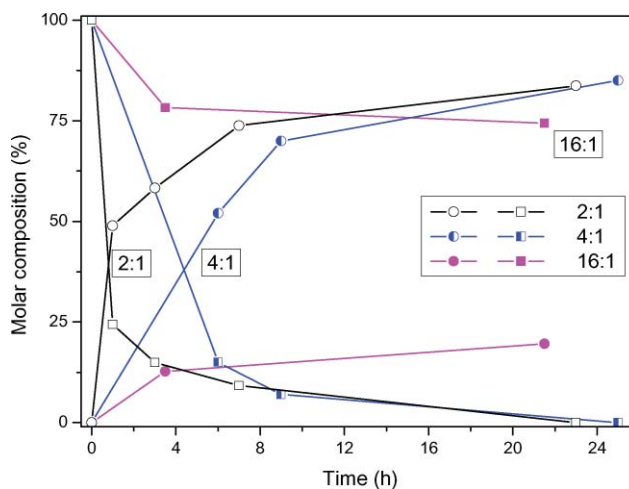

Fig. 2 Conversion of benzyl alcohol (■) and formation of benzaldehyde (●) as a function of the initial molar ratio of benzyl alcohol and $Fe(NO_3)_3 \cdot 9H_2O$ at 50 °C under conventional heating and aerobic conditions.

$$18\,Fe(NO_3)_2 + \cancel{15\,H_2O} \rightleftharpoons 4\,Fe_2O_3 + 10\,Fe(NO_3)_3 + 6\,NO + \cancel{15\,H_2O}$$
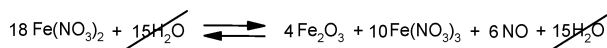
Scheme 3 (Auto)decomposition of iron(II)nitrate reproduces iron(III).

The role of iron(III) in the oxidation of benzyl alcohol is purely catalytic by coordinating the oxidant to the alcohol. Even though there is a combination of nitrate and iron(III) in one salt, a molar ratio of benzyl alcohol and $Fe(NO_3)_3 \cdot 9H_2O$ of 100 : 1 at 50 °C is insufficient to bring the reaction to completion. The conversion completely flattens off after a few hours, see Fig. 1.

Although overall iron(III) remains in its original oxidative state, the counter-ion in its original salt form has changed into the oxide-salt thus lowering the iron(III) concentration in solution by precipitation during the reaction.

Formation of (by-)products

Throughout the reaction at various temperatures, the formation of two byproducts has been observed, namely benzyl nitrite[18] and benzyl nitrate.[19] The proposed sequence of reactions during
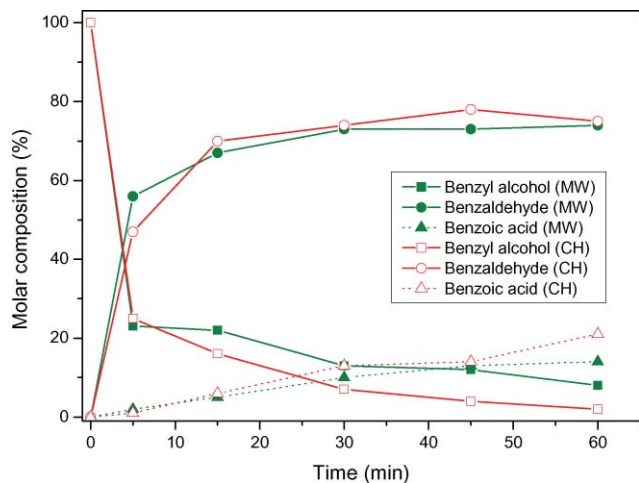
Fig. 3 Time–molar composition plot of the oxidation of benzyl alcohol at a molar ratio of benzyl alcohol and $Fe(NO_3)_3 \cdot 9H_2O$ of 4 : 1 at 100 °C under comparable conventional heating (CH) and microwave (MW) heating (aerobic conditions).

the oxidation of benzyl alcohol to benzaldehyde are depicted in Schemes 4 and 5.

In Scheme 4 the postulated reactions lead to a 2 : 1 molar ratio of benzyl alcohol and $Fe(NO_3)_3 \cdot 9H_2O$. To rationalize the observation that a 4 : 1 molar ratio nearly leads to completion, the reactions as proposed in Scheme 5 should also be integrated. Water and oxygen act as an oxidant in this process by reactivating NO.

Scheme 5 Reactions rationalizing a higher than 2 : 1 ratio in stoichiometry of benzyl alcohol and $Fe(NO_3)_3 \cdot 9H_2O$.

Molar ratio benzyl alcohol and $Fe(NO_3)_3 \cdot 9H_2O$

An increase in the amount of iron(III)nitrate, with respect to benzyl alcohol, leads to an increase of the reaction rate at 50 °C. See Fig. 2 for the time–conversion plots.

At a molar ratio of 16 : 1 (benzyl alcohol : $Fe(NO_3)_3 \cdot 9H_2O$) at room temperature, benzyl alcohol was found to be saturated with $Fe(NO_3)_3 \cdot 9H_2O$ affording a homogeneous solution.[20] Larger amounts of $Fe(NO_3)_3 \cdot 9H_2O$ resulted in two liquid phases. In that case, the bottom layer primarily consists of inorganic salt, melting point 47 °C, while the top layer is rich in benzyl alcohol. The heterogeneous nature of such reaction systems hampers a simple kinetic evaluation of the oxidation process.

Each reaction mixture with varying amounts of $Fe(NO_3)_3 \cdot 9H_2O$ eventually forms a substantial amount of red-brown sediment on the reactor wall. An XPS analysis of the sediment points to a mixture of FeO_x and $FeNO_x$. The formation of sediment is explained by Schemes 2 and 3.

Almost full conversion within one hour was achieved at 100 °C when a 4 : 1 molar ratio of benzyl alcohol and $Fe(NO_3)_3 \cdot 9H_2O$

Scheme 4 Reactions rationalizing a 2 : 1 ratio in stoichiometry of benzyl alcohol and $Fe(NO_3)_3 \cdot 9H_2O$.

was applied giving a selectivity of 75% to benzaldehyde, see Fig. 3. Three important issues are noteworthy. Firstly, under saturated conditions (16 : 1) the reactions appear to level off at 25% conversion, which is in line with the results obtained in Fig. 1. Secondly, over-oxidation leading to benzoic acid has been observed in all cases, which implicates the presence of an optimum for the conversion to benzaldehyde. And in the third place, high temperatures should be avoided due to instability of the byproducts during this oxidation.[21]

Results of microwave heating

In a next step, the influence of microwave heating on the course of the oxidation of benzyl alcohol was assessed at temperatures of 50 °C and 100 °C. These two temperature levels were primarily used to gain insight into the potential of microwave heating (MW) compared to conventional heating (CH), as claimed by Jachuck *et al.*[4] The molar compositions of benzaldehyde and benzyl alcohol in the reaction mixture are shown in Fig. 3 and 4.

Experiments with conventional heating and microwave heating at 50 °C and 100 °C can be directly compared due to similar reaction vessels, stirring speeds and heating profiles. Surprisingly, no significantly higher reaction-rate with microwave heating was observed at 100 °C for the experimental conditions (4 : 1 molar ratio of benzyl alcohol and $Fe(NO_3)_3 \cdot 9H_2O$). Subsequently, for the same initial reaction conditions at 50 °C for a 16 : 1 molar ratio of benzyl alcohol and $Fe(NO_3)_3 \cdot 9H_2O$ again no beneficial effect was observed (Fig. 4).
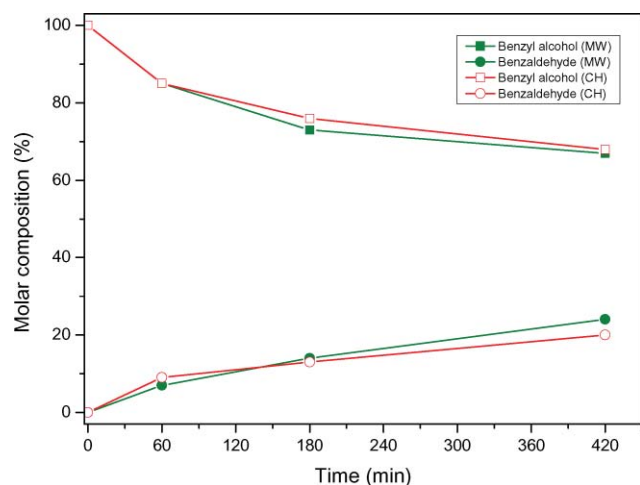
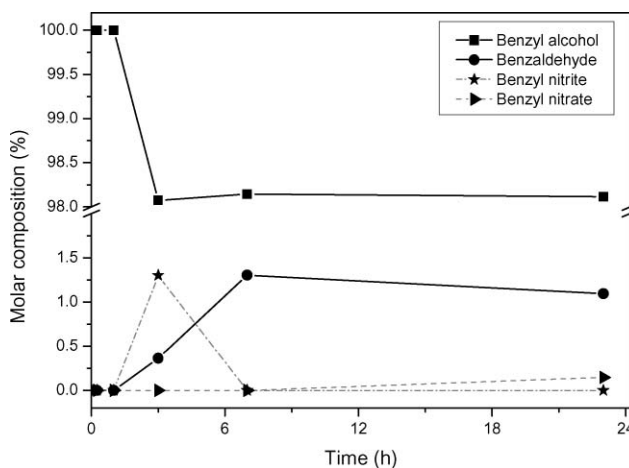**Fig. 4** Time–molar composition plot of the oxidation of benzyl alcohol at a molar ratio of benzyl alcohol and $Fe(NO_3)_3 \cdot 9H_2O$ of 16 : 1 at 50 °C under comparable conventional heating (CH) and microwave (MW) heating (aerobic conditions).
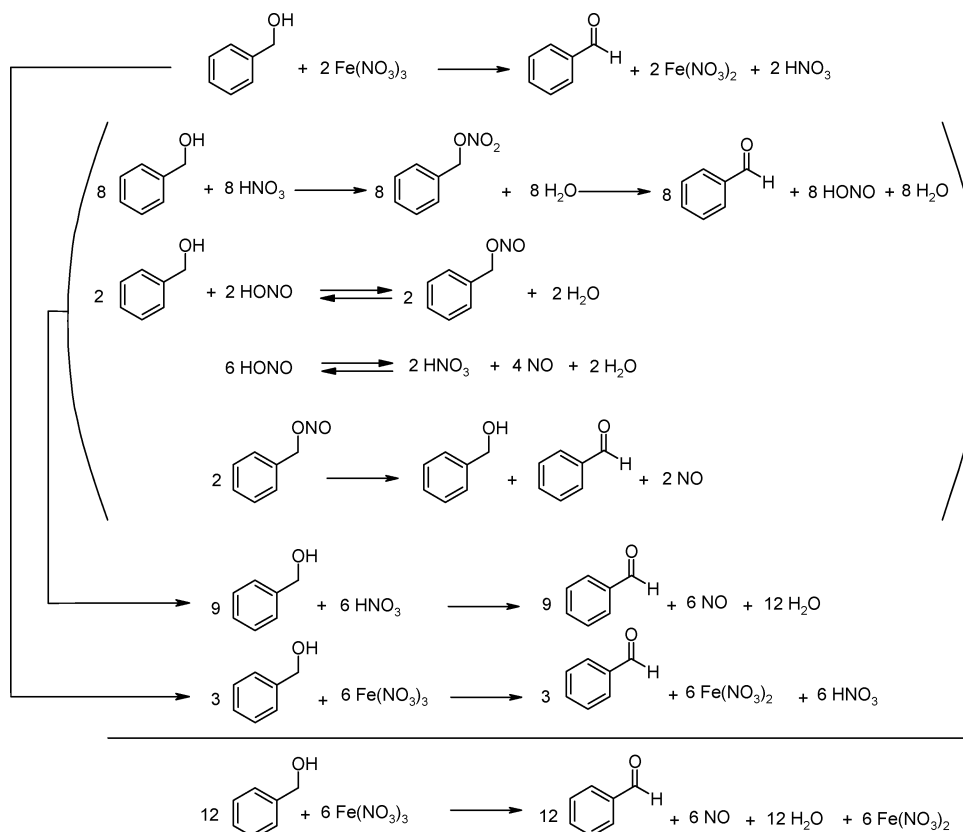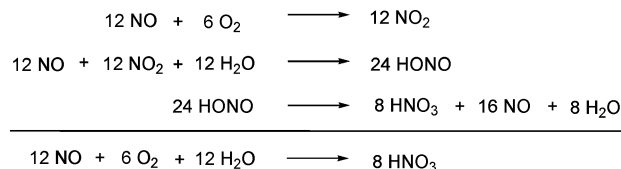
Conclusions

Direct comparison (*i.e.* open vessel, same stirrer speed, same heating-up rate and internal temperature measurements) of the oxidation of benzyl alcohol with iron(III)nitrate nonahydrate under atmospheric conditions for homogeneous (initially) and heterogeneous reaction mixtures did not reveal any positive microwave effect. Under anaerobic conditions an increased

amount of iron(III)nitrate nonahydrate is necessary to reach full conversion of benzyl alcohol.

Based on the results obtained for both conventional and microwave heating it is concluded that the conventional batch heating procedure should be recommended as the method of choice for a scalable process. This conclusion is supported by the observation that any microwave-induced reaction-rate enhancement is lacking when the heating conditions are systematically compared. In our group, the transfer of batch processes to a flow reactor has demonstrated to occur with preservation of kinetics and reaction rates.[22] Processing in a continuous mode is not preferable due to the necessity of aerobic conditions for completion of the reaction with the minimal economical amount of oxidant, the formation of a sediment during the reaction and the evolution of nitric fumes. The tremendously high heating rate as a result of a strong absorption of microwave energy by the reaction mixture leads to the conclusion that microwave heating is not the preferred method for safe operation on larger scales. These high heating rates lead to a rapid increment of temperature (and pressure) when the reaction is performed in a closed system with indirect temperature control. Accurate temperature control is a prerequisite for assignment of microwave effects on the rates of chemical reactions.

Experimental

In our setup, a commercially available, automated multimode microwave oven, MicroSynth from Milestone s.r.l. (Italy), was used. This oven operates at 2.45 GHz and is temperature-controlled by a fiber-optic sensor. During our microwave experiments the maximum power was set at 100 W. The average power input was 18 W (50 °C) and 76 W (100 °C). The reaction mixture was analysed by ^{1}H NMR, GC-MS and GC-FID and conversion was determined by ^{1}H NMR. ^{1}H NMR spectra were recorded in $CDCl_3$ with a Varian Mercury 200 MHz with the aid of 1,3,5-tri-*tert*-butylbenzene as the internal standard. The proton chemical shifts were calibrated to tetramethylsilane (TMS). GC analyses were performed using a CP-Chiralsil-Dex CB (25 m × 0.25 mm) column with a FID detector with the aid of tetradecane as the internal standard or Zebron ZB-35 (30 m × 0.25 mm) column with a MS detector. The XPS (X-ray photoelectron spectroscopy) measurements were carried out with a VG Escalab MKII spectrometer, equipped with a dual Al/Mg Kα X-ray source and a hemispherical analyzer with a five-channeltron detector. Spectra were obtained using the aluminium anode (Al Kα = 1486.6 eV) operating at 300 W and a constant pass energy of 20 eV with a background pressure of 2×10^{-9} mbar.

Typical procedure for the oxidation of benzyl alcohol with iron(III)nonahydrate

Benzyl alcohol (2.0 mL, 19.4 mmol) and 1,3,5-tri-*tert*-butylbenzene (20 mg, 0.082 mmol) as internal standard were introduced in a 10 mL two neck round-bottomed flask, and heated in an oil bath or microwave oven. When the mixture reached the selected temperature, $Fe(NO_3)_3 \cdot 9H_2O$ (0.48 g, 1.2 mmol) was added, and the reaction was started. When the desired reaction time was reached, the reaction mixture was

eluted over a short silica column with a 5 μm-filter attached to the end, with an excess of diethyl ether. The diethyl ether phase was dried with MgSO₄, filtered, and evaporated to yield the product(s). ¹H NMR (CDCl₃, 200 MHz) typical signals δ (ppm) 1.35 (s, 27H, 1,3,5-tri-*tert*-butylbenzene), 4.70 (s, 2H, benzyl alcohol), 5.43 (s, 2H, benzyl nitrate), 5.71 (s, 2H, benzyl nitrite), 8.12 (d, 2H, benzoic acid), 10.03 (s, 1H, benzaldehyde).

Acknowledgements

References

1 I. R. Baxendale and M. R. Pitts, *Chem. Today*, 2006, **24**, 41.
2 T. N. Glasnov and C. O. Kappe, *Macromol. Rapid Commun.*, 2007, **28**, 395.
3 A. De la Hoz, A. Diaz-Ortiz and A. Moreno, *Chem. Soc. Rev.*, 2005, **34**, 164.
4 R. J. J. Jachuck, D. K. Selvaraj and R. S. Varma, *Green Chem.*, 2006, **8**, 29.
5 A. Cornélis and P. Laszlo, *Synthesis*, 1985, **10**, 909.
6 A. Loupy, *Microwaves in Organic Synthesis*, WILEY-VCH, Weinheim, 2006.
7 M. H. C. L. Dressen, B. H. P. Van de Kruijs, J. Meuldijk, J. A. J. M. Vekemans and L. A. Hulshof, *Org. Process Res. Dev.*, 2007, **11**, 865.
8 T. Nishiguchi and M. J. Bougauchi, *Org. Chem.*, 1989, **54**, 3001.
9 (*a*) A. Cornélis and P. Laszlo, *Synthesis*, 1980, 849; (*b*) S. E. Martin and D. F. Suárez, *Tetrahedron Lett.*, 2002, **43**, 4475.
10 M. M. Heravi, D. Ajami and M. M. Mojtahedi, *Chem. Commun.*, 1999, 833.
11 J.-D. Lou, L.-H. Zhu, Y.-C. Ma and L. Li, *Synth. Commun.*, 2006, **36**, 3061.
12 J.-D. Lou, X.-X. Cai, F. Li, L. Li and C.-L. Gao, *Synth. React. Inorg. Met.-Org. Nano-Met. Chem.*, 2006, **36**, 599.
13 R. S. Varma and R. Dahiya, *Tetrahedron Lett.*, 1997, **38**, 2043.
14 Experimental of ref. 4: The reactant was prepared at room temperature by dissolving solid Fe(NO₃)₃.9H₂O in the benzyl alcohol solution. The mixture was stirred thoroughly and filtered using a Fisherbrand1 filter paper. Experiments were performed using the continuous isothermal reactor under the influence of microwave irradiation for a range of residence times (3–17 s) corresponding to different flow rates (1–5 mL min⁻¹) and different microwave intensities (0 W to 39 W). The feed was pumped through the reactor using an HPLC pump and the heat transfer fluid (water) was circulated through the heat transfer zone of the reactor at 120 mL min⁻¹ by using a peristaltic pump.
15 Y. Shang and G. Van Weert, *Hydrometallurgy*, 1993, **33**, 273.
16 A. I. Vogel, *Vogel's textbook of quantitative chemical analysis*, 5th edn, Burnt Mill, Longman Scientific & Technical, 1989, 326.
17 Y. Shang and G. Van Weert, *Hydrometallurgy*, 1993, **33**, 255.
18 A. Cornélis, P. Y. Herzé and P. Laszlo, *Tetrahedron Lett.*, 1982, **23**, 5035.
19 A. Baruah, B. Kalita and N. C. Baruam, *Synlett*, 2000, **7**, 1064.
20 The molar ratio of 16 : 1 (benzyl alcohol : Fe(NO₃)₃.9H₂O) at room temperature leads to saturation of Fe(NO₃)₃·9H₂O in benzyl alcohol which is the reaction condition of the article of ref. 4.
21 P. Gray and A. Williams, *Chem. Rev.*, 1959, **59**, 239.
22 Unpublished results of transfer from batch-wise to flow conditions (FlowSynth of Milestone srl).

The green solvent ethyl lactate: an experimental and theoretical characterization†

Santiago Aparicio* and Rafael Alcalde

Ethyl lactate is a green, and economically viable, alternative to traditional solvents whose extensive use and scale-up to industrial level requires a deep and accurate knowledge of its properties in wide pressure–temperature ranges. In this work, the pressure–volume–temperature and pressure–viscosity–temperature behaviors are reported together with several derived properties of remarkable importance for process design purposes. The structure of the liquid is analyzed at the microscopic level using the Density Functional Theory and from classical molecular dynamics simulations. It is shown the competing effect of intra and intermolecular hydrogen bonding mainly through preferred positions. The predictive ability of the forcefield used for molecular dynamics simulations is studied, showing good results for most of the considered properties. Monte Carlo/Gibbs ensemble simulations were carried out to predict the phase equilibria of the fluid, considering the absence of experimental data.

Introduction

The problem of solvents is ubiquitous to most of the chemical and related industries,[1] because they are present not only for production and purification purposes but they appear also in the final products, thus they affect the whole product cycle. The world demand of solvents is forecasted to increase in the next years,[2,3] and although the use of compounds with strong effects on the environment will decrease,[2] as a consequence of international regulations, the industrial needs will lead to an increased demand of new fluids. The use of solvents is at a multi-ton scale, the world demand is approaching 20 million metric tons per year.[3] Together with the volatile character and very poor environmental and toxicological profiles of the most commonly used compounds, there is a need for alternative solvents that may replace the present ones.[1,4–6] Several approaches within the green chemistry framework have been proposed in the last few years;[1] supercritical fluids and ionic liquids being the most promising and extended ones among academia, if specialized literature is analyzed.[7,8] In spite of the promising characteristics of these alternative fluids, their extension to large scale industrial applications is very scarce nowadays, especially for ionic liquids.[9] Moreover, the technological and economical viability of these alternative solvents is still under study and thus their extension to large-scale industrial processes would not be straightforward and it would require several years together with systematic

and costly studies. Hence, other alternative organic solvents, with characteristics more similar to the traditional ones, may be considered and studied if their properties are adequate both from technological and environmental viewpoints. The industrial replacement of traditional solvents for these alternative organic solvents may be faster considering that the technologies required for their use are similar to the present ones and thus the economical costs of the replacement would be lower than for the other alternatives. Moreover, the industry probably would be less reluctant to get involved in the transition toward these solvents because of their similarities to the present ones.

Among these alternative organic solvents with adequate properties, ethyl lactate (EL) is one of the most promising ones.[10] EL is the main member of the lactate esters family. It has very favourable toxicological properties,[11] it does not show any potential health risks, it is not teratogenic, and it readily undergoes metabolic hydrolysis because of estearase enzymatic activity to ethyl alcohol and lactic acid, this last compound being a natural metabolite in humans. Moreover, the low toxicity of EL may be inferred from its FDA (USA Food and Drug Administration) approved use in food products. The ecotoxicity of EL is very low,[12] and thus its environmental profile is very adequate considering that it is completely biodegradable in a very short time. In case of vapors release, EL is a non-ozone depleting fluid. From an economical viewpoint, the replacement of traditional solvents by EL is clearly favoured considering that the recently developed technologies[13–16] allow its production from carbohydrate feedstocks at very low and competitive prices. Moreover, the use of carbohydrates as a starting point in its production leads to a renewable product, and thus sustainable, not rising from petrochemical sources. The reduced energy use in its production decreases its costs but also the effect on the environment. Moreover, the production of EL from carbohydrate feedstocks is not a competition to food because

Department of Chemistry, University of Burgos, 09001, Burgos, Spain.
E-mail: sapar@ubu.es; Fax: +34 947 258831; Tel: +34 947 258062

† Electronic supplementary information (ESI) available: AIM analysis for EL monomer (Fig. S1), NBO analysis for EL monomer (Fig. S2), experimental density and derived properties (Table S1), fitting parameters of TRIDEN correlation of density (Table S2), dynamic viscosity (Table S3), fitting parameters for correlation of viscosity (Table S4), viscosity–derived coefficients (Table S5), MK Atomic charges (Table S6), forcefield parameters (Tables S7–S10). See DOI: 10.1039/b811909k

low-cost agricultural waste may be considered as a source of carbohydrates. Although the open literature on uses of EL, pure or mixed, is not very extensive, reported results show that it may be applied successfully for different processes as its used as a cleaning solvent,[17] for the manufacturing of magnetic[18] and electronic devices,[19] or for applications ranging from the pharmaceutical[20] to the paint industries.[21]

The replacement of any solvent by a new one requires a deep and accurate knowledge of the properties for the selected candidate in wide pressure/temperature ranges to carry out cost-effective and reliable process design for the application required,[22] thus allowing to keep the production targets. A detailed analysis of the literature shows that thermophysical data for EL are almost absent, only some properties at conditions close to the ambient ones may be found.[23–26] This absence of reliable information hinders any development of processes for EL, and thus the main objective of this work is to provide these values. The measurement of properties as a function of pressure and temperature is very time consuming and economically costly,[27] thus the studied properties have to be selected according to their importance, both from practical and basic science purposes. In this work, the results of pressure–volume–temperature (PVT) and pressure–dynamic viscosity–temperature (PηT) studies on EL are reported. PVT measurements were carried out considering they provide most of the thermodynamic information for the studied fluid, and the values of density and derived coefficients such as isothermal compressibility of thermal expansion coefficients are required for many industrial purposes. Moreover, the knowledge of the PηT behavior, and of its derived pressure and temperature coefficients, is of great importance for any fluid, considering how this property affects the heat or mass transfer processes or their use in the design of relevant operations such as fluids pumping or boilers.

Although the experimental measurement of physical properties is the most accurate and straightforward way of getting the required data, the theoretical prediction of these properties is also very important considering the cost of measurements and the impossibility of obtaining values for all the possible conditions. Thus, in this work a theoretical study is carried out with two main objectives: (*i*) to analyze the molecular level structure of EL studying its hydrogen-bonding ability and (*ii*) to develop predictive tools that allow to infer microscopic structure/macroscopic properties relationships. This theoretical study would provide valuable information on the way that EL molecules develop intermolecular interactions, their effect on the fluid structure, and thus a basis on which to analyze the effect of possible solute molecules on fluid EL properties and thus the solvent ability of EL. The theoretical study was carried out using three different approaches: (*i*) Density Functional Theory (DFT), to study the short range interactions and the energetics and structure of EL molecules, (*ii*) classical molecular dynamics simulations (MD), to study the long-range fluid structure and to provide a predictive tool for the EL macroscopic properties and (*iii*) Monte Carlo simulations, to predict phase equilibria.

As the *S*-enantiomer is the prevailing one, in this study, all the experimental and theoretical studies were performed only for this isomer.

Results and discussion

Density Functional Theory computations

The optimized structure of EL in the gas phase calculated at the B3LYP/6–311++g** theoretical level is reported in Fig. 1. The main feature that should control the EL liquid structure is its ability to develop intra (among the hydroxyl hydrogen and carbonyl and/or alkoxy oxygens) and intermolecular hydrogen bonding. The ability to develop intramolecular hydrogen bonding relies on the relative position of the hydroxyl hydrogen respective to the oxygens in the EL molecule. It has been previously reported for the smallest member of the lactate family, methyl lactate (ML),[28] that in the gas phase: (*i*) hydroxyl groups tends to eclipse carbonyl groups, and thus intramolecular interaction is preferentially developed with the carbonyl oxygen, and (*ii*) intramolecular hydrogen bonding among hydroxyl hydrogen and carbonyl oxygen is strong and the out-of-plane movement of the hydroxyl hydrogen, that weakens the interaction, evolves through a large torsional barrier. Nonetheless, this barrier decreases on going to solution because of the competing effect of possible intermolecular interactions. Results reported in Fig. 1 show the behavior for EL very close to that previously reported for ML, the distance and angle between the hydroxyl hydrogen and carbonyl oxygen allows the development of strong intramolecular hydrogen bonding. The electrostatic potential energy surface (ESP) shows regions of negative values for hydroxyl and carbonyl oxygens, whereas the alkoxy oxygen is clearly embedded within the positive, hydrophobic, region rising from the ethyl chain. Hence, the interaction among hydroxyl and carbonyl groups should be preferred than the possible one between hydroxyl and alkoxy groups; the increase of the alkyl chain length in comparison with ML[28] reinforces the preference for the first interaction position. The dipole moment calculated for EL is 10.5% larger than for ML,[28] this is in agreement with the effect rising from the larger alkyl chain.
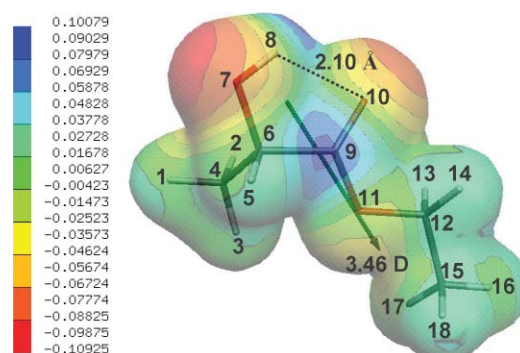
Fig. 1 Optimized gas phase structure of the most stable, lower energy, conformer for EL monomer computed at the B3LYP/6–311++g** theoretical level. Atom color code: gray = carbon, white = hydrogen, and red = oxygen. Arrow shows calculated dipole moment whose value is also reported in the Figure. Dashed line shows intramolecular hydrogen bonding. Electrostatic potential mapped on an electronic density surface isovalue of 0.0005 au is reported together with the map color legend.

The infrared spectra was also computed for the optimized geometry reported in Fig. 1, the hydroxyl stretching band was obtained at 3550.8 cm^{-1}, this band is in good agreement with

This journal is © The Royal Society of Chemistry 2009

the experimental gas phase value reported in the literature for the monomer (3562 cm⁻¹).²⁹ The theoretical values obtained for EL are red-shifted by 3.3 cm⁻¹ in comparison with ML,²⁸ which is in agreement with the experimental 3.5 cm⁻¹ red-shifting.²⁹ This red-shifting correlates with the slight increase for O–H distance (0.0001 Å) on going from ML to EL, and thus it shows a slightly stronger intramolecular hydrogen bond for EL probably due to inductive effects²⁹ because of the larger alkyl chain. The comparison among theoretical and literature²⁹ infrared spectra show that in the gas phase the monomer structure reported in Fig. 1 prevails over other possible isomers.²⁸ Although gas results provide valuable structural information on EL, it has been previously reported²⁸ the strong effect of surrounding media on lactate intramolecular hydrogen bonding. This effect was studied using the IEF-PCM approach in which the solvent media are treated as a continuum. Hence, in Fig. 2 we report the variation of the O–H stretching frequency for the EL monomer, as a function of the dielectric constant used to simulate the solvent. To allow a straightforward comparison, the structure reported in Fig. 1 was directly calculated for different values of the dielectric constant without optimization. The experimental value of dielectric constant for EL is 15.70 at 298.15 K,²³ thus it is a moderately polar solvent. The increasing dielectric constant leads to a red-shifting of the O–H stretching frequency in comparison with gas phase values. If we compare the gas value for EL and the value obtained when EL molecules are surrounded by a continuous media, which dielectric constant is that of EL, a 39.1 cm⁻¹ red-shifting is obtained, and thus intramolecular hydrogen bonding seems to be strengthened in going to solution. But this is a simplified view of the problem, because when the dielectric constant of the surrounding media increases, the hydroxyl hydrogen tends to move out of plane, and thus the development of intramolecular hydrogen bonding is hindered in spite of the red-shifting obtained. Moreover, this effect is reinforced if the molecules of the surrounding media are able to act as acceptor/donors of hydrogen bonding, although this effect can not be analyzed through the IEF-PCM approach because it considers a continuous surrounding media

instead of a discrete molecular one. Thus, we have calculated the optimized structures of EL as a function of the dielectric constant of the surrounding media, the values of the dihedral angle that shows the position of the hydroxyl hydrogen regarding the carbonyl oxygen (8–7–6–9 in Fig. 1) are reported in Fig. 3. Results reported show that as the polarity of the surrounding media increases, the dihedral angle first increases sharply (up to ~$\varepsilon = 10$) and then slowly, reaching an asymptotic value of 57.5°. This dihedral is 49.90° when $\varepsilon = 15.7$, and thus the position of the hydroxyl hydrogen in a fluid, which polarity mimics that of EL is clearly out of plane, hence intramolecular hydrogen bonding is remarkably weakened and hydroxyl hydrogens would be able to develop intermolecular hydrogen bonding with neighbour EL molecules. This is in agreement with the increasing O–H distance with increasing ε, Fig. 3, and with the large red-shifting obtained for its stretching frequency (258.1 cm⁻¹ on going from $\varepsilon = 1$ to $\varepsilon = 79$). Nonetheless, this interpretation has to be confirmed with the molecular dynamics results, in which EL molecules are treated explicitly instead of the continuum model used to describe the surrounding medium in IEF-PCM approach.
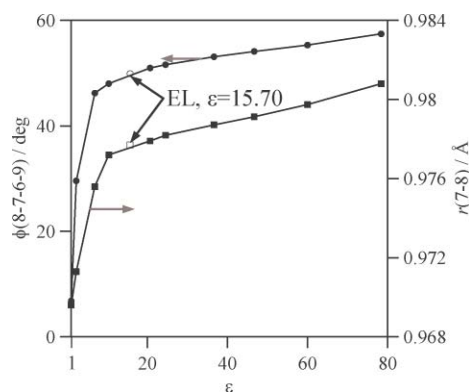
Fig. 3 (●) 8–7–6–9 dihedral angle, and (■) O7–H8 bond distance, in EL computed at the B3LYP/6–311++g** theoretical level using and IEF–PCM approach as a function of the dielectric constant, ε, of the solvent. Values obtained from structure optimization for each value of the dielectric constant. Atom numbering as in Fig. 1.

To analyze the characteristics of the intramolecular hydrogen bonding in EL monomer in more depth, we have carried out Atoms in Molecules (AIM)³⁰ and Natural Bond Orbital (NBO)³¹ studies; all the calculations were done for the monomer optimized structure in the gas phase, Fig. 1. Results of AIM calculations are summarized in Fig. S1 (ESI),† the first evidence of H-bonding according to the AIM formalism is the existence of a bond path between two atoms and the existence of a bond critical point, BCP, in the middle of the path.³²,³³ The molecular graph reported in Fig. S1a (ESI)† keeps the Lewis bonding scheme in the molecule, intramolecular H-bonding between H8 and O10 positions is clearly inferred from this Figure. A second AIM criterion according to the AIM formalism to define an H-bond considers that electron density at BCP, ρ_{BCP}, and the laplacian of that electron density, $\nabla^2\rho_{BCP}$, must be within the 0.002–0.035 and 0.024–0.139 ranges, respectively, (both in atomic units);³²,³³ this criterion is also fulfilled by the H8···O10 interaction. The values of ρ_{BCP} and $\nabla^2\rho_{BCP}$ for the H8···O10 are large, and thus this is a strong H-bond (ρ_{BCP} and $\nabla^2\rho_{BCP}$ are
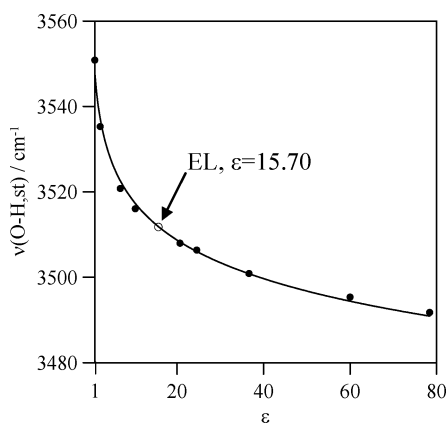

Fig. 2 O–H stretching IR vibrational frequency in EL monomer computed at the B3LYP/6–311++g** theoretical level using and IEF-PCM approach as a function of the dielectric constant, ε, of the solvent. Dielectric constant for EL obtained from ref. 23. Frequency scaled with a factor 0.96. Data calculated for the structure reported in Fig. 1 without optimization.

~70% of the top limit in the defined ranges). The $\nabla^2\rho_{BCP}$ is reported in Fig. S1b (ESI)† close to the studied intramolecular H-bond, we should remember that $\nabla^2\rho_{BCP} < 0$ shows charge concentration, whereas $\nabla^2\rho_{BCP} > 0$ indicates charge depletion. The large charge depletion between H8 and O10 corresponds to the strong H-bond, however the charge concentration on H8 is not polarised toward O10.

NBO analysis provides valuable information on the energy of H-bonds. The interaction O7–H8$\cdots$O10 should be determined by the hyperconjugation induced charge transfer between the O10 electron lonely pairs (donor) and the antibonding orbitals for the O7–H8 bond (acceptor), $n_O \to \sigma^*_{O-H}$. This hyperconjugation effect is analyzed in Fig. S2 (ESI),† the calculated second order perturbation energy, $E(2)$, is surprisingly low for the charge transfer of both oxygen lone pairs. For the first lone pair, $E(2) < 0.5$ kcal mol^{-1}, the interaction between the orbital for this pair and that for σ^*_{O-H} is clearly hindered both because of the shapes and phases reported in Fig. S2 (ESI);† moreover, the orbital for the lone pair has a 59/41% s/p relationship, whereas for σ^*_{O-H} it is 80/20%. For the second lone pair, a larger value of $E(2)$ is obtained, and although this value would contribute to stabilize the hydrogen bond, it is low considering the small value for the energy difference among the donor and the acceptor, Fig. S2 (ESI).† The orbital for the second oxygen lone pair is almost a pure p orbital, 0.1/99.9% s/p relationship, and thus its properties are very different to those for σ^*_{O-H}, hence although hyperconjugation is produced for this H-bond, it is not as high as for other H-bonds. Moreover, the Fock matrix element between the donor and acceptor NBO orbitals, F_{ij}, is very low, Fig. S2 (ESI),† which is the main reason of the low $E(2)$ values.

As both in gas and liquid phases EL would be composed not only by monomers but also by multimers, several association complexes formed by 2, 3 and 4 EL molecules are also analyzed and reported in Fig. 4. Several dimers may be considered for EL, with different topologies and thus with different H-bonding strengths. We report the two most stable calculated structures, Fig. 4: (*i*) symmetric dimers with two reciprocal O–H$\cdots$C=O interactions leading to an 8-ring structure (2A) and (*ii*) dimers rising from the insertion of the O–H group of a molecule into the intramolecular H-bond of a second one leading to a disrupted 5-ring structure (2B). 2A dimer is slightly more stable than 2B, this is in agreement with literature results,[29] although the energy difference between both dimers reported here (0.37 kcal mol^{-1}) is lower than the one previously calculated (1.20 kcal mol^{-1} at B3LYP/6–31g* or 2.39 kcal mol^{-1} at MP2/6 + 31 + g* theoretical levels),[29] probably due to a larger basis set used in this work. In dimer 2A both H-bonds are totally symmetric and with the same length, whereas for 2B one of the H-bonds is larger, and thus weaker. The calculated IR spectra
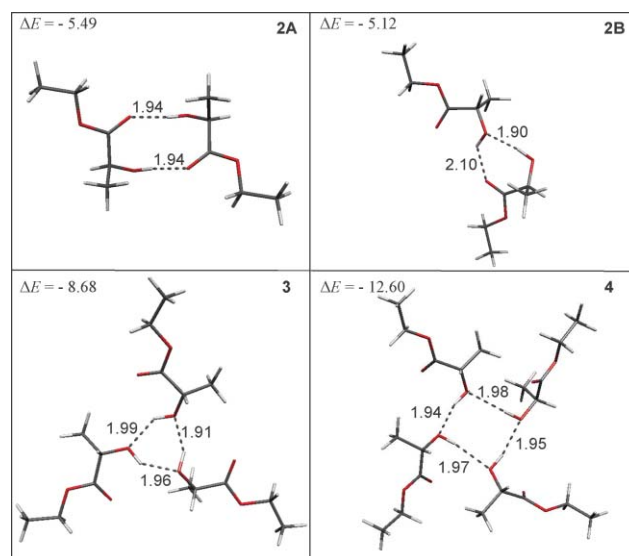
Fig. 4 Optimized gas phase structures of the most stable, lower energy, multimers of EL computed at the B3LYP/6–311++g** theoretical level. Atom color code: gray = carbon, white = hydrogen, and red = oxygen. ΔE = counterpoise corrected binding energies in kcal mol^{-1}. Distances in Å.

for both dimers is in good agreement with the experimental one, a value of 3483.6 cm^{-1} is calculated for the asymmetric O–H stretching band, which experimental value is 3517 cm^{-1}.[29] For 2B, two peaks are calculated at 3433.9 and 3514.5 cm^{-1}, the assignment of experimental bands for this dimer is not totally resolved but several peaks in the 3500–3550 cm^{-1} are obtained.[29]

The AIM analysis of dimers is reported in Fig. 5 and Table 1, results support the existence of bond paths that define H-bonds for both dimers. For 2A, both H-bonds are totally equivalent as the values of ρ_{BCP} and $\nabla^2\rho_{BCP}$ show, these values are large and point to strong H-bonding. BCPs for O5$\cdots$H31 and O19$\cdots$H13 interactions, Fig. 5, are well defined by the behavior of the Laplacian of electron density reported in Fig. 5, the contour plots for both H-bonds are equivalent, thus justifying their similarities. The study of 2B dimer shows that the two H-bonds involved are disimilar, the O24–H31$\cdots$O3 interaction (hydroxyl–hydroxyl type) is clearly stronger than the O3–H13$\cdots$O19 one (hydroxyl–carbonyl type), Table 1. $\nabla^2\rho$ shows a stronger charge concentration in the region between donor and acceptor for the hydroxyl–hydroxyl interaction, which is also inferred from the larger ρ_{BCP}. NBO analysis for both dimers supports AIM conclusions, Table 2. For 2A dimer, the hyperconjugation induced charge transfer between acceptor

Table 1 AIM analysis of EL multimers computed in gas phase at the B3LYP/6–311++g** theoretical level. Electron density at BCP, ρ_{BCP}, Laplacian of electron density at BCP, $\nabla^2\rho_{BCP}$, for the H-bonds. Multimers as in Fig. 6 and 7

	H-bond	ρ_{BCP}/a.u.	$\nabla^2\rho_{BCP}$/a.u.	H-bond	ρ_{BCP}/a.u.	$\nabla^2\rho_{BCP}$/a.u.	H-bond	ρ_{BCP}/a.u.	$\nabla^2\rho_{BCP}$/a.u.	H-bond	ρ_{BCP}/a.u.	$\nabla^2\rho_{BCP}$/a.u.
2A	O5$\cdots$H31	0.023	0.089	O19$\cdots$H13	0.023	0.089	—	—	—	—	—	—
2B	O3$\cdots$H31	0.027	0.096	O19$\cdots$H13	0.018	0.067	—	—	—	—	—	—
3	O8$\cdots$H27	0.023	0.077	O22$\cdots$H45	0.029	0.091	O40$\cdots$H9	0.025	0.082	—	—	—
4	O40$\cdots$H9	0.022	0.076	O22$\cdots$H45	0.025	0.089	O58$\cdots$H27	0.024	0.078	O8$\cdots$H63	0.023	0.078
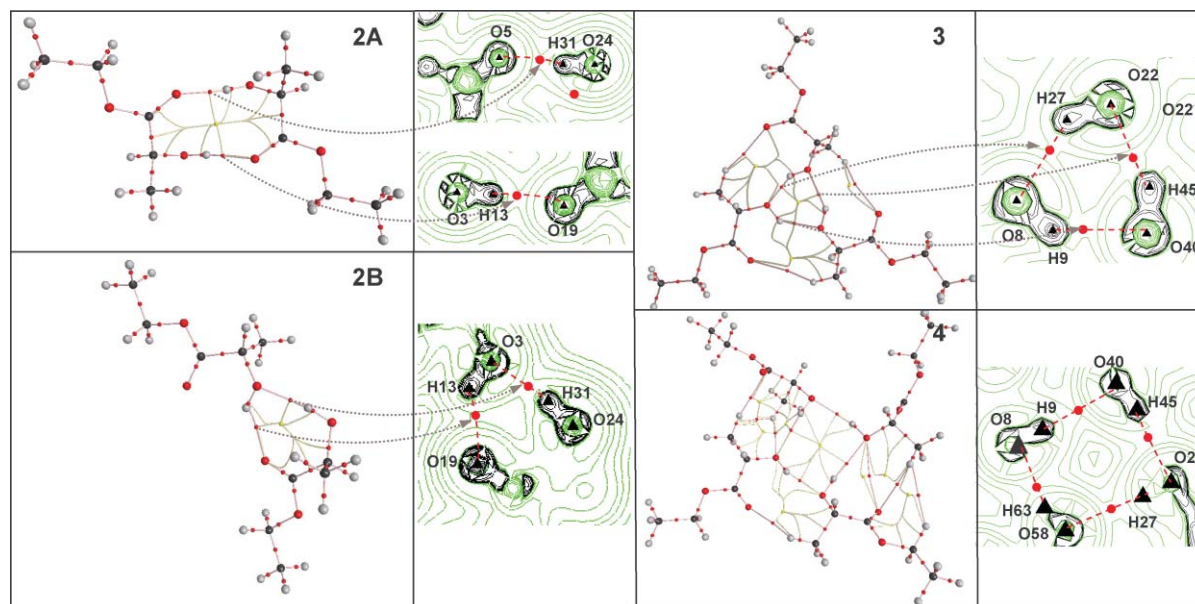
Fig. 5 AIM analysis for EL multimers. (a) Molecular graphs; small red dots represent bond critical points (BCP), small yellow dots represent ring critical points (RCP), pink lines represent bond paths, yellow lines represent ring paths, large dots represent attractors (atoms). (b) Contour plot for the Laplacian of electron density, $\nabla^2\rho$, in the vicinity of several hydrogen bonds; red dot represents BCP for hydrogen bonding, red dashed line represents bond path for hydrogen bonds, green curves represent positive isosurface values of $\nabla^2\rho$ and black curves represent negative isosurface values of $\nabla^2\rho$.

Table 2 NBO analysis of EL multimers computed in the gas phase at the B3LYP/6–311++g** theoretical level. Second order perturbation energy, $E(2)$, energy difference among the donor and the acceptor, ΔE, and Fock matrix element between the donor and acceptor, F_{ij}. Multimers as in Fig. 5. All hyperconjugation induced charge transfers are of $n_O \rightarrow \sigma^*_{O-H}$ type, from the oxygen lone pairs (pair 1 or 2) to corresponding antibonding O–H orbital

|	Donor	Donor pair	Acceptor	$E(2)$/kcal mol⁻¹	ΔE/a.u.	F_{ij}/a.u.
2A	O5	Pair 1	H31–O24	3.74	1.16	0.059
		Pair 2		3.82	0.74	0.049
	O19	Pair 1	H13–O3	3.73	1.16	0.059
		Pair 2		3.81	0.74	0.049
2B	O3	Pair 1	H31–O24	2.10	0.98	0.041
		Pair 2		8.18	0.81	0.073
	O19	Pair 1	H13–O3	1.40	1.13	0.036
		Pair 2		1.86	0.70	0.033
3	O8	Pair 1	H27–O22	3.54	0.97	0.052
		Pair 2		6.23	0.80	0.064
	O22	Pair 1	H45–O40	1.79	0.96	0.037
		Pair 2		12.50	0.81	0.090
	O40	Pair 1	H9–O8	2.23	0.97	0.042
		Pair 2		8.83	0.81	0.076
4	O8	Pair 1	H63–O58	3.40	0.93	0.050
		Pair 2		5.98	0.77	0.061
	O40	Pair 1	H9–O8	1.72	0.92	0.036
		Pair 2		12.00	0.78	0.086
	O22	Pair 1	H45–O40	2.14	0.93	0.040
		Pair 2		8.48	0.78	0.073
	O58	Pair 1	H27–O22	3.40	0.93	0.051
		Pair 2		5.88	0.76	0.061

and donor is equivalent for both H-bonds. Moreover, for each H-bond the calculated second order perturbation energy for each oxygen donor pair is almost equivalent, because although for the first pair the energy difference between donor and acceptor is larger, F_{ij} is also larger. For 2B dimer, $E(2)$ values are clearly larger for the hydroxyl–hydroxyl interaction, being the $E(2)$ associated with the second oxygen donor pair remarkably larger. This large $E(2)$ value is the main cause of the stronger H-bond for the hydroxyl–hydroxyl interaction in 2B, and of the small energetic difference between 2A and 2B dimers, Fig. 4. The molecular origin of this large $E(2)$ value is in the large F_{ij}, the symmetry of donor and acceptor orbitals allow an efficient charge transfer between them.

Trimers and tetramers are reported in Fig. 4, large stabilization energies are obtained for both complexes. H-bonds are formed through hydroxyl/hydroxyl interactions leading to cyclic structures. The AIM analysis of the cyclic trimer shows that the three H-bonds are very similar from a topological viewpoint, Table 1, only the interaction for O22···H45 position shows a slightly stronger interaction. Nevertheless, the shapes of the contour plots for the Laplacian of electron density, Fig. 5, show almost equivalent charge depletions between donors and acceptors for the three H-bonding positions. NBO results reported in Table 2 for the trimer confirms the AIM results, the calculated second order perturbation energy for the O22···H45 interaction is stronger, although the energy difference between donor and acceptor is equivalent for the three H-bonds, the larger F_{ij} value for the O22···H45 position justifies this behavior because of the shapes and phases of the involved orbitals. Moreover, the interaction with the first lone pair of oxygens for the three H-bonds is clearly less efficient than with the second pair because of the larger energy difference between donor and acceptor and their lower orbital symmetry. Results for the cyclic tetramer are analogous to those for the trimer, AIM analysis shows symmetric charge depletions for all the H-bonds, and NBO results point to preferred interactions through the second oxygen lone pair for the four positions.

Thermophysical properties

The pressure/temperature effect on the main properties of EL (in the ranges of 278.15–358.15 K and 0.1–60 MPa, for density, or 1–70 MPa, for dynamic viscosity) are reported in Tables S1–S5 (ESI)† and Fig. 8–10. Fitting coefficients of density according to the *TRIDEN* equation[34] and of dynamic viscosity with a Tait-like equation are also reported.[35]

Literature density data for EL are very scarce,[24–26] and, to our knowledge, all the reported values have been measured only at atmospheric pressure, hence a full comparison with our data is not possible. Nevertheless, percentage deviations of our 0.1 MPa density data (close to atmospheric conditions) with literature data are very low, thus deviations of 0.03% with the data reported in ref. 25 at 298.15 K and 0.08, 0.12 and 0.11% with the data reported in ref. 24 at 298.15, 308.15 and 318 K, respectively, are obtained. Literature viscosity data are even scarcer, the extrapolation of our data to 0.1 MPa leads to a value 5% larger than the value reported in ref. 24 and 3% larger than the one reported in ref. 36, both at 298.15 K.

Density increases with pressure for isotherms and decreases with temperature for isobars, Fig. 6a, as we may expect. Density values are relatively large, thus pointing to an efficient packing, both by steric and intermolecular interaction effects. To obtain more information about the EL structure from PVT
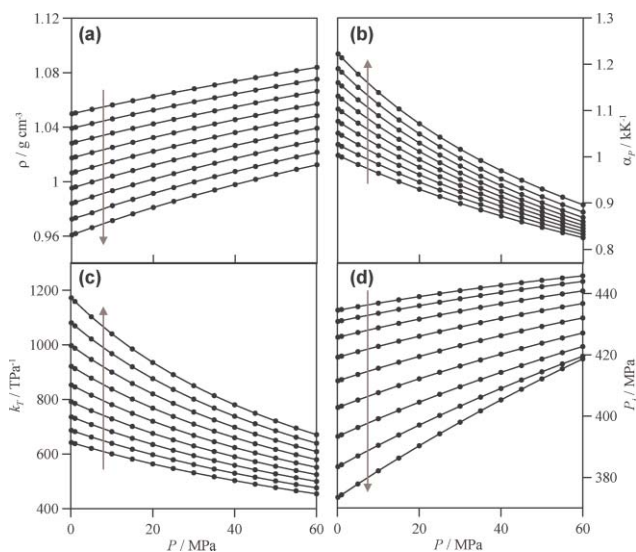

Fig. 6 (●) Experimental density, ρ, and calculated isobaric thermal expansivity, α_P, isothermal compressibility, k_T, and internal pressure, P_i, as a function of pressure, P, for different temperatures. Lines: TRIDEN fitting function for density (parameters from Table S2, ESI)† and guide-lines for the remaining properties. Arrows indicate increasing temperature: 278.15 to 358.15 K in 10 K steps.

data, the Sanchez-Lacombe[37] equation of state, SL-EOS, was applied, with its parameters obtained from least-squares fitting of experimental density results, Table 3. SL-EOS has proved to be useful for the description of PVT behavior for many different fluids,[38–40] although it is a purely physical lattice-fluid model it allows valuable information on the efficiency of the molecular packing and on the available free volumes in the fluids to be inferred, this information being obtained from the fitted model parameters. Very low percentage deviations are obtained for EL, despite the simplicity of the model and considering that it is a three-parametric EOS, thus this simple EOS is able to represent accurately the behavior of this complex fluid over the wide pressure/temperature ranges studied. The molar hard-core volume is the main parameter obtained from the SL-EOS analysis; it may be interpreted as the total volume, without free space, of one mole of particles. Thus, the free volume, V_F, in liquid EL can be obtained from eqn (1):

$$V_F = V - \upsilon^* r \tag{1}$$

Where V is the experimental molar volume, for each temperature and pressure, and $\upsilon^* r$ is the hard-core volume from SL-EOS, Table 3. Free volume is a very important property for any solvent because it is strongly related with properties such as gas solubility or solute solvation. V_F reported in Fig. 7, shows moderate values increasing with temperature and decreasing with pressure. The available V_F can be related with three main factors: (*i*) esteric effects, that contribute to increase it, (*ii*) the extension of hydrogen bonding, that decrease V_F and (*iii*) the dynamics of these interactions. The shape of EL allows an efficient packing through intermolecular interactions, H-bonded complexes, Fig. 4, lead to low void spaces because of the preferred orientations of EL molecules. The extension of hydrogen bonding interactions should determine the efficiency of the packing. Although any EL molecule can develop H-bonds through three different positions (carbonyl oxygen, alkoxy oxygen and hydroxyl group), and thus a hydrogen bonding dynamic network with high cooperativity of remarkable cohesive nature may be obtained, previously reported dielectric relaxation spectroscopy, DRS, results have discarded the existence of associates larger than tetramers,[23] which is in agreement with the moderate free volumes. In fact, there is a strong linear correlation among the intensity of the relaxation amplitude of the DRS peak assigned to multimers and the values of free volume, Fig. 7c, thus showing how the extension of multimers' aggregation determines the values of free volume.

Isobaric thermal expansivity, α_P, and isothermal compressibility, k_T, are also reported in Fig. 6; both properties show the regular behavior of most fluids: decreasing with increasing pressure along isotherms and increase with increasing

Table 3 Parameters of Sanchez-Lacombe equation of state obtained by fitting to experimental PVT data for EL. T^*, P^*, ρ^* reducing characteristic parameters, r segment number of one molecule, ε^* segment interaction energy, υ^* segment volume and %AAD percentage absolute average deviation of the fitting to experimental data

[a]P^*/MPa	[a]r	[a]ε^*/J mol^{-1}	[b]T^*/K	[b]ρ^*/kg m^{-3}	[b]υ^*/cm^3 mol^{-1}	[b]Hard-core volume ($\upsilon^* \times r$)/cm^3 mol^{-1}	%AAD
549.2	13.0	4295.3	516.6	1160.4	7.82	101.7	0.09

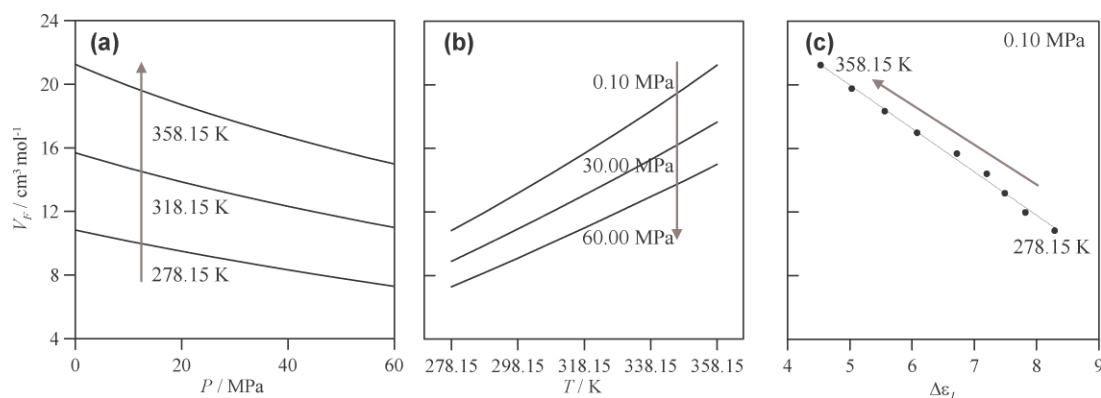[a] Fitted parameters. [b] Calculated parameters.

Fig. 7 Free volume, V_F, of liquid EL, estimated from the Sanchez-Lacombe equation of state with parameters from Table 2. (a) Panel shows isothermal results with the arrow indicating increasing temperatures (from bottom to top), (b) Panel shows isobaric results with the arrow indicating increasing pressures (from top to bottom) and (c) panel shows relationship between V_F and relaxation amplitude for multimeric associates obtained from DRS studies[23] at 0.1 MPa with the arrow indicating increasing temperatures (from right to left).

temperature along isobars. k_T is related with the extension of the H-bonding, compounds with the ability of developing spatial networks would have lower compressibilities.[41] Although for EL the possibility of developing H-bond networks is discarded, its compressibility is moderately low, thus pointing to efficient interactions among molecules.

Internal pressure, P_i, is reported in Fig. 6. This property contains very valuable information on the structure of the fluid because of its relationship with cohesive forces. Nonetheless, the differences between P_i and cohesive energy density, c, should be remarked, considering that both properties are equivalent only for non-associated fluids, whereas for associated ones, $c > P_i$.[42] c is a measure of the total molecular cohesion, because it is the sum to all attractive intermolecular forces per unit volume that are broken when the fluid is vaporized to the ideal gas state. However, P_i is the change in internal energy per mole when the fluid undergoes a very small isothermal expansion, thus this expansion does not necessarily disrupt all the intermolecular forces, and P_i is mainly affected by weak intermolecular forces (dispersive, repulsive and weakly dipolar), which are strongly affected by the intermolecular distance. One of the main characteristics of any H-bond is that they restrict the motion of molecules into the packing of a liquid, and although H-bonds are distance dependent, they do not markedly affect the internal pressure of a fluid.[42,43] Thus, we have tried to relate the difference between c and P_i properties with the strength of intermolecular forces, the interaction energy assigned to specific intermolecular forces (strong dipole–dipole and hydrogen bonding), U_{sp}, could be defined as:[42,43]

$$U_{sp} = cV_i - P_iV_i \qquad (2)$$

Where, V_i is the molar volume. To calculate c parameter we use the vaporization enthalpy obtained from the literature at 298.15 K ($\Delta H_{vap} = 52.5$ kJ mol^{-1}),[44] thus, all the calculations were carried out at 298.15 K and 0.1 MPa. The experimental literature ΔH_{vap} data leads to a $U_{sp} = 0.27$ kcal mol^{-1}, this value is remarkably low if it is compared with the H-bond strengths reported in Fig. 4 for the main studied multimers. It is also too low considering the large dipole moment of EL reported in Fig. 1 that should also contribute to U_{sp}. Several reasons may

be considered for this discrepancy. (i) P_i values are too high because the method proposed in this work for estimation of internal pressure is not accurate. To explore this possibility we have carried out the same analysis for methanol, for which U_{sp} has been determined from experimental P_i data,[43] thus using our previously reported P_i data[45] we obtain $U_{sp} = 5.69$ kcal mol^{-1} which is just 0.76% larger than the value obtained from experimental P_i. Hence, the reported values for P_i obtained from PVT data are reliable. (ii) ΔH_{vap} data are too low, although there is a slight discrepancy among the data reported in the literature, all of them are in the 50–53 kJ mol^{-1} range.[18,44,46] Nevertheless, ΔH_{vap} data are reported for mixtures of enantiomers[46] or it is not indicated which enantiomer has been studied.[44] Thus, we have calculated ΔH_{vap} using the Pitzer-Carruth-Kobayashi group contribution method,[47] leading to $\Delta H_{vap} = 57.1$ kJ mol^{-1}, thus $U_{sp} = 1.37$ kcal mol^{-1} is obtained, this value is still too low, in fact if we consider that P_i values are accurate, ΔH_{vap} should be ~30% larger than the value reported in ref. 43. Hence, in our opinion, the trend to form cyclic aggregates through H-bonding in EL is at least partially affected by the very small isothermal expansion for which P_i is defined; at least 30% of P_i should be originated in H-bonds and strong dipolar interactions.

Dynamic viscosity data are plotted in Fig. 8 as a function of pressure and temperature, and pressure–viscosity, α_η, and temperature–viscosity, β_η, derived coefficients are reported in Table S5 (ESI).† Moderate viscosities are obtained in the whole pressure/temperature ranges studied, this is important for any heat or mass transfer operations in which this solvent could be applied because too high viscosity values would hinder its application. As a rule, the stronger the intermolecular forces the higher the viscosity, and thus these forces are obviously weakened upon temperature increases and reinforced with increasing pressure. Pressure effect on viscosity changes on going from low to high temperatures, whereas for $T \leq 298.15$ K the behavior is clearly non-linear, for $T > 298.15$ K an almost linear increase with pressure is obtained. The pressure effect on viscosity is frequently explained according to eqn (3):
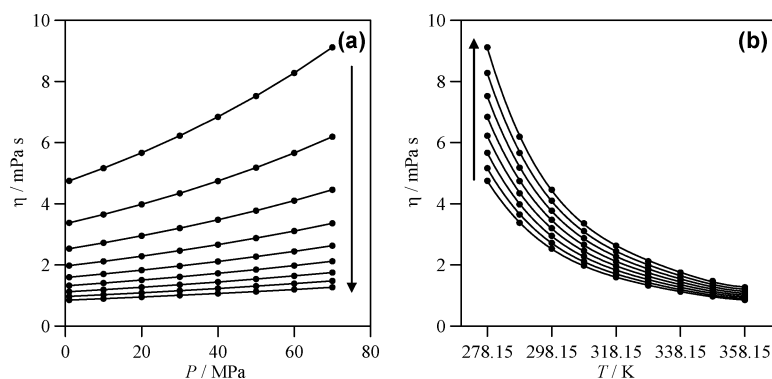
$$\eta_{isothermal} = \eta_p \exp(PV^\#/RT) \qquad (3)$$

Fig. 8 (●) Experimental dynamic viscosity, η, as a function of pressure, P, and temperature, T, for EL. From top to bottom in (a) 278.15 to 358.15 K in 10 K steps and (b) 70, 60, 50, 40, 30, 20, 10 and 1 MPa. Lines: fitting function (parameters from Table S4, ESI).† Arrows indicate (a) increasing temperature and (b) increasing pressure.

Where η_p is a pre-exponential factor and $V^{\#}$ is the activation volume. The fits to eqn (3) show very low deviations. $V^{\#}$ is calculated for all the studied isotherms and reported in Fig. 9a, a clearly non linear behavior is obtained showing remarkable larger values for the lower temperatures and then an almost linear variation. This behavior shows that viscosity is more pressure dependent at lower than higher temperatures because of the stronger intermolecular forces at the lower temperatures and considering the larger free volume available, which allows a better flow, at higher ones. This is supported by the α_η behavior reported in Table S5 (ESI),† whereas for 298.15 K, an increase of 70 MPa leads to a 5.5% increase in α_η, at 358.15 K it increases by 3.4%. The temperature behavior of viscosity reported in Fig. 8b is even more complex, with a remarkable viscosity increase for $T < 298.15$ K. Temperature effect on viscosity was tried to fit to an Arrhenius type behavior, at low temperatures there is a deviation from this behavior, in fact results are more accurately fitted to a Volger-Fulcher-Tamman (VFT) equation. Nevertheless, to obtain the values of the activation energy, E_a, Arrhenius fits were done for $T > 298.15$ K for each isobar, with results reported in Fig. 9b. E_a increases in an almost linear way for the pressure range studied, with values in good agreement with the H-bonding energies reported in Fig. 4 and with the previously reported DRS results.

Molecular dynamics simulations

Results obtained from these simulations infer more detailed information about molecular level structure in the studied fluid. We have considered OPLS-AA forcefield[48] for all the simulations, parameters used are reported in Tables S6–S10.† To validate the reported forcefield parameterization, and thus to assure the reliability of structural features inferred from the simulations, calculated properties were compared with experimental ones. In Fig. 10, density and isobaric thermal expansivity comparisons are reported. Simulated densities are always larger than experimental ones with deviations roughly 3–4% for the pressure/temperature ranges studied. The use of Merz-Singh-Kollman, MK, charges may lead to a larger coulombic energetic contribution that would be the origin of the larger densities. Predictions on isobaric thermal expansivity allow inferring if the simulations are able to capture the changes on density with temperature at constant pressure; this is of great importance because of the stronger temperature effect on intermolecular forces if compared with pressure effect. Predicted α_P values are always 10–20% lower than experimental ones, this is in agreement with stronger intermolecular forces in the model system, nevertheless, the temperature trend is properly captured by the simulations. Although these deviations may seem too large, they are in the common range of predicted properties,
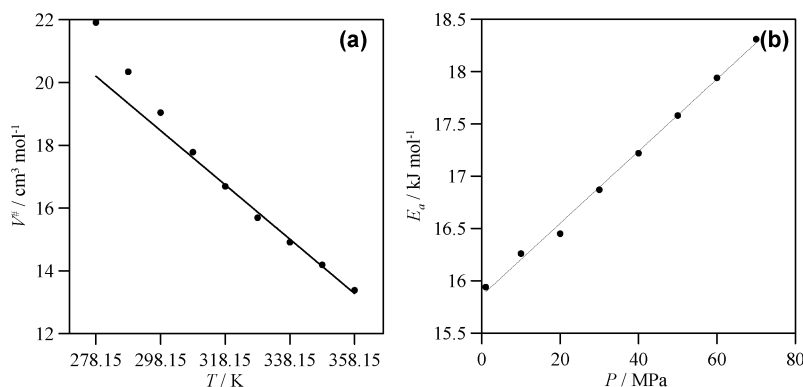

Fig. 9 (a) Activation volume, $V^{\#}$, and (b) Arrhenius activation energy, E_a, calculated from eqn (3) and Arrhenius equation for experimental viscosity data reported in Table S3 (ESI).† Lines: linear fits. In (a) linear fit for $T > 298.15$ K to show deviations at lower temperatures.
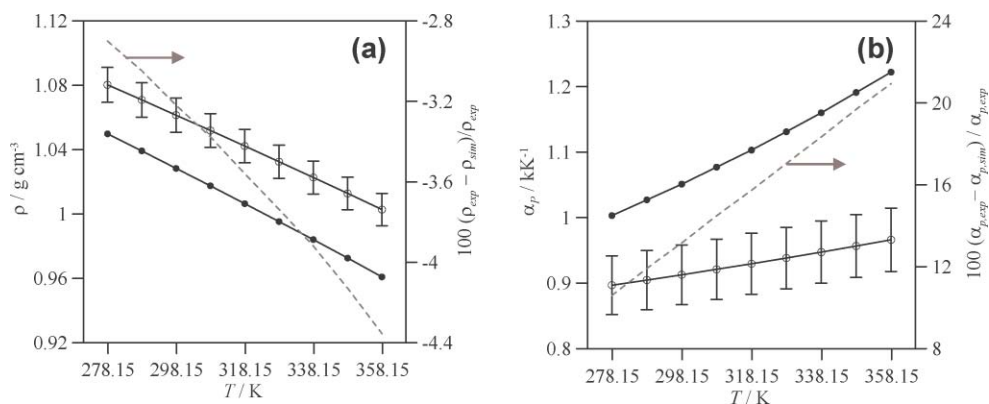
Fig. 10 Comparison between (●) experimental and (○) calculated density, ρ, and isobaric thermal expansivity, α_P, for EL at 0.1 MPa as a function of temperature. Simulated values, *sim* subindex, calculated from OPLS-AA molecular dynamics. Continuous lines showed for guiding purposes.

the degree of agreement over the studied pressure/temperature ranges is reasonable, considering the purely predictive character of the model and the complexity of the studied fluid, and should allow reliable insights into EL properties and structure. The calculated intermolecular interaction energy, E_{int}, is reported in Fig. 11, although the predicted E_{int} are larger than the ones inferred from the experimental vaporization enthalpy,[44] the values show strong intermolecular interactions that are weakened upon increasing temperature. E_{int} for EL is larger than the one previously reported for ML,[28] this behavior is in agreement with the increasing vaporization enthalpy upon alkyl chain length increase.[46]
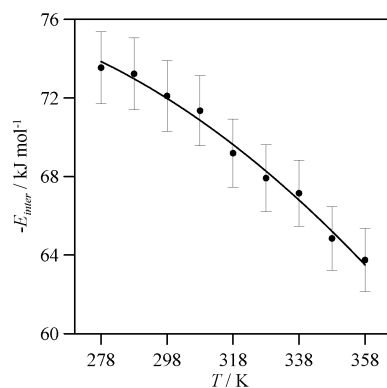
Fig. 11 Intermolecular interaction energy, E_{int}, for EL at 0.1 MPa as a function of temperature calculated from OPLS-AA molecular dynamics simulations.

Structural features are analyzed using radial distribution functions for selected pairs, RDFs, Fig. 14 and 15. A very important factor that should be analyzed in molecular dynamics simulations is the effect of the simulations' length on the predictions, thus we have carried out simulations for longer times to study if the structural features are affected. In a previous work, we reported the long residence times of EL in H-bonded clusters through DRS results,[23] thus although self-diffusion coefficients for EL are not too low (as the molecular dynamics predicted values show), simulations should be extended to a time that assures reliable structural results. In Fig. 12 we report RDFs for the pair 8–10 (hydroxyl hydrogen-carbonyl oxygen) for different

Fig. 12 Site–site radial distribution function, $g(r)$, for the 8–10 pair in EL calculated from OPLS-AA molecular dynamics simulations at 298 K and 0.1 MPa. Atom numbering as in Fig. 1. (black line) simulation time 500 ps, (gray line) simulation time 2 ns.

simulation times; this pair is the most important one to analyze intermolecular H-bonding as reported in Fig. 4. RDFs are not remarkably affected by a simulation time 4-times larger, peaks positions and intensities remain constant and thus simulations are reliable for the studied lengths.

Intermolecular H-bonding may be developed through three main positions: (*i*) OH···OC (positions 8–10, Fig. 1), (*ii*) OH···OH (positions 8–7, Fig. 1) and (*iii*) OH···O_{ALKOXY} (position 8–11, Fig. 1). The energetic and structural analysis reported in previous sections have showed that interactions through 8–10 and 8–7 positions are formed, whereas 8–11 H-bonding should be discarded because of steric hindrance. For the most stable studied dimers, Fig. 4, 8–10 and 8–7 interactions are present (although 8–10 prevails over 8–7), whereas cyclic higher aggregates are produced by 8–7 interactions. Thus, the analysis of RDFs for these pairs would lead to information on the prevailing associates in the liquid phase. The analysis of results reported in Fig. 13, first discards the 8–11 H–bonding thus confirming gas phase DFT results. H-bonding through 8–10 and 8–7 positions are clearly inferred from the sharp and intense peaks obtained, RDFs show maxima at 1.95 Å for both positions but interaction through 8–10 is clearly stronger than through
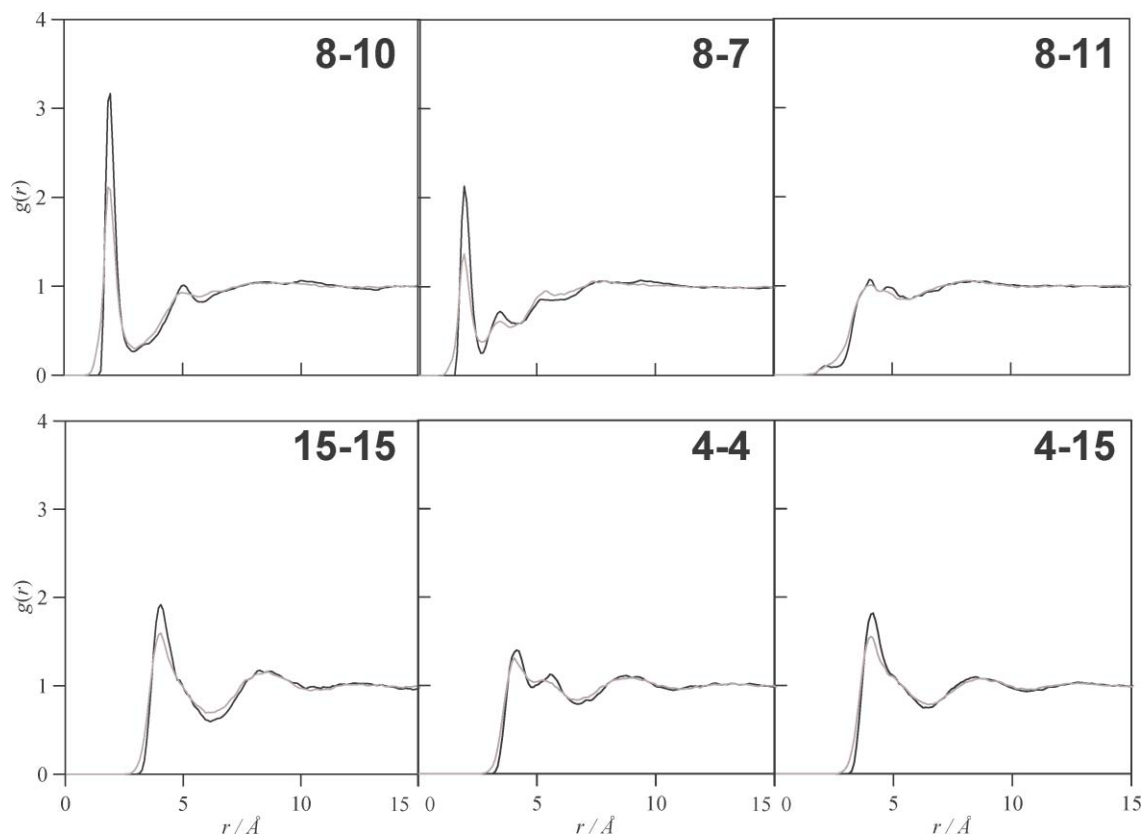
Fig. 13 Site–site radial distribution functions, $g(r)$, for EL calculated from OPLS-AA molecular dynamics simulations at (black line) 278 K, 0.1 MPa and (gray line) 358 K, 0.1 MPa. Atom numbering as in Fig. 1.

8–7 (peak maximum is 48.8% larger), thus dimers would prevail over higher associates reported in Fig. 4 (specially 2A formed through 8–10 interactions) in spite of the large stabilization energies reported in Fig. 4. Nonetheless, 8–7 H-bonding is also present in liquid EL. RDFs for EL are larger than the ones previously reported for ML,[23] which is in agreement with stronger H-bonding. RDFs for 8–10 and 8–7 interaction show small weak features beyond the first sharp peak with maxima at 5.05 and 3.50 Å, respectively, thus pointing to at least a second solvation shell and a certain degree of cooperativity in the H-bonding. The temperature effect on 8–10 and 8–7 RDFs is very similar, first peak maxima decreases 33.2 and 35.8%, respectively, on going from 278 to 358 K, hence the strength of both interactions is almost the same, which is in agreement with the strength of dimers reported in Fig. 4. Pressure effect is not reported in Fig. 13 because it is almost negligible for both positions in the pressure range studied.

We have also analyzed in Fig. 13 the RDFs for the head (position 4, Fig. 1) and tail (position 15, Fig. 1) methyl groups. RDFs for tail–tail interactions (15–15) show two well defined solvation shells at 4.10 and 8.25 Å, whereas for head–head interactions (4–4) a weaker peak appears also at 4.10 Å and a second shell at 8.75 Å. The cross head–tail interaction shows two shells at 4.10 and 8.45 Å. Hence, we may infer the existence of a continuous apolar domain within liquid EL.

To study EL conformation in the liquid phase it is important to analyze the possibility of developing intramolecular hydrogen bonding competing with intermolecular interactions. We report

in Fig. 14 the probability distribution function for two important dihedral angles that show the relative position of hydroxyl and carbonyl groups within EL molecules. The first dihedral, 7–6–9–10 (atom code Fig. 1), shows a well defined peak at 21°, thus showing that hydroxyl and carbonyl groups are slightly out of plane. Moreover, the 8–7–6–9 dihedral distribution shows a maximum at 73°, thus the development of intramolecular H-bonding between the hydroxyl hydrogen and the carbonyl oxygen is clearly hindered, the hydroxyl group is moved out of plane if compared with the obtained monomer in the gas phase, Fig. 1. These results are in good agreement with the monomer

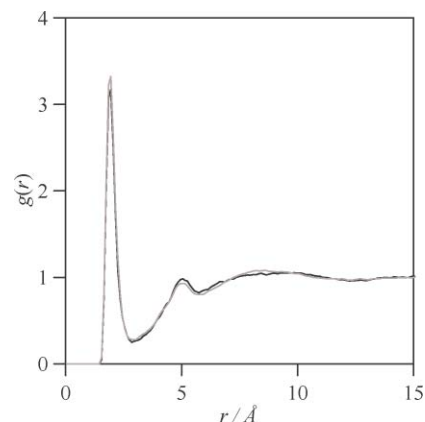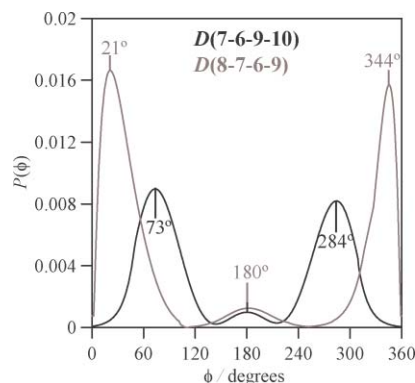**Fig. 14** Intramolecular dihedral angle distribution function for EL calculated from OPLS-AA molecular dynamics simulations at 298 K and 0.1 MPa. Atom numbering as in Fig. 1.
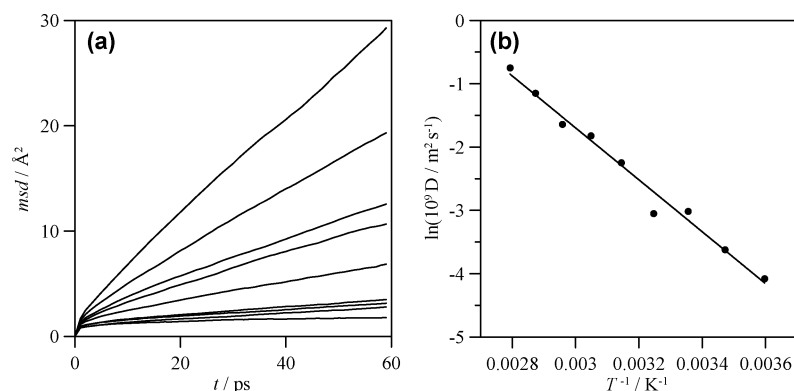
Fig. 15 Mean square displacement, *msd*, and self-diffusion coefficient, *D*, for EL calculated from OPLS-AA molecular dynamics simulations as a function of temperature. In panel (a) 278–358 K in 10 K steps from bottom to top. In panel (b) symbols show calculated *D* values according to Einstein's relation from *msd* and line shows fit to Arrhenius' equation.

values reported in Fig. 3 as a function of the dielectric constant of the surrounding media, and more remarkably with the values of dihedrals for dimer 2A reported in Fig. 4 (25 and 66° for 7–6–9–10 and 8–7–6–9 dihedrals, respectively). Thus, intramolecular H-bonding in liquid EL almost vanishes to develop intermolecular interactions mainly through 2A cyclic dimers.

The dynamic behavior of EL was studied using the self-diffusion coefficient, *D*, calculated from the Einstein relation:

$$D = \frac{1}{6} \lim_{t \to \infty} \frac{d}{dt} \left\langle \Delta r(t)^2 \right\rangle \qquad (4)$$

where the quantity in brackets is the mean square displacement, *msd*. In Fig. 15, the *msd* calculated from the molecular dynamics simulation is reported for the first 60 ps of simulation (after equilibration) as a function of temperature. A linear behavior is observed leading to the *D* coefficients from the slope of the linear fittings. To the best of our knowledge, there is no literature data for EL *D* coefficients, thus no comparison is possible between predicted and experimental data. Nonetheless, low diffusion coefficients are obtained, which is in agreement with the large intermolecular interaction energies reported in Fig. 11. The calculated coefficients approximately follow an Arrhenius behavior, Fig. 15b, from which the activation energy

for diffusion may be calculated, the 34.1 kJ mol⁻¹ value shows a strongly interacting fluid with low molecular mobility.

Monte Carlo/Gibbs ensemble. Phase equilibria predictions

A detailed analysis of the literature shows the absence of phase equilibria studies for EL, only vapor pressure data may be found in ref. 44, in fact, not even any critical data is reported for this compound. This absence of data hinders the development of common predictive models used in the industry for the analysis and design of processes, such as equations of state, in which EL would be involved. Hence, we have carried out Monte Carlo/Gibbs ensemble[49] simulations to predict EL phase equilibria, in conjunction with the remaining properties reported in this work, to obtain a full picture of the behavior of this relevant fluid. The critical properties were calculated from the simulated data using the law of rectilinear diameters and a scaling law, assuming an Ising exponent $\beta = 0.325$. In Fig. 16, the vapor–liquid coexistence curve together with vapor pressure data are reported. A good agreement is obtained between experimental and calculated vapor pressure data, whereas the absence of saturation density data hinders any comparison. These phase equilibria data should be considered as an initial

Fig. 16 (a) Vapor–liquid coexistence curve and (b) vapor pressure for EL. (●) Calculated from Monte Carlo simulations with OPLS-AA forcefield and parameters reported in Tables S6–S10 (ESI),† (+) calculated critical point and (gray line) in panel (b), experimental values from ref. 44. Values within panel (a) show calculated critical point.

estimation until experimental data is available, nevertheless the quality of vapor pressure predictions points to accurate equilibria data from these Monte Carlo simulations.
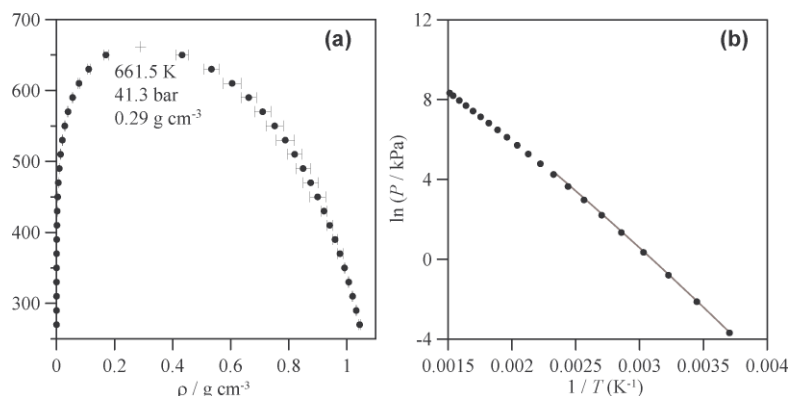
Conclusions

A wide scope study on EL structure and properties is reported using a combined experimental/theoretical approach. EL structure in the liquid phase is characterized by remarkable intermolecular associations through H-bonding, leading to mainly cyclic dimers although the presence of higher complexes such as cyclic trimers or tetramers is also important. Intermolecular interactions are developed through hydroxyl/carbonyl interactions, whereas the alkoxy position is sterically hindered to develop H-bonding. Alkylic groups tend to arrange in apolar domains across the fluid with tail/tail (terminal ethyl groups) arrangements. These complexes have remarkable association energies and their formation leads to a weakening of the intramolecular H-bonding through an out-of-plane movement of the hydroxyl group in EL. Calculated intermolecular interaction energies show a highly structured fluid, with low molecular mobility leading to low self-diffusion coefficients. Thermophysical properties reported show a dense fluid with moderate viscosity, which is a candidate suitable to be applied in different industrial fields.

Experimental

Materials

EL ((−)-Ethyl (*S*)-2-hydroxypropionate, CAS Number 687–47–8, 99.7% purity from gas chromatography, water content < 0.05% from Karl Fischer coulometric titration) was purchased from Fluka. It is a colorless and clear liquid that was degassed by ultrasound before any measurement and used without any additional purification.

PVT behavior

The apparatus used in the PVT measurements was previously described in detail.[45,50] The system is installed around a high-pressure vibrating tube densimeter. The cell temperature is controlled and measured to $\pm 1 \times 10^{-2}$ K and the pressure was kept constant to $\pm 5 \times 10^{-3}$ MPa and measured to $\pm 1 \times 10^{-2}$ MPa. The pressure transducer and thermometer were previously calibrated through well defined and traceable procedures. For proper apparatus calibration, a 14-parameter equation was used[50] with *n*-hexane (Fluka, 99.9%) and water (Millipore, resistivity 18.2 mΩ cm) as reference fluids.[51] The effect of sample viscosity on density readings is below the accuracy limit of measurements ($\pm 1 \times 10^{-4}$ g cm^{-3}), thus raw data without viscosity corrections were used in this work.

Experimental density data were fitted to the 10-parameter *TRIDEN* equation developed by Ihmehls and Gmehling.[34] From the fitting equation the derived properties isobaric thermal expansivity, α_P, isothermal compressibility, k_T, and internal pressure, P_i, were calculated.[52]

PηT behavior

Viscosity measurements were carried out using an electromagnetic viscometer VINCI Tech. EV1000.[35] Sample temperature is controlled and measured to $\pm 1 \times 10^{-2}$ K and pressure to $\pm 1 \times 10^{-2}$ MPa. Temperature and pressure sensors were previously calibrated through traceable procedures. Apparatus calibration was done using certified oils provided by the manufacturer. Viscosity accuracy was estimated to be ±1% in the full scale.

Experimental viscosity data were fitted for the whole pressure-temperature range to a 7-parameters Tait-like equation.[52,53] Pressure-viscosity, α_η, and temperature-viscosity, β_η, coefficients were calculated from fitting coefficients.

DFT calculations

DFT calculations were carried out with the Gaussian 03 package[54] according to Density Functional Theory (DFT), using the Becke gradient corrected exchange functional[55] and Lee-Yang-Parr correlation functional[56] with three parameters (B3LYP)[57] method. 6–311++g** basis set was used along this work. Calculations in solution were carried out using the self-consistent reaction field approach (SCRF) with the solvent treated as a continuum using the integral equation formalism of the PCM approach (IEF-PCM).[58] The cavity in which the solute is placed in the IEF-PCM approach was built using the united atom model in all the cases, a value of 1.2 was used to scale all the radii and 70 tesserae to divide the spherical surfaces. Atomic charges were calculated to fit the electrostatic potential[59] according to the Merz-Singh-Kollman (MK)[60] scheme. Interaction energies for complexes, ΔE, were calculated as the differences among the complex and sum of EL monomer energies at the same theoretical level, with basis set superposition error (BSSE) corrected through the counterpoise procedure.[61]

Molecular dynamics simulations

Classical molecular dynamics simulations were carried out using the TINKER molecular modelling package.[62] All simulations were performed in the NPT ensemble; the Nosé-Hoover method[63] was used to control the temperature and pressure of the simulation system. The motion equations were solved using the Verlet Leapfrog integration algorithm.[64] The molecular geometries were restrained according to the shake algorithm.[65] Long-range electrostatic interactions were treated with the smooth particle mesh Ewald method.[66] The simulated systems consist of cubic boxes with 200 molecules to which periodic boundary conditions were applied in three directions. The simulations were performed using a cutoff $L/2$ Å radius for the non-bonded interactions, L being the box side. Initial boxes were generated using the PACKMOL program[67] that uses the BOX-QUACAN[68] local-minimization method to obtain adequate starting configurations. These boxes were minimized according to the MINIMIZE program in the TINKER package to a 0.01 kcal mol^{-1} Å^{-1} *rms* gradient, then several heating and quenching steps in the NVT ensemble up to 500 K were performed after which a 100 ps NVT equilibration molecular dynamics simulation was run at the set temperature; finally, from the output NVT simulation configuration, a run of 500 ps

(time step 1 fs) in the NPT ensemble at the set temperature and pressure was run, from which the first 100 ps were used to ensure equilibration (checked through constant energy) and the remaining 400 ps for data collection. EL was described according to the so-called Optimized Potential for Liquid Simulations (all atom version) OPLS-AA.[48] MK charges obtained through B3LYP/6–311++g** calculations were used in the simulations.

Monte Carlo/Gibbs ensemble simulations

Coupled–decoupled[69] dual cutoff[70] configurational bias[71] simulations using the MF-CPN strategy[72] were performed using MCCCS Towhee code in the NVT-Gibbs ensemble.[49] Ewald sum method was used to handle the columbic interactions. Vapor–liquid coexistence calculations require a 2-box simulation, the probability of the molecule transfer move between both boxes was set to achieve one accepted movement every 5–10 cycles, where a cycle is N moves (with N being the number of molecules). The probability of the remaining moves was set to 0.002 for volume changes, to 0.01 for type 1 aggregation volume bias moves, and equally divided between translation, rotation and configurational bias regrowths. OPLS-AA forcefield was applied with the same parameters as for molecular dynamics simulations. Simulations were performed on 200 total EL molecules. Systems were equilibrated for 50 000 cycles (1×10^7 Monte Carlo Steps) and the production runs of 40 000 cycles (8×10^6 Monte Carlo Steps) were broken into 20 blocks for error estimation.

Acknowledgements

References

1 J. M. DeSimone, *Science*, 2002, **297**, 799.
2 R. Höfer and J. Bigorra, *Green Chem.*, 2007, **9**, 203.
3 *World solvents. Industry study with forecast to 2007 & 2012 for 14 countries & six regions*, The Freedonia Group, Cleveland, 2003.
4 R. A. Sheldon, *Green Chem.*, 2005, **7**, 267.
5 C. Capello, U. Fischer and K. Hungerbühler, *Green Chem.*, 2007, **9**, 927.
6 W. M. Nelson, *Green solvents for chemistry: perspectives and practice*, Oxford University Press, New York, 2003.
7 N. V. Plechkova and K. R. Seddon, *Chem. Soc. Rev.*, 2008, **37**, 123.
8 J. M. DeSimone, W. Tumas, (Eds.), *Green Chemistry using liquid and supercritical carbon dioxide*, Oxford University Press, New York, 2003.
9 P. L. Short, *Chem. Eng. News*, 2006, **84**, 15.
10 J. C. Warner, A. S. Cannon and K. M. Dye, *Environ. Impact Assess. Rev.*, 2004, **24**, 775.
11 J. J. Clary, V. J. Feron and J. A. van Velthuijsen, *Regul Toxicol. Pharmacol.*, 1998, **27**, 88.
12 C. T. Bowner and R. Hooftman, *Chemosphere*, 1998, **37**, 1317.
13 N. Asthana, A. K. Kolah, D. R. Vu, C. T. Lira and D. Miller, *Org. Process Res. Dev.*, 2005, **9**, 599.
14 J. Gao, X. M. Zhao, L. Y. Zhou and Z. H. Huang, *Chem. Eng. Res. Des.*, 2007, **85**, 525.
15 D. J. Benedict, S. J. Parulekar and S. P. Tsai, *Ind. Eng. Chem. Res.*, 2003, **42**, 2282.
16 O. Sánchez, G. Vidriales, E. Morales and E. Ortiz, *Chem. Eng. J.*, 2006, **117**, 123.
17 K. Trychta, D. A. Sandberg and M. Henry, *Pollution Prevention Rev.*, 2001, **44**, 33.
18 S. M. Nikles, M. Piao, A. M. Lane and D. E. Nikles, *Green Chem.*, 2001, **3**, 109.
19 W. Den, F. Ko and T. Huang, *IEEE T. Semicond. M.*, 2002, **15**, 540.
20 F. Mottu, A. Laurent, D. A. Rufenach and E. Doelker, *PDA J. Pharm. Sci. Technol*, 2000, **54**, 456.
21 D. L. White, J. A. Bardole, Paint and Finish Removers. In: *Kirk-Othmer encyclopedia of chemical technology*, John Wiley and Sons, New York, 2000.
22 R. Dohrn and O. Pfohl, *Fluid Phase Equilibr.*, 2002, **194–197**, 15.
23 S. Aparicio, S. Halajian, R. Alcalde, B. García and J. M. Leal, *Chem. Phys. Lett.*, 2008, **454**, 49.
24 J. Chen and H. Chu, *J. Chem. Eng. Data*, 2007, **52**, 650.
25 J. M. Resa, J. M. Goenaga, A. I. Sanchez and M. Iglesias, *J. Chem. Eng. Data*, 2006, **51**, 1294.
26 S. Peña, R. Murga, M. T. Sanz and S. Beltrán, *Fluid Phase Equilibr*, 2005, **230**, 197.
27 J. D. Raal, A. Muhlbauer, *Phase Equilibria: Measurement and Computation*, CRC, Washington DC, 1997.
28 S. Aparicio, *J. Phys. Chem. A*, 2007, **111**, 4671.
29 N. Borho and M. A. Suhm, *Org. Biomol. Chem.*, 2003, **1**, 4351.
30 R. F. W. Bader, *Atoms in Molecules: a Quantum Theory*, Oxford University Press, Oxford, 1990.
31 A. E. Reed, L. A. Curtiss and F. Weinhold, *Chem. Rev.*, 1988, **88**, 899.
32 U. Koch and P. L. A. Popelier, *J. Phys. Chem.*, 1995, **99**, 9747.
33 P. L. A. Popelier, *J. Phys. Chem.*, 1998, **102**, 1873.
34 E. C. Ihmehls and J. Gmehling, *Ind. Eng. Chem. Res.*, 2001, **40**, 4470.
35 S. Aparicio, R. Alcalde, B. García, J. M. Leal, *J. Phys,. Chem.*, Submitted.
36 J. A. Riddick, W. B. Bunger, T. K. Sakano, *Organic Solvents: Physical Properties and Methods of Purification*, Wiley–Interscience, New York, 1986.
37 I. C. Sanchez and R. H. Lacombe, *Macromolecules*, 1978, **11**, 1145.
38 B. Coto, F. Mossner, C. Pando, R. G. Rubio and J. A. R. Renuncio, *Fluid Phase Equilibr.*, 1997, **133**, 89.
39 K. Gauter and R. A. Heidemann, *Ind. Eng. Chem. Res.*, 2000, **39**, 1115.
40 H. Machida, Y. Sato and R. L. Smith, *Fluid Phase Equilibr.*, 2008, **264**, 147.
41 M. Rodnikova and J. Barthel, *J. Mol. Liq.*, 2007, **131–132**, 121.
42 M. J. R. Dack, *Chem. Soc. Rev.*, 1975, **4**, 211.
43 E. V. Ivanov and V. K. Abrosimov, *J. Struct. Chem.*, 2005, **46**, 856.
44 M. Temprado and J. S. Chickos, *Thermochim. Acta*, 2005, **435**, 49.
45 S. Aparicio, B. García, R. Alcalde, M. J. Dávila and J. M. Leal, *J. Phys. Chem. B*, 2006, **110**, 6933.
46 J. S. Chickos and W. E. Acree Jr, *J. Phys. Chem. Ref. Data*, 2003, **32**, 519.
47 G. F. Carruth and R. Kobayashi, *Ind. Eng. Chem. Fundam.*, 1972, **11**, 509.
48 W. L. Jorgensen, D. S. Maxwell and J. Tirado–Rives, *J. Am. Chem. Soc.*, 1996, **118**, 11225.
49 J. R. Errington and A. Z. Panagiotopoulos, *J. Phys. Chem. B*, 1998, **102**, 7470.
50 B. García, S. Aparicio, R. Alcalde, M. J. Dávila and J. M. Leal, *Ind. Eng. Chem. Res.*, 2004, **43**, 3205.
51 E. W. Lemmon, M. O. McLinden, D. G. Friend, Thermophysical Properties of Fluid Systems. In: *NIST Chemistry WebBook, NIST Standard Reference Database Number 69*, Eds. P. J. Linstrom, and W. G. Mallard, National Institute of Standards and Technology, Gaithersburg MD, June 2005, (http://webbook.nist.gov).
52 M. J. Dávila, S. Aparicio, R. Alcalde, B. García and J. M. Leal, *Green Chem.*, 2007, **9**, 221.
53 M. J. P. Comuñas, A. Baylaucq, C. Boned and J. Fernández, *Int. J. Thermophys.*, 2001, **22**, 749.
54 M. J. Frisch, G. W. Trucks, H. B. Schlegel, G. E. Scuseria, M. A. Robb, J. R. Cheeseman, J. A. Montgomery, Jr., T. Vreven, K. N. Kudin, J. C. Burant, J. M. Millam, S. S. Iyengar, J. Tomasi, V. Barone, B. Mennucci, M. Cossi, G. Scalmani, N. Rega, G. A. Petersson, H. Nakatsuji, M. Hada, M. Ehara, R. Toyota, R. Fukuda, J. Hasegawa, M. Ishida, T. Nakajima, Y. Honda, O. Kitao, H. Nakai, M. Klene, X. Li, J. E. Knox, H. P. Hratchian, J. B. Cross, C. Adamo, J. Jaramillo, R. Gomperts, R. E. Stratmann, O. Yazyev, A. J. Austin, R. Cammi, C. Pomelli, J. W. Ochterski, P. Y. Ayala, K. Morokuma, G. A. Voth, P. Salvador, J. J. Dannenberg, V. G. Zakrzewski, S. Dapprich, A. D. Daniels, M. C. Strain, O. Farkas, D. K. Malick, A. D. Rabuck,

K. Raghavachari, J. B. Foresman, J. V. Ortiz, Q. Cui, A. G. Baboul, S. Clifford, J. Cioslowski, B. B. Stefanov, G. Liu, A. Liashenko, P. Piskorz, I. Komaromi, R. L. Martin, D. J. Fox, T. Keith, M. A. Al-Laham, C. Y. Peng, A. Nanayakkara, M. Challacombe, P. M. W. Gill, B. Johnson, W. Chen, M. W. Wong, C. Gonzalez, J. A. Pople, J. A. Gaussian, *03 (Revision C.02)*, Gaussian, Inc., Wallingford CT, 2004.

55 A. D. Becke, *Phys. Rev. A*, 1988, **38**, 3098.
56 C. Lee, W. Yang and R. G. Parr, *Phys. Rev. B*, 1988, **37**, 785.
57 A. D. Becke, *J. Chem. Phys.*, 1993, **98**, 5648.
58 E. Cances and B. Mennucci, *J. Math. Chem.*, 1998, **23**, 309.
59 U. C. Singh and P. A. Kollman, *J. Comput. Chem.*, 1984, **5**, 129.
60 B. H. Besler, K. M. Merz and P. A. Kollman, *J. Comput. Chem.*, 1990, **11**, 431.
61 S. Simon, M. Duran and J. J. Dannenberg, *Chem. Phys.*, 1996, **105**, 11024.

62 J. W. Ponder, J. W. TINKER, *Software tool for molecular design*. 4.2 ed, *Washington University School of Medicine*, 2004.
63 W. G. Hoover, *Phys. Rev. A*, 1985, **31**, 1695.
64 M. P. Allen, D. J. Tildesley, *Computer Simulation of Liquids* Clarendon Press: Oxford, UK, 1989.
65 J. P. Rickaert, G. Ciccotti and H. J. Berendsen, *J. Comput. Phys.*, 1977, **23**, 327.
66 U. L. Essmann, M. L. Perera, T. Berkowitz, H. Darden, H. Lee and L. G. Pedersen, *J. Chem. Phys.*, 1995, **103**, 8577.
67 J. M. Martínez and L. Martínez, *J. Comput. Chem.*, 2003, **24**, 819.
68 A. Friedlander, J. M. Martínez and S. A. Santos, *Appl. Math. Opt.*, 1994, **30**, 235.
69 M. G. Martin and J. I. Siepmann, *J. Phys. Chem. B*, 1999, **103**, 4508.
70 T. J. H. Vlugt, M. G. Martin, B. Smit, J. I. Siepmann and R. Krishna, *Mol. Phys.*, 1998, **94**, 727.
71 J. I. Siepmann and D. Frenkel, *Mol. Phys.*, 1992, **75**, 59.
72 M. G. Martin and A. L. Frischknecht, *Mol. Phys.*, 2006, **104**, 2439.

This journal is © The Royal Society of Chemistry 2009

An environmentally benign solvent-free Tishchenko reaction

Daniel C. Waddell and James Mack*

Herein, we describe the solvent-free ball milling Tishchenko reaction. Using high speed ball milling and a sodium hydride catalyst, the Tishchenko reaction was performed for aryl aldehydes in high yields in 0.5 hours. The reaction is not affected by the type of ball bearing used and can be successful when conducted in a liquid nitrogen environment.

Introduction

Environmental concerns about solvent-based chemistry have stimulated a renewed interest in the study of chemical reactions under solvent-free conditions.[1–3] Although most of the research conducted in this area has been performed by using a mortar and pestle, high speed ball milling (HSBM) is an attractive solvent-free method that has started to gain attention. In the HSBM method, a ball bearing is placed inside a vessel that is shaken at high speeds.[4,5] The high speed attained by the ball-bearing has enough force to make an amorphous mixture of the reagents that subsequently facilitate a chemical reaction.

The use of commericial ball mills have allowed these reactions to be scaled up to industrial levels, therefore understanding organic reactions using this methodology can significantly reduce solvent waste.[4,6–9] We recently reported that the rate of the Baylis–Hillman reaction is increased under HSBM conditions and we developed a safe solvent-free method for the reduction of esters.[10,11] In this work, we describe the Tishchenko reaction under these novel conditions.

The conversion of aldehydes to their dimeric esters, better known as the Tishchenko reaction (Scheme 1) has been known for more than a hundred years.[12] This reaction is heavily used in industry,[13] and it is inherently environmentally benign since it utilizes catalytic conditions and is 100% atom economic. Over the years, chemists have looked to develop new reagents that are more efficient than the aluminum based catalysts traditionally used. Metal catalysts such as alkali metals,[14–17] alkali metal oxides, lanthanides,[18–22] and many others have been developed towards the improvement of Tishchenko chemistry. Unfortunately, many of these catalysts react sluggishly with aromatic aldehydes or provide the ester product in low yield.[23–25] It was demonstrated that catalytic diisobutylaluminum hydride (DIBAL-H) reacts with aliphatic aldehydes to give the dimeric ester but it does not give the Tishchenko product with aryl
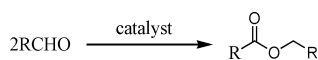
aldehydes.[24] Catalysts such as lithium bromide and lanthanide catalysts undergo the Tishchenko reaction with aryl aldehydes in high yield, but long reaction times (2–3 days) are required.[25] One of the simplest and cheapest catalysts that has been used for the generation of benzyl benzoate from benzaldehyde has been sodium hydride. Although sodium hydride is generally thought of as a non-nucleophilic base,[26] Swamer and Hauser demonstrated in refluxing benzene that benzaldehyde can be converted to benzyl benzoate in moderate yield.[27] Since benzaldehyde was the lone example in this report, the scope and limitations of the Tishchenko reaction using sodium hydride as the catalyst are still absent from the literature. Further, the use of benzene as the solvent under these conditions significantly increases the health risk, especially on large scale. We thought the use of high speed ball milling under solvent-free conditions would afford us the possibility of using sodium hydride as the catalyst, while avoiding the use of benzene. Further, we predicted that under HSBM conditions catalytic activity would be very high due to the high concentration of materials in the reaction vials.

Results and discussion

Our results are summarized in Table 1. We started our process by reacting various aryl aldehydes in the presence of a catalytic amount of sodium hydride. We attempted 1% and 2% mol catalyst but found the reaction was most effective with 10% sodium hydride. Typically, the reactions were conducted in a custom made $1/2'' \times 2''$ inch screw-capped stainless steel vial and milled with a $1/8''$ inch stainless steel ball-bearing in a Spex certiprep mixer/mill 8000M open to the atomsphere for 30 minutes (Scheme 2). At the conclusion of the reaction the products were recrystallized with 95% ethanol and dried over a Hirsch funnel. Liquid products were isolated from extraction with the minimal amount of methylene chloride.[28] Upon isolation ^{1}H NMR, ^{13}C NMR and GC-MS were compared to literature values to confirm product formation. We were able to convert benzaldehyde to benzyl benzoate in as little
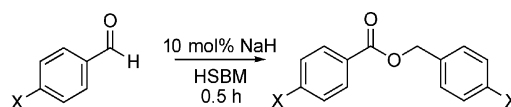

Scheme 1 Tishchenko reaction.

University of Cincinnati, 301 Clifton Court, Cincinnati, OH, USA.
E-mail: james.mack@uc.edu; Fax: +1 513 556 9239;
Tel: +1 513 556 9249

Scheme 2 Conducting the Tishchenko reaction under solvent-free ball milling conditions.

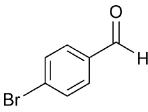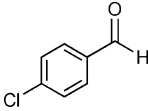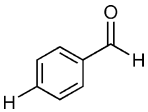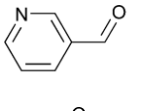**Table 1** Tishchenko reaction of aryl aldehydes using 10% sodium hydride catalyst
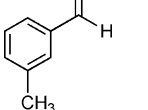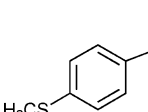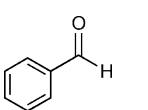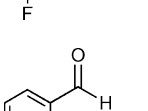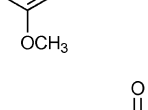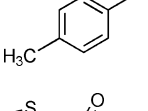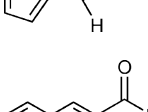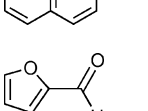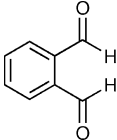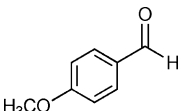
Entry	Substrate	Time (hrs)	% Conversion	% Yield	TOF
1	4-bromobenzaldehyde (Br)	2	>99	91	2.5
2	4-chlorobenzaldehyde (Cl)	0.5	>99	92	10
3	benzaldehyde (H)	0.5	>99	98	10
4	pyridine-3-carbaldehyde	0.5	86	80	10
5	3-methylbenzaldehyde (CH₃)	2	94	86	2.5
6	4-(methylthio)benzaldehyde (H₃CS)	2	>99	93	2.5
7	3-fluorobenzaldehyde (F)	0.5	>99	91	10
8	3-methoxybenzaldehyde (OCH₃)	2	>99	97	2.5
9	4-methylbenzaldehyde (H₃C)	2	80	69	2.5
10	thiophene-2-carbaldehyde	2	80	70	2.5
11	2-naphthaldehyde	16	95	91	1
12	furan-2-carbaldehyde	2	86	69	2.5

Table 1 *(Contd.)*

Entry	Substrate	Time (hrs)	% Conversion	% Yield	TOF
13	phthalaldehyde	2	>99	93	2.5
14	4-methoxybenzaldehyde (H₃CO)	16	>99	97	1

as 30 minutes under HSBM conditions compared to 5 hrs in solution.[27] The turnover frequencies (TOF's) were determined from complete conversion.[29]

Our success with aryl aldehydes led us to investigate the Tishchenko reaction of aliphatic and α,β unsaturated aldehydes. Using sodium hydride as the catalyst we attempted the ball milled Tishchenko reaction with 3-phenylpropional, pentanal, and 1,2,3,6-tetrahydro-benzaldehyde. Our results showed that straight chain non-hindered aldehydes such as 3-phenylpropional and pentanal gives only a small amount of the dimeric ester with these substrates; with the majority of the products arising from aldol condensation chemistry. However, when sterically hindered aldehydes are used, such as 1,2,3,6-tetrahydro-benzaldehyde the dimeric ester is the major product and we observed no product resulting from the aldol condensation. α,β unsaturated systems such as cinnamaldehyde and 2-butenal gave a mixture of products which included the expected dimeric ester as well as products which arise from conjugate additon into the double bond. We also examined the reaction with acetaldehyde for the preparation of ethyl acetate but instead of obtaining ethyl acetate under these conditions the reaction resulted in the formation of a polymer.[30]

Since the Tishchenko reaction is catalyzed by various metals, we wanted to investigate the role of the ball material on this reaction. Using the dimerization of benzaldehyde to form benzyl benzoate as the benchmark, we explored the affect of ball material on the Tishchenko reaction under HSBM conditions. Benzaldehyde and 10 mol% sodium hydride was ball milled for fifteen minutes and the % conversion was analyzed by ¹H NMR. The reactions were conducted in dupilcate and run with a 1/8″ stainless steel ball, 1/8″ brass ball and in the absence of a ball. In this particular reaction we saw similar % conversion irrespective of the ball material used, each giving ~30% conversion. The most surprising result is that we observed the reaction was just as sucessful in the absence of a ball bearing. This suggests the high speed movement of the vial provides enough energy to cause this reaction. We thought since benzaldehyde is a liquid, a ball may not be needed in order create the proper mixing at the molecular level for this reaction to take place. To test this hypothesis, we ball milled *p*-chlorobenzaldehyde, a solid, to determine if the reaction procedes in the absence of a ball. To our surprise, after 30 minutes of milling the reaction proceeded in similar yield to reactions

conducted with brass and stainless steel balls (~99% conversion). This suggests at least for this particular reaction that the shaking of the vial has enough energy to make an amorphous mixture of the reagents to provide a chemical reaction even without a ball!

On very large scale, ball milled reactions can generate a signifigant amount of heat, thus we wanted to conduct these reactions in the Spex Certiprep freezer mill in a liquid nitrogen environment to determine the feasibility of the reaction under low temperature conditions. Using our typical conditions, *p*-chlorobenzaldehyde and sodium hydride was placed inside a reaction vial and cooled to −196 °C. The reaction was milled for 30 minutes at which point it was allowed to warm to room temperature. ^{1}H NMR and GC-MS both confirmed the presence of the expected dimeric ester of *p*-chlorobenzaldehyde (~5% yield). This demonstrates the ability to conduct ball milling experiments in a low temperature environment which would allow this process to be implemented with highly exothermic reactions.

In an attempt to avoid handling sodium hydride, we wanted to generate our catalyst in situ. Sodium formate is known under certain condtions to break down to sodium hydride and carbon dioxide.[26,31,32] We thought we could use sodium formate, which is safe and very easy to handle as a direct precusor to the sodium hydride catalyst. Unfortunately, after ball milling benzaldehyde and sodium formate for 16 hours we saw no evidence of the desired dimeric ester. It has been shown that various metal catalyst can facilitate the disproportion of sodium formate to sodium hydride and carbon dioxide.[33–36] We tested whether a combination of catalytic sodium formate (10 mol%) and palladium tetrakistriphenylphospine (1 mol%) would lead to the generation of the sodium hydride catalyst. Using this mixture along with benzaldehyde we were able to generate trace amounts of benzyl benzoate after milling for 44 hours (Scheme 3).
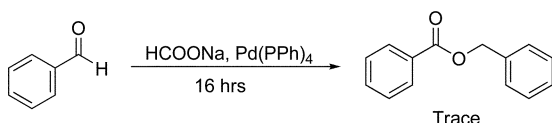
Scheme 3 Generation of sodium hydride catalyst from sodium formate and palladium tetrakistriphenylphosphine.

In addition to sodium hydride, we also investigated other benign catalysts that could give high yields of the Tishchenko reaction using ball milling conditions. Ball milling benzaldehyde with catalysts such as lithium bromide and calcium oxide did not provide the desired dimeric ester but rather gave unreacted starting material. We custom made vials out of nickel and molybdenum to investgate if these metals would lead to Tishchenko products, however, neither of these gave the dimeric ester product even under long milling times. It was reported that benzaldehyde can be converted to benzyl benzoate using magnesium metal as the catalyst in refluxing toluene.[37] We ball milled *p*-chlorobenzaldehyde along with magnesium metal and observed >95% yield of expected dimeric ester. We are in the process of making magnesium vials to determine if the magnesium vial itself will be a sutiable catalyst under these conditions.

Conclusions

In conclusion, we report an environmentally benign method for the Tishchenko reaction using solvent-free ball milling conditions. We used sodium hydride as the catalyst instead of the more traditional aluminum catalyst which allowed the reaction to procede in high yield and short reaction times. We discovered in this particular reaction the type of ball used has little to no affect on the yield or rate of the reaction and the reaction proceeded equally well without the addition of a ball. We also observed the ball milled Tishchenko reaction can take place while the vial is immersed in a liquid nitrogen environment. Currently, we are in the process of creating a magnesium vial that is expected to act as the catalyst as well. Ball milling is a novel method for conducting organic reactions. With a better understanding of how these reactions procede we will be able to make significant strides in the development of various solvent-free reactions.

Experimental

All NMR spectra were recorded on a Bruker Avance 400 spectrometer. Deuterated NMR solvents were obtained from Cambridge Isotope Laboratories, Inc., Andover MA, and used without further purification. *p*-bromobenzaldehyde, *p*-chloro-benzaldehyde, *p*-anisaldehyde, benzaldehyde, *p*-tolualdehyde, *p*-(methylthio)benzaldehyde, *m*-anisaldehyde, napthaldehyde, 2-thiophenecarboxaldehyde and sodium hydride were purchased from Acros Organics and used without further purification. *m*-Fluorobenzaldehyde, *m*-tolualdehyde and 1,2-phthalic carboxaldehyde were purchased from Sigma-Aldrich and used without further purification. Ball milling was carried out in a 8000M SpexCertiprep Mixer/Mill. Ball milling under a liquid nitrogen was carried out in a 6750 SpexCertiprep Freezer/Mill. Ball bearings were purchased from Small Parts incorporated. Custom made vials were made by the machine shop at the University of Cincinnati with metal rods purchased from ESPICorp Inc.

Typical procedure

Benzaldehyde (0.22 g, 2.07 mmol), and sodium hydride (0.004 g, 0.2 mmol) were added to a custom-made 2″ by 1/2″ screw capped stainless steel vial along with a 1/8″ inch stainless steel ball bearing. The vial was placed in an 8000M Spex Certiprep mixer/mill and the contents were ball milled for 0.5 h. The resulting mixture was dissolved in methylene chloride[28] (15 mL) and washed with 10% HCl (15 mL). The organic layer was dried over anhydrous $MgSO_4$ and the solvent was evaporated under reduced pressure. This afforded benzyl benzoate in > 98% yield.

Notes and references

1 K. Tanaka and F. Toda, *Chem. Rev.*, 2000, **100**, 1025–1074.
2 K. Tanaka, *Solvent-Free Organic Synthesis*, Wiley-VCH, Cambridge, 2003.
3 G. Rothenberg, A. P. Downie, C. L. Raston and J. L. Scott, *J. Am. Chem. Soc.*, 2001, **123**, 8701–8708.
4 C. Suryanarayana, *Prog. Mater Sci.*, 2000, **46**, 1–184.
5 L. Takacs, *Prog. Mater Sci.*, 2002, **47**, 355–414.
6 V. V. Boldyrev, *J. Mater. Sci.*, 2004, **39**, 5117–5120.
7 M. A. Mikhailenko, T. P. Shakhtshneider and V. V. Boldyrev, *J. Mater. Sci.*, 2004, **39**, 5435–5439.

8 G. Kaupp, *CrystEngComm*, 2003, **5**, 117–133.
9 G. Kaupp, *CrystEngComm*, 2006, **8**, 794–804.
10 J. Mack and M. Shumba, *Green Chem.*, 2007, **9**, 328–330.
11 J. Mack, D. Fulmer, S. Stofel and N. Santos, *Green Chem.*, 2007, **9**, 1041–1043.
12 W. Tischtschenko, *Chem. Zentralbl*, 1906, 1.
13 T. Seki, T. Nakajo and M. Onaka, *Chem. Lett.*, 2006, **35**, 824–829.
14 R. Crimmin Mark, G. M. Barrett Anthony, S. Hill Michael and A. Procopiou Panayiotis, *Org. Lett.*, 2007, **9**, 331–333.
15 M. A. Pasha and B. Ravindranath, *Indian J. Chem. Sect B*, 1985, **24B**, 1068–1069.
16 O. P. Tormakangas and A. M. P. Koskinen, *Tetrahedron Lett.*, 2001, **42**, 2743–2746.
17 F. J. Villani and F. F. Nord, *J.Am.Chem.Soc.*, 1947, **69**, 2605–2607.
18 K. Yokoo, N. Mine, H. Taniguchi and Y. Fujiwara, *J. Organomet. Chem.*, 1985, **279**, C19–C21.
19 H. Beberich and P. W. Roesky, *Angew. Chem. Int. Ed.*, 1998, **37**, 1569–1571.
20 M. R. Burgstein, H. Berberich and P. W. Roesky, *Chem. Eur. J.*, 2001, **7**, 3078–3085.
21 G. B. Deacon, A. Gitlits, P. W. Roesky, M. R. Burgstein, K. C. Lim, B. W. Skelton and A. H. White, *Chem. Eur. J.*, 2001, **7**, 127–138.
22 J. Mlynarski, J. Jankowska and B. Rakiel, *Tetrahedron: Asymmetry*, 2005, **16**, 1521–1526.
23 S.-y. Onozawa, T. Sakakura, M. Tanaka and M. Shiro, *Tetrahedron*, 1996, **52**, 4291–4302.
24 Y.-S. Hon, Y.-C. Wong, C.-P. Chang and C.-H. Hsieh, *Tetrahedron*, 2007, **63**, 11325–11340.
25 M. M. Mojtahedi, E. Akbarzadeh, R. Sharifi and M. S. Abaee, *Org. Lett.*, 2007, **9**, 2791–2793.
26 P. Caubere, *Top. Curr. Chem.*, 1978, **73**, 105–124.
27 F. W. Swamer and C. R. Hauser, *J.Am.Chem.Soc.*, 1946, **68**, 2647–2649.
28 Using the minimal amount of ethyl acetate is just as effective in this procedure for isolating the desired product.
29 J. Takehara, S. Hashiguchi, A. Fujii, S. -i. Inoue, T. Ikariya and R. Noyori, *Chem. Commun.*, 1996, 233–234.
30 Conducting the same reaction in refluxing toluene gives the same polymeric material.
31 R. A. W. Johnstone, A. H. Wilby and I. D. Entwistle, *Chem. Rev.*, 1985, **85**, 129–170.
32 T. A. Bryson, J. M. Jennings and J. M. Gibson, *Tetrahedron Lett.*, 2000, **41**, 3523–3526.
33 D. E. Linn, Jr., R. B. King and A. D. King, Jr., *J. Organomet. Chem.*, 1988, **355**, C1–C4.
34 Y. Ben-David, M. Gozin, M. Portnoy and D. Milstein, *J. Mol. Catal.*, 1992, **73**, 173–180.
35 X. Li, X. Wu, W. Chen, F. E. Hancock, F. King and J. Xiao, *Org. Lett.*, 2004, **6**, 3321–3324.
36 A. Schlatter, M. K. Kundu and W.-D. Woggon, *Angew. Chem. Int. Ed.*, 2004, **43**, 6731–6734.
37 P. I. Schorigin, W. Gussewa and A., *Chem. Ber.*, 1933, **66**, 1435.

Biodegradable pyridinium ionic liquids: design, synthesis and evaluation

Jitendra R. Harjani,[a] Robert D. Singer,[b] M. Teresa Garcia[c] and Peter J. Scammells*[a]

A range of ionic liquids (ILs) with a pyridinium cation were synthesised and their biodegradability was evaluated using the CO_2 Headspace test (ISO 14593). ILs bearing an ester side chain moiety were prepared from either pyridine or nicotinic acid and showed high levels of biodegradation under aerobic conditions and can be classified as 'readily biodegradable'. In contrast, pyridinium ILs with alkyl side chains showed significantly lower levels of biodegradability in the same test. The utility of the biodegradable IL **6c** as a reaction solvent for the Diels–Alder reaction was also investigated.

Introduction

Ionic liquids (ILs) have earned themselves a reputation as excellent reaction media. Earlier applications of ILs were mainly as electrolytes, solvents and extractants. The scope of their application is now broader and covers their use as reaction media, fuel cells, optical fluids, solar cells, energetic materials, heat transfer fluids and lubricants, to name only a few.[1] In chemical synthesis, the initial interest in the use of ILs was mainly to realize their advantages for transition metal mediated catalysis in biphasic reaction systems.[2] With time, this was further broadened by utilising them for catalysis using supported IL phases,[3] designing task-specific (functionalized) ILs for catalysis,[4] using ILs as supports for the substrates[5] and designing novel materials.[6] The properties of ILs, such as broad solvating ability, good thermal and chemical stability, non-volatility and non-flammability under operational conditions, not only adds to their versatility, but may make them a safer substitute to conventional solvents. ILs as reaction media can offer better reaction selectivity, higher reaction yields and reusability. These advantages further add to their green attributes. Although, some of these properties, such as good chemical stability, volatility *etc.*, have been challenged, it is notable that not all the ILs have all these ideal properties.[7] By varying the cations and anions that constitute their structure, it is typically possible to design ILs with the desired solvent characteristics for the chemical process of interest. The only principles of green chemistry which may disqualify ILs as a green solvent replacements are the necessity to 'use safer solvents and reaction conditions' and 'design chemicals and products to degrade after use'.[8] Designing ILs that are safe to release in to the environment

would address both of these issues. As ILs make a transition from academic curiosities to commercial commodities, their environmental impact is certainly concerning.[9] Rightfully so, the life cycle assessment of newer chemicals (such as ILs) and designing benign chemicals are now considered as an integral part of green chemistry.[10]

In contrast to the other possible fates of any chemical released into the environment, biodegradation appears to be the cleanest ultimate fate for any compound. This natural process of decay is an intensive collective endeavor of a number of microbes with different metabolic capabilities, ultimately leading to the formation of non-toxic inorganic products such as carbon dioxide, water and/or biomass. The assessment of environmental impact of ILs has mainly centered on the evaluation of their toxicity,[10b,11] however it is known that a refractory organic substance, if released in to the environment, would bio-accumulate and may eventually lead to chronic toxic effects.[12] Earlier investigations have also indicated that structural features, such as alkyl chain length, that can decrease resistance to microbial attack may also increase the toxicity of the ILs.[13] As suitable structural design has helped integrate low toxicity with high biodegradability in some commercial products in the past (*e.g.* drilling fluids), we believe that appropriately designing the ILs may lead to the solvents with desired attributes that would not pose problems to the environment.[12]

Our initial investigations on the evaluation of biodegradability of ILs were centered on the most commonly used imidazolium based ILs. The biodegradability of this class of ILs increased if the ester group was integrated in to the structure, however the amide group did not have any significant influence.[14] The ester group derived from a C_2 acid and C_5 linear alcohol on the imidazolium side chain and the octyl sulfate anion together enhances the ready biodegradability of the IL to meet the standard 60% cutoff value in 28 days.[15]

Our interest in assessing the biodegradability of the pyridinium based ILs (another commonly used class of ILs) was due to their popularity as ionic solvents. Our curiosity was peaked by the results reported by Engberts and Hulst *et al.*[16] Their research on the pyridinium based amphiphiles showed high vulnerability of their products to enzymatic attack. Their results were also

[a] *Medicinal Chemistry and Drug Action, Monash Institute of Pharmaceutical Sciences, Monash University, Parkville, 3052, Victoria, Australia. E-mail: peter.scammells@vcp.monash.edu.au; Fax: +61 3 99039582; Tel: +61 3 9903 9542*
[b] *Department of Chemistry, Saint Mary's University, Halifax, Nova Scotia, B3H 3C3, Canada*
[c] *Department of Surfactant Technology, IIQAB-CSIC, Jordi Girona 18–26, 08034, Spain. E-mail: mtgbet@iiqab.csic.es; Fax: +34 93 204 5904; Tel: +34 93 400 6100*

suggestive of very low toxicity of these compounds. Around the same time, the results on the study of biodegradability of some cationic surface active compounds with pyridinium head group also indicated the susceptibility of the pyridinium ring towards the microbial attack.[17] While our studies were underway, Docherty *et al.* measured biodegradability of 1,3-dialkylpyridinium bromides using the OECD 301 A (DOC Die-Away Test), and found that pyridinium bromide with a linear C_6 side chain mineralized completely after 49 days of incubation, and with a linear C_8 side chain, mineralization occurred after 25 days.[18] ^{1}H NMR, DNA-PCR-DGGE and TDN analysis established that the pyridinium ring is metabolized in the process of biodegradation. Very recently, Jastorff *et al.* investigated a family of unsubstituted and substituted 1-*n*-alkylpyridinium halides for biodegradation.[19] The disappearance of the substrates was monitored by HPLC (with UV detection) to calculate their primary biodegradation. However, as respirometric parameters (O_2 depletion/CO_2 formation) were not used for the measurement of mineralization, the method does not reflect the ready biodegradability of the compounds tested. Being interested by these reports, we sought to systematically investigate the ready biodegradability of the pyridinium based ILs/salts derived from pyridine and nicotinic acid, a relatively inexpensive natural product that can be used to incorporate the pyridinium core in the IL moiety.[20]

Results and discussion

Target ionic liquids were prepared using standard methodology. This initially involved alkylation of pyridine or the appropriate 3-substituted pyridine with an alkyl halide to afford the corresponding pyridinium halide (Scheme 1). Alternative anions were subsequently introduced by a metathesis reaction with sodium octyl sulfate, potassium hexafluorophosphate or lithium bis(trifluormethanesulfonimide).
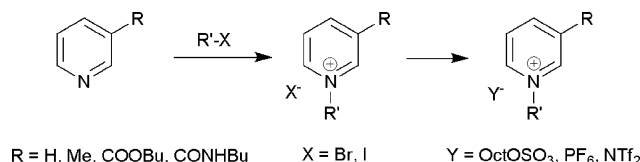
Scheme 1 Synthesis of pyridinium ILs.

Pyridinium salts with C_4 linear alkyl chains at position 1 (compounds **1a**, **c** and **d**) did not show high levels of biodegradability (Fig. 1). The presence of the methyl group at the 3-position of the pyridine ring helps induce the asymmetry in the structure, rendering the salt **2a** liquid at room temperature, but certainly does not help improve the biodegradability of the IL. The 1-butylpyridinium salts based on Br^-, PF_6^- and NTf_2^- showed only 1–3% biodegradability over a 28 day period, unless octyl sulfate was employed as the anion. The biodegradability as high as 37–40% was attained by the incorporation of an octyl sulfate counter ion, which is obviously an effect induced by the anion. These observations on the resistance of 1-butylpyridinium salts towards biodegradation are consistent with the earlier results documented by Docherty[18] and Jastorff *et al.*[19] 1-Alkylpyridinium bromides with linear C_{10} and C_{16} substituents (**3** and **4**) showed poor biodegradability at 9% and 0%, respectively.
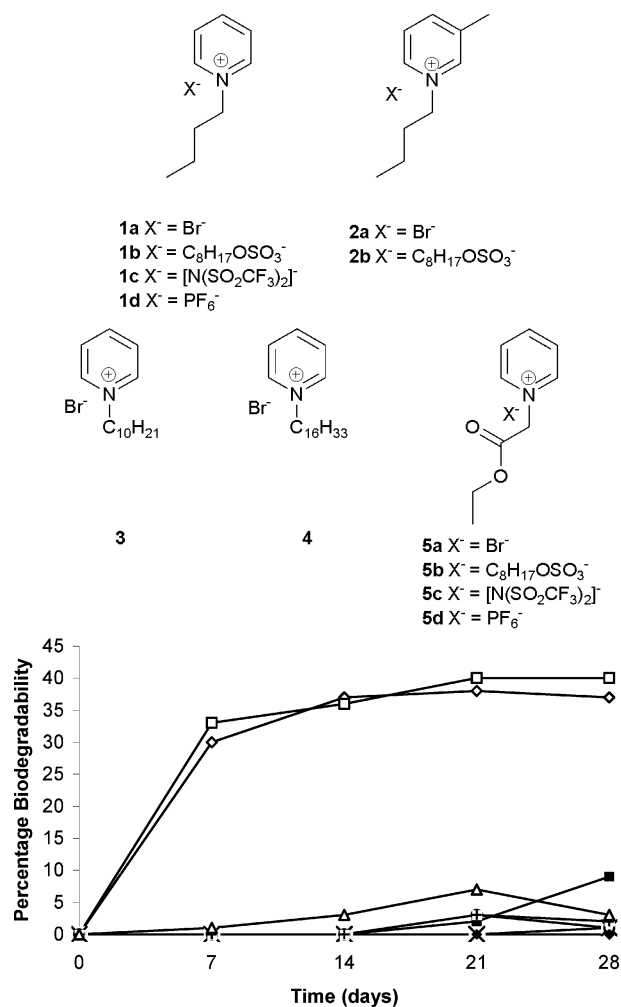
Fig. 1 Percentage biodegradability of the alkyl pyridinium based quaternary salts **1a** (○), **1b** (□), **1c** (+), **1d** (△), **2a** (×), **2b** (◇), **3** (■) and **4** (♦).

The introduction of the ester group seems to have a profound effect on the biodegradability of these salts.[21] The quaternary salt **5a** derived from two simple starting materials, pyridine and ethyl bromoacetate and the corresponding octyl sulfate IL, **5b**, both showed a comparable biodegradability at 87 and 89% respectively (Fig. 2). The biodegradability attained by these compounds after the first 7 days was 71 and 74% respectively (Fig. 2). As the halide ion is not likely to have significant influence on biodegradability, these results indicate that the pyridinium nucleus is not refractory and that appropriate structural manipulations of this core can lead to compounds with good ready biodegradability values. It is also worth noting that the presence or absence of the octyl sulfate anion (which is generally known to have positive influence on the ready biodegradability) seems to have only a meagre influence on the overall high biodegradability values. The exchange of bromide ion with NTf_2^- produces a low viscosity IL **5c** and with PF_6^- produces a solid **5d** which is sparingly solubility in water. Both **5c** and **5d** contain fluorine in the anion component and show ready biodegradability at 64 and 86% respectively, both above the 60% threshold (Fig. 2). It is also notable that in this series the NTf_2^- based IL offers lower (by 23% on average) biodegradability than the corresponding Br^-,

This journal is © The Royal Society of Chemistry 2009

5a X⁻ = Br⁻
5b X⁻ = C₈H₁₇OSO₃⁻
5c X⁻ = [N(SO₂CF₃)₂]⁻
5d X⁻ = PF₆⁻

6a X⁻ = I⁻
6b X⁻ = C₈H₁₇OSO₃⁻
6c X⁻ = [N(SO₂CF₃)₂]⁻
6d X⁻ = PF₆⁻

7a X⁻ = I⁻
7b X⁻ = C₈H₁₇OSO₃⁻

8a X⁻ = I⁻
8b X⁻ = C₈H₁₇OSO₃⁻

Fig. 2 Percentage biodegradability of alkyl pyridinium based quaternary salts with ester group appended on the side chain; **5a** (×), **5b** (+), **5c** (▲) and **5d** (□).
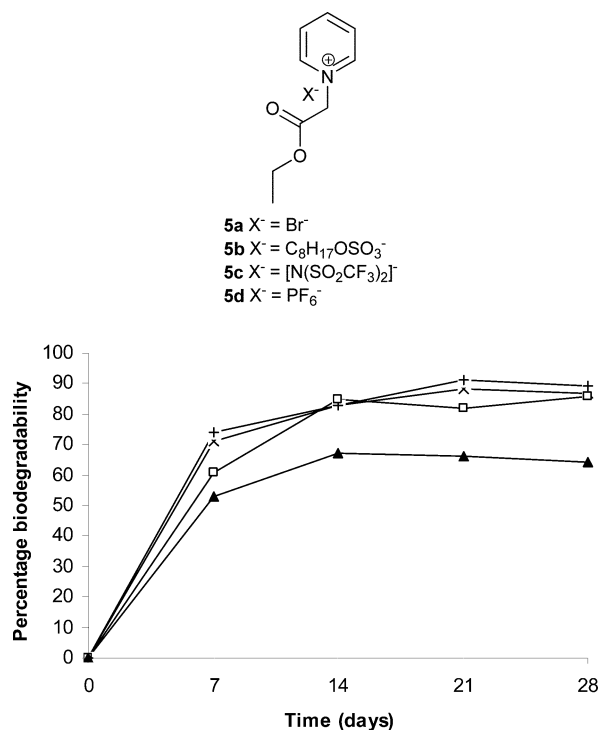
Fig. 3 Percentage biodegradability of alkyl pyridinium based quaternary salts derived from nicotinic acid; **6a** (△), **6b** (×), **6c** (♦), **6d** (+), **7b** (■) and **8b** (○).

OctOSO₃⁻ and PF₆⁻ counterparts. This may, in part, be because of the lack of water miscibility of the NTf₂⁻ based IL. The good biodegradability of ILs with fluorine containing anions such as NTf₂⁻ and PF₆⁻ is particularly significant as the ILs with these anions possess good solvent characteristics and these anions are amongst the most commonly encountered in ILs.

ILs derived from nicotinic acid in which the ester moiety was incorporated into the 3-position of the pyridinium cation were also investigated. Synthesizing the ILs from biorenewable chemicals such as nicotinic acid, as opposed to petrochemicals such as pyridine is acknowledged as a good argument in favor of sustainable development of products.[22] Butyl nicotinate was synthesized from nicotinic acid and was subjected to quaternization with alkyl iodides, mainly because of the reduced nucleophilicity of the nitrogen on the pyridine ring. The quaternization of butyl nicotinate with methyl iodide produced **6a**. The *N*-alkylation of butyl nicotinate with butyl iodide followed by anion metathesis yields **7b**. Both **6a** and **7b** offer promising biodegradability at 72 and 84%, respectively (Fig. 3). The octyl sulfate containing **6b**, the triflimide based **6c** and the hexafluorophosphate containing IL **6d** were synthesized from quaternary iodide **6a** showed biodegradability at 75, 68 and 75% respectively (Fig. 3). It is notable that **6a–d** showed greater than 60% biodegradability within the first seven days of incubation. The increased biodegradability of **7b** over **6b** is perhaps because of an increase in the lipophilicity of cation. This finding is consistent with previous studies in which cations with longer alkyl side chains were found to be more biodegradable.[14,19] The simple primary amide *N*-butyl nicotinamide derived from nicotinic acid and butyl amine was used to synthesize the nicotinamide based IL **8b**. The ready biodegradability of 30%
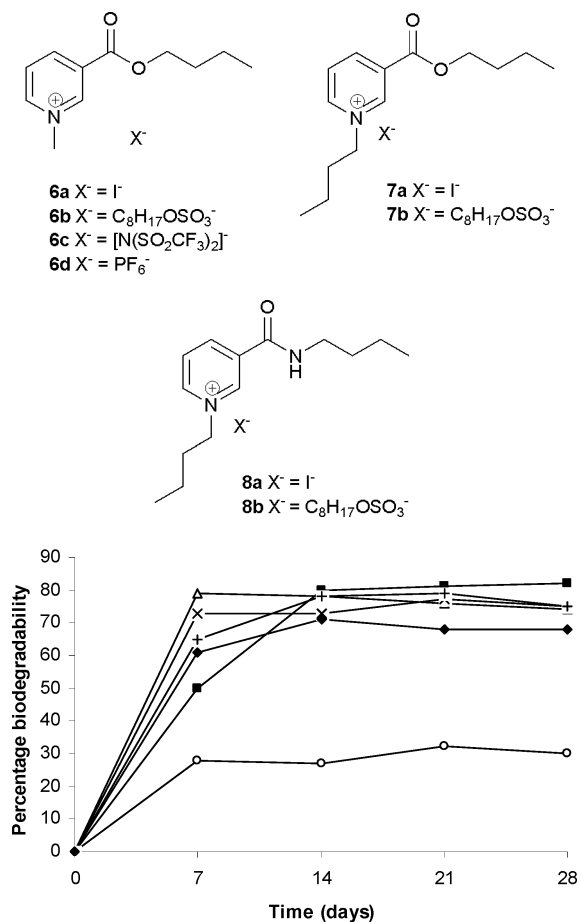
(Fig. 3) after a standard 28 day period perhaps indicates the recalcitrance of the nicotinamide derived IL under the test conditions. This inertness of amide containing IL is consistent with our earlier observations on the imidazolium series under similar test conditions.[14] The resistance of amides towards biodegradation has also been documented earlier in the design of biodegradable imidazolium ILs.[12]

Compounds which undergo 60% mineralization in 28 days using methods based on respirometry are defined as "readily biodegradable". Levels of 60% mineralization also may indicate the use of test substances for the production of biomass (which is eventually but not immediately used as a source of energy) and thus this value may equate to higher levels of ultimate biodegradation (around 90%) and even higher values of primary biodegradation (at least > 90%). It is important to note that the tests for ready biodegradability are generally performed under the most stringent conditions of lower microbial population and with the test substance as the sole source of carbon. Also, the concentration of the test substance is unrealistically higher than what would normally be observed in a practical scenario in the environment or a typical waste water treatment plant. Therefore 60% biodegradability obtained by these methods indicates that the test substance should undergo speedy and complete biodegradation upon release into an aquatic environment. Not

surprisingly, the tests for ready biodegradability have had a long history of successful applications.

A preliminary investigation into the use of the biodegradable ionic liquid (BIL), 3-(butoxycarbonyl)-1-methylpyridinium triflimide (**6c**), as a reaction solvent has also been conducted. We chose the Diels–Alder reaction for this purpose as this cycloaddition is one of the most extensively used methods to construct six membered carbo- and heterocyclic compounds.[23] This reaction has been investigated well not only in the Lewis acidic ILs,[24] but also in the 'second generation' neutral ILs.[25] In the neutral ILs the rates of this reaction are increased by doping the IL with Lewis acid catalysts[26] or mineral acid catalysts.[27] The combination of neutral ILs with ultrasound[28] or microwave[29] has also proved useful in enhancing the rate of this reaction. It has been demonstrated that ILs not only offers an advantage as a reaction media, but also exert effects on the rates[30] and selectivity[31] of Diels–Alder reaction when compared with the conventional solvents. The reaction has also been investigated in the imidazolium based BILs by our group.[32] Accordingly, the plethora of comparative data available for Diels–Alder reactions in covalent solvents and ionic liquids made it an obvious choice for the evaluation of the novel ionic liquids reported herein.

Cyclopentadiene was used as the diene component, as it is one of the most commonly used reactive diene in Diels–Alder reactions. The reaction of cyclopentadiene with methyl acrylate afforded 70% product after 24 h and 97% after 72 h (Table 1, Entry 1). A range of other dienophiles, including methyl vinyl

ketone (Entry 2), dimethylacetylene dicarboxylate (Entry 3), maleic anhydride (Entry 4), *N*-phenylmaleimide (Entry 5) and dimethyl maleate (Entry 6) were also investigated. In all cases, the dienophiles reacted readily with cyclopentadiene in the BIL **6c** to produce the corresponding Diels–Alder adduct in good to nearly quantitative yields. It is notable that the reactivity is dictated by the electron deficient character of the dienophile, which also indirectly influences the reaction time and selectivity. The reactive dienophiles also offer excellent *endo* selectivity. The crude products in all the cases were isolated by extracting the reaction mixture with diethyl ether. The purity of IL was ascertained by ^{1}H NMR and can be reused after evaporating the traces of diethyl ether under reduced pressure. The products in all the cases were purified by column chromatography and the *endo*:*exo* ratio in all the cases was determined by ^{1}H NMR.

Conclusions

It can be concluded that ionic liquids with a pyridinium cation bearing an ester containing substituent at positions 1 or 3 show excellent biodegradability. The biodegradability does not seem to significantly depend on the anion, although some effects are apparent. The high ready biodegradability values attest the earlier claims of tendency of the pyridine ring to mineralize.[16–19] In contrast, 1-alkylpyridinium ILs with linear C_4, C_{10} and C_{16} showed relatively low levels of biodegradability. Although the presence of linear alkyl chains is an important factor in designing biodegradable compounds as they can act as potential sites for attack by oxygenases,[10b,14b] no significant improvement was detected for these 1-alkylpyridinium bromides. However, as ionic liquids with longer alkyl chains have been proven to be more toxic,[15b,33] further studies are underway to clarify if their resistance towards biodegradation in the ready biodegradability tests could be related to their toxic effects on the biological activity of the aerobic micro-organisms.
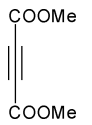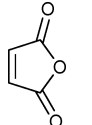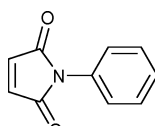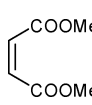
The biodegradable ionic liquid (BIL), 3-(butoxycarbonyl)-1-methylpyridinium triflimide (**6c**), was demonstrated to be a viable reaction medium as exemplified with the Diels–Alder reaction. In general, high yields and *endo* selectivities were observed.

Experimental

Synthesis

Nicotinic acid (Sigma-Aldrich, 98%), lithium triflimide (Aldrich, 97%), potassium hexafluorophosphate (Fluka, 98%), sodium octyl sulfate (Sigma, ~95%), methyl iodide (Sigma-Aldrich, 99%), butyl iodide (Fluka ≥ 98%), 1-butanol (BDH, 99%), thionyl chloride (Fluka, ≥ 99%), ethyl bromoacetate (Merck, > 98%), toluene (Merck, GR, ≤ 0.03% H_2O), acetonitrile (Merck, Chromatography grade, ≤ 0.02% H_2O), diethyl ether (Merck, GR, ≤ 0.03% H_2O), butyl amine (Sigma-Aldrich, 99.5%), pyridine (BDH, 98%) and triethylamine (Sigma-Aldrich, 99%) were procured from the commercial supplier and used without any pre-treatment. The ^{1}H and ^{13}C NMR spectra of the purified products were recorded in $CDCl_3$ (Cambridge Isotope Laboratories Inc., 99.8% D) or DMSO d_6 (Cambridge Isotope Laboratories Inc., 99.9% D) on a Bruker Avance

Table 1 Diels–Alder reactions in 3-(butoxycarbonyl)-1-methyl-pyridinium triflimide (**6c**)

Entry	Dienophile	Reaction time	Isolated yield[a]	*endo*:*exo* ratio[b]
1	COOMe	72 h	97%	76:24
2	COMe	72 h	57%	79:21
3	COOMe / COOMe	2 h	97%	100:0
4	maleic anhydride	10 min	100%	100:0
5	*N*-phenylmaleimide	10 min	97%	100:0
6	COOMe / COOMe	18 h	95%	95:5

[a] Isolated by column chromatography. [b] Determined by ^{1}H NMR.

DPX 300 spectrometer at 300 and 75.4 MHz, respectively. Low resolution mass spectra using electrospray ionisation (ES-MS) were obtained using a Micromass Platform II instrument. Unless otherwise stated, cone voltage was 20 eV.

Butyl nicotinate

Thionyl chloride (81.30 mmol) was gradually added to the suspension of nicotinic acid (40.65 mmol) in toluene (100 mL) maintained at room temperature. The reaction mixture was heated at 100 °C for 24 h, to assure the quantitative formation of the nicotinic acid chloride (as a hydrochloride salt). After decanting the solution of unreacted thionyl chloride in toluene, the acid chloride was washed with diethyl ether (4 × 50 mL) and then treated with dichloromethane (100 mL). The reaction mixture was cooled under dry ice and gradually treated with triethylamine (81.30 mmol) followed by 1-butanol (81.30 mmol). The reaction mixture was stirred at room temperature for 24 h and then treated with water and stirred vigorously to yield a clear dichloromethane layer. Butyl nicotinate, being a water insoluble Brønsted base, was separated and purified by treating the organic layer with 6 N HCl solution (20 mL). The acidic aqueous layer was first extracted with dichloromethane (2 × 20 mL), and treated with an aqueous base, ammonium hydroxide, to release the pure ester. The ester was separated by extraction of the aqueous layer with dichloromethane (2 × 20 mL), followed by drying and evaporation at reduced pressure. Yield 50%. ^{1}H NMR (CDCl$_3$): δ 0.97–1.02 (t, J = 7.4 Hz, 3H), 1.43–1.55 (m, 2H), 1.73–1.83 (m, 2H), 4.36–4.40 (t, J = 6.6 Hz, 2H), 7.40–7.44 (m, 1H), 8.31–8.35 (m, 1H), 8.77–8.79 (m, 1H), 9.23–9.24 (m, 1H). ^{13}C NMR (CDCl$_3$): δ 13.8, 19.3, 30.8, 65.4, 123.4, 126.5, 137.1, 151.0, 153.4, 165.4. ES-MS (+ ve): m/z, 180.0 [M + 1]$^+$.

N-Butyl nicotinamide

The acid chloride was prepared and purified as per the procedure described above. The reaction mixture was cooled under dry ice and gradually treated with butyl amine (122 mmol). After stirring at room temperature for 3 h, the reaction mixture was treated with water and stirred vigorously to yield a clear dichloromethane layer. The isolation of product was carried out by quenching the reaction mixture with water, followed by drying and evaporation of the dichloromethane at reduced pressure. Yield 52%. ^{1}H NMR (CDCl$_3$): δ 0.96–1.01 (t, J = 7.2 Hz, 3H), 1.38–1.50 (m, 2H), 1.59–1.69 (m, 2H), 3.46–3.53 (m, 2H), 6.15 (bs, 1H), 7.37–7.41 (m, 1H), 8.10–8.14 (m, 1H), 8.72–8.74 (m, 1H), 8.95–8.96 (m, 1H). ^{13}C NMR (CDCl$_3$): δ 13.8, 20.2, 31.6, 40.0, 123.4, 130.7, 135.1, 148.2, 151.9, 165.9. ES-MS (+ ve): m/z, 179.0 [M + 1]$^+$.

General procedures for the synthesis of pyridinium halides (1a, 2a, 3, 4, 5a and 6a)[34]

To the solution of pyridine/3-substituted pyridine (33.3 mmol) in toluene (20 mL), was added alkyl halide (40.0 mmol) at room temperature, followed by stirring at room temperature for 1 h under nitrogen. The reaction mixture was then stirred at 110 °C for 24 h. In the case of **5a** and **6a**, the reactions were heated at 70 °C and 45 °C, respectively. In all the cases, the completion of the reaction was marked by the separation of either the dense IL

layer or solid from the initially obtained clear and homogenous mixture of amine and alkyl halide in toluene. The product was isolated by decanting the toluene layer to remove the unreacted starting materials and solvent. Subsequently, the quaternary salt was washed with diethyl ether (4 × 20 mL) and each time the ether layer was separated from the quaternary halide by decantation. In some cases, the ether washings resulted in the formation of a solid. The solid was purified by dissolving in acetonitrile (20 mL) and precipitation with diethyl ether (60–70 mL). In each case, the IL/salt was finally dried at a reduced pressure to get rid of all the volatile organic compounds. These quaternary salts (except **6a**) being hygroscopic, were handled under nitrogen at each stage of synthesis and purification.

1-Butylpyridinium bromide (1a). Yield 96%. ^{1}H NMR (CDCl$_3$): δ 0.89–0.94 (t, J = 7.4 Hz, 3H), 1.33–1.43 (m, 2H), 1.96–2.06 (m, 2H), 4.96–5.01 (t, J = 7.5 Hz, 2H), 8.11–8.16 (m, 2H), 8.50–8.56 (m, 1H), 9.59–9.62 (m, 2H). ^{13}C NMR (CDCl$_3$): δ 13.4, 19.1, 33.7, 61.5, 128.4, 145.2. ES-MS (+ ve): m/z, 136.3 [M–Br]$^+$; ES-MS (−ve): m/z, 79.1 and 81.1 [Br]$^-$.

1-Butyl-3-methylpyridinium bromide (2a). Yield 96%. ^{1}H NMR (CDCl$_3$): δ 0.94–0.99 (t, J = 7.4 Hz, 3H), 1.37–1.49 (m, 2H), 1.99–2.09 (m, 2H), 2.66 (s, 3H), 4.95–5.00 (t, J = 7.5 Hz, 2H), 7.98–8.03 (m, 1H), 8.24–8.27 (m, 1H), 9.31–9.33 (m, 1H), 9.46 (s, 1H). ^{13}C NMR (CDCl$_3$): δ 13.5, 18.6, 19.3, 33.8, 61.4, 127.8, 139.6, 142.4, 144.7, 145.6. ES-MS (+ ve): m/z, 150.1 [M–Br]$^+$; ES-MS (−ve): m/z, 78.9 and 80.8 [Br]$^-$.

1-Decylpyridinium bromide (3). Yield 96%. ^{1}H NMR (DMSO d_6): δ 0.81–0.85 (t, J = 5.6 Hz, 3H), 1.22–1.26 (m, 14H), 1.89–1.93 (m, 2H), 4.64–4.69 (t, J = 6.8 Hz, 2H), 8.16–8.20 (m, 2H), 8.61–8.66 (m, 1H), 9.21–9.23 (m, 2H). ^{13}C NMR (DMSO d_6): δ 13.7, 21.9, 25.2, 28.3, 28.5, 28.6, 28.7, 30.7, 31.1, 60.4, 127.9, 144.7, 145.4. ES-MS (+ ve): m/z, 220.2 [M–Br]$^+$; ES-MS (−ve): m/z, 79.0 and 81.0 [Br]$^-$.

1-Hexadecylpyridinium bromide (4). Yield 92%. ^{1}H NMR (DMSO d_6): δ 0.80–0.85 (t, J = 6.6 Hz, 3H), 1.21–1.26 (m, 26H), 1.89–1.93 (m, 2H), 4.65–4.70 (t, J = 7.5 Hz, 2H), 8.16–8.21 (m, 2H), 8.61–8.66 (m, 1H), 9.23–9.24 (m, 2H). ^{13}C NMR (DMSO d_6): δ 13.8, 22.0, 25.3, 28.3, 28.6, 28.7, 28.8, 28.9, 29.0, 30.7, 31.2, 60.5, 128.0, 144.7, 145.40. ES-MS (+ ve): m/z, 304.4 [M–Br]$^+$; ES-MS (−ve): m/z, 79.0 and 81.0 [Br]$^-$.

1-(2-Ethoxycarbonyl)methylpyridinium bromide (5a). Yield 89%. ^{1}H NMR (DMSO d_6): δ 1.24–1.29 (t, J = 7.2 Hz, 3H), 4.21–4.28 (q, J = 7.1 Hz, 2H), 5.68 (s, 2H), 8.23–8.27 (m, 2H), 8.70–8.75 (m, 1H), 9.05–9.07 (m, 2H). ^{13}C NMR (DMSO d_6): δ 13.9, 60.2, 62.2, 127.7, 146.2, 146.7, 166.3. ES-MS (+ ve): m/z, 166.1 [M − Br]$^+$; ES-MS (−ve): m/z, 79 and 81 [Br]$^-$.

3-(Butoxycarbonyl)-1-methylpyridinium iodide (6a). Yield 98%. ^{1}H NMR (DMSO d_6): δ 0.92–0.97 (t, J = 7.4 Hz, 3H), 1.39–1.52 (m, 2H), 1.70–1.79 (m, 2H), 4.39–4.45 (m, 5H), 8.24–8.29 (m, 1H), 8.95–8.98 (m, 1H), 9.19–9.21 (m, 1H), 9.52 (s, 1H). ^{13}C NMR (DMSO d_6): δ 13.4, 18.4, 29.9, 48.4, 66.0, 127.8, 129.2, 144.6, 146.5, 148.7, 161.6. ES-MS (+ ve): m/z 194.0 (M–I)$^+$; ES-MS (−ve, 70 eV): m/z, 126.8 [I]$^-$.

3-(Butoxycarbonyl)-1-butylpyridinium iodide (7a). Butyl nicotinate (33.3 mmol) was treated with butyl iodide

(166.5 mmol) at room temperature and the reaction mixture was heated at 140 °C for 48 h, while been stirred under nitrogen atmosphere. The resultant reaction mixture was treated with water (40 mL) and stirred for 10 min. The aqueous quaternary iodide solution was purified by extracting it with diethyl ether (3 × 20 mL). A light yellowish brown liquid was obtained by freeze drying the purified aqueous solution and further drying for 24 h at 50 °C under reduced pressure. Yield 70%. ^{1}H NMR (DMSO d_6): δ 0.90–0.97 (m, 6H), 1.29–1.50 (m, 4H), 1.70–1.77 (m, 2H), 1.89–1.94 (m, 2H), 4.39–4.43 (t, J = 6.5 Hz, 2H), 4.69–4.74 (t, J = 7.5 Hz, 2H), 8.26–8.31 (m, 1H), 8.97–9.00 (m, 1H), 9.28–9.30 (m, 1H), 9.59 (s, 1H). ^{13}C NMR (DMSO d_6): δ 13.3, 13.5, 18.5, 18.7, 30.0, 32.7, 60.9, 66.1, 128.3, 130.0, 145.0, 145.8, 147.8, 161.7. ES-MS (+ ve): m/z 236.3 (M–I$^-$)$^+$; ES-MS (–ve, 70 eV): m/z, 126.9 [I]$^-$.

1-Butyl-(3-butylcarbamoyl)pyridinium iodide (8a). Butyl iodide (30.64 g, 166.5 mmol) was added to the solution of N-butylnicotinamide (5.933 g, 33.3 mmol) in toluene (20 mL) under nitrogen atmosphere. The reaction mixture was heated at 110 °C for 48 h, while maintaining the inert atmosphere. Toluene was evaporated at a reduced pressure and the resultant product was treated with water (50 mL). The crude aqueous quaternary iodide solution was extracted with diethyl ether (4 × 20 mL). A light yellow liquid was obtained by freeze drying the purified aqueous solution and subsequent drying under reduced pressure for 24 h at 50 °C. Yield 74%. ^{1}H NMR (CDCl$_3$): δ 0.93–1.03 (m, 6H), 1.37–1.51 (m, 4H), 1.71–1.79 (m, 2H), 2.02–2.12 (m, 2H), 3.46–3.53 (m, 2H), 4.89–4.94 (t, J = 7.5 Hz, 2H), 8.09–8.14 (m, 1H), 8.66–8.69 (m, 1H), 9.11–9.16 (m, 2H), 10.05 (s, 1H). ^{13}C NMR (CDCl$_3$): δ 13.5, 13.8, 19.4, 20.3, 31.2, 33.5, 40.3, 62.1, 128.4, 134.9, 143.6, 145.1, 145.9, 160.8. ES-MS (+ ve): m/z 235.3 (M–I$^-$)$^+$; ES-MS (–ve, 70 eV): m/z, 126.9 [I]$^-$.

General procedure for the synthesis of pyridinium octyl sulfates (1b, 2b, 5b, 6b, 7b and 8b)[35]

The quaternary salt (2 mmol) was dissolved in water to obtain a clear solution. The aqueous solution of quaternary halide was treated with the aqueous solution of sodium octyl sulfate (1.54 mmol in case of **1b**, **2b** and **5b** or 2 mmol in case of **6b**, **7b** and **8b** in 10 mL of water) and the resultant was stirred for 10 min. The product was isolated by solvent extraction using dichloromethane (3 × 10 mL). The extracts were dried over anhydrous MgSO$_4$ and evaporated under reduced pressure to yield the required product.

1-Butylpyridinium octyl sulfate (1b). Yield 90%. ^{1}H NMR (CDCl$_3$): δ 0.84–0.89 (t, J = 6.8 Hz, 3H), 0.93–0.98 (t, J = 7.4 Hz, 3H), 1.26–1.45 (m, 12H), 1.61–1.71 (m, 2H), 1.94–2.04 (m, 2H), 4.00–4.05 (t, J = 6.8 Hz, 2H), 4.76–4.81 (t, J = 7.4 Hz, 2H), 8.06–8.11 (m, 2H), 8.44–8.49 (m, 1H), 9.17–9.18 (m, 2H). ^{13}C NMR (CDCl$_3$): δ 13.6, 14.2, 19.4, 22.7, 26.0, 29.3, 29.4, 29.7, 31.9, 33.8, 62.0, 67.8, 128.7, 145.2, 145.5. ES-MS (+ ve): m/z, 136.3 [M–C$_8$H$_{17}$OSO$_3^-$]$^+$; ES-MS (–ve): m/z, 209.3 [C$_8$H$_{17}$OSO$_3$]$^-$.

1-Butyl-3-methylpyridinium octyl sulfate (2b). Yield 93%. ^{1}H NMR (CDCl$_3$): δ 0.85–0.89 (t, J = 6.8 Hz, 3H), 0.93–0.98 (t, J = 7.2 Hz, 3H), 1.26–1.45 (m, 12H), 1.61–1.71 (m, 2H), 1.93–2.03 (m, 2H), 2.62 (s, 3H), 4.01–4.05 (t, J = 6.9 Hz, 2H), 4.74–4.79

(t, J = 7.5 Hz, 2H), 7.93–7.97 (m, 1H), 8.19–8.22 (m, 1H), 8.94–8.96 (m, 1H), 9.02 (s, 1H). ^{13}C NMR (CDCl$_3$): δ 13.6, 14.2, 18.7, 19.4, 22.7, 26.0, 29.3, 29.4, 29.7, 31.9, 33.8, 61.8, 67.7, 128.0, 139.9, 142.6, 145.0, 145.5. ES-MS (+ ve): m/z, 150.1 [M–Br$^-$]$^+$; ES-MS (–ve): m/z, 209.1 [C$_8$H$_{17}$OSO$_3$]$^-$.

1-(2-Ethoxycarbonyl)methylpyridinium octyl sulfate (5b). Yield 83%. ^{1}H NMR (DMSO d_6): δ 0.84–0.88 (t, J = 5.7 Hz, 3H), 1.25–1.29 (m, 12H), 1.45–1.47 (m, 2H), 3.65–3.69 (t, J = 6.8 Hz, 3H), 4.21–4.28 (q, J = 7.1 Hz, 2H), 5.65 (s, 2H), 8.22–8.27 (m, 2H), 8.69–8.74 (m, 1H), 9.02–9.05 (m, 2H). ^{13}C NMR (DMSO d_6): δ 13.9, 22.0, 25.5, 28.6, 28.7, 29.0, 31.2, 60.3, 62.3, 65.4, 127.8, 146.3, 146.7, 166.3. ES-MS (+ ve): m/z, 166.1 [M – C$_8$H$_{17}$OSO$_3^-$]$^+$; ES-MS (–ve): m/z, 209.1 [C$_8$H$_{17}$OSO$_3$]$^-$.

3-(Butoxycarbonyl)-1-methylpyridinium octyl sulfate (6b). Quantitative. ^{1}H NMR (CDCl$_3$): δ 0.85–0.90 (t, J = 6.5 Hz, 3H), 0.97–1.02 (t, J = 7.4 Hz, 3H), 1.26–1.35 (m, 10H), 1.42–1.66 (m, 4H), 1.76–1.86 (m, 2H), 3.91–3.96 (t, J = 6.9 Hz, 2H), 4.43–4.48 (t, J = 6.8 Hz, 2H), 4.72 (s, 3H), 8.24–8.29 (m, 1H), 8.88–8.91 (m, 1H), 9.26 (s, 1H), 9.59–9.61 (m, 1H). ^{13}C NMR (CDCl$_3$): δ 13.8, 14.2, 19.2, 22.8, 26.0, 29.4, 29.5, 29.7, 30.6, 31.9, 49.9, 67.3, 67.7, 128.8, 130.7, 144.8, 146.5, 150.0, 161.5. ES-MS (+ve): m/z 194.0 [M – C$_8$H$_{17}$OSO$_3^-$]$^+$; ES-MS (–ve): m/z, 209.0 [C$_8$H$_{17}$OSO$_3$]$^-$.

3-(Butoxycarbonyl)-1-butylpyridinium octyl sulfate (7b). Yield 93%. ^{1}H NMR (DMSO d_6): δ 0.84–0.97 (m, 9H), 1.25–1.52 (m, 16H), 1.70–1.80 (m, 2H), 1.87–1.97 (m, 2H), 3.64–3.69 (t, J = 6.6 Hz, 2H), 4.39–4.43 (t, J = 6.6 Hz, 2H), 4.69–4.74 (t, J = 7.5 Hz, 2H), 8.26–8.30 (m, 1H), 8.97–9.00 (m, 1H), 9.27–9.29 (m, 1H), 9.59 (s, 1H). ^{13}C NMR (DMSO d_6): δ 13.2, 13.5, 13.8, 18.5, 18.7, 22.0, 25.5, 28.6, 28.7, 29.0, 30.0, 31.2, 32.7, 60.9, 65.4, 66.1, 128.4, 130.0, 145.0, 145.8, 147.9, 161.7. ES-MS (+ve): m/z 236.2 [M – C$_8$H$_{17}$OSO$_3^-$]$^+$; ES-MS (–ve): m/z, 209.1 [C$_8$H$_{17}$OSO$_3$]$^-$.

3-(Butylcarbamoyl)-1-butylpyridinium octyl sulfate (8b). Yield 87%. ^{1}H NMR (DMSO d_6): δ 0.82–0.95 (m, 9H), 1.25–1.60 (m, 18H), 1.88–1.98 (m, 2H), 3.30–3.37 (m, 2H), 3.65–3.69 (t, J = 6.6 Hz, 2H), 4.63–4.68 (t, J = 7.5 Hz, 2H), 8.23–8.28 (m, 1H), 8.89–8.91 (m, 1H), 8.98–9.02 (m, 1H), 9.18–9.20 (s, 1H), 9.43 (s, 1H). ^{13}C NMR (CDCl$_3$): δ 13.5, 13.9, 14.2, 19.5, 20.4, 22.8, 26.0, 29.3, 29.4, 29.7, 31.2, 31.9, 33.8, 40.7, 62.4, 68.2, 128.4, 135.8, 143.7, 144.9, 146.5, 161.0. ES-MS (+ve): m/z 235.1 [M – C$_8$H$_{17}$OSO$_3^-$]$^+$; ES-MS (–ve): m/z, 209.1 [C$_8$H$_{17}$OSO$_3$]$^-$.

General procedure for the synthesis of pyridinium triflimides (1c, 5c and 6c)

The quaternary halide (2 mmol) was dissolved in water (10 mL) to obtain a clear solution. The aqueous solution of quaternary halide was treated with the aqueous solution of bis(trifluormethanesulfonimide) lithium salt (2.2 mmol, 0.631 g in 10 mL water) and the resultant was stirred for 10 min. The product was isolated by solvent extraction using dichloromethane (2 × 10 mL). The extracts were dried over anhydrous MgSO$_4$ and evaporated under reduced pressure to yield the required product. As expected, all triflimide based ILs were low viscosity liquids at room temperature.

1-Butylpyridinium triflimide (1c). Yield 97%. ^{1}H NMR (DMSO d_6): δ 0.89–0.94 (t, J = 7.4 Hz, 3H), 1.24–1.37 (m, 2H), 1.86–1.98 (m, 2H), 4.58–4.63 (t, J = 7.4 Hz, 2H), 8.13–8.17 (m, 2H), 8.57–8.62 (m, 1H), 9.07–9.09 (m, 2H). ^{13}C NMR (DMSO d_6): δ 13.2, 18.7, 32.6, 60.6, 119.48 (–CF$_3$), 128.1, 144.7, 145.4. ES-MS (+ve): m/z, 136.2 ([M – [N(SO$_2$CF$_3$)$_2$]$^-$]$^+$; ES-MS (–ve): m/z, 280.0 [N(SO$_2$CF$_3$)$_2$]$^-$.

1-(2-Ethoxycarbonyl)methylpyridinium triflimide (5c). Yield 93%. ^{1}H NMR (DMSO d_6): δ 1.24–1.29 (t, J = 7.1 Hz, 3H), 4.22–4.29 (q, J = 7.1 Hz, 2H), 5.65 (s, 2H), 8.21–8.26 (m, 2H), 8.68–8.73 (m, 1H), 9.03–9.05 (m, 2H). ^{13}C NMR (DMSO d_6): δ 13.8, 60.3, 62.3, 119.5 (–CF$_3$), 127.8, 146.3, 146.7, 166.3. ES-MS (+ve): m/z, 166.1 ([M – [N(SO$_2$CF$_3$)$_2$]$^-$)$^+$; ES-MS (–ve) 280.0 [N(SO$_2$CF$_3$)$_2$]$^-$.

3-(Butoxycarbonyl)-1-methylpyridinium triflimide (6c). Yield 92%. ^{1}H NMR (CDCl$_3$): δ 0.96–1.01 (t, J = 7.4 Hz, 3H), 1.41–1.53 (m, 2H), 1.75–1.85 (m, 2H), 4.43–4.48 (t, J = 6.8 Hz, 2H), 4.52 (s, 3H), 8.12–8.16 (m, 1H), 8.93–8.95 (m, 2H), 9.14 (s, 1H). ^{13}C NMR (DMSO d_6): δ 13.4, 18.5, 30.0, 48.3, 66.1, 119.5 (CF$_3$), 127.9, 129.5, 144.7, 146.7, 148.8, 161.7. ES-MS (+ve): m/z, 194.1 [M – [N(SO$_2$CF$_3$)$_2$]$^-$]$^+$; ES-MS (–ve): m/z, 280.0 [N(SO$_2$CF$_3$)$_2$]$^-$.

General procedure for the synthesis of pyridinium hexafluorophosphates (1d, 5d and 6d)[36]

The quaternary salt (2 mmol) was dissolved in water (10 mL) to obtain a clear solution. The aqueous solution of quaternary halide was treated with the aqueous solution of potassium hexafluorophosphate (2.4 mmol, 0.405 g in 10 mL water) and the resultant was stirred for 10 min. The product was isolated by solvent extraction using dichloromethane (2 × 10 mL). The extracts were dried over anhydrous MgSO$_4$ and evaporated under reduced pressure to yield the desired product.

1-Butylpyridinium hexafluorophosphate (1d). Yield 89%. ^{1}H NMR (DMSO d_6): δ 0.89–0.94 (t, J = 7.4 Hz, 3H), 1.24–1.36 (m, 2H), 1.86–1.96 (m, 2H), 4.58–4.63 (t, J = 7.4 Hz, 2H), 8.12–8.16 (m, 2H), 8.56–8.61 (m, 1H), 9.05–9.07 (m, 2H), ^{13}C NMR (DMSO d_6): δ 13.2, 18.7, 32.6, 60.7, 128.1, 144.7, 145.4. ES-MS (+ve): m/z, 136.2 [M – PF$_6$$^-$]$^+$; ES-MS (–ve): m/z, 144.9 [PF$_6$]$^-$.

1-(2-Ethoxycarbonyl)methylpyridinium hexafluorophosphate (5d). Yield 70%. ^{1}H NMR (DMSO d_6): δ 1.24–1.29 (t, J = 7.2 Hz, 3H), 4.21–4.29 (q, J = 7.1 Hz, 2H), 5.65 (s, 2H), 8.21–8.26 (m, 2H), 8.68–8.73 (m, 1H), 9.02–9.04 (m, 2H). ^{13}C NMR (DMSO d_6): δ 13.9, 60.3, 62.3, 127.8, 146.2, 146.8, 166.3 ppm. ES-MS (+ve): m/z, 166.1 [M – PF$_6$$^-$]$^+$; ES-MS (–ve): m/z, 145.0 [PF$_6$]$^-$.

3-(Butoxycarbonyl)-1-methylpyridinium hexafluorophosphate (6d). Yield 86%. ^{1}H NMR (DMSO d_6): δ 0.92–0.97 (t, J = 7.4 Hz, 3H), 1.40–1.52 (m, 2H), 1.70–1.80 (m, 2H), 4.39–4.44 (m, 5H), 8.22–8.27 (m, 1H), 8.95–8.98 (m, 1H), 9.16–9.18 (m, 1H), 9.52 (s, 1H). ^{13}C NMR (DMSO d_6): δ 13.5, 18.5, 30.0, 48.3, 66.2, 127.9, 129.5, 144.7, 146.6, 148.8, 161.7. ES-MS (+ve): m/z, 194.0 [M – PF$_6$$^-$]$^+$; ES-MS (–ve): m/z, 145.0 [PF$_6$]$^-$.

General procedure for Diels–Alder reactions in BIL 6c

The dienophile (1.66 mmol) was added to 3-(butoxycarbonyl)-1-methylpyridinium triflimide (**6c**) (0.5 mL) and the mixture was stirred well for 1–3 min. Cyclopentadiene (2.33 mmol) was added and the reaction mixture was stirred at room temperature for the time specified in the Table 1. Diels–Alder adducts were extracted with diethyl ether (3 × 20 mL), the extracts were dried over anhydrous MgSO$_4$ and evaporated under reduced pressure to yield the crude products. All crude products were purified using column chromatography with ethyl acetate/petroleum spirits (ranging from 5% to 30% ethyl acetate) as an eluent. The ^{1}H and ^{13}C NNMR spectra of these products were identical to those previously reported in the literature.

ISO 14593-Carbon dioxide head space test

To evaluate the biodegradability of the test ILs, the "CO$_2$ Headspace" test (ISO 14593) was also applied. This method allows the evaluation of the ultimate aerobic biodegradability of an organic compound in an aqueous medium at a given concentration of microorganisms by analysis of inorganic carbon. The test IL, as the sole source of carbon and energy, was added at a concentration of 40 mg/L to a mineral salt medium. These solutions were inoculated with activated sludge collected from an activated sludge treatment plant, washed and aerated prior to use and incubated in sealed vessels with a headspace of air. Biodegradation (mineralization to carbon dioxide) was determined by measuring the net increase in the total organic carbon (TOC) levels over time compared with unamended blanks. Sodium n-dodecyl sulfate (SDS) was used as reference substance. The tests ran for 28 days. The extent of biodegradation was expressed as a percentage of the theoretical amount of inorganic carbon (ThIC) based on the amount of test compound added initially.

Acknowledgements

Notes and References

1 M. Smiglak, A. Metlen and R. D. Rogers, *Acc. Chem. Res.*, 2007, **40**, 1182–1192.
2 (*a*) P. Wasserscheid and W. Keim, *Angew. Chem., Int. Ed.*, 2000, **39**, 3772–3789; (*b*) J. Dupont, R. F. de Souza and P. A. Z. Suarez, *Chem. Rev.*, 2002, **102**, 3667–3691.
3 M. H. Valkenberg, C. de Castro and W. F. Hoelderich, *Green Chem.*, 2002, **4**, 88–93.
4 (*a*) Z. Fei, T. J. Geldbach, D. Zhao and P. J. Dyson, *Chem. Eur. J.*, 2006, **12**, 2122–2130; (*b*) S.-g. Lee, *Chem. Commun.*, 2006, 1049–1063.
5 W. Miao and T. H. Chan, *Acc. Chem. Res.*, 2006, **39**, 897–908.
6 T. Fukushima and T. Aida, *Chem. Eur. J.*, 2007, **13**, 5048–5058.
7 (*a*) P. Wasserscheid, *Nature*, 2006, **439**, 797; (*b*) S. Chowdhury, R. S. Mohan and J. L. Scott, *Tetrahedron*, 2007, **63**, 2363–2389.
8 T. Welton, *Green Chem.*, 2008, **10**, 483.
9 (*a*) J. H. Davis, Jr. and P. A. Fox, *Chem. Commun.*, 2003, 1209–1212; (*b*) D. Adam, *Nature*, **407**, 938–940.
10 (*a*) K. Kümmerer, *Green Chem.*, 2007, **9**, 899–907; (*b*) J. Ranke, S. Stolte, R. Störmann, J. Arning and B. Jastorff, *Chem. Rev.*, 2007, **107**, 2183–2206.

11 (*a*) M. Matsumoto, K. Mochiduki and K. Kondo, *J. Biosci. Bioeng.*, 2004, **98**, 344–347; (*b*) C. Pretti, C. Chiappe, D. Pieraccini, M. Gregori, F. Abramo, G. Monni and L. Intorre, *Green Chem.*, 2006, **8**, 238–240; (*c*) S. Stolte, M. Matzke, J. Arning, A. Boeschen, W.-R. Pitner, U. Welz-Biermann, B. Jastorff and J. Ranke, *Green Chem.*, 2007, **9**, 1170–1179.

12 R. S. Boethling, E. Sommer and D. DiFiore, *Chem. Rev.*, 2007, **107**, 2207–2227.

13 (*a*) K. M. Docherty, and C. Kulpa, Abstracts of Papers, 231st ACS National Meeting, Atlanta, GA, United States, March 26–30, 2006, 2006, IEC-174; (*b*) J. Ranke, K. Moelter, F. Stock, U. Bottin-Weber, J. Poczobutt, J. Hoffmann, B. Ondruschka, J. Filser and B. Jastorff, *Ecotoxicol. Environ. Safe.*, 2004, **58**, 396–404.

14 (*a*) N. Gathergood and P. J. Scammells, *Aust. J. Chem.*, 2002, **55**, 557–560; (*b*) N. Gathergood, M. T. Garcia and P. J. Scammells, *Green Chem.*, 2004, **6**, 166–175.

15 (*a*) N. Gathergood, P. J. Scammells and M. T. Garcia, *Green Chem.*, 2006, **8**, 156–160; (*b*) M. T. Garcia, N. Gathergood and P. J. Scammells, *Green Chem.*, 2005, **7**, 9–14.

16 (*a*) A. Roosjen, J. Šmisterová, C. Driessen, J. T. Anders, A. Wagenaar, D. Hoekstra, R. Hulst and J. B. F. N. Engberts, *Eur. J. Org. Chem.*, 2002, 1271–1277; (*b*) D. Pijper, E. Bulten, J. Šmisterová, A. Wagenaar, D. Hoekstra, J. B. F. N. Engberts and R. Hulst, *Eur. J. Org. Chem.*, 2003, 4406–4412.

17 E. Grabińska-Sota and J. Kalka, *Environ. Int.*, 2003, **28**, 687–690.

18 K. M. Docherty, J. K. Dixon and C. F. Kulpa, Jr., *Biodegradation*, 2007, **18**, 481–493.

19 S. Stolte, S. Abdulkarim, J. Arning, A.-K. Blomeyer-Nienstedt, U. Bottin-Weber, M. Matzke, J. Ranke, B. Jastorff and J. Thoeming, *Green Chem.*, 2008, **10**, 214–224.

20 Commercial grade nicotinic acid is priced at ~9.716 AU \$/mole (79 \$/kg) in Sigma-Aldrich catalogue.

21 J. R. Harjani, R. D. Singer, M. T. Garcia and P. J. Scammells, *Green Chem.*, 2008, **10**, 436–438.

22 (*a*) S. T. Handy, *Chem. Eur. J.*, 2003, **9**, 2938–2944; (*b*) G. Imperato, B. Koenig and C. Chiappe, *Eur. J. Org. Chem.*, 2007, 1049–1058.

23 J. Sauer and R. Sustmann, *Angew. Chem., Int. Ed. Engl.*, 1966, **5**, 211–230.

24 (*a*) C. W. Lee, *Tetrahedron Lett.*, 1999, **40**, 2461–2464; (*b*) A. P. Abbott, G. Capper, D. L. Davies, R. K. Rasheed and V. Tambyrajah, *Green Chemistry*, 2002, **4**, 24–26.

25 (*a*) D. A. Jaeger and C. E. Tucker, *Tetrahedron Lett.*, 1989, **30**, 1785–1788; (*b*) T. Fischer, A. Sethi, T. Welton and J. Woolf, *Tetrahedron Lett.*, 1999, **40**, 793–796; (*c*) P. Ludley and N. Karodia, *Tetrahedron Lett.*, 2001, **42**, 2011–2014.

26 (*a*) G. Silvero, M. J. Arevalo, J. L. Bravo, M. Avalos, J. L. Jimenez and I. Lopez, *Tetrahedron*, 2005, **61**, 7105–7111; (*b*) I. Hemeon, C. DeAmicis, H. Jenkins, P. Scammells and R. D. Singer, *Synlett*, 2002, 1815–1818.

27 A. Kumar and S. S. Pawar, *J. Org. Chem.*, 2007, **72**, 8111–8114.

28 J. L. Bravo, I. Lopez, P. Cintas, G. Silvero and M. J. Arevalo, *Ultrason. Sonochem.*, 2006, **13**, 408–414.

29 I. Lopez, G. Silvero, M. J. Arevalo, R. Babiano, J. C. Palacios and J. L. Bravo, *Tetrahedron*, 2007, **63**, 2901–2906.

30 (*a*) C. E. Song, E. J. Roh, S.-g. Lee, W. H. Shim and J. H. Choi, *Chem. Commun.*, 2001, 1122–1123; (*b*) Y. Xiao and S. Malhotra, *Tetrahedron Lett.*, 2004, **45**, 8339–8342.

31 M. J. Earle, P. B. McCormac and K. R. Seddon, *Green Chem.*, 1999, **1**, 23–25.

32 S. Bouquillon, T. Courant, D. Dean, N. Gathergood, S. Morrissey, B. Pegot, P. J. Scammells and R. D. Singer, *Aust. J. Chem.*, 2007, **60**, 843–847.

33 (*a*) R. S. Boethling, Designing Safer Chemicals, *ACS Symp. Ser.*, 1996, **640**, 156; (*b*) P. H. Howard, R. S. Boethling, W. Stiteler, W. Meylan and J. Beauman, *Sci. Total Environ.*, 1991, **109/110**, 635; (*c*) R. S. Boethling, *Cationic Surfactants, Surfactant Science Series Vol. 53*, Marcel Dekker, New York, 1994, pp. 95–135.

34 P. J. Dyson, M. C. Grossel, N. Srinivasan, T. Vine, T. Welton, D. J. Williams, A. J. P. White and T. Zigras, *J. Chem. Soc. Dalton Trans.*, 1997, 3465–3469.

35 P. Wasserscheid, R. van Hal and A. Boesmann, *Green Chem.*, 2002, **4**, 400–404.

36 J. G. Huddleston, A. E. Visser, W. M. Reichert, H. D. Willauer, G. A. Broker and R. D. Rogers, *Green Chem.*, 2001, **3**, 156–164.

Solvent-free Diels–Alder reactions of *in situ* generated cyclopentadiene†

David Huertas, Melinda Florscher and Veljko Dragojlovic*

A solvent-free Diels–Alder reaction was carried out by heating a mixture of dicyclopentadiene and a dienophile. Cyclopentadiene, formed *in situ*, reacted with the dienophile in a thermodynamically controlled reaction. Besides being solvent-free, the described procedure allows for almost complete utilization of dicyclopentadiene and avoids handling of noxious and hazardous cyclopentadiene. The reaction worked well with dienophiles such as maleic anhydride and unsaturated esters. However, unsaturated acids were not suitable dienophiles, yielding Diels–Alder adducts in a low yield.

Introduction

The Diels–Alder reaction is one of the most important methods for formation of six-membered rings.[1] Cyclopentadiene is one of the dienes frequently used in Diels–Alder reactions. It is unstable under ordinary conditions and, at room temperature, dimerizes into dicyclopentadiene. Usually it is obtained by cracking of dicyclopentadiene and is used immediately in a reaction. Cyclopentadiene has a rather strong and disagreeable odor and cracking has to be done in a fumehood. Furthermore, while retro Diels–Alder reactions are well known and have been extensively used in organic synthesis,[2] with numerous examples of an *in situ* generated diene being trapped by a more reactive dienophile,[3] other than a report of a solvent-free reaction of dicyclopentadiene with ethylene under high temperarature and pressure in an autoclave[4] and a similar process described in a patent,[5] dicyclopentadiene as an *in situ* source of cyclopentadiene has received relatively little attention. That is surprising given both its importance and safety implications. Pure cyclopentadiene has to be stored at a low temperature (–20 °C). Under ordinary conditions it undergoes a spontaneous and highly exothermic dimerization into dicyclopentadiene[6] and has been implicated in a fatal accident.[7] Moreover, only about 2/3 of dicyclopentadiene can be cracked.[8] The rest of it forms oligomers, which require

Wilkes Honors College of Florida Atlantic University, 5353 Parkside Drive, Jupiter, FL 33458, USA. E-mail: vdragojl@fau.edu; Fax: 561-799-8602; Tel: 561-799-8012
† Electronic supplementary information (ESI) available: Additional experimental details and ¹H NMR spectra of the isolated compounds. See DOI: 10.1039/b813485e

considerably higher temperature for cracking. Thus, when cyclopentadiene is obtained by cracking of dicyclopentadiene, one can expect, at best, an overall 65–70% reaction yield with respect to dicyclopentadiene. Therefore, a procedure that allows use of dicyclopentadiene directly would have important practical advantages. Finally, such a procedure may allow isolation of stereoisomers that are not commonly produced in a Diels–Alder reaction of cyclopentadiene. Recently, Diels–Alder reactions under solvent-free conditions in the presence of a catalyst[9] or under microwave irradiation[10] have been reported. A retro Diels–Alder reaction of oxanorbornenes under solvent-free conditions and microwave irradiation afforded the corresponding products in high yields.[11] A patent that describes preparation of 5-norbornene-2-carboxylic acid by heating dicyclopentadine with acrylic acid at ambient pressure in the presence of a free radical inhibitor[12] will be discussed in detail in the Results and Discussion section.

We have developed a solvent-free procedure in which cyclopentadiene generated *in situ* is used in a Diels–Alder reaction (Scheme 1). Advantages of this procedure are that cyclopentadiene reacts as it is generated and thus there are neither safety problems associated with use of cyclopentadiene nor problems with formation of oligomers. As a result, most of the starting dicyclopentadiene is utilized. Furthermore, as the reaction is done at a relatively high temperature (162–206 °C), thermodynamically preferred reaction products are obtained. Ordinarily, Diels–Alder reactions involving cyclopentadiene proceed under kinetic conditions to give predominantly or exclusively the *endo* isomer.[13] By adjusting the reaction times, one can obtain either the *exo* or *endo* isomer as the major
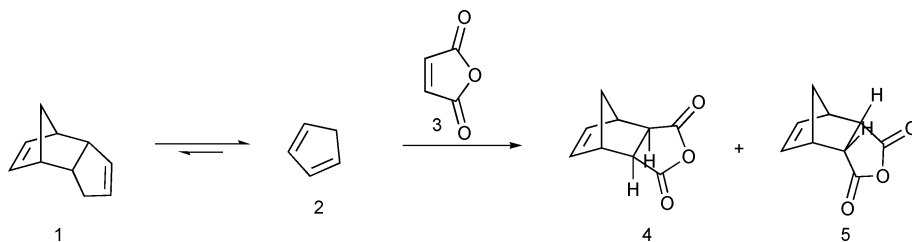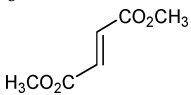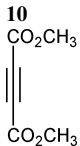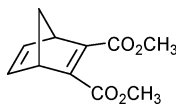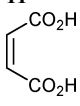

Scheme 1

Table 1 Solvent-free Diels–Alder reactions of *in situ* generated cyclopentadiene

Entry	Dienophile	Reaction time/min	Products	Yield (*exo/endo*)	Procedure
1	**3**	15–22	**4/5**	37%[a] : 35%[a,c]	A
2	**3**	8–10	**5**	32%[a] (1:6)[b]	A
3	**6**	25	**7/8**	78%[a] (57:35)[b]	A
4	(structure) **CO₂CH₃ / H₃CO₂C**	15	**9**	83%[a]	A
5	**10** CO₂CH₃ / CO₂CH₃ (alkyne)	12	(norbornene diester structure) CO₂CH₃ / CO₂CH₃	88%[a]	A
6	**11** CO₂H / CO₂H	5	**12** **4/5**	<10%[d]	B
7	**13** CO₂H / HO₂C	5	**4/5**	~20%[d]	B
8	**14** CO₂H / CO₂H (alkyne)	5	(norbornene diacid structure) CO₂H / CO₂H	0	B
9	**15** (benzoquinone structure) O / O	5	**16** (structure) O / O **18**	~5%[d]	B

[a] Isolated yield. [b] GC ratio. [c] Product was 95:5 endo/exo mixture according to GC analysis. [d] Estimated yield based on the amount of recovered material and GC analysis.

reaction product. Finally, by avoiding use of a reaction solvent this is a "greener" procedure compared to traditional Diels–Alder reactions.

Results and discussion

Reactions of dicyclopentadiene with dienophiles were relatively fast (5–25 min). In addition, none, or very little, of the byproducts such as tri- and tetracyclopentadienes, which are formed in the course of an ordinary cracking, were observed and one did not have to isolate or handle noxious and unstable cyclopentadiene.

Usually, in a Diels–Alder reaction the diene is used in an excess. However, in this case, use of the diene precursor, dicyclopentadiene, in an excess resulted in lower yields and lower purity of the products. In particular, a larger amount of cyclopentadiene oligomers were formed. Therefore, we opted for use of a small excess of the dienophile. Thus, reaction of

dicyclopentadiene with 2.30 equivalents (1.15 equivalents with respect to *in situ* generated cyclopentadiene) of maleic anhydride gave 5-norbornene-2,3-dicarboxylic anhydride cleanly and in good yield (Table 1, entry 1). Very little of the cyclopentadiene oligomers were formed (<5% according to GC-MS analysis). It was important to keep the reaction times within the optimal range. The reaction should be run until the reaction mixture turns dark yellow and the reflux stops. Shorter reaction times resulted in an incomplete reaction, while longer reaction times gave charred products and lower yields. The reaction was successfully scaled up to 0.6 mol scale (67.6 g maleic anhydride and 49.8 mL dicyclopentadiene in a 300 mL round bottom flask). As there was some foaming in the course of the reaction, it may be tempting to use larger flasks. Furthermore, a larger reaction flask would allow for a more efficient heat transfer. Interestingly, use of larger reaction vessels resulted in charred products and lower yields. Use of smaller reaction vessels (10 mL round bottom flask for 75 mmol, 200 mL for 0.3 mol and 300 mL

for 0.6 mol reaction) gave better results. Overall, our experience was that it was best to use the smallest possible flask, which should be ~1/3 filled.

Both dicyclopentadiene and cyclopentadiene react with maleic anhydride in the presence of a free radical catalyst to give polymers.[14] However, while a solvent-free reaction of cyclopentadiene with ethylene under high pressure and high temperature gave norbornene in an acceptable yield,[4] to our knowledge reaction of neat dicyclopentadiene with maleic anhydride has not been investigated. In contrast to a Diels–Alder reaction conducted at ambient temperature,[15] the reaction was thermodynamically controlled and a mixture of *exo* and *endo* isomers in approximately equilibrium amounts was obtained. The reaction time was only 15–22 minutes which compares favorably with the standard procedure for obtaining a thermodynamic mixture of *exo* and *endo* isomers by equilibrating the *endo* isomer at 190 °C for 1.5 hours.[16] A small excess of maleic anhydride ensured complete utilization of cyclopentadiene and simplified the work up. The isolated yield of a mixture of *exo*- and *endo*-5-norbornene-2,3-dicarboxylic anhydride was ~72% (average of five runs, Table 1, entry 1). Remaining *endo*-isomer can be re-equilibrated according to a literature procedure[16] to give an overall yield of ~60% of the *exo*-compound. It has been reported that the thermodynamic mixture contains 57% and 43% of *exo* and *endo* isomers by Craig,[16] or 54% and 46% of *exo* and *endo* isomers by Pincock *et al.*[17] Our results were similar, and the equilibrium mixtures contained a small excess of the *exo* isomer. These results are in contrast to recent calculations, according to which the *endo* isomer is more stable by 1.9 kJ/mol.[18]

The *endo* isomer was obtained as the major reaction product when the conversion was kept low by keeping the reaction time short. Attempts to increase the amount of *endo* isomer by slow addition of dicyclopentadiene, either manually or by use of syringe drive, failed. Reproducibility was very poor, with both yields and *exo/endo* ratios varying considerably between the individual trials. The amount of the starting maleic anhydride did not appear to play a role. Thus, the reaction times, yields of the reaction products and *exo/endo* ratio were about the same when maleic anhydride was used in 2–6 equivalent amounts (1–3 equivalents with respect to *in situ* generated cyclopentadiene). The best yield (32% of a 6:1 mixture of *endo* and *exo* isomers) of the *endo* product was obtained when dicyclopentadiene was added to an excess (4.50 equivalents) of boiling maleic anhydride (206 °C) and the reaction time was kept short (Table 1, entry 2). Craig reported that a reaction of maleic anhydride and cyclopentadiene at 190 °C for 10 minutes gave an 82:18 ratio of *endo* and *exo* isomers.[16]

When the reaction was done at 206 °C on a mixture that corresponded to 50% conversion (37.5 mmol of 5-norbornene-2,3-dicarboxylic anhydride, 37.5 mmol of maleic anhydride and

Table 2 Solvent-free reaction of cyclopentadiene with maleic anhydride on a mixture that corresponds to 50% conversion

Entry	Added adduct[a]	Time	Isolated Yield (*exo/endo*)
1	*exo*	4′30″	44% : 42%
2	*endo*	5′30″	36% : 35%
3	*exo/endo* (1:1)	5′	41% : 39%

[a] Reaction conditions: 37.5 mmol of Diels–Alder adduct and 37.5 mmol of maleic anhydride were heated for 2 minutes followed by addition of 16.25 mmol of dicyclopentadiene. Heating was continued for the time indicated.

32.5 mmol of dicyclopentadiene), an approximately thermodynamic ratio of *exo* and *endo* isomers was obtained in only 5 minutes (Table 2). Interestingly, the reaction outcome was about the same regardless of whether the added 5-norbornene-2,3-dicarboxylic anhydride was the *exo*-isomer, the *endo*-isomer, or a 1:1 mixture of the *exo* and *endo* isomers. Yields were slightly better compared to a reaction of maleic anhydride and cyclopentadiene (Table 1, entry 1). Under the same conditions, equilibration of a pure *endo* isomer took 15 minutes.

Esters (Table 1, entries 3–5) worked very well and yields were very good. The reaction products were those expected for a Diels–Alder reaction run under a thermodynamic conditions. As the Diels–Alder reaction usually gives a kinetic (*endo*) product, this is a way to obtain a thermodynamic product. Dimethyl maleate gave *exo* and *endo* isomers in a 57:35 ratio (Table 1, entry 3). There was some isomerization of dimethyl maleate into dimethyl fumarate and a small amount (~5%, GC analysis, not isolated) of dimethyl *trans*-5-norbornene-2,3-dicarboxylate was observed (GC analysis, Scheme 2). Both dimethyl fumarate and dimethyl acetylenedicarboxylate gave the corresponding Diels–Alder adducts cleanly and in high yields (Table 1, entries 4 and 5).

Carboxylic acids were not suitable substrates for this reaction (Table 1, entries 6–8). Complex mixtures that consisted mainly of insoluble, presumably polymeric, material were obtained accompanied by small amounts of Diels–Alder adducts. Reaction of dicyclopentadiene with maleic acid gave very little (<10% according to GC-MS analysis) of a ~1:1 mixture of *exo* and *endo* isomers of 5-norbornene-2,3-dicarboxylic anhydride (Table 1, entry 6). It is known that upon heating, maleic acid isomerizes into fumaric acid, which in turn isomerizes into maleic anhydride.[19] Fumaric acid gave a somewhat better yield of the anhydrides (Table 1, entry 7) and it may be possible to optimize the reaction conditions to improve the yield. However, since maleic anhydride itself works quite well there was no apparent reason to attempt such an exercise. According to the previously mentioned patent, a solvent-free reaction between dicyclopentadiene and acrylic acid works well in the presence of a free radical inhibitor such as hydroquinone.[12] While it
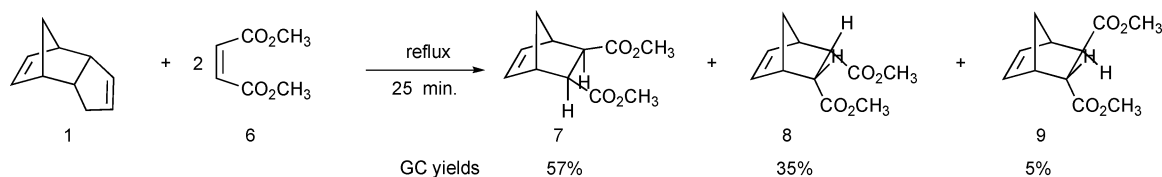
Scheme 2

was stated that 5-norbornene-2-carboxylic acid was isolated in 89% yield, there was no mention of the *exo/endo* ratio and very few experimental details were provided. In our hands, the reaction was rather slow and heating of dicyclopentadiene prior to addition of a dienophile resulted in formation of a large amount of tri- and tetracyclopentadienes. As expected, addition of a free radical inhibitor prevented polymerization of acrylic acid, but had no effect on oligomerization of *in situ* generated cyclopentadiene. Thus, the best result we obtained was ~40% yield of 5-norbornene-2-carboxylic acid. We found that a slow reverse addition (dicyclopentadiene to a boiling acrylic acid in the presence of hydroquinone) gave better results and 5-norbornene-2-carboxylic acid was obtained in ~60% yield (~1:1 *endo/exo* mixture isolated as the corresponding methyl esters). As addition of a free radical inhibitor only prevents polymerization, such modification does not address thermal instability of acids, which is the main problem when using maleic and fumaric acids.

Reaction of dicyclopentadiene with an excess of molten 1,4-benzoquineone was extremely vigorous. Within ~5 minutes most of the reaction mixture was a charred solid. Extraction yielded the Diels–Alder adduct and dehydrogenated product **18** in a low yield accompanied by a considerable amount of hydroquinone (Table 1, entry 9).

Conclusion

We have developed an environmentally friendly methodology for Diels–Alder reactions of cyclopentadiene by using dicyclopentadiene directly in the reaction, without previous cracking, and by conducting the reactions under solvent-free conditions. Reaction products were obtained in multi-gram quantities. Limitations of the described procedure include use of thermally unstable dienophiles, such as benzoquinone and unsaturated acids. The Meinwald and Hudak article, as well as previously published patents, provide complementary procedures, which may be useful for reactions involving low boiling and polymerizable dienophiles.[4,5,12] Somewhat less reactive dienophiles, such as esters and maleic anhydride, worked very well and gave a thermodynamic mixture of *exo* and *endo* isomers. This is a "point reaction" – there is a relatively narrow range of optimal conditions and deviation from them reduces the yield.[20] Although there are some limitations to the choice of suitable dienophiles, advantages of the process are that it generates no waste, maximizes incorporation of starting materials into products, is done under ambient pressure, is solvent-free, utilizes no other reagents nor catalysts, avoids safety hazards associated with handling of cyclopentadiene and thus conforms to most of the twelve green chemistry principles.[21] Finally, and perhaps most importantly, it allows for a fast and convenient preparation of thermodynamic products of Diels–Alder reactions.

Experimental

^{1}H NMR spectra were recorded on a Bruker Avance 400 spectrometer. GC-MS analyses were performed by means of Agilent 6890 N Gas Chromatograph equipped with HP-5MS 30 m × 0.25 mm column (Cat. No. 19091S-433) and Agilent 5973 N MSD. Dicyclopentadiene, maleic anhydride, maleic acid, fumaric acid, acetylene dicarboxylic acid, dimethyl maleate, dimethyl fumarate, dimethyl acetylene dicarboxylate and 1,4-benzoquinone were purchased from Acros Organic and used without further purification. Acetone, hexanes and ethyl acetate were purchased from Fisher Scientific Company and used without further purification. Deuterated solvents and silica gel were purchased from Aldrich Chemical Company and used without further purification. Separations were done either by column chromatography or by preparative radial thin layer chromatography (Harrison Chromatotron). All of the isolated products were known compounds and gave satisfactory ^{1}H NMR and GC-MS data.

Procedure A

Dienophile (75 mmol) was placed in a 10 mL round bottom flask equipped with a condenser. It was heated with stirring until it began to boil. Dicyclopentadiene (5.35 mL, 32.5 mmol) was added in a single portion and the reaction was continued until the reflux stopped and the reaction mixture turned yellow. *Exo* and *endo* isomers were separated by radial thin layer chromatography (Harrison Chromatotron) eluting with ethyl acetate:hexanes (1:4 by volume) in the case of dimethyl *cis*-5-norbornene-2,3-dicarboxylate or ethyl acetate:acetone:hexanes (1:2:6 by volume) in the case of 5-norbornene-2,3-dicarboxylic anhydride. Other products were purified by column chromatography eluting with ethyl acetate:hexanes (1:3 by volume).

Procedure B

Diene (75 mmol) and dicyclopentadiene (5.35 mL, 32.5 mmol) were placed in a 10 mL round bottom flask equipped with a condenser. The mixture was heated to reflux for the time indicated (Table 1, entries 6–9). Products were extracted from the solid residue with ethyl acetate and analyzed by GC-MS.

Acknowledgements

Notes and references

1 K. Takao, R. Munakata and K. Tadano, *Chem. Rev.*, 2005, **105**, 4779–4807; E. J. Corey, *Angew. Chem., Int. Ed.*, 2002, **41**, 1650–1667; K. C. Nicolaou, S. A. Snyder, T. Montagnon and G. Vassilikogiannakis, *Angew. Chem., Int. Ed.*, 2002, **41**, 1668–1698; U. Pindur, G. Lutz and C. Otto, *Chem. Rev.*, 1993, **93**, 741–761.

2 B. Rickborn, *Organic Reactions (New York)*, 1998, **52**, 1–393; A. Ichihara, *Synthesis*, 1987, 207–222; J. L. Ripoll, A. Rouessac and F. Rouessac, *Tetrahedron*, 1978, **34**, 19–40.

3 J. H. M. Lange, A. J. H. Klunder and B. Zwanenburg, *Tetrahedron Lett.*, 1988, **29**, 2365–2368; D. Mackay, D. Papadopoulos and N. J. Taylor, *J. Chem. Soc. Chem. Commun.*, 1992, 325–327; R. N. Warrener, M. A. Houghton, A. C. Schultz, F. R. Keene, L. S. Kelso, R. Dash and D. N. Butler, *Chem. Commun.*, 1996, 1151–1152.

4 J. Meinwald and N. J. Hudak, *Organic Syntheses Coll.*, 1963, **4**, 738, http://www.orgsyn.org/orgsyn/pdfs/CV4P0738.pdf, accessed on April 13, 2008.

5 U. Takashi and K. Shoichi, Jpn. Kokai Tokkyo Koho (1974), JP, 49–048650 A (in Japanese), *Chem. Abstr.*, 1974, **81**, 135555.

6 D. J. am Ende, D. C. Whritenour and J. W. Coe, *Org. Process Res. Dev.*, 2007, **11**, 1141–1146.

7 A. Starkie and S. Rowe, *Chem. Br.*, 1996, **32(2)**, 34–8.

8 R. B. Moffett, *Organic Syntheses Coll.*, 1963, **4**, 238, http://www.orgsyn.org/orgsyn/pdfs/CV4P0238.pdf, accessed on April 13, 2008.

9 F. Fringuelli, R. Girotti, F. Pizzo and L. Vaccaro, *Org. Lett.*, 2006, **8**, 2487–2489; S. Imachi and M. Onaka, *Tetrahedron Lett.*, 2004, **45**, 4943–4946; J. Long, J. Hu, X. Shen, B. Ji and K. Ding, *J. Am. Chem. Soc.*, 2002, **124**, 10–11; D. Bradley, *Chemistry in Britain*, 2002, **38**, 42–45; M. Avalos, R. Babiano, J. L. Bravo, P. Cintas, J. L. Jimenez, J. C. Palacios and B. C. Ranu, *Tetrahedron Lett.*, 1998, **39**, 2013–2016.

10 A. Loupy, F. Maurel and A. Sabatie-Gogova, *Tetrahedron*, 2004, **60**, 1683–1691.

11 M. Bortolussi, R. Bloch and A. Loupy, *J. Chem. Res. (S)*, 1998, 34–35.

12 Y. Murakami, M. Asagai, and I. Yamane, Jpn. Kokai Tokkyo Koho (2000), JP, 2000–319222 A (in Japanese). A mechanical translation is available on the Japanese Patent Office web site: http://www.jpo.go.jp/.

13 D. Suárez and J. A. Sordo, *Chem. Commun.*, 1998, 385–386; R. Gleiter and M. C. Böhm, *Pure Appl. Chem.*, 1983, **55**, 237–244; M. Kakushima, *Can. J. Chem.*, 1979, **57**, 2564–2568.

14 N. G. Gaylord and A. B. Deshpande, *Journal of Macromolecular Science, Part A*, 1977, **11**, 1795–1807; N. G. Gaylord, A. B. Deshpande and M. Martan, *J. Polym. Sci. Polym. Letters Ed.*, 1976, **14**, 679–682.

15 W. J. Sheppard, *J. Chem. Educ.*, 1963, **40**, 40–41.

16 D. Craig, *J. Am. Chem. Soc.*, 1951, **73**, 4889–4892.

17 R. E. Pincock, K. R. Wilson and T. E. Kiovsky, *J. Am. Chem. Soc.*, 1967, **89**, 6890–6897.

18 L. Rulíšek, P. Šebek, Z. Havlas, R. Hrabal, P. Čapek and A. Svatoš, *J. Org. Chem.*, 2005, **70**, 6295–6302.

19 W. D. Robinson and R. A. Mount, *Kirk-Othmer Encycl. Chem. Technol.*, 1981, **14**, 778–779.

20 S. Turner, *Design of Chemical Synthesis*, Elsevier, Amsterdam, 1976, 21–22.

21 P. T. Anastas and J. C. Warner, *Green Chemistry: Theory and Practice*, Oxford University Press, Oxford, 1998.

Pd nanoparticles immobilized on sepiolite by ionic liquids: efficient catalysts for hydrogenation of alkenes and Heck reactions

Ranting Tao, Shiding Miao, Zhimin Liu,* Yun Xie, Buxing Han, Guimin An and Kunlun Ding

Palladium-sepiolite catalysts were prepared by immobilizing Pd^{2+} on sepiolite using an ionic liquid containing a guanidine cation, followed by reduction with hydrogen at 150 °C. The resulting composites were characterized by different techniques. X-Ray photoelectron spectroscopy analysis showed that the loaded Pd existed mainly in the form of Pd^0, with a small amount of its oxides, and distributed uniformly on sepiolite with particle size about 5 nm, as confirmed by transmission electron microscopy examination. X-Ray diffraction analysis indicated that the sepiolite retained its original structure after deposition of Pd nanoparticles. The activities of the Pd-sepiolite catalysts for hydrogenations of some alkenes (e.g., cyclohexene and 1,3-cyclohexdiene) and Heck reactions were investigated. It was demonstrated that the as-prepared catalysts exhibited very high efficiency for these reactions.

Introduction

With the development of green chemistry, the design and preparation of green catalysts have attracted much attention recently, among which heterogeneous catalysts have been widely investigated. Natural clays are environmentally friendly materials, which are good catalyst supports because of their crystalline structures and large surface areas. Sepiolite, a kind of natural clay mineral with a formula of $Si_{12}Mg_8O_{30}(OH)_6(OH_2)_4 \cdot 8H_2O$, has a very special place among natural clay minerals due to its relatively high surface area and excellent ability to adsorb molecular, ionic, and polymeric species.[1,2] Similar to other types of silicate minerals, it contains continuous two-dimensional tetrahedral sheets of T_2O_5 (T = Si, Al, Be,…), but has no continuous octahedral sheets.[3] Owing to its special structure and properties, sepiolite has been widely used in a variety of industrial applications.[4–6]

Ionic liquids (ILs), possessing negligible vapor pressure, reasonable thermal stability, strong ability to dissolve a wide range of organic, inorganic and organometallic compounds, have promising applications in many fields.[7,8] In particular, ILs offer new opportunities for the development of catalytic materials. In industrial processes, heterogeneous catalysis is generally preferred to homogeneous catalysis, since the separation of the product and recovery of the catalyst are made easier.[9] Therefore, the immobilization of ILs onto solid supports and the preparation of heterogeneous catalysts assisted by ILs have attracted significant attention.[10–12] For example, Brønsted acid ILs were immobilized on solid supports, which displayed excellent recyclability and high activity for a range of esterification and nitration reactions.[13] Choline hydroxide was supported on MgO and shown to be an efficient catalyst for the aldol reaction for a range of aldehyde and ketone substrates.[14] Metal nanoparticles (e.g. Pd, Rh, Ru, etc.) were supported on different solid supports with the aid of ILs, exhibiting high efficiency for hydrogenations of alkenes and arenes.[15,16] The main advantage of using the supported IL system is that it requires significantly reduced amounts of the ionic media, which is favorable from an economic and toxicological point of view.

In our previous work, we developed an approach to support noble metal nanoparticles (e.g., Ru, Rh) on natural clays by ILs, and the resultant catalysts showed high efficiency for hydrogenations of benzene[16] and cyclohexene.[17] In this work, we extended this approach to immobilize Pd nanoparticles on sepiolite with the aid of an IL, aiming at developing new green catalysts. The as-prepared Pd catalysts were characterized in detail by different techniques, including X-ray photoelectron spectroscopy (XPS), thermogravimetric analysis (TG), scanning electron microscopy (SEM), transmission electron microscopy (TEM), inductively coupled plasma-atomic emission spectrometer (ICP-AES), X-ray diffraction (XRD), N_2 sorption, and their catalytic activities for hydrogenations of alkenes and Heck reactions were investigated. The combination of sepiolite as a support with an IL may widen the application of sepiolite and help develop new kinds of green catalysts as well.

Experimental

Starting materials

The sepiolite clay, provided by the Mingyang company, was first treated as follows. 10 g of sepiolite was immersed in 20 mL of 1 M HNO_3 solution at room temperature with stirring for 24 h. Then, the suspension was filtered and the resulting solid was washed with deionized water for ten times before drying at 105 °C for 24 h. The treated clay was pulverized and sieved down to 120 mesh, which was designated as SH.

Institute of Chemistry, The Chinese Academy of Sciences, Beijing, 100190, China. E-mail: liuzm@iccas.ac.cn

Other reagents including HNO₃ (65%–68%), HCl (36%–38%), PdCl₂, cyclohexene (AR), *N*,*N*-dimethylformamide (AR), methyl acrylate (AR) and triethylamine (AR) were purchased from the Beijing Chemical Reagent Company. 1,3-Cyclohexdiene was obtained from ACROS, and iodobenzene (98%) was provided by Alfa Aesar. The ILs (including 1,1,3,3-tetramethylguanidine trifluoroacetic acid, TMG⁺TFA⁻; 1,1,3,3-tetramethylguanidine lactic acid, TMG⁺LA⁻ and 1,1,3,3-tetramethylguanidine acetic acid, TMG⁺AA⁻) were synthesized directly by neutralization of 1,1,3,3-tetramethylguanidine (TMG) with proportionable acid based on the procedures reported previously.[18,19]

Preparation of SH-IL-Pd catalysts

The catalyst SH-IL-Pd containing 1.0 wt% Pd (denoted as SH-IL-1.0%Pd) was prepared in the following way. 10.0 g of the activated sepiolite (*i.e.*, SH) was dispersed in 50 mL of aqueous solution containing 0.7 g of TMG⁺TFA⁻, and stirred for about 6 h. Then the sepiolite was separated *via* centrifugation, and treated with fresh IL aqueous solution again. These procedures were repeated three times. The sepiolite treated with IL aqueous solution was dried at 105 °C for 24 h and named SH-IL. 1.0 g of SH-IL was redispersed in 10.0 mL of H₂PdCl₄ (1M PdCl₂ + 2M HCl) aqueous solution with a concentration of 1.0 mg/mL. Then the clay was dried at 60 °C under vacuum after the water was removed *via* evaporation, and denoted as SH-IL-Pd²⁺. SH-IL-Pd²⁺ was hydrogenated with H₂ at 150 °C for 4 h, resulting in a composite, designated as SH-IL-1.0 wt%Pd, since the mass content of Pd in the composite was 1.0 wt%, calculated on the basis of the amounts of the clay and the PdCl₂ used. The catalyst containing 2.5 wt% Pd was synthesized following the same procedure, named SH-IL-2.5%Pd. Instead of TMG⁺TFA⁻, other ILs including TMG⁺LA⁻, TMG⁺AA⁻ and TMG were also used to prepare the Pd catalysts in the similar way.

Characterization

TG measurements were performed on a thermal analyzer (NETZSCH STA 409 PC/PG) with a heating rate of 3 °C/min. SEM examination was carried out on a scanning electron microscope (JEOL, JSM-4300) operated in a high-vacuum mode at 15 kV, which provided general textural information of the samples. The SEM samples were sputter-coated with gold before observation. TEM observation was performed on a transmission electron microscope (JEOL, JEM 1011) at an operating voltage of 100 kV, and the images were electronically captured using a CCD camera. XPS data of the as-prepared samples were obtained with an ESCALab220i-XL electron spectrometer from VG Scientific using 300 W MgKα radiation. The base pressure was about 3×10^{-9} mbar. The binding energies were referenced to the C 1s line at 284.8 eV from adventitious carbon. XRD was performed on a X'PERT SW X-ray diffractometer operated at 30 kV and 100 mA with CuKα radiation. The loading content of Pd in the catalysts was determined by ICP-AES (VISTA-MPX). The nitrogen sorption analysis was performed on an ASAP-2405N instrument at liquid nitrogen temperature.

Catalytic activity test

To evaluate the catalytic characteristics of the as-prepared samples, hydrogenations of some alkenes (*e.g.*, cyclohexene, 1,3-cyclohexdiene, styrene and 1-hexene) and Heck reactions were investigated. Hydrogenation reactions were carried out in a 50 mL stainless steel autoclave with a magnetic stirrer at 300 rpm. In a typical experiment, 12 mmol of alkene and the required amount of catalyst were placed in the reactor, and the air in the reactor was then replaced by H₂ five times. After H₂ was charged into the reactor up to 2.0 MPa, the reactor was moved to an oil bath at the desired temperature. The temperature of the oil bath was controlled with a temperature controller (Haake D3) with an accuracy of 0.1 °C. The pressure of the reaction system was monitored using a pressure transducer (Foxboro/ICT model 93). As the H₂ pressure remained unchanged, the product was collected *via* centrifugation (12000 rpm) and analyzed by a gas chromatograph (Agilent 4890 D) equipped with an Innovax capillary column and a Varian FID-GC flame ionization detector.

The Heck reaction was performed as follows. Iodobenzene (2.0 mmol), methyl acrylate (2.2 mmol), triethylamine (Et₃N, 2.4 mmol), and 2 mg of SH-IL-1.0wt%Pd composite were added into a 7 mL stainless steel autoclave with a magnetic stirrer. Then the reactor was sealed and placed in an air bath of 140 °C. After a desired reaction time, the autoclave was cooled by ice water. The product was dissolved by *N*,*N*-dimethylformamide (DMF, 10.0 mL) and analyzed by GC-MS. Conversion was determined from the amount of consumed iodobenzene. Bromobenzene instead of iodobenzene was also used to test the activity of the catalyst in the similar way.

Results and discussion

Characterization of the catalysts

Before being used as catalysts, SH, SH-IL, and SH-IL-Pd were characterized in detail by means of different techniques, including XPS, TG, SEM, TEM, ICP-AES, XRD, and N₂ sorption analysis.

The XPS analysis was used to detect the oxidation state of all species in the composites. Fig. 1a shows the survey spectrum of SH-IL-1.0wt%Pd, which indicates that no element Cl was detectable, suggesting that PdCl₂ was completely converted during the H₂ reduction process. From Fig. 1a, it is obvious that element N was present in the composites. Fig. 1b illustrates the N 1s spectrum, in which the peak centered at 400.6 eV is attributed to N species bounding to =C and –C, which originated from the cation of the IL, suggesting that IL existed in the composites. Fig. 1c displays the XPS spectrum of Pd 3d. Compared to the binding energy values of Pd 3d in pure palladium metal,[20] both the predominant peak at 335.2 eV and the deconvolved peak at 340.8 eV are attributed to Pd⁰ species, and the peaks at 337.1 eV and 342.9 eV are assigned to the partially oxidized palladium species, which may result from the slight oxidation of Pd⁰. From XPS analysis, it can be deduced that the Pd⁰ species are predominant in the composites. XPS analysis shows that the Pd content on the surface of SH-IL-Pd was about 0.94%, which is almost identical with the initial quantities of Pd (1.0 wt%), implying that the Pd nanoparticals were mainly decorated on the surface of sepiolite. The loading content of Pd
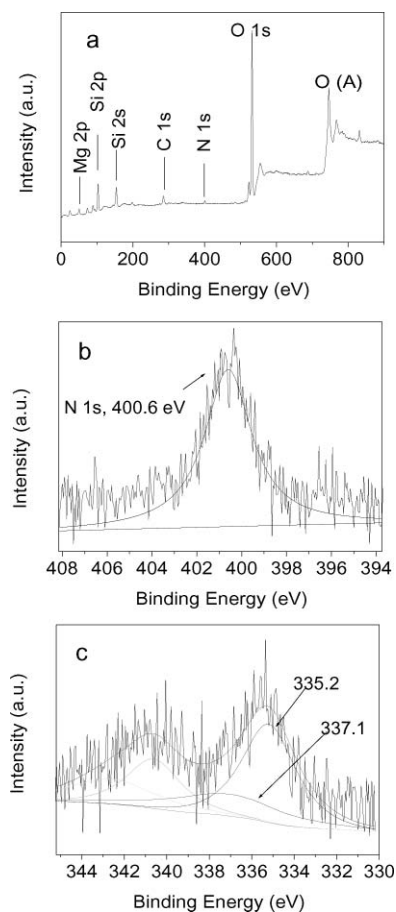
Fig. 1 XPS spectra of SH-IL-1.0wt%Pd: (a) survey spectrum, (b) N 1s, (c) Pd 3d.

in SH-IL-1.0wt%Pd was also determined by ICP-AES. It was demonstrated that the Pd content was 0.95 wt%, nearly equal to the value obtained from XPS analysis, further confirming that the Pd nanoparticles were uniformly distributed on the sepiolite support.

To determine the loading content of IL on the sepiolite support, TG analysis for SH and SH-IL was carried out from room temperature to 700 °C at a heating rate of 3 °C min^{-1}. At 700 °C, the residual contents of SH and SH-IL were 92.8 wt% and 91.2 wt%, respectively, which gives the information that the IL was indeed immobilized on the sepiolite support, and the loaded IL content was about 1.6 wt%.

The microstructure and morphology of the resultant composites were examined by SEM and TEM. The SEM images of SH-IL-1.0wt%Pd, as shown in Fig. 2, indicate that the sepiolite exhibited fibrous structure with an average diameter of about 100 nm and length in the range from 20 nm to 2 μm. Some fibers congregated into bundles, and a great deal of sepiolite fibers stacked up, leading to pores with different sizes. The TEM images provided more information about the morphology of SH and SH-IL-1.0wt%Pd. Fig. 2c shows a typical TEM image of SH, which indicates that sepiolite is composed of fibers with smooth surfaces. For the SH-IL-1.0wt%Pd composite, the surface of the fiber became rough, and there were numerous nanoparticles attached along the fibers. It is clear that the particle size was less than 5 nm, as shown in Fig. 2d; moreover,

the TEM image also shows that the particle size distribution of the particles located on the rods was very narrow.

The samples, SH, SH-IL, SH-IL-1.0wt%Pd, and SH-TMG, were also examined by XRD analysis. It was shown that these four samples exhibited almost identical XRD patterns, which suggests that the sepiolite in SH-IL, SH-IL-Pd, and SH-TMG retained its original structure without any damage. There is no expansion or collapse of the sepiolite framework, which suggests that no IL was impregnated into the channels of sepiolite. This is different from our previous work, in which the IL was intercalated into the interlayers of montmorillonite and expanded them to some extent.[16] In the pattern of SH-IL-Pd, no detectable diffraction peak was assigned to Pd species in the wide angle range, which indicates that there were no large Pd particles in the SH-IL-Pd composites.

To verify the changes of the surface area and porous characteristics of the sepiolite in SH-IL and SH-IL-Pd, the as-prepared samples were evaluated by N_2 sorption analysis. Fig. 3 shows the corresponding isothermal curves of SH-IL-1.0wt%Pd, which belongs to type IV sorption isotherms with hysteresis loop of type H1 according to the IUPAC classification.[21] The other samples (e.g. SH, SH-IL, SH-IL-2.5wt%Pd) exhibited similar sorption isotherms to the SH-IL-1.0wt%Pd composite, implying the immobilization of IL and Pd nanoparticles did not destroy the main structure of the sepiolite. The specific surface areas of the samples were achieved by the BET method (Brunauer-Emmett-Teller) in the relative pressure range of 0.05–0.20 from nitrogen desorption isotherms,[22] and the pore size distribution was determined by the BJH method (Barrett-Joyner-Halenda). The specific surface area of the clay decreased from 72.3 m^2/g for the sepiolite activated by nitric acid to 40.5 m^2/g for SH-IL due to the immobilization of the IL, and further to 34.6 m^2/g for SH-IL-Pd, which may result from the deposition of Pd nanoparticles on the surface of sepiolite. The small hysteresis of the composite indicates less mesoporosity present in the sepiolite. From the N_2 sorption analysis, it is known that the total pore volume is reduced from 0.13 mL/g for SH to 0.09 mL/g for SH-IL composites, and to 0.07 mL/g for SH-IL-Pd, due to the absorption of IL and the deposition of Pd nanoparticles. Furthermore, the pore size distribution is much broader and has no significant change after the deposition of Pd nanoparticles in the composite.

Catalytic activities for hydrogenations and Heck Reactions of the catalysts

To evaluate their catalytic characteristics, the as-prepared SH-IL-Pd composites were used to catalyze the hydrogenations of some alkenes, including cyclohexene, 1-hexene, styrene and 1,3-cyclohexdiene, at different conditions, and the results are listed in Table 1. Both 1-hexene and styrene could almost completely convert into hexane and ethyl benzene within 0.5 h, respectively, at 60 °C and initial H_2 pressure of 2 MPa with a substrate/Pd molar ratio of 5000 (Table 1, entries 1 and 2). The conversion of cyclohexene could approach 100% within 1 h with cyclohexane as the only product under the same conditions (Table 1, entry 3). The turnover frequencies (TOFs), defined as moles of substrate consumed per mole of palladium per hour, could reach 10000 or 5000 h^{-1}, suggesting that the SH-IL-Pd catalyst was very
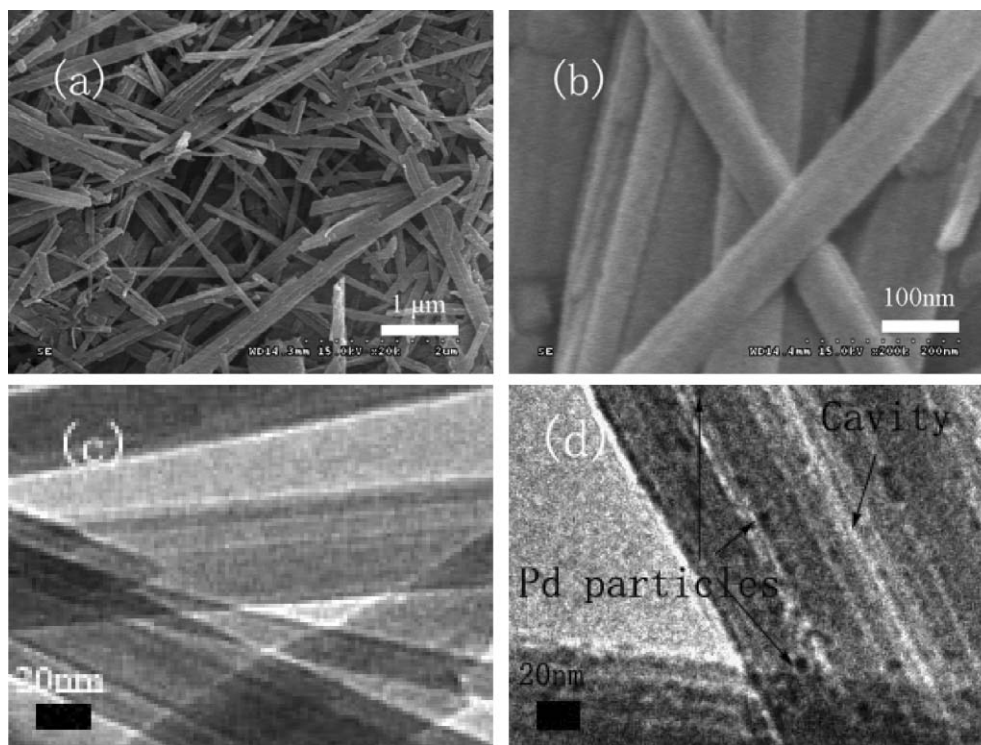
Fig. 2 SEM images of SH (a), (b); and TEM images of SH (c) and SH-IL-Pd (d).
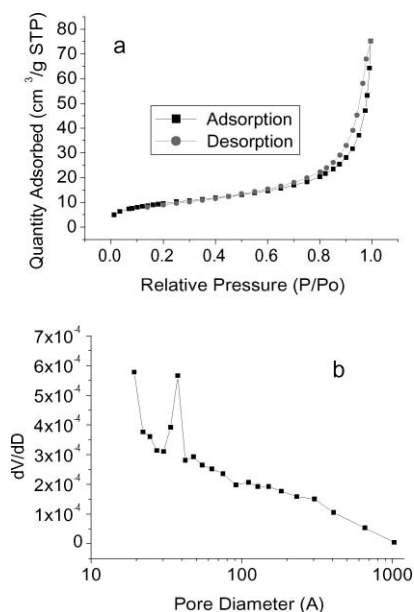
Fig. 3 Nitrogen sorption isotherms (a) and pore size distribution (b) of SH-IL-1.0wt%Pd.

active for these reactions. Taking the cyclohexene hydrogenation as an example, the stability of the SH-IL-1.0wt%Pd catalyst was investigated. It was demonstrated that there was almost no activity loss after the catalyst was reused for five times for this reaction (Table 1, entries 3–7), indicating that the as-prepared catalyst was rather stable. TEM observation for the five-time reused catalyst also support this, which shows that the Pd nanoparticles were still firmly adhered on the surface

of sepiolite and no remarkable aggregation of Pd nanoparticles occurred after the catalyst was reused for five times, as shown in Fig. 4.
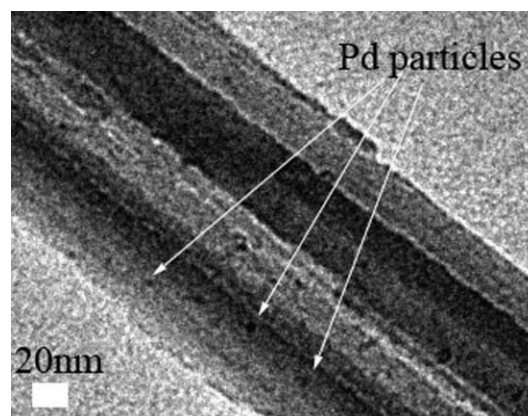
Fig. 4 TEM image of the SH-IL-1.0wt%Pd catalyst after it was reused for five times for hydrogenation of cyclohexene.

The SH-IL-1.0wt%Pd catalyst also exhibited a good activity for cyclohexene hydrogenation at lower temperatures (*e.g.*, Table 1, entries 8 and 9), but the TOFs decreased with decreasing temperature. The influence of Pd content on the hydrogenation was also investigated. For example, the SH-IL-2.5wt%Pd composite was used to catalyze the hydrogenation of cyclohexene, which displayed comparable activity with SH-IL-1.0wt%Pd at the C_6H_{10}/Pd molar ratio of 5000, as shown in Table 1 (entry 11). However, this catalyst was less active than SH-IL-1.0%Pd when the C_6H_{10}/Pd molar ratio was 10000, as listed in Table 1 (entries 10 and 12). This might result from the slight increment of Pd

Table 1 Results of catalyst performance in hydrogenations of alkenes[a]

Entry	Catalyst	Substrate	Substrate/Pd (mol/mol)	T/°C	$P(H_2)$/MPa	Time/h	Conversion (%)	TOF/h^{-1}
1	SH-IL-1.0%Pd	1-Hexene	5000	60	2	0.5	>99.0	10000
2	SH-IL-1.0%Pd	Styrene	5000	60	2	0.5	>99.0	10000
3	SH-IL-1.0%Pd	Cyclohexene	5000	60	2	1	>99.0	5000
4[b]	SH-IL-1.0%Pd	Cyclohexene	5000	60	2	1	>99.0	5000
5[c]	SH-IL-1.0%Pd	Cyclohexene	5000	60	2	1	>99.0	5000
6[d]	SH-IL-1.0%Pd	Cyclohexene	5000	60	2	1	>99.0	5000
7[e]	SH-IL-1.0%Pd	Cyclohexene	5000	60	2	1	>99.0	5000
8	SH-IL-1.0%Pd	Cyclohexene	5000	40	2	2	98.0	2450
9	SH-IL-1.0%Pd	Cyclohexene	5000	20	2	6	98.2	833
10	SH-IL-1.0%Pd	Cyclohexene	10000	60	2	2	>99.0	5000
11	SH-IL-2.5%Pd	Cyclohexene	5000	60	2	1	>99.0	5000
12	SH-IL-2.5%Pd	Cyclohexene	10000	60	2	2	88.0	4400
13[f]	SH-IL-1.0%Pd	1,3-Cyclohexdiene	5000	60	2	3.5	>99.0	1428
14	SH-IL-2.5%Pd	Cyclohexene	5000	60	2	0.5	95.0	—
15	Pd/C, 5%Pd	Cyclohexene	5000	60	2	0.5	80.2	—
16[g]	SH-IL-1.0%Pd	Cyclohexene	5000	60	2	1	>99.0	5000

[a] The amount of cyclohexene was 12 mmol. [b] SH-IL-1.0%Pd reused for the second time for cyclohexene hydrogenation. [c] SH-IL-1.0%Pd reused for the third time for cyclohexene hydrogenation. [d] SH-IL-1.0%Pd reused for the fourth time for cyclohexene hydrogenation. [e] SH-IL-1.0%Pd reused for the fifth time for cyclohexene hydrogenation. [f] The product is cyclohexene. [g] The amount of cyclohexene was 100 mmol.

particle size in the SH-IL-2.5%Pd composite. For comparison, the commercially available catalyst Pd/C (5 wt%Pd) was used to catalyze the cyclohexene hydrogenation. As shown in Table 1 (entries 14 and 15), the catalyst prepared in this work was more active than the Pd/C catalyst.

1,3-Cyclohexdiene hydrogenation was selected to investigate the activity of the catalyst SH-IL-1.0wt%Pd for selective hydrogenation. It was demonstrated that the catalyst showed high activity for the selective hydrogenation of 1,3-cyclohexdiene, and cyclohexene was the main product. For instance, at 60 °C and the initial H_2 pressure of 2 MPa with a C_6H_8/Pd molar ratio of 5000, the conversion of cyclohexdiene could reach 99% within 3.5 hours, and the selectivity for cyclohexene could approach 97.6%. This phenomenon was similar to that reported previously,[15] which originated from the properties of Pd metallic nanoparticles. Alkadienes are much more strongly adsorbed by the Pd nanoparticles than alkenes, which resulted in preferential hydrogenation of the alkadiene to the alkene. Moreover, the small size of the Pd nanopartilces is also favorable in enhancing the selectivity.

The Pd catalysts mediated with other ILs including TMG$^+$LA$^-$, TMG$^+$AA$^-$ and TMG, were also used to catalyze cyclohexene hydrogenation. It was demonstrated that these catalysts exhibited almost identical activity for this reaction, suggesting that 1,1,3,3-tetramethylguanidine cation played a key role in immobilizing the Pd nanoparticles on sepiolite.

Besides the catalyst for hydrogenation reactions, Pd is also an active catalyst for Heck reactions. For example, Clark et al. supported Pd nanoparticles on porous materials derived from starch in acetone solution, and the resultant Pd catalysts exhibited excellent activities for the Heck reaction of iodobenzene with methyl acetate under microwave irradiation.[23] In this work, the catalytic activity of the SH-IL-1.0wt%Pd catalyst for Heck reaction was investigated using the model reaction of iodobenzene and methyl acrylate to give methyl cinnamate. The reaction of iodobenzene (1.0 equiv) and methyl acrylate (1.1 equiv) with the molar ratio of iodobenzene/Pd = 10000 was performed

at 140 °C containing triethylamine (Et$_3$N, 1.2 equiv) under solvent-free conditions. The conversion of iodobenzene could reach 100% within 65 min, and no production of biphenyl was detected. This indicates that the catalyst had high efficiency for this Heck reaction. However, as the reaction time was prolonged from 65 min to 20 h, a little cinnamic acid was obtained, which may result from ester hydrolysis of methyl cinnamate. The stability of SH-IL-1.0wt%Pd for the Heck reaction of iodobenzene with methyl acetate was examined by performing this reaction for 5 consecutive runs, and no noticeable activity loss was observed, suggesting that this catalyst was also stable for the Heck reaction. Bromobenzene instead of iodobenzene was investigated for Heck reaction under the same conditions. Unfortunately, the catalyst displayed little activity for this reaction.

To explore the scalability of the as-prepared SH-IL-Pd catalyst, SH-IL-1.0%Pd was used to catalyze hydrogenation of 100 mmol cyclohexene and Heck reaction of 16 mmol iodobenzene with methyl acrylate, respectively. It was demonstrated that the catalyst was still very effective for cyclohexene hydrogenation as the amount of cyclohexene increased (as listed in Table 1, entry 16), and it was also very active for Heck reaction of iodobenzene and methyl acrylate with the increment of iodobeneze.

Conclusions

In summary, the sepiolite supported Pd catalysts were successfully prepared with the aid of ILs, and the as-prepared catalysts exhibited very high efficiency for hydrogenations of alkenes and Heck reaction of iodobenzene and methyl acrylate. Moreover, these catalysts were very stable and could be reused without activity loss. These catalysts combined the advantages of natural clay and ILs, resulting in environmentally friendly materials, which are expected to find promising applications in industrial catalysis.

Acknowledgements

References

1 J. Santarén, J. Sanz and E. Ruiz-Hitzky, *Clay Miner.*, 1990, **38**, 63.
2 E. Ruiz-Hitzky, *J. Mater. Chem.*, 2001, **11**, 86.
3 W. X. Kuang, G. A. Facey, C. Detellier, B. Casal, J. M. Serratosa and E. Ruiz-Hitzky, *Chem. Mater.*, 2003, **15**, 4956.
4 M. A. Aramendia, V. Borau, C. Jimenez, J. M. Marinas, A. Porras, F. J. Urbano and L. Villar, *J. Mol. Catal.*, 1994, **94**, 131.
5 A. Corma and R. M. Martin-Aranda, *Appl. Catal. A.*, 1993, **105**, 271.
6 A. Corma, S. Iborra, S. Miquel and J. Primo, *J. Catal.*, 1998, **173**, 315.
7 R. Sheldon, *Chem. Commun.*, 2001, 2399.
8 Y. Chauvin, L. Mussman and H. Olivier, *Angew. Chem. Int. Ed. Engl.*, 1995, **34**, 2698.
9 E. Lindner, T. Schneller, F. Auer and H. A. Mayer, *Angew. Chem. Int. Ed.*, 1999, **38**, 2154.
10 C. P. Mehnert, E. J. Mozeleski and R. A. Cook, *Chem. Commun.*, 2002, 3010–3011.
11 A. Riisager, R. Fehrmann, S. Flicker, R. Hal, M. Haumann and P. Wasserscheid, *Angew. Chem. Int. Ed.*, 2005, **44**, 815–819.
12 V. I. Pârvulescu and C. Hardacre, *Chem. Rev.*, 2007, **107**, 2615–2665.
13 K. Qiao, H. Hagiwara and C. Yokoyama, *J. Mol. Catal. A*, 2006, **246**, 65.
14 S. Abelló, F. Medina, X. Rodríguez, Y. Cesteros, P. Salagre, J. E. Sueiras, D. Tichit and B. Coq, *Chem. Commun.*, 2004, 1096.
15 J. Huang, T. Jiang, H. Gao, B. X. Han, Z. M. Liu, W. Wu, Y. Chang and G. Zhao, *Angew. Chem. Int. Ed.*, 2004, **43**, 1397.
16 S. D. Miao, Z. M. Liu and B. X. Han, *Angew. Chem. Int. Ed.*, 2006, **45**, 266.
17 S. D. Miao, Z. M. Liu and B. X. Han, *J. Phys. Chem. C*, 2007, **111**, 2185.
18 M. Hirao, H. Sugimoto and H. Ohno, *J. Electrochem. Soc.*, 2000, **147**, 4168.
19 N. M. M. Mateus, L. C. Branco, N. M. T. LourenKo and C. A. M. Afonso, *Green Chem.*, 2003, **5**, 347.
20 J. F. Silvain and O. Fouassier, *Sur. Interface Anal.*, 2004, **36**, 769.
21 K. S. W. Sing, D. H. Everett and R. A. W. Haul, *Pure Appl. Chem.*, 1985, **57**, 603.
22 E. P. Barret, L. G. Joyner and P. P. Halenda, *J. Am. Chem. Soc.*, 1951, **73**, 373.
23 V. L. Budarin, J. H. Clark, R. Luque, D. J. Macquarrie and R. J. White, *Green Chem.*, 2008, **10**, 382.

Isobutane/butene alkylation on microporous and mesoporous solid acid catalysts: probing the pore transport effects with liquid and near critical reaction media

V. R. Sarsani[a,b] and Bala Subramaniam*[a,b]

The alkylation of isobutane with 1-butene was investigated on microporous (β-zeolite) and mesoporous (silica supported heteropolyacids) catalysts in a slurry reactor. The reaction was investigated in the range of 25–100 bar and 15–95 °C in liquid phase and in near critical reaction media with either dense CO_2 or dense ethane as diluent, partially replacing the excess isobutane. At 75 °C, the selectivity towards trimethylpentanes (TMP) in the liquid phase is 70%+ initially, but decreases with time on all the catalysts investigated. While near-critical reaction mixtures were employed in order to enhance pore diffusion rates, the conversion and selectivity profiles obtained with such mixtures are comparable to those obtained with liquid phase reaction mixtures in both microporous and mesoporous catalysts. This implies that pore diffusion effects play a limited role at higher temperatures (75–95 °C). In contrast, the liquid phase results at sub-ambient temperatures indicate that the catalyst is deactivated before the TMPs diffuse out of the pores, indicating that pore diffusion effects play an important role in the deactivation process at low temperatures. Our results suggest that novel approaches that enhance the pore-diffusion rates of the TMPs at lower temperatures must be pursued.

Introduction

The alkylation of isobutane with light olefins (C_3–C_5) is a refinery process used to produce alkylates, which constitute about 13% of the U.S. gasoline pool. Trimethylpentanes (TMPs) are the most desired compounds with high octane numbers within the alkylates. Within reformulated gasoline, the isobutane alkylates not only provide a high octane number with low vapor pressure but also the desired combination of low levels of sulfur, olefins and aromatics. Due to the consequences of the 1990 Clean Air Act and phasing out of MTBE, it is anticipated that the isobutane alkylate will play an even more significant role as refiners worldwide attempt to comply with environmental mandates such as reduction in volatile organic compounds, sulfur and nitrogen oxides.

The most widely used catalysts in industry today for isobutane/olefin (I/O) alkylation are H_2SO_4 and HF. The use of environmentally benign solid acids as catalysts to replace these toxic mineral acids continues to be a major challenge of green chemistry and green engineering. To date, while there are claims of pilot scale plants[1] and even a commercial scale plant,[2] rapid catalyst deactivation by fouling hampers the commercial development utilizing solid acids. Detailed reviews on the subject

can be found elsewhere.[3–6] The current manuscript presents investigations aimed at better understanding the causative factors behind the rapid deactivation of solid acid catalysts by fouling. A better understanding of the pore size, temperature and solvent effects on catalyst deactivation is important for chemists and engineers to rationally develop practically viable solid acid catalysts. The work presented in this paper is thus relevant to green chemistry.

Researchers at Shell[7] were one of the first groups to report a systematic study in a back-mixed slurry reactor to evaluate the activity of zeolites. Through a simple kinetic model, the authors reported that the I/O ratio is the most important parameter that determines alkylate selectivity and catalyst life time. Amongst various zeolites tested, the authors found that beta zeolite is the most promising catalyst for high activity and catalyst lifetime. Lercher's group has been active in systematically studying the mechanistic aspects of isobutane alkylation in a continuous slurry reactor on beta zeolites[8] and more recently on Y[9] and X zeolites.[10] Froment's group has recently reported detailed mechanistic pathways of the reaction using studies in a plug flow reactor and by following the product distribution carefully at short time on stream (TOS). Single event kinetic modeling has been used to identify all the possible reactions.[11] In these referenced reports, microporous acid catalysts were evaluated. The present study complements these studies by also including mesoporous acid catalysts for investigation.

Rapid catalyst deactivation by fouling is widely accepted as the major hindrance to commercial development. Use of

[a]Center for Environmentally Beneficial Catalysis, Lawrence, KS 66045, USA
[b]Department of Chemical and Petroleum Engineering, University of Kansas, Lawrence, KS 66045, USA. E-mail: bsubramaniam@ku.edu; Fax: +1-785-864-6051; Tel: +1-785-864-2903

Table 1 Composition and physical properties of zeolites

Catalyst	Total Surface area (m^2/g)	Internal S.A (m^2/g)	SiO_2, Al_2O_3 (wt%)	SO_4 (wt%)	Na_2O (wt%)
Beta zeolite	671	618	93.53, 5.98	0.22	0.27
USY	797	749	75.75, 22.56	0.98	0.71

supercritical (*sc*) reaction media is one way to reduce the de-activation process *in situ* by enhancing the transport properties. Early studies on the use of supercritical media for isobutane alkylation focused on operating above the critical point of the reaction mixture. However, the high temperatures (> 140 °C) needed to achieve the critical point lead to cracking products on strong solid acids, like sulfated zirconia,[12] Y zeolites,[13] heteropolyacids,[14] adversely affecting the selectivity towards the desired products. Salinas *et al.*[15] partly circumvent the high cracking activity at elevated temperatures by employing lower acid strength zeolites with high Si/Al ratios. Clark and Subramaniam[16] reported on the use of CO_2 as a diluent to yield supercritical mixtures at lower temperatures and demonstrated steady C_8 alkylates production activity during isobutane/butene alkylation with zeolites and sulfated zirconia in a fixed bed reactor. However, the yield of alkylates was very low, less than 10%. All of the aforementioned studies in *sc* media are based on plug flow reactor studies and hence the I/O ratios in the reactor are lower compared to a well back-mixed system. The role of the media in the aforementioned studies was not fully understood.

Using mesoporous solid acid catalysts (SiO_2-supported Nafion® or SAC-13 and heteropolyacids), it was shown that improved C_8 yields can be obtained in a CSTR with CO_2-based supercritical feed mixtures.[17] By systematic pressure tuning studies, it was demonstrated that for the SAC-13 catalyst, the optimum conditions which maximize steady alkylates production are 95 °C, 80 bar, an olefin space velocity (OSV) of 0.05 h^{-1}, and a molar I/O ratio of 5 : 1 with 70 mol% CO_2 in the feed. Under these conditions, various heteropolyacid catalysts were evaluated and found that the maximum steady C_8 alkylate selectivity was 25%, but still much lower compared to the current industrial processes (70%+).[18]

Corma and coworkers investigated zeolites and sulfated zirconia at temperatures of 0 °C and 50 °C and conclude that the optimum temperature to obtain desired alkylates depends on the acid strength, which determines the relative rates of cracking, alkylation and oligomerization.[19] Olah and coworkers reported the effect of acid strength in their study with liquid acids (trifluoromethanesulfonic acid with trifluoroacetic acid/water) and report that $H_0 = -10.7$ is the optimum acid strength.[20]

It is generally agreed that weak Brønsted acid sites catalyze only oligomerization.[21] Some of the literature reports indicate that CO_2 adsorbs strongly on the acid sites and that it can reduce the acid strength of the catalyst. Olah and coworkers report that liquid carbon dioxide acts as a competing weak base and decreases the acidity of the system, thereby affecting product quality. Their study was based on isobutane/isobutylene alkylation on liquid acids like HF, H_2SO_4 and CF_3SO_3H. However, the authors are uncertain about the extent of inhomogeneity in the reaction mixture with CO_2.[22] A recent report also confirms that CO_2 can act as a Lewis base interacting with strong Lewis acids in solutions.[23] Ruthven and coworkers report that CO_2 adsorbs strongly compared to propane on a zeolitic catalyst.[24]

The main objective of the present work is to systematically investigate reaction media effects on conversion and TMP selectivity using diluents like dense CO_2 and ethane on various solid acid catalysts. The extraction of heavy compounds by the near critical media is evaluated in a back-mixed slurry reactor with both microporous and mesoporous supported catalysts to clearly distinguish the effect of pore-diffusion limitations in these catalysts. Further, the low temperature (ambient/sub-ambient) region is explored to reduce the coke precursor formation rates and more effectively balance the coke removal rates. The results also shed light on the physico-chemical aspects of the reaction.

Experimental

Catalysts

Four different catalysts are used in this study. The zeolite catalysts were procured from GraceDavison. The beta zeolite (SMR 5-9858-01062) has a Si/Al ratio of 13 and USY zeolite (SMR 5-9858-01061) has Si/Al ratio of 3. The compositions, along with basic physical properties are listed in the Table 1. Zeolites were used in the powder form as received. The SEM images of these zeolites indicate that the particle size ranges from 1–10 μm. The supported heteropolyacid catalyst, 62% TPA/SiO_2, was prepared as reported previously, but using *n*-butanol as solvent during impregnation.[25] The SiO_2-supported Nafion® catalysts (SAC-13) were supplied (in the form of pellets) by BASF Catalysts. The TPA/SiO_2 and SAC-13 catalysts are size-reduced and sieved to 62–105 μm prior to use.

The 62% TPA/SiO_2 catalyst was pretreated *in situ* under flowing nitrogen at 175 °C for 1 h. The SAC-13 catalyst was pretreated *in situ* under flowing nitrogen at 150 °C for 3 h. The BET surface area (SA) and BJH pore volume (PV) measurements for these mesoporous catalysts were made using a Micromeretics Gemini instrument, employing nitrogen physisorption. Detailed pore size distribution on beta zeolites was experimentally measured by Micromeritics ASAP analyzer at DuPont.

Chemicals

The compressed gases used in the study, isobutane (Instrument purity grade, > 99.5%; Lot no. 102-51-02346-A2), 1-butene (Chemical purity grade, > 99.0%; Lot no. 102-51-02345-A1) and ethane (Chemical purity grade, > 99.0%), were procured from Matheson Tri-gas Inc. Liquified CO_2 (Airgas) of 99.995% purity was used.

Experimental setup

The details of the experimental setup are described elsewhere.[17,26] Briefly, the catalyst is suspended as slurry in a continuous, back-mixed slurry reactor. Premixed I/O mixture and diluents (if any) are pumped separately using syringe pumps (500D from Teledyne Isco). Before admitting the feed mixture, the reactor is brought to the desired pressure and temperature with isobutane (when no diluent is used) or with isobutane and diluent in the same molar ratio as in the feed mixture. The products were analyzed online by gas chromatography (Agilent 6890 N), equipped with an FID, and a DB-Petro 100 m column (J & W Scientific), with a total analysis time of 90 min for each injection. The following definitions are used in discussing the results of this work.

$$Conversion = 1 - \frac{(Butenes\ mass)_{effluent}}{(Butenes\ mass)_{feed}}$$

$$C_8\ Selectivity = \frac{(Mass\ of\ all\ C_8's)_{effluent}}{(Mass\ of\ all\ C_{5+}\ components)_{effluent}}$$

$$TMP/C_8\ Selectivity = \frac{(Mass\ of\ all\ TMPs)_{effluent}}{(Mass\ of\ all\ C_8's)_{effluent}}$$

Results and discussion

Catalyst characterization

The total microporous pore volume (pore dia < 20 Å) is 0.222 cc/g, while the total pore volume for pore dia > 20 Å is 0.064 cc/g. Within pore sizes of 20–100 Å, the major fraction of pore volume is within 20–45 Å. The volume in inter-crystalline pores of large diameter (> 100 Å) is about 20% of the total pore volume (of pore sizes > 20 Å). The SEM images of zeolites shown in Fig. 1a (beta zeolite) and Fig. 1b (USY zeolite) depict that the crystallite sizes are on the order of 100 nm. The BET surface area and pore volume for mesoporous supported catalysts are discussed later.

Conversion and selectivity results

Liquid phase experiments

Initial experiments are conducted in the liquid phase with particular attention to the change in product distribution with TOS, which provides insights into the deactivation mechanism. By operating at a relatively long reactor residence time (ratio of volume of the reaction mixture to that of total volumetric flow rate at the exit) of ~6.7 h, the initial product distribution is closely followed. At the beginning, the I/O ratios are very high since the reactor contains only isobutane. Model predictions suggest that high I/O ratios in the reactor favor C_8 alkylate yields.[26]

Fig. 2 gives the product distribution on beta zeolite in liquid phase at 75 °C, 40 bar, OSV = 0.11 h⁻¹, I/O = 5.0. Several key observations are made from this experiment (see Figs. 2a–2c).

• As seen in Fig. 2a, almost complete butene conversion (99.5%+) is achieved up to 12 h, thereby providing a high
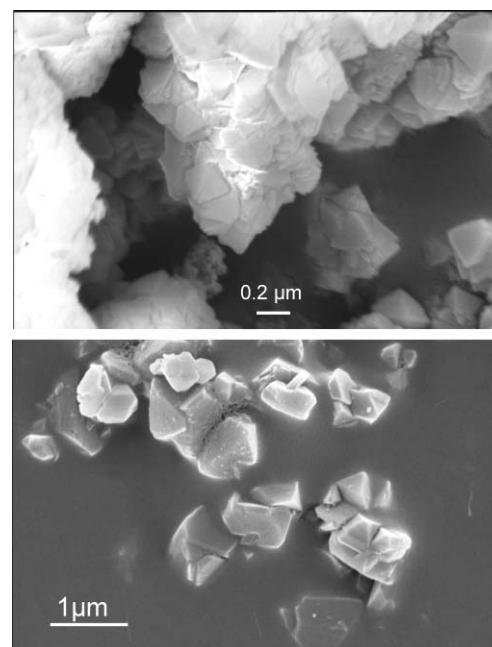

Fig. 1 SEM images of (a) beta zeolite; (b) USY zeolite.
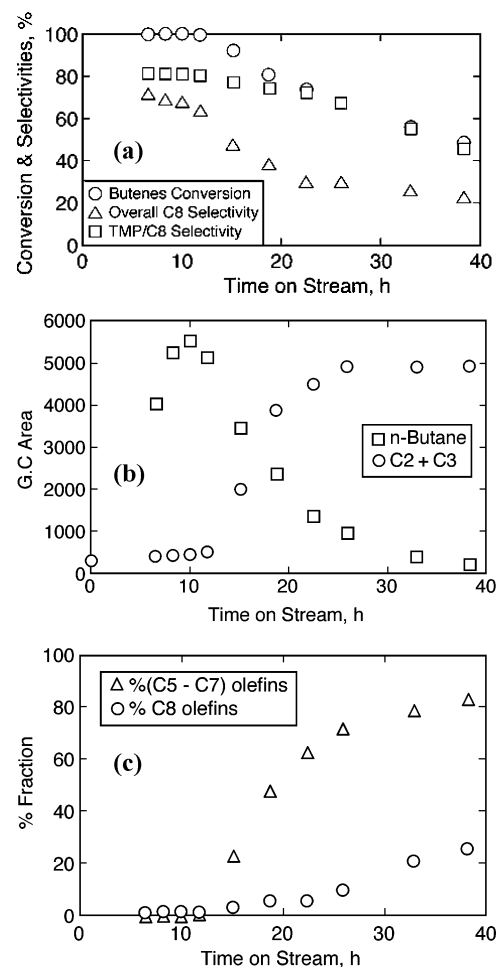

Fig. 2 Temporal profiles on beta zeolite (75 °C, 40 bar, OSV = 0.11 h⁻¹, I/O = 5.0): (a) conversion and selectivity profiles; (b) light ends; (c) olefins.

I/O ratio in the reactor (CSTR) that favors the formation of the desired products, the trimethylpentanes. The formation of TMPs is high during this period (Fig. 2a), but decreases after 12 h, similar to that reported in the literature.[7,9]

• The decrease of 'self alkylation' activity (tracked by *n*-butane formation) is observed after 12 h (Fig. 2b), which indicates the decrease of hydride transfer activity and hence an important measure of catalyst lifetime, a correlation first noted by Lercher's group.[9]

• The formation of olefins within the C_5–C_7 fraction, C_8 olefins and C_2, C_3 olefins is observed starting at about the same TOS of 12 h and increases with time (Fig. 2c). This indicates the onset of cracking reactions at about the same TOS when catalyst deactivation is observed.

• Within the C_5–C_7 fraction, the olefinic content reaches as high as 83%, with the fraction of C_5 olefin being dominant (74%). However, the fraction of C_8 olefins among C_8's is only about 26% at longer TOS (see Fig. 2c).

• The selectivity towards heavier compounds (C_9^+) increases from 15% to about 50% until TOS of 23 h and then decreases (not shown in Fig. 2).

These observations show that the catalyst deactivation is concurrent with decrease in self-alkylation, build up of olefins from cracking and oligomerization reactions. Other insights from these results are discussed in the appropriate sections below.

Reaction media effects on zeolites: pressure tuning studies with ethane

Simulations based on the Peng–Robinson equation of state (PREOS) were performed to obtain the critical properties of the reaction mixtures containing isobutane, butene, 2,2,4 TMP, CO_2 and ethane, as summarized in Table 2. The compositions in the table represent pure reactant, and reactants with partial/complete conversion of butenes to 2,2,4 TMP with either CO_2 or ethane as diluent. Details may be found elsewhere.[26] Based on the simulations, isothermal pressure tuning studies at 75 °C have been performed with *sc*-ethane as the solvent, with pressures ranging from 52–100 bars. At constant 1-butene space velocity and ethane flow rates, conversion and selectivity profiles were obtained at various fixed pressures at 75 °C. This pressure tuning is similar, in principle, to that reported for Fischer-Trøpsch synthesis with *n*-hexane[28] and

isobutane/butene alkylation with CO_2 as diluents.[17] In a typical experiment, the feed mixture contained about 74% (molar) ethane, the rest being made up of an I/O mixture at a molar ratio of 5.

The absence of any possible side effects of the diluent, ethane or its impurities is verified with the following experiment. After loading the pretreated catalyst, dense ethane is pumped to the reactor and maintained at 80 bar, 75 °C. After 2 h of exposure time at reaction conditions, isobutane is flowed into the reactor system until about 10 times the volume of the reactor to replace all the ethane with isobutane, after which the typical liquid phase experiment is started. The results show similar profiles to the liquid phase experiment without exposing the catalyst to ethane, confirming the absence of any adverse effects of ethane on catalyst activity and lifetime.

Figures 3a and 3b show the conversion and the TMPs/C_8 selectivity profiles respectively during the pressure tuning studies on beta zeolite. In all cases, the results point to catalyst deactivation. The conversion stabilizes in the case of the mild pressure (52 bar) ethane experiment (Fig. 3a), while in the liquid
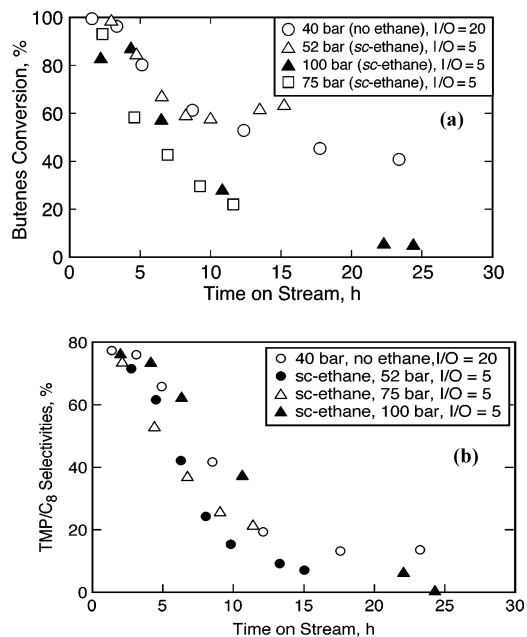
Fig. 3 Temporal profiles on beta zeolite (75 °C, OSV = 0.11 h^{-1}); (a) 1-butene conversion, (b) TMP/C_8 selectivity.

Table 2 Predicted critical properties of reactant/product mixtures with ethane/CO_2 as diluents (Estimated using PREOS)[26]

Isobutane (mol%)	1-Butene (mol%)	CO_2 (mol%)	Ethane (mol%)	2,2,4 TMP (mol%)	$(T_c)_{mix}$ (°C)	$(P_c)_{mix}$ (bar)
25	5	70	0	0	67	74
21	1	70	0	4	78	89
20	0	70	0	5	81	92
25	5	0	70	0	78	55
21	1	0	70	4	90	63
20	0	0	70	5	93	65
20	4	0	76	0	70	55
16	0	0	76	4	82	64
15	3	0	82	0	62	55
12	0	0	82	3	71	62
10	2	0	88	0	53	53
8	0	0	88	2	59	59

phase (no ethane) run, the TMPs/C$_8$ selectivity stabilizes at about 14% (Fig. 3b). Thus, the high initial TMP/C$_8$ selectivity is not stabilized even with the use of dense ethane as the diluent. Note that in these experiments, the comparison of the ethane-based experiments are made with a liquid phase experiment such that the (I + diluent)/O ratio is 20 in both cases. The diluent is either additional isobutane or the supercritical fluid solvent (either CO$_2$ or ethane). In this manner, the olefin residence times are unaffected in these experiments. However, the I/O ratios inside the reactor are different, which could affect the selectivity. To better understand the effect of feed I/O ratio on activity and catalyst life, the conversion and selectivity profiles of the experiments with feed I/O ratios of 5 and 20 (under otherwise identical conditions) are plotted with dimensionless time (defined as ratio of time on stream to that of reactor residence time) in Fig. 4. With identical olefin space velocity of 0.11 h^{-1}, the reactor residence times for I/O ratios of 5 and 20 are calculated to be 6.7 h and 1.7 h respectively. Fig. 4 clearly shows that the I/O ratio does not affect the catalyst activity or selectivity significantly. It must be noted that at startup, the reactor contains isobutane only and that the results are compared across a duration of less than six reactor residence times which are insufficient to achieve a steady state even without catalyst deactivation.
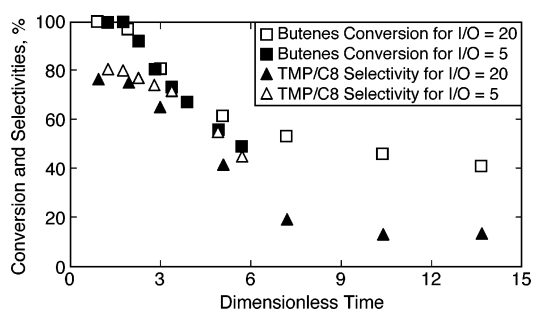

Fig. 4 Comparison of conversion and selectivity profiles for molar feed I/O ratios of 5 and 20 (beta zeolite, 75 °C, 40 bar, OSV = 0.11 h^{-1}, liquid phase).

Activity at ambient/sub-ambient temperatures

Sub-ambient temperatures are used in both HF and H$_2$SO$_4$ based commercial processes. Hence, low temperature activity in the case of zeolites was explored since at sub-ambient temperatures, the coke precursor formation rates are expected to be much slower. Further, the TMPs are thermodynamically favored over DMHs at lower temperatures. Fig. 5a compares the performance of beta zeolite in liquid phase operation at 75 °C, 31 °C and 15 °C, under otherwise identical conditions. The conversion profiles of the low temperature experiments seem to be identical, but different from the profiles at 75 °C. As explained in the previous section, a steady state is possible only after a TOS of 40 h. Hence, the apparent steady activity until ~12 h at 75 °C is only representative of the initial conversion.

To better understand the intrinsic activity, % TMP yields, expressed as a percentage of the maximum possible theoretical yields that can be achieved at steady state, are plotted in Fig. 5b. Because these are profiles from a CSTR at unsteady state, the plots also show that the deactivation started before 15 h. Note
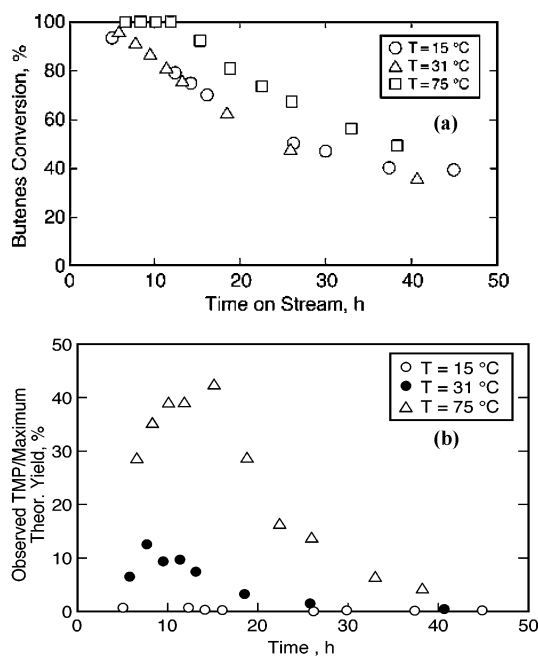

Fig. 5 Comparison of temporal profiles at various temperatures on beta zeolite (40 bar, OSV = 0.11 h^{-1}, molar feed I/O = 5.0); (a) 1-butene conversion; (b) TMP yields.

that while the TMP yields start to decrease beyond 15 h at 75 °C, they decrease much earlier (TOS of 8 h) at 31 °C. Negligible TMPs are observed at sub-ambient temperatures. These results indicate that the catalyst is deactivated before the TMPs diffuse out of the pores. Further, an experiment with dense ethane was conducted at 30 °C to see if the activity can be stabilized at low temperatures. The reaction in this case is expected to proceed in a gas-expanded liquid phase, as reviewed recently.[27] It is clear that the activity declines continuously with time and the overall selectivity towards C$_8$'s is less than 10% after TOS of 20 h (see Fig. 6). It suggests that the enhanced diffusion rate in the expanded phase is not sufficient to ameliorate the deactivation process.
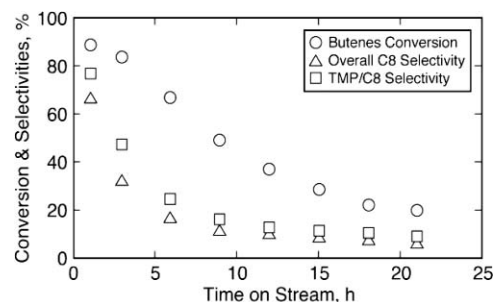
Fig. 6 Temporal conversion and selectivity profiles on beta zeolite with dense ethane (73 mol% in feed) in liquid phase (30 °C, 40 bar, OSV = 0.11 h^{-1}, molar feed I/O = 5.0).

Reaction media effects on mesoporous solid acids

Some reports have indicated that the media effects in microporous zeolitic catalysts are effective only on the processes occurring on the outer surface of these catalysts.[16,29] Since the
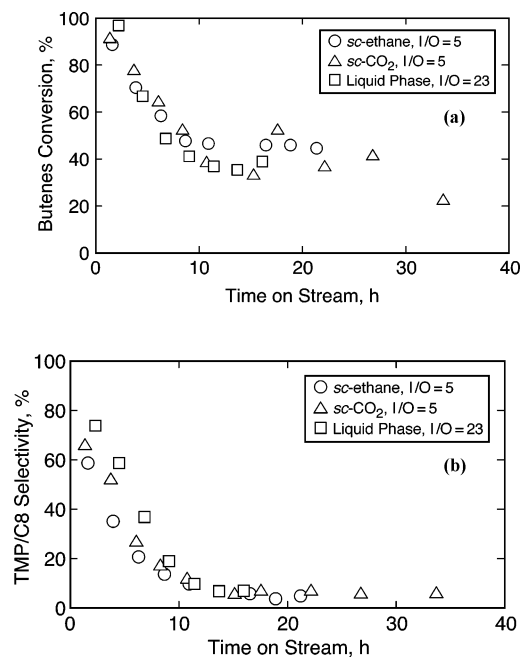
Fig. 7 Comparison of temporal conversion profiles on 62%TPA/SiO₂ (62–105 μm) with various media (95 °C, 40 bar, OSV = 0.11 h⁻¹, molar fee I/O = 5.0); (a) 1-butene conversion; (b) TMP/C₈ selectivity.

reaction media effects observed with ethane are not appreciable on zeolites, a new batch of heteropolyacids (62% HPA/SiO₂) was also investigated with dense ethane, and the results compared with dense CO₂ and liquid phase operation. Figs. 7a and 7b compare the conversion and selectivity profiles of these experiments. The conversion and the TMP/C₈ selectivity stabilize at longer TOS of about 15–20 h in all the cases. These results indicate that the use of CO₂ *vs.* ethane as diluent does not alter the conversion/selectivity profiles and that the media effects are not appreciable for stabilizing the high initial TMP selectivity. This suggests that the desired reaction *via* intermolecular hydride transfer step is not diffusion controlled. Note that the higher temperature (95 °C) used with these catalysts is because of their lower acid strength compared to that of beta and USY zeolites.

For comparison purposes, liquid phase experiments (with no additional diluents) were also conducted with USY, 62% HPA/SiO₂ and SAC-13 catalysts with molar feed I/O ratio of 5, at 40 bar and olefin space velocity of 0.11 h⁻¹. Such a comparison of initial activity for various catalysts is summarized in Table 3. It is interesting to note that despite lower than complete conversion (even at 95 °C) in case of HPA/SiO₂ and SAC-13, the TMP/C₈ selectivity is significant. The observed

Table 3 Comparison of initial activity and selectivity of various solid acid catalysts [molar feed I/O ratio = 5, 40 bar, olefin space velocity = 0.11 h⁻¹]

Catalyst	Conversion (%)	TMP/C₈	Overall C₈'s	C₅–C₇	C₉+
USY zeolite[a]	100	90	82	15	3
Beta zeolite[a]	100	81	71	14	15
62% HPA/Silica[b]	97	72	70	12	18
SAC-13[b]	94	64	55	23	22

[a] 75 °C. [b] 95 °C.

activity in zeolites is generally retained longer (TOS of 10 h) as compared to less than a few hours in the case of HPA/SiO₂ and SAC-13. However, considering that the acid site density (ASD) of SAC-13 is an order of magnitude lower compared to zeolites and that HPA/SiO₂ has an intermediate ASD between those of SAC-13 and zeolites, the results indicate that the net butene flow rate per acid site controls the observed duration of steady selectivity. This phenomenon was also pointed out recently by Lercher's group, based on their study on X zeolites.⁹ The net butene flow rate per acid site is greater in the case of SAC-13 and HPA/SiO₂. The results on catalyst lifetime also suggest that deactivation of catalysts occurs site by site.

The physical properties of the spent mesoporous catalysts are characterized and compared to those of the fresh catalyst. The results are shown in Table 4. SAC-13 catalyst does not show any substantial loss of any surface area or pore volume but heteropolyacids lose greater than 98% surface area and pore volume in case of liquid phase experiments, but retain properties better when either dense CO₂ or ethane is used as diluent. Despite these variations, all catalysts show deactivation with decreasing TMP/C₈ selectivity with TOS, indicating that deactivation is not caused by pore blocking, at least on the SAC-13 catalyst. These results suggest that the deactivation on mesoporous catalysts should be studied in more detail.

Conclusions

This study represents a systematic evaluation of reaction media effects in highly active microporous and mesoporous solid acid catalysts. The liquid phase experiments in the back-mixed slurry reactor, with long reactor residence times provide a framework for comparing the initial activity of various solid acid catalysts. The zeolitic catalysts showed excellent selectivity towards TMP production, followed by HPA/SiO₂ and SAC-13 catalysts.

Table 4 Characteristics of spent mesoporous catalysts, compared to fresh batches

Catalyst	BET SA (m²/g)	Pore Volume (cc/g)	Avg. Pore Dia (Å)
SAC-13 N, Fresh	129	0.51	162
SAC-13 N, spent (liquid phase, 95 °C, 40 bar, I/O = 5)	133	0.54	145
SAC-13 N, spent (sc-ethane, 95 °C, 95 bar, I/O = 5)	117	0.45	118
62%HPA/SiO₂, Fresh	220	0.29	48
62%HPA/SiO₂, spent (liquid, 95 °C, 40 bar, I/O = 23)	3.2	0.005	75
62%HPA/SiO₂, spent (liquid, 95 °C, 40 bar, I/O = 5)	4.2	0.008	83
62%HPA/SiO₂, spent (sc-ethane, 95 °C, 95 bar, I/O = 5)	38.3	0.09	72
62%HPA/SiO₂, spent (sc-CO₂, 95 °C, 95 bar, I/O = 5)	25.1	0.06	72

The use of either *sc* ethane or *sc*CO$_2$ as a diluent to replace the excess isobutane in the feed provides similar conversion and TMP selectivity profiles indicating that there are negligible adsorption effects due to the use of CO$_2$ with the acid catalysts. Further, the conversion and selectivity profiles obtained with supercritical feed mixtures are comparable to those obtained in liquid phase experiments. These results demonstrate that reaction media effects are not significant during isobutane alkylation at higher temperatures (75–95 °C) implying that the desired alkylate forming reaction *via* the intermolecular hydride transfer step is not diffusion controlled at these temperatures.

The conversion and selectivity results at low temperatures show that the catalyst is deactivated even before the TMPs are transported out of the pores, thereby indicating that pore diffusion rates play an important role in the deactivation process at low temperatures. These results suggest that novel approaches that enhance the pore diffusion rates at lower temperatures need to be pursued.

The results presented here bridge the gap between alkylation reactions conducted in the liquid and supercritical phases, and have provided a better understanding of the physicochemical sequence of events occurring in solid acid catalyzed alkylations. An effort is currently underway in our laboratory to study the intrinsic adsorption, desorption and pore-transport rates of reactant and product molecules using a Tapered Element Oscillatory Microbalance (TEOM) on various solid acids under non-reactive conditions. The results of such TEOM investigations help discern if a chosen solid acid catalyst is a viable candidate for facile transport of the reactant and product molecules, a prerequisite for attaining stable catalyst activity.

Acknowledgements

References

1 J. A. Kocal, *Green Chemistry Conference*, Washington D.C. June, 2005.
2 A. Gaffney, *Annual CREL meeting*, Washington University, St. Louis, 2006.
3 A. Corma and A. Martinez, *Catal. Rev.-Sci. Eng.*, 1993, **35**, 483.
4 P. Rao and S. R. Vatcha, *Oil Gas J.*, 1996, **94**, 56.
5 J. Weitkamp and Y. Traa, *Catal. Today*, 1999, **49**, 193.
6 R. Gläser, *Chem, Eng. Techol.*, 2007, **30**, 557.
7 K. P. deJong, C. M. A. M. Mesters, D. G. R. Peferoen, P. T. M. van Brugge and C. de Groot, *Chem. Eng. Sci.*, 1996, **51**, 2053.
8 G. S. Nivarthy, Y. He, K. Seshan and J. A. Lercher, *J. Catal.*, 1998, **176**, 192.
9 A. Feller, A. Guzman, I. Zuazo and J. A. Lercher, *J. Catal.*, 2004, **224**, 80.
10 C. Sievers, I. Zuazo, A. Guzman, R. Olindo, and J. A. Lercher, *AIChE Annual Meeting*, Salt Lake City, 2007.
11 G. Martinis and G. Froment, *Ind. Eng. Chem. Res.*, 2006, **45**, 940; G. Martinis and G. Froment, *Ind. Eng. Chem. Res.*, 2006, **45**, 954.
12 G. Funamoto, S. Tamura, K. Segawa, K. Wan and M. Davis, *Res. Chem. Intermed.*, 1998, **24**, 449.
13 L. Fan, I. Nakamura, S. Ishida and K. Fujimoto, *Ind. Eng. Chem. Res.*, 1997, **36**, 1458.
14 P. Y. Gayraud, N. Essayem and J. C. Vedrine, *Stud. Surf. Sci. Catal.*, 2000, **130C**, 2549.
15 A. L. M. Salinas, D. Kong, Y. B. Taarit and N. Essayem, *Ind. Eng. Chem. Res.*, 2004, **43**, 6355.
16 M. Clark and B. Subramaniam, *Ind. Eng. Chem. Res.*, 1998, **37**, 1243.
17 C. J. Lyon, B. Subramaniam and C. Pereira, *Stud. Surf. Sci. Catal.*, 2001, **139**, 221.
18 V. R. Sarsani, Y. Wang and B. Subramaniam, *Ind. Eng. Chem. Res.*, 2005, **44**, 6491.
19 A. Corma, *Appl. Catal. A*, 1994, **111**, 175.
20 G. A. Olah, P. Batamack, D. Deffieux, B. Torok, Q. Wang, A. Molnar and G. K. S. Prakash, *Appl. Catal. A*, 1996, **146**, 107.
21 A. Feller, A. Guzman, I. Zuazo and J. A. Lercher, *Stud. Surf. Sci. Catal.*, 2003, **145**, 67.
22 G. A. Olah, E. Marinez, B. Torok and G. K. S. Prakash, *Catal. Lett.*, 1999, **61**, 105.
23 P. W. Bell, A. J. Thote, Y. Park, Ram B. Gupta and C. B. Roberts, *Ind. Eng. Chem. Res.*, 2003, **42**, 6280.
24 F. Brandani and D. M. Ruthven, *Ind. Eng. Chem. Res.*, 2004, **43**, 8339.
25 Y. Wang, A. Y. Kim, S. S. Li, L. Wang, C. H. F. Peden, and B. C. Bunker, in *Shape-Selective Catalysis: Chemical Synthesis and Hydrocarbon Processing*, ed. C. Song, C., M. M. Garces, and Y. Sugi, Am. Chem. Soc., Washington, DC, 1998.
26 V. R. Sarsani, Ph.D. Dissertation, University of Kansas, 2007.
27 P. G. Jessop and B. Subramaniam, *Chem. Rev.*, 2007, **107**, 2615.
28 D. Bochniak and B. Subramaniam, *AIChE J.*, 1998, **44**, 1889.
29 R. Gläser and J. Weitkamp, *Ind. Eng. Chem. Res.*, 2003, **42**, 6294.

Aerobic oxidation of alcohols using various types of immobilized palladium catalyst: the synergistic role of functionalized ligands, morphology of support, and solvent in generating and stabilizing nanoparticles†

Babak Karimi,*[a] Asghar Zamani,[a] Sedigheh Abedi[a] and James H. Clark[b]

Preparation and characterization of a variety of immobilized palladium catalyst, based on either ligand functionalized amorphous or ordered mesoporous silica, is described. The resulting Pd-loaded materials act as efficient catalyst for the oxidation of a variety of alcohols using molecular oxygen and air. Our studies show that in the case of supported palladium catalyst on hybrid amorphous silica, the nature of ligand and the solvent could effectively control the generation of nanoparticles. Furthermore, we have found that nanoparticles with smaller size and higher activity were generated from the anchored palladium precursor when the aerobic oxidation of alcohols was carried out in α,α,α-trifluorotoluene (TFT) instead of toluene. On the other hand, in the case of aerobic oxidation reactions by using supported palladium catalyst on hybrid SBA-15, the combination of organic ligand and ordered mesoporous channels resulted in an interesting synergistic effect that led to enhanced activity, prevention of Pd nanoparticles agglomeration, and finally generation of a durable catalyst.

Introduction

The selective oxidation of alcohols to form carbonyl compounds is one of the most fundamental transformation in both laboratory and industrial synthetic chemistry.[1] Reagents that are traditionally used for these oxidations such as stoichiometric Cr(VI) salts,[1a,2] DMSO-coupled reagents,[3] or hypervalent iodines,[4] are often toxic and show poor atom efficiency and their use thereby presents significant environmental issues which render them impractical. The recent Technology Vision 2020 report published by the Council for Chemical Research highlights selective oxidation of organic compounds as one of the critical challenges facing the chemical industry;[5] Dioxygen-coupled strategies are the most attractive means of attaining this goal.[6] This has resulted in much attention being recently directed toward the development of new protocols for the aerobic oxidation of alcohols using transition-metal catalysts.[7] Among them, palladium-based catalysts show promising catalytic activity, and different types of palladium-based homogeneous[8] and heterogeneous catalysts[9] in the form of metal complexes or nanoparticles have been reported.[10] However, they often require high catalyst loading and the vast majority of them still use homogeneous palladium catalyst/ligand systems which are of limited practical application on an industrial scale owing to the difficulties in recovering and the reusing the expensive metals and ligands from the reaction mixture. One means to circumvent this problem is the design and synthesis of new improved heterogeneous catalysts with superior activity as well as high reusability. In this regard a few heterogeneous Pd catalysts including Pd/C,[9a] Pd-hydrotalcite,[9c–d] Pd/TiO2[9b,g] have been reported. However, these heterogeneous Pd systems suffer from high catalyst loading and/or low catalytic activities or limited substrate scope. Recently, the application of palladium nanoparticles dispersed in an organic polymer has also been disclosed for the aerobic oxidation of alcohols.[10] However, this heterogeneous system also suffers from high catalyst loading (up to 5 mol%) and the organic polymers in these protocols are very expensive and potentially susceptible to oxidative degradation under oxidation conditions. There are a few excellent catalysts including hydroxyapatite supported palladium (Pd-HAP),[9f,11a] Au-CeO2,[11b] Au-Pd/TiO2,[11c] Pt/PS-PEG-NH2,[11d] and PI-Au,[11e] but most of them produce only high turnover frequencies at elevated (~ 160 °C) temperatures. Furthermore, a major problem is that palladium agglomeration and the formation of palladium black can cause catalyst deactivation in many cases. To address these issues, we have recently reported in a preliminary communication that hybrid ordered mesoporous (SBA-15) silica is a very suitable support in preparing a highly recoverable palladium-based catalyst for the aerobic oxidation of alcohols.[12] We have also demonstrated for the first time that the combination of an organic ligand and ordered mesoporous channels resulted in an interesting synergistic effect that led to enhanced activity, the prevention of the agglomeration of the Pd nanoparticles, and the generation of a durable catalyst for

[a]*Department of Chemistry, Institute for Advanced Studies in Basic Sciences (IASBS), P.O. Box 45195–1159, Gava Zang, Zanjan, Iran. E-mail: karimi@iasbs.ac.ir; Fax: +98-241-4214949; Tel: +98-241-4153225*
[b]*Clean Technology Centre, University of York, York, Yorkshire, UK YO10 5DD. E-mail: jhc1@york.ac.uk; Fax: +44 1904 432705; Tel: +44 1904 432559*

† Electronic supplementary information (ESI) available: experimental procedures; characterization of the catalysts; schemes and figures. See DOI: 10.1039/b805824e

aerobic oxidation of alcohols. Herein, we present the preparation and characterizations of a variety of supported palladium catalyst based on both functionalized amorphous and SBA-15 silica and discuss more fully our findings concerning the synergistic effect of functionalized ligand, the structure of support, and the nature of solvent in generating and stabilizing Pd nanoparticles during the aerobic oxidation of alcohols. We also describe the effect of above-mentioned issues on aspects such as substrate scope and recycling behavior of catalysts.

Results and discussion

### Preparation and characterization of catalysts

In contrast to organic polymers, inorganic supports like silica show advantages such as mechanical stability and resistance against aging, solvent, chemical reagents, and high temperature.[13] Therefore, an important recent strategy to convert a homogeneous process into a heterogeneous one is to covalently introduce the active site onto large surface area inorganic solids through an organic entity (flexible space)

to create organic-inorganic hybrid (interphase) catalysts.[14] An interphase is defined as a region within a material in which a stationary (organic-inorganic hybrid catalyst) and mobile compound (solvent and reagent) penetrate each other at a molecular level. According to the definition, an interphase catalyst (or pre-catalyst) is composed of three parts: an inert matrix (support), a flexible organic spacer, and an active center.[14b] Therefore, owing to the partial mobility of the reactive center, an interphase catalyst is able to simulate homogeneous reaction conditions, and at the same time it has the advantage of easy separation and recovery of the heterogeneous catalysts. In the present study, we use the interphase strategy to synthesize three different kinds of supported palladium pre-catalyst onto both amorphous and ordered mesoporous silica for application as heterogeneous catalyst for the aerobic oxidation of alcohols. The preparation procedure to obtain the catalyst (Cat **1**, Pd@SiO$_2$-L$_1$) is demonstrated in Scheme 1.[15]

Catalyst **1** was characterized by atomic absorption spectroscopy (AA), thermogravimetric analysis (TGA), and DRIFT-IR spectroscopy.[15] From the TGA analysis of L$_1$@SiO$_2$, it was calculated that the loading of the bipyridyl ligand bound to the
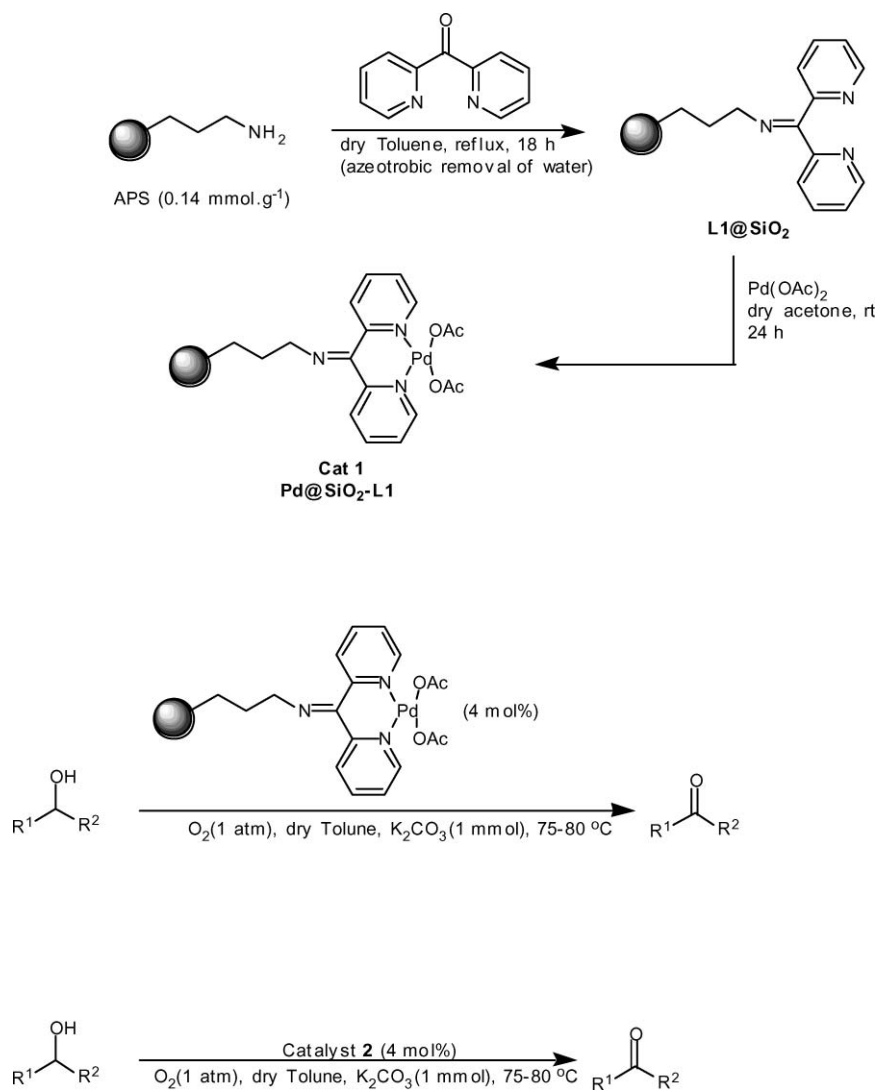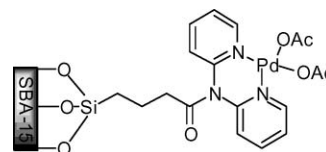

Scheme 1
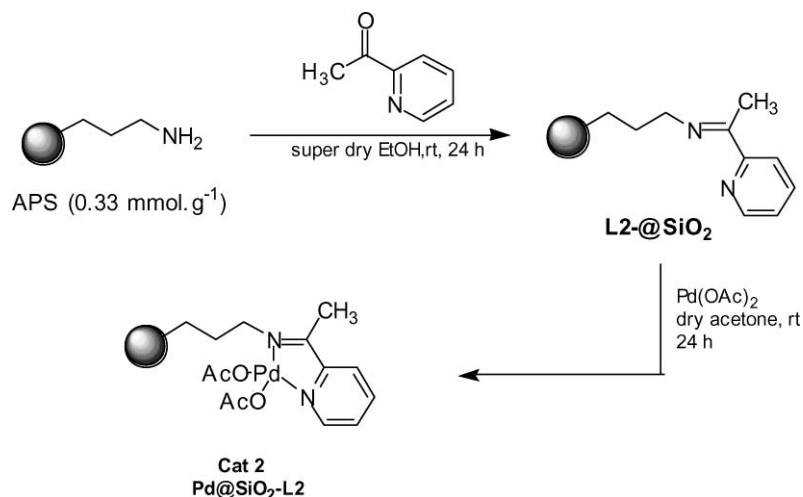
Scheme 2

silica surface was 0.13 mmol.g^{-1}. The loading of palladium in **1** was determined using AA and shows a loading at 0.120 ± 0.001 mmol.g^{-1}. This indicates that more than 90% of the surface-bound ligand were complexed with palladium.†[15]

The second catalyst (Cat **2**, Pd@SiO$_2$-L$_2$) was synthesized by APS (0.33 mmol.g^{-1}) precursor using a known procedure with slight modifications (Scheme 2).[16]

TGA analysis was used to determine the amount of ligand incorporated into APS.† Weight loss is mainly divided into three regions: below 100 °C, 150 °C–400 °C and 400–614 °C. Weight loss 30–151 °C was assigned to the loss of adsorbed water (1.8%). The large weight loss between 480–615 °C was owing to the decomposition of covalently bonded organic groups (4.6%). The amount of ligand anchored on the surface of L$_2$@SiO$_2$ was found to be 0.28 mmol.g^{-1}. This data was further confirmed by elemental analysis. The catalyst **2** (Pd@SiO$_2$-L$_2$) was then prepared by stirring a mixture of L$_2$@SiO$_2$ (4 g) and Pd(OAc)$_2$ (0.112 g, 0.5 mmol) in dry acetone (100 mL) at room temperature for 24h. After stirring, the resulting solid was filtered, and washed with acetone until the washings were colourless and dried at 95 °C overnight to afford Pd@SiO$_2$-L$_2$. The amount of palladium anchored on the surface of **2** was found to be 0.08 mmol.g^{-1} (corresponding to 28% of the ligands available) on the basis of atomic absorption spectroscopy. To determine the thermal stability, TGA analysis of **2** was also conducted in air from room temperature to 700 °C, and typical weight loss curves have been shown.† This sample shows a weight loss of a small amount of loosely bound water (less than 2%) below 200 °C. This is followed by a weight loss of about 9.1% between 350 and 500 °C due to the decomposition of organic ligand bound palladium complex. There after, an additional loss of 3.2% is observed, probably resulting principally decomposition of free anchored imine complex (see supporting information).

In order to prepare the third catalyst (Pd@SBA-15-L$_3$, **3**), we chose to employ the ordered mesoporous silicate SBA-15[17] as a support for a bidentate ligand because it has regular porosity, and high surface area. In addition, it is well known that organic groups inside large pore mesoporous materials are more accessible than those on amorphous silica. Therefore we reasoned that SBA-15, owing to the above-mentioned

property, might be better suited as a support for preparing heterogeneous Pd catalysts. SBA-15 was obtained from pluronic P123 (EO$_{20}$PO$_{70}$EO$_{20}$, EO = ethylene oxide, PO = propylene oxide, M$_{AV}$ = 5800, Aldrich) as a lyotropic ligand that was liquid crystal templated, and (EtO)$_4$Si under acidic conditions following the reported literature procedure.[17b] The resulting SBA-15 was then functionalized with a bipyridylamide ligand followed by complexation with Pd(OAc)$_2$ to give the corresponding immobilized catalyst **3** (Scheme 3).†

Scheme 3

A typical nitrogen adsorption/desorption type IV profile with a sharp hysteresis loop, which is characteristic of the highly ordered mesoporous materials, was obtained for **3** (Fig. 1a).

A BET surface area of 455 m^2.g^{-1} and a total pore volume of 0.76 cm^3.g^{-1} were obtained for the material. Thus values are smaller than those for the starting SBA-15 (864 m^{2}g^{-1}). BJH calculations showed an average pore diameter of 7.6 nm for **3**, a value which is in good agreement with the pore diameter estimated from the TEM image (Figs. 4a, b). On the basis of the AA analysis of a solution obtained by washing the catalyst with nitric acid, the amount of palladium loading on **3** was found to be 0.022 ± 0.001 mmol.g^{-1}. We used such a low loading in order to minimize catalyst leaching.

Catalysis. We next examined the ability of the palladium loaded hybrid silicates (Cat **1–3**) to actually catalyze the aerobic oxidation of alcohols. Initially we focused our attention on the aerobic oxidation of benzyl alcohol under the same reaction conditions (80 °C, TFT or toluene as solvent, K$_2$CO$_3$ as base, 1 atm O$_2$ (balloon filled)) in order to compare our new catalyst **2** with catalyst **1**[15] and catalyst **3**[12] reported earlier (Table 1).

Although all catalysts were able to furnish the corresponding benzaldehyde in excellent yield within the indicated time
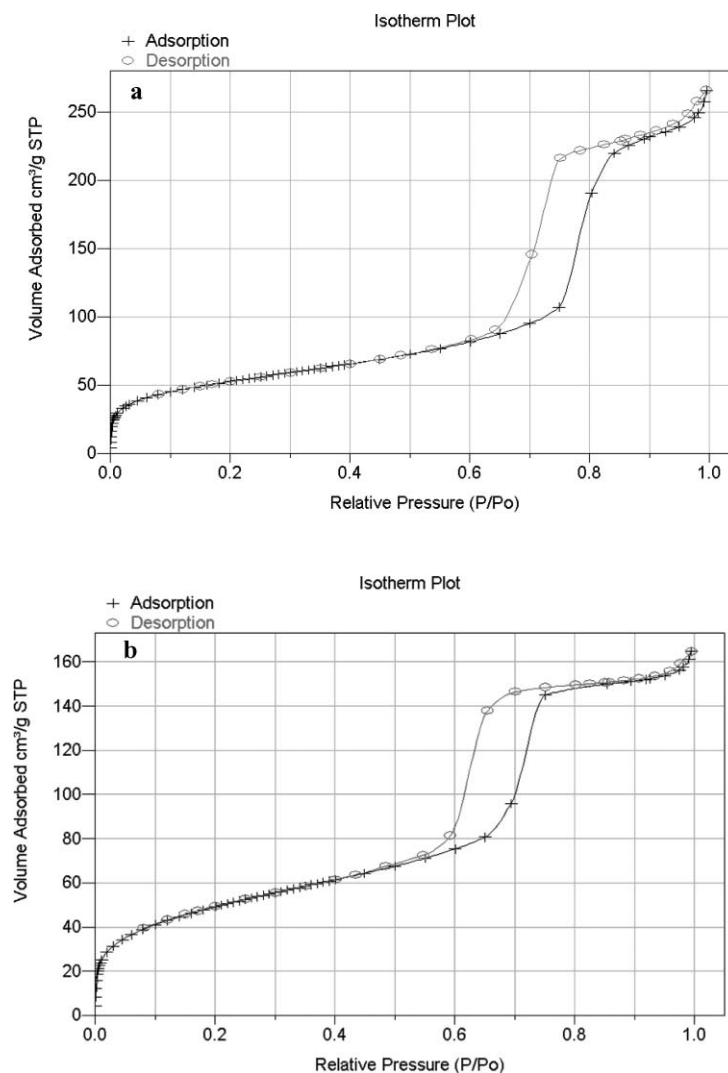
Fig. 1 The isotherm plot of a sample of Catalyst **3**: (a) before the first reaction cycle and; (2) after the first reaction cycle.

obviously, catalyst **2** in TFT (entry 11) and catalyst **3** in both TFT and toluene (entries 14, 15) exhibited higher catalytic activities than that of catalyst **1** (entries 3, 4).

It is worth mentioning that catalyst **2** in TFT (equivalent to 0.4 mol% Pd) is even more effective than the same catalyst sample in toluene (entry 11 vs. 12). Moreover, our preliminary investigations showed that catalyst **2** in TFT and toluene gave consistent activity in 5 and 6 subsequent reactions and exhibited $TON_{TFT} = 2500$ and $TON_{Tol} = 187$, respectively at 80 °C, with almost quantitative yield of the product. To clarify the above mentioned observations, we have studied the evolution of **2** by means of transmission electron microscopy (TEM) analysis. Interestingly, inspection of the TEM image of a sample of catalyst **2** after recovery from the aerobic oxidation of benzyl alcohol in TFT and toluene clearly indicates, the generation of Pd nanoparticles onto the surface of amorphous SiO_2 (Fig. 2).

Furthermore, the images show that the oxidation reaction using catalyst **2** in *TFT clearly favors production of smaller metal nanoparticles than those obtained in toluene.* It is well-known that the catalyst performance can be very sensitive to particle size because the surface structure and electronic properties can change greatly within the nano-size range.[18] Moreover, it has been demonstrated that the catalytic activity of Pd nanoparticles increases with decreasing their average size.[19] Therefore, it would be logical to speculate that the increase in the size of the nanoparticles onto the surface of **2** in toluene is the reason why the process is slower than in TFT.

This observation might be due to the fact that TFT more efficiently caps many of the free metallic surface sites of the nanoparticles and provides fewer sites for the Ostwald ripening process.[20] On the other hand, the lower catalytic activity (higher catalyst loading) of **2** in toluene is probably due to generation of a smaller amount of nanoparticles of the bigger size throughout the silica surface due to larger nanoparticle aggregations. We may expect that in the case of **1** ($Pd@SiO_2-L_1$) and **3** (Pd@SBA-15-L_3), TFT will result in rapid nucleation of a great number of smaller Pd nanoparticles compared to toluene and therefore cause a similar solvent effect. However, as can be seen from the data in Table 1 neither **1** nor **3** showed this effect (entries 3 vs. 4 and 14 vs. 15).

Therefore it seems that in the case of **1** and **3** other factors should also be taken into account. On the basis of our previous

Table 1 Oxidation of benzyl Alcohol by Various Palladium supported Catalyst with Molecular Oxygen and Air

Entry	Catalyst/support	x (mol%)	solvent	time (h) O$_2$	time (h) air	yield (%)^{a,b} O$_2$	yield (%)^{a,b} air
1	**1**/SiO$_2$[15]	4.0	toluene	8	12	>99 (85)	>99
2	**1**/SiO$_2$	4.0	TFT^c	8	12	>99	>99
3	**1**/SiO$_2$	4.0	toluene	2	2	7	5
4	**1**/SiO$_2$	4.0	TFT	2	2	11	9
5	**2**/SiO$_2$	3.2	toluene	1.25	1.25	>99	>99
6	**2**/SiO$_2$	2.0	toluene	3	3	>99	>99
7	**2**/SiO$_2$	1.0	toluene	7	7	>99	>99
8	**2**/SiO$_2$	0.4	TFT	1.5	2	>98	>98
9	**2**/SiO$_2$	0.2	TFT	4	—	>98	—
10	**2**/SiO$_2$	0.2	Toluene	2	—	35	—
11	**2**/SiO$_2$	0.2	TFT	2	—	51	—
12	**3**/SBA-15[12]	0.4	toluene	3.5	5.5	>99 (83)	>99
13	**3**/SBA-15	0.4	TFT	3.5	5	>99	>99
14	**3**/SBA-15	0.4	toluene	2	—	72	—
15	**3**/SBA-15	0.4	TFT	2	—	73	—
16	NHC-Pd/IL@SiO$_2$[23]	5	toluene	12	—	Nd	—
17	NHC-Pd/IL@SiO$_2$[23]	5	TFT	12	—	Nd	—

^{a} GC yield unless otherwise stated. ^{b} Yields in parentheses refer to isolated pure products. ^{c} TFT = α,α,α-trifluorotoluene.
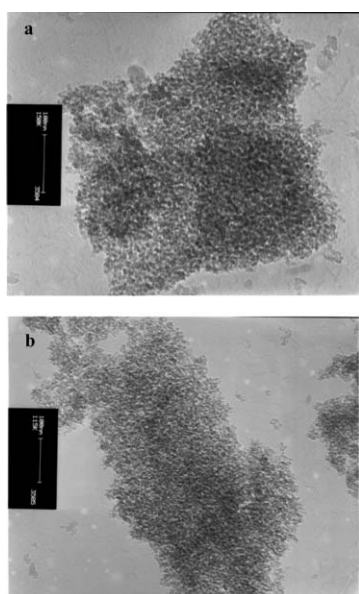

Fig. 2 TEM images of the recovered catalyst **2**. (a) After the first reaction cycle in toluene (particle size in the range of 6–17 nm and an average particle size ≈10 nm); (b) After the first reaction cycle in TFT (particle size in the range 3–14 nm and an average particle size ≈6.7).

studies, we also found that catalyst **1** requires high catalyst concentration (up to 4 mol%, 80 °C, 8 h) and it also suffers from the disadvantage of prolonged reaction time and a significant reduction in its catalytic activity after three reaction cycles.[15] At first glance, one might conclude that this catalytic deactivation is due to Pd leaching from the solid to the solution. However, both individual AA analysis of the solution of each three reaction cycles and hot-filtration test indicates no Pd species that leached into the solution.[15] To gain better insight into the structural

changes, the recovered sample of **1** has also been studied by means of TEM to try to find a reason for its rapid deactivation. Fig. 3 shows a typical TEM (in dark-field mode) image of **1** after the third cycle of aerobic oxidation of benzyl alcohol. It can be seen, this material shows extensive agglomeration of palladium with an irregular size distribution above 100 nm.

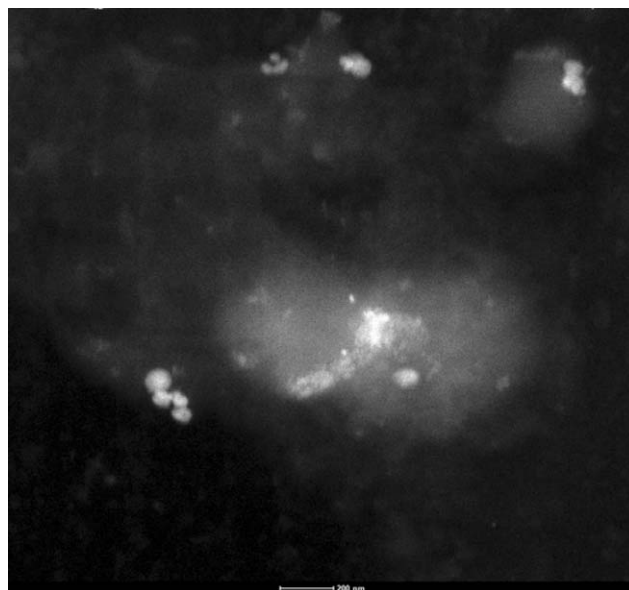**Fig. 3** Dark-field TEM image of catalyst **1** after the third reaction cycle.

This result clearly shows that Pd-agglomeration is the major reason for deactivation of catalyst **1** just after the third cycle. One reason the process is so much more prominent in the case of both **2** and **3** than in **1** is presumably owing to smooth hydrolysis of un-complexed imino group in **1** during the oxidation reaction

using the water by-product. Unfortunately, we have not yet been able to obtain any evidence for the hydrolyzed bipyridyl ketone that leached from catalyst **1**. However, TGA analysis of the recovered catalyst **1** showed a slight decrease in the weight loss as compared with the fresh catalyst, in support of the above proposal.

The lack of binding provides a means of rapid sintering of small palladium particles throughout the surface of silica and produce very large (much less reactive) palladium clusters. This may also explain why the catalyst **1** shows similar behaviour in both TFT and toluene, *i.e.* in the absence of a well-bonded ligand, Pd agglomeration would rapidly result in catalyst deactivation regardless to the small difference in the stabilizing ability of TFT compared to toluene. This observation also highlights *the crucial role of anchored ligands in generating and stabilizing nanoparticles during a typical catalytic process.*

With regard to material **3** we have reported in an earlier communication[12] that at 0.4 mol% it is an efficient and durable heterogeneous catalyst for the aerobic oxidation of a wide range of alcohols including benzyl alcohol itself. In this study, we have found that the catalytic activity and durability of **3** was not significantly altered by changing the solvent from toluene to TFT (Table 1, entries 14 vs. 15). Moreover, after the first oxidation cycle using **3** (Table 1, entry 8) to afford benzaldehyde in 83% isolated yield (>99% conversion), the recovered catalyst exhibited consistent catalytic activity in 12 consecutive reactions (total TON $\cong$ 3000 at 80 °C),[12] which is much higher than those observed in the case of both **1** and **2**. To find a reason for this high reactivity and more importantly, high durability of **3** at a molecular level, TEM analysis has also been performed on a sample of **3** before and after catalysis. Fig. 4 shows representative TEM images of **3** before the first cycle of aerobic oxidation both perpendicular (Fig. 4a) and across (Fig. 4b) to the hexagonally uniformed channels of $\approx$7 nm in size. On the other hand, Fig. 4c shows a representative TEM image of the same sample of **3** after recovery from the first cycle of aerobic oxidation of benzyl alcohol. By comparing these two set of TEM images before and after the first reaction cycle, we can see that Pd nanoparticles with regular size ($\leq$ 7 nm) were mostly generated inside the highly ordered channels and that the nanoarchitecture of the catalyst (SBA-15 channels) largely survived.[21]

Moreover, the N_2 adsorption-desorption analysis of the recovered catalyst (Fig. 1b) showed a very similar isotherm to those of the fresh catalyst **3** (Fig. 1a) with relatively sharp adsorption and desorption branches in the P/P_0 range of 0.5–0.8. This strongly indicates a relatively narrow mesopore size distribution even in the recovered catalyst, although the total pore volume decreases from 0.76 to 0.57 cm^3 g^{-1}. This result also suggests that most of the nanometre-scaled void space and channels of the host SBA-15 remain open, although a small portion of the channels may be blocked by Pd nanoparticles (Fig. 2b). In order to better clarify the role of bipyridyl ligands in our protocol we set up two sets of controlled experiments. First, we prepared a new catalyst in which SBA-15 lacking organic ligands was loaded with Pd(OAc)$_2$ with the same Pd loading as **3**. The oxidation of benzyl alcohol was then conducted under the same reaction condition using this catalyst. Interestingly, we found that the corresponding benzaldehyde was produced in >99% conversion after 5 hours in the first experiment. However,
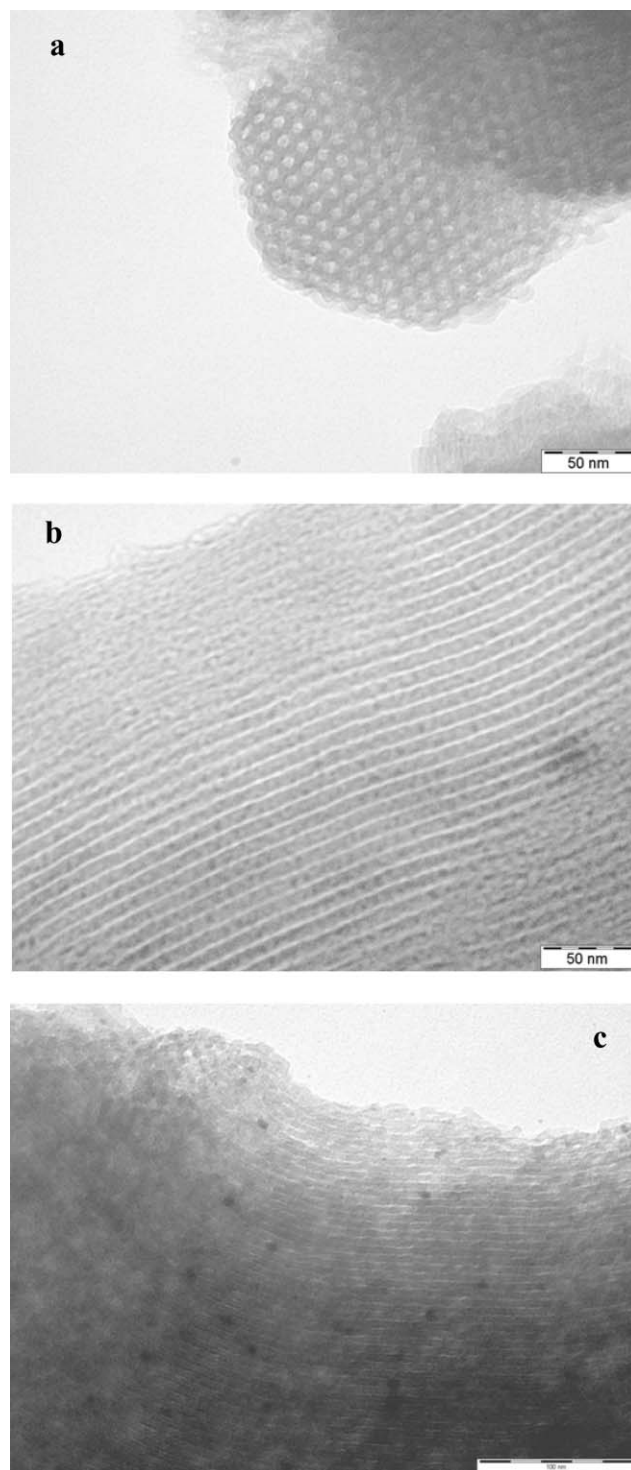

Fig. 4 TEM images of fresh catalyst **3**. (a) Perpendicular to the channels; (b) across the channels; (c) TEM image of the recovered catalyst **3** across the channels, well-dispersed palladium nanoparticles with a relatively regular size can clearly be seen inside the channels.

when the oxidation of benzyl alcohol was repeated for two subsequent runs with the same catalyst sample, the catalyst activity was dramatically decreased. The significant deactivation of the material along with a color change to dark grayish is presumably due to the formation of large palladium clusters (palladium black) onto the outer surface of SBA-15.[12] In the

second experiment, the SBA-15 with 3-cyanopropyl group was loaded with Pd(OAc)₂ and the resulting pale yellow solid was tested for catalytic activity in the same process. In this case, the solid catalyst showed a high degree of leaching and also the corresponding benzaldehyde was produced in low (less than 25%) yield after 5 h due to the rapid formation of Pd-black. Therefore, we believe that the bipyrydyl ligands in catalyst **3** provide a means of uniform distribution of mononuclear palladium center throughout the solid support, to ensure controlled nanoparticle formation mostly inside the ordered mesoporous channels of SBA-15.[12] We can also explain why the catalyst **3** shows high and the same catalytic activity in both TFT and toluene. The cooperation of functionalized organic ligand (the bipyridine ligand) inside the ordered mesoporous channels and size restriction imposed by meso-channels of the parent SBA-15 resulted in an interesting synergistic effect enhancing the activity, *preventing Pd nanoparticles agglomeration*, and producing an inherently *durable catalyst* independent of the choice of TFT or toluene. Much to our surprise, our recently developed silica supported N-heterocyclic carbene palladium/ionic liquid catalysts that have been shown to be highly efficient and recyclable catalysts for the Heck reaction, were ineffective in oxidizing benzyl alcohol under similar reaction conditions to those of catalysts **1–3** (Table 1, entries 16, 17).[22] The reasons for this latter observation are under investigation.

Aerobic oxidation of alcohols using catalyst 2. The scope and failure of catalyst **2** was also examined. As summarized in Table 2, benzylic and allylic alcohols are generally excellent substrates for this catalyst with electron-rich alcohols having the fastest reaction rates. However, electronic effects do not seem to have a significant effect on the isolated yields for electron-rich and electron-poor benzylic alcohols.

In general, many of the previously reported homogeneous transition metal complexes are unable to catalyze the oxidation of alcohols that can chelate Pd(II) catalyst, as a starting material or product, because the strong coordination to metal centers deactivates the catalyst. However, the successful oxidation of benzoin and furfuryl alcohol as model substrates shows a superior capability of **2** in oxidizing similar substrates (Table 2, entries 9, 13). Catalyst **2** in particular showed excellent reactivity for the selective oxidation of various types of allylic alcohols yielding the corresponding α,β-unsaturated carbonyl compounds in excellent yields (Table 2, entries 14–17). It is worth mentioning that in the oxidation of allylic alcohols, C=C double bonds remained intact without an intramolecular hydrogen transfer. Secondary benzylic alcohols were also efficiently oxidized into the corresponding ketone (Table 2, entries 10–13). Even the reaction under air (balloon filled) instead of oxygen proceeded well, thus indicating that the reaction is not markedly retarded by the concentration of dissolved oxygen in the solvent. Unfortunately, using **2**, aliphatic alcohols such as 1-octanol and 2-octanol and 4-phenyl cyclohexanol proved to be poor substrates, yielding the corresponding carbonyl compound in 13%, 21%, and 18% yields, respectively (Table 2, entries 18–20).

To determine whether the catalyst **2** is functioning in a heterogeneous manner, or whether it is merely a reservoir for more active soluble forms of Pd, various heterogeneity tests were performed. First, the reaction of benzyl alcohol was conducted

in the presence of catalyst **2** for 1 hour until a conversion of 55% was reached. Then the solid was hot-filtered and transferred to another Schlenk flask containing K₂CO₃ in TFT at 80 °C under O₂ atmosphere. The catalyst free solution was then allowed to continue to react, but no further reaction took place even after 12 h. Furthermore, our primarily investigation using AA analysis indicates that no Pd species leached into solution within the detection limit. Nevertheless, it is difficult at this stage to exactly attribute the actual catalytic activity solely to the ligand-bound Pd or to Pd nanoparticles. It would not be also surprising if the supported Pd nanoparticles serve as a reservoir for a trace of non-detectable Pd particles which react *via* a homogeneous pathway.[22] To better clarify this issue, we have also conducted a *three-phase-test* with a heterogeneous alcohol (Scheme 4).
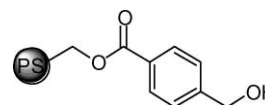
Scheme 4

Unfortunately, this substrate was decomposed during the oxidation reaction so that we have detected the decomposed alcoholic part of the solid in the reaction solution. We are now searching to obtain a more suitable solid alcohol for this purpose and we will present the results in due course.

Experimental

Preparation of aminopropyl silica (APS)

Mesoporous silica gel (average pore diameter 60 Å) was activated by refluxing in concentrated hydrochloric acid (6 M) for 24 h and then washed thoroughly with the deionized water and dried before undergoing chemical surface modification. Refluxing the activated silica gel (10 g) with 3-aminopropyltrimethoxysilane (1.5 mmol) in dry toluene for 18 h. The solid materials were filtered off and washed with hot toluene for 12 h in a continuous extraction apparatus (Soxhlet) and then dried in oven at 110 °C overnight to give the surface bound amine (APS) group at a loading *ca.* 0.14 mmol g⁻¹ (by elemental analysis and back titration).
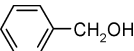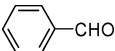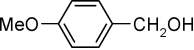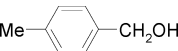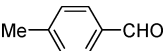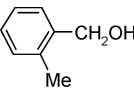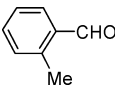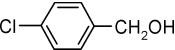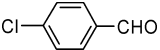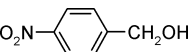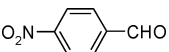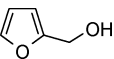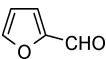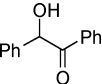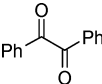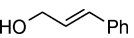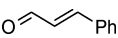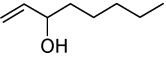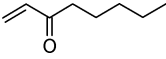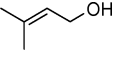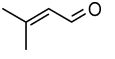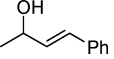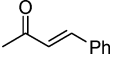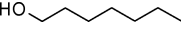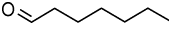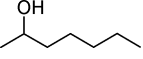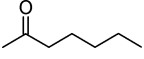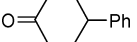
Preparation of surface bound bipyridyl ligand (L₁@SiO₂)

The resulting AMPS (0.14 mmol.g⁻¹, 5 g) was allowed to react with 2,2′-dipyridyl ketone (1 mmol, 0.184 g, Aldrich) in refluxing toluene with continuous removal of water using a Dean–Stark trap. The solid was filtered off and was washed thoroughly with hot toluene and ethanol to remove unreacted ketone. It was dried in air at 110 °C overnight to furnish the corresponding surface bound bidentate ligand **1** at a loading *ca.* 0.13 mmol g⁻¹ (Determined by TGA analysis).

Preparation of Pd@SiO₂-L₁ (Cat 1)

The catalyst was prepared by stirring a mixture of surface bound ligand **1** (4 g) and palladium acetate (0.52 mmol, 0.117 g, Merck) in dry acetone (100 mL) at room temperature for 24 h. After stirring the resulting white brown solid was filtered, washed with large volume of acetone, ethanol and ether. It was then dried in

Table 2 Oxidation of Alcohols by Catalyst **2** in TFT with Molecular Oxygen and Air

Entry	Substrate	Product	Pd (mol%)	time (h) O₂	time (h) air	yield (%)[a] O₂	yield (%)[a] air
1	Ph–CH₂OH	Ph–CHO	0.4	1.5	2	98	98
2	MeO–C₆H₄–CH₂OH	MeO–C₆H₄–CHO	0.2	4	—	97	—
3			0.1	3	3	100	100
4	Me–C₆H₄–CH₂OH	Me–C₆H₄–CHO	0.2	3	1.5	95	95
5	2-Me-C₆H₄–CH₂OH	2-Me-C₆H₄–CHO	0.7	10	—	91	—
6	Cl–C₆H₄–CH₂OH	Cl–C₆H₄–CHO	0.3	8	15	93	95
7	O₂N–C₆H₄–CH₂OH	O₂N–C₆H₄–CHO	0.2	24	—	78	—
9	furfuryl–CH₂OH	furfuryl–CHO	0.2	2	—	92	—
10	Ph–CH(OH)–Me	Ph–CO–Me	0.4	2.5	4	>99	100
			0.2	8.5	—	>99	—
11	Ph–CH(OH)–Et	Ph–CO–Et	0.4	2.5	4	97	95
12	Ph–CH(OH)–Ph	Ph–CO–Ph	0.4	10	—	100	—
13	Ph–CH(OH)–CO–Ph	Ph–CO–CO–Ph	0.4	4	7	100	97
14	HO–CH₂–CH=CH–Ph	O=CH–CH=CH–Ph	2	5	8	94	96
15	oct-1-en-3-ol	oct-1-en-3-one	2	7	10	100	94
16	3-methylbut-2-en-1-ol	3-methylbut-2-enal	2	5	8	100	100
17	4-phenylbut-3-en-2-ol	4-phenylbut-3-en-2-one	2	7	10	98	97
18	HO–CH₂–(CH₂)₅–CH₃	O=CH–(CH₂)₅–CH₃	3	24	—	13[b]	—
19	2-heptanol	2-heptanone	3	24	—	21	—
20	HO–C₆H₁₀–Ph	O=C₆H₉–Ph	3	24	—	18	—

[a] GC yield based on an internal standard method unless otherwise stated. [b] A trace amount of the corresponding esters (≈ 4%) and carboxylic acid (≈ 11%) were formed.

an oven at 95 °C overnight to furnish the corresponding catalyst **1** at a loading *ca.* 0.12 ± 0.01 mmol g^{-1} (Determined by TGA analysis and atomic absorption spectroscopy (AA)).

Preparation of (L$_2$@SiO$_2$)

2-acetylpyridine (0.605 g, 5 mmol) was added to a mixture of the oven dried AMPS (0.33 mmol.g^{-1}, 5 g) in super dry ethanol (150 mL) in a 250 mL round bottomed flask. The reaction mixture was stirred at 60 °C for 24 h. The ligand-grafted silica was filtered at the reaction temperature and the resulting solid and was washed thoroughly with hot toluene and ethanol to remove un-reacted ketone. It was dried in air at 95 °C overnight to furnish the corresponding surface bound bidentate ligand L$_2$@SiO$_2$ at a loading *ca.* 0.28 mmol g^{-1} (Determined by TGA analysis).

Preparation of Pd@SiO$_2$-L$_2$ (Cat 2)

The catalyst was prepared by stirring a mixture of surface bound ligand L$_2$@SiO$_2$ (4 g) and palladium acetate (0.50 mmol, 0.112 g, Merck) in dry acetone (100 mL) at room temperature for 24 h. After stirring the yellow solid was filtered, washed with large volume of acetone until washing were colourless. It was then dried in an oven at 95 °C overnight to furnish the corresponding catalyst **2** (Scheme S2, ESI†) at a loading *ca.* 0.080 ± 0.001 mmol g^{-1} (Determined by TGA analysis (Figure S5b) and atomic absorbtion spectroscopy (AA)).

Preparation of SBA-15

The synthesis of SBA-15 has been achieved using known procedure described by Stucky and his co-workers (see ref. 17b). In a typical preparation procedure, 4.0 g of Pluronic P123 (Aldrich, average Mw ≅ 5800) was dissolved in 30 g of water and 120 g of 2 M HCl solution with stirring at 35 °C. Then 8.50 g of tetraethoxysilane (TEOS) was added into that solution with stirring at 35 °C for 20 h. The mixture was aged at 80 °C overnight without stirring. The solid was filtered off and washed thoroughly with hot ethanol/water using a Soxhelet apparatus for 18 h to remove the surfactant molecules. It was dried in air at 110 °C overnight.

Preparation of SBA-15 surface bound carboxylic acid

The preparation of SBA-15 surface bound carboxylic acid was achieved according to the known procedure described by Clark *et al.*:[24] The resulting SBA-15 (6 g) was allowed to react with 3-cyanopropyltriethoxysilan (2 mmol, 0.462 g, Fluka) in refluxing dry toluene (150 mL) under nitrogen for 24 h. The solid was filtered off and was washed thoroughly with hot toluene and ethanol. It was dried in air at 90 °C overnight to furnish the corresponding surface bound cyanopropyl group at a loading *ca.* 0.33 mmol g^{-1} (Determined by elemental analysis). The absorption band at 2256 cm^{-1} along with bands 2900–3000 cm^{-1} clearly indicates the attachment of cyanopropyl group onto the surface of SBA-15 (Fig. 1). The CN-SBA-15 was hydrolyzed by heating in 50% (v/v) aqueous sulfuric acid at 150 °C for 3h. After cooling to room temperature, the resulting solid was filtered off and filter cake was washed with an excess of deionized water. Drying in an oven at 110 °C overnight furnished the

corresponding SBA-15-COOH with approximately the same loading.

Preparation of Pd@SBA-15-L$_3$ (Cat 3)

The ligand **A** was first prepared by stirring a mixture of surface-bound carboxylic acid (5 g), 2,2′-bipyridylamine (1.7 mmol, 0.291 g, Aldrich) and dicyclohexylcarbodiimide (1.7 mmol, 0.350 g, Merck) in dry THF (150 mL) at reflux temperature for 72 h. The solid was filtered off and washed thoroughly with hot ethanol using a Soxhelet apparatus for 18 h to remove both the urea by-products and unreacted starting materials. It was then dried in an oven at 110 °C overnight to furnish the corresponding surface-bound bipyridyl amide **A** at a loading *ca.* 0.2 mmol g^{-1} (Determined by TGA and elemental analysis, Fig. 2). The catalyst was then prepared by stirring a mixture of surface bound ligand **A** (4 g) and palladium acetate (0.11 mmol, 0.025 g, Merck) in dry acetone (100 mL) at room temperature for 24 h. After stirring, the white brown solid was filtered, washed with acetone, ethanol and ether in order to remove any adsorbed palladium on the surface. It was then dried in an oven at 95 °C overnight to furnish the corresponding catalyst **3** at a loading *ca.* 0.022 ± 0.001 mmol g^{-1} (atomic absorption spectroscopy (AA)).

General experimental procedure for oxidation using molecular oxygen

A mixture of K$_2$CO$_3$ (1 mmol) and catalyst **1** (0.18 g, ~0.4 mol% of Pd) in TFT (5 mL) was prepared in a two-necked flask. The flask was then evacuated (water aspirator) and refilled with pure oxygen for three times (balloon filled). To this solution the alcohol (1 mmol, in 1 mL TFT) was then injected and the resulting mixture was stirred at 80 °C under an oxygen or air atmosphere (for the indicated time in the Table 2). After completion of the reaction, the reaction mixture was filtered off and the catalyst rinsed twice with CH$_2$Cl$_2$ (5 mL) the excess of solvent was removed under reduced pressure to give the corresponding carbonyl compounds.

Conclusions

The preparation and characterization of a variety of supported palladium catalysts based on ligand functionalized amorphous and ordered mesoporous silicas (SBA-15) were described. The resulting Pd-loaded materials act as highly efficient catalysts for the oxidation of a variety of alcohols using molecular oxygen and air. The catalysts show high thermal stability and could be recovered and reused for several reaction cycles in a batch-wise system depending on their structures of the support, function-alized ligand, and the solvent. This study shows that in the case of supported palladium catalyst on hybrid amorphous silica (catalysts **1** and **2**), the nature of the ligand could significantly affect the generation and the distribution of nanoparticles onto the solid surface. Furthermore, we have found that nanoparticles with smaller size were generated from the anchored palladium precursor when the aerobic oxidation of alcohols were carried out in TFT instead of toluene. Our studies using TEM analysis of the samples before and after catalysis, show that in the case of supported palladium catalyst on hybrid amorphous silica, the nature of the ligand could effect the generation of nanoparticles.

Furthermore, we have found that nanoparticles with smaller size were generated from the anchored palladium precursor when the aerobic oxidation of alcohols were carried out in TFT instead toluene. On the other hand, in the case of aerobic oxidation reactions using supported palladium catalyst on hybrid SBA-15, the combination of organic ligand and ordered mesoporous channels resulted in an interesting synergistic effect enhancing catalytic activity, preventing Pd nanoparticles agglomeration, and enabling generation of a durable catalyst. Based on this study, a typical reactivity and durability sequence is: **3**/toluene ≈ **3**/TFT > **2**/TFT > **2**/toluene >> **1**/TFT ≈ **1**/toluene. Both catalysts **3** and **2** show high TOFs of approximately 18150 h^{-1} and 7230 h^{-1-} in the oxidation of 1-phenylethanol at 150 °C under solvent-free conditions. These results may find wide potential applications in designing other types of transition metal nanocatalysts. Further applications of this approach with other transition metal based nanoparticles are currently underway in our laboratories.

Acknowledgements

Notes and references

1 (*a*) M. Hudlicky, *Oxidation in Organic Chemistry*, ACS Monograph Series; American Chemical Scociety, Washington DC, 1990; (*b*) R. A. Sheldon, and J. K. Kochi, *Metal Catalyzed Oxidationd of Organic Compounds*, Academic Press, New York, 1984.

2 S. V. Ley, and A. Madfin, *Comprehensive Organic Synthesis*, B. M. Trost, I. Fleming, S. V. Ley, Eds.; Pergamon: Oxford, U.K., 1991; *vol.* **7**, pp 251–289.

3 A. Mancuso and D. Swern, *Synthesis*, 1981, 165.

4 (*a*) D. B. Dess and J. C. Martin, *J. Org. Chem.*, 1983, **48**, 4155; (*b*) D. B. Dess and J. C. Martin, *J. Am. Chem. Soc.*, 1991, **113**, 7277.

5 *Vision 2020 Catalysis Report* (www.ccrhq.org/vision/index/roadmaps.catrep.html).

6 (*a*) For recent reviews see: R. A. Sheldon, I. W. C. E. Arend and A. Dijksman, *Catal. Today*, 2000, **57**, 157; (*b*) B. Z. Zhan and A. Thompson, *Tetrahedron*, 2004, **60**, 2917.

7 (*a*) R. A. Sheldon, *Green Chem.*, 2000, **2**, G1; (*b*) P. T. Anastas, L. B. Bartlett, M. M. Kirchhoff and T. C. Williamson, *Catal. Today*, 2000, **55**, 11.

8 (*a*) K. Kaneda, Y. Fujii and K. Morioka, *J. Org. Chem.*, 1996, **61**, 4502; (*b*) K. Kaneda, Y. Fujii and K. Ebitani, *Tetrahedron Lett.*, 1997, **38**, 9023; (*c*) K. P. Peterson and R. C. Larock, *J. Org. Chem.*, 1998, **62**, 3185; (*d*) T. Nishimura, T. Onoue, K. Ohe and S. Uemura, *Tetrahedron Lett.*, 1998, **39**, 6011; (*e*) T. Nishimura, T. Onoue, K. Ohe and S. Uemura, *J. Org. Chem.*, 1999, **64**, 6750; (*f*) G.-J. T. Brink, I. W. C. E. Arends and R. A. Sheldon, *Science*, 2000, **287**, 1636; (*g*) K. Hallman and C. Moberg, *Adv. Synth. Catal.*, 2001, **343**, 260; (*h*) M. J. Schultz, C. C. Park and M. S. Sigman, *Chem. Commun.*, 2002, 3034; (*i*) D. R. Jensen, M. J. Schultz, J. A. Mueller and M. S. Sigman, *Angew. Chem. Int. Ed.*, 2003, **42**, 3810; (*j*) G.-J. T. Brink, I. W. C. E. Arends and R. A. Sheldon, *Adv. Synth. Catal.*, 2002, **344**, 355; (*k*) T. Nishimura and S. Uemura, *Synlett*, 2004, 201; (*l*) S. Paavola, K. Zetterberg, T. Privalov, I. Csöregh and C. Moberg, *Adv. Synth. Catal.*, 2004, **346**, 237; (*m*) T. Iwasawa, M. Tokunaga, T. Obora and Y. Tsuji, *J. Am. Chem. Soc.*, 2004, **126**, 6554; (*n*) M. J. Schultz, S. S. Hamilton, D. R. Jensen and M. S. Sigman, *J. Org. Chem.*, 2005, **70**, 3343; (*o*) T. Iwasawa, M. Tokunaga, Y. Obora and Y. Tsuji, *J. Am. Chem. Soc.*, 2004, **126**, 6554; (*p*) For a recent review on palladium catalyzed oxidation of alcohols see: J. Muzart, *Tetrahedron*, 2003, **59**, 5789; (*q*) For recent interesting reviews on palladium catalyzed aerobic oxidations of organic chemicals see: S. S. Stahl, *Angew. Chem. Int. Ed.*, 2004, **43**, 3400; (*r*) T. Nishimura and S. Uemura, *Catal. Surv.*

Jpn., 2000, **4**, 135; (*s*) B. A. Steinhoff, A. E. King and S. S. Stahl, *J. Org. Chem.*, 2006, **71**, 1861.

9 (*a*) T. Mallat and A. Baiker, *Catal. Today*, 1994, **19**, 274; (*b*) K. Ebitani, Y. Fujie and K. Kaneda, *Langmuir*, 1999, **15**, 1907; (*c*) T. Nishimura, N. Kakiuchi, M. Inoue and S. Uemura, *Chem. Commun.*, 2000, 1245; (*d*) N. Kakiuchi, Y. Maeda, T. Nishimura and S. Uemura, *J. Org. Chem.*, 2001, **66**, 6620; (*e*) N. Kakiuchi, M. Nishimura, M. Inoue and S. Uemura, *Bull. Chem. Soc. Jpn.*, 2001, **74**, 165; (*f*) K. Moroi, K. Yamaguchi, T. Hara, T. Mizugaki, K. Ebitani and K. Kaneda, *J. Am. Chem. Soc.*, 2002, **124**, 11572; (*g*) K.-M. Choi, T. Akita, T. Mizugaki, K. Ebitani and K. Kaneda, *New. J. Chem.*, 2003, **27**, 324; (*h*) K. Mori, T. Hara, T. Mizugaki, K. Ebitani and K. Kaneda, *J. Am. Chem. Soc.*, 2004, **126**, 10657; (*i*) U. R. Pillai and E. Sahle-Demessie, *Green Chem.*, 2004, **6**, 161.

10 (*a*) Y. Uozumi and R. Nakao, *Angew. Chem. Int. Ed.*, 2003, **42**, 3810; (*b*) B. Corain, K. Jerabek and P. Centomo, *Angew. Chem. Int. Ed.*, 2004, **43**, 959; (*c*) Z. Hou, N. Theyssen, A. Brinkmann and W. Leitner, *Angew. Chem.Int. Ed.*, 2005, **44**, 1346; (*d*) M. S. Kwon, N. Kim, C. M. Park, J. S. Lee, K. Y. Kang and J. Park, *Org. Lett.*, 2005, **7**, 1077; (*e*) Z. Hou, N. Theyssen and W. Leitner, *Green Chem.*, 2007, **9**, 127; (*f*) K. Hara, S. Tayama, H. Kano, T. Masuda, S. Takakusagi, T. Kondo, K. Uosaki and M. Sawamura, *Chem. Commun.*, 2007, 4280; (*g*) For an excellent recent study of aerobic oxidation of alcohols in supercritical carbon dioxide using supported palladium nanoparticles on hybrid mesoporous silica see: Z. Hou, N. Theyssen, A. Bronkmann, K. V. Klementiev, W. Grünert, M. Bühl, W. Schmidt, B. Spliethoff, B. Tesche, C. Weidenthaler and W. Leitner, *J. Catal.*, 2008, **258**, 315.

11 (*a*) K. Mori, T. Hara, T. Mizugaki, K. Ebitani and K. Kaneda, *J. Am. Chem. Soc.*, 2004, **126**, 10657; (*b*) A. Abad, P. Concepción, A. Corma and H. García, *Angew. Chem. Int. Ed.*, 2005, **44**, 4066; (*c*) D. I. Enache, J. K. Edwards, P. Landon, B. Solsona-Espiriu, A. F. Carley, A. A. Herzing, M. Watanabe, C. J. Kiely, D. W. Knight and G. J. Huchings, *Science*, 2006, **311**, 362; (*d*) Y. M. A. Yamada, T. Arakawa, H. Hocke and Y. Uozumi, *Angew. Chem. Int. Ed.*, 2007, **46**, 704; (*e*) H. Miyamura, R. Matsubara, Y. Miyazaki and S. Kobayashi, *Angew. Chem. Int. Ed.*, 2007, **46**, 4151.

12 B. Karimi, S. Abedi, J. H. Clark and V. Budarin, *Angew. Chem. Int. Ed.*, 2006, **45**, 4776.

13 P. Panster and S. Wieland, *Applied Homogeneous Catalysis with Organometallic Compounds* Vol. **2** (Eds. B. Cornils, W. A. Hermann, VCH, Weinheim, 1996, pp. 605–623.

14 (*a*) A. Corma and H. Garcia, *Chem. Rev.*, 2002, **102**, 3879; (*b*) Z. L. Lu, E. Lindner and H. A. Mayer, *Chem. Rev.*, 2002, **102**, 3543; (*c*) D. E. De Vos, M. Dams, B. F. Sels and P. A. Jacobs, *Chem. Rev.*, 2002, **102**, 3615; (*d*) A. P. Wight and M. E. Davis, *Chem. Rev.*, 2002, **102**, 3589; (*e*) J. H. Clark and D. J. Macquarrie, *Chem. Commun.*, 1998, 853.

15 B. Karimi, A. Zamani and J. H. Clark, *Organometallics*, 2005, **24**, 4695.

16 S. Paul and J. H. Clark, *Green Chem.*, 2003, **5**, 635.

17 (*a*) D. Zhao, J. Feng, Q. Huo, N. Melosh, G. H. Fredrickson, B. F. Chmelka and G. D. Stucky, *Science*, 1998, **279**, 548; (*b*) D. Zhao, Q. Huo, J. Feng, B. F. Chmelka and G. D. Stucky, *J. Am. Chem. Soc.*, 1998, **120**, 6024.

18 (*a*) A. T. Bell, *Science*, 2003, **299**, 1688; (*b*) D. R. Rolison, *Science*, 2003, **299**, 1698; (*c*) M. A. El-Sayed, *Acc. Chem. Res.*, 2001, **34**, 257.

19 (*a*) R. Narayanan and M. A. El-Sayed, *J. Am. Chem. Soc.*, 2003, **125**, 8340; (*b*) Y. Li, E. Boone and M. A. El-Sayed, *Langmuir*, 2002, **18**, 4921; (*c*) J.-L. Bars, U. Specht, J. S. Bradley and D. G. Blackmond, *Langmuir*, 1999, **15**, 7621.

20 (*a*) A. Howard, C. E. J. Mitchell and R. G. Egdell, *Surf. Sci.*, 2002, **515**, L504; (*b*) A. Imre, D. L. Beke, E. Contier-Moya, I. A. Szabo and E. Gillet, *Appl. Phys. A*, 2000, **71**, 19.

21 (*a*) For recent examples of the preparation and the use of metal nanoparticles deposited on ordered porous solids see: C. Yang, P. Liu, Y. Ho, K. Chiu and C. Chao, *Chem. Mater.*, 2003, **15**, 275; (*b*) J. Zhu, Z. Konya, V. F. Puntes, I. Kiricsi, C. X. Miao, J. W. Ager, A. P. Alivisatos and G. A. Somorjai, *Langmuir*, 2003, **19**, 4396; (*c*) J. He, T. Kunitake and A. Nakao, *Chem. Mater.*, 2003, **15**, 4401; (*d*) T. F. Baumann and J. H. Satcher, *Chem. Mater.*, 2003, **15**, 3745; (*e*) Y. Guari, C. Thieuleux, D. Mehdi, C. Reye, R. J. P. Corriu, S. Gomez-Gallardo, K. Philippot and B. Chaudret, *Chem. Mater.*, 2003, **15**,

2017; (*f*) S. D. Jackson, G. D. McLellan, G. Webb, L. Conyers, B. T. Keegan, S. Matter, S. Simpson, P. B. Wells, D. A. Whan and R. Whyman, *J. Catal.*, 1996, **162**, 10; (*g*) G. Jacobs, F. Ghadiali, A. Pisanu, A. Borgna, W. Alvarez and D. E. Resasco, *Appl. Catal. A*, 1999, **188**, 79; (*h*) S. Mandal, D. Roy, R. V. Chaudhari and M. Sastry, *Chem. Mater.*, 2004, **16**, 3714; (*i*) C. P. Mehnert, D. W. Weaver and J. Y. Ying, *J. Am. Chem. Soc.*, 1998, **120**, 12289.

22 B. Karimi and D. Enders, *Org. Lett.*, 2006, **8**, 1237.

23 (*a*) For some examples of metal colloids as reservoirs for homogeneous metal species, see: S. Tasler and B. H. Lipshutz, *J. Org. Chem.*, 2002, **64**, 1190; (*b*) I. W. Davis, L. Matty, D. L. Hughes and P. J. Reider, *J. Am. Chem. Soc.*, 2001, **123**, 10139.

24 (*a*) Andrew J. Butterworth, James H. Clark, Paul H. Walton and Simon J. Barlow, *Chem. Commun.*, 1996, 1859; (*b*) Jacob A. Elings, Rachida Ait-Meddour, James H. Clark and Duncan J. Macquarrie, *Chem. Commun.*, 1998, 2707.

Selective aerobic oxidative dibromination of alkenes with aqueous HBr and sodium nitrite as a catalyst†

Ajda Podgoršek,[a] Marco Eissen,[b] Jens Fleckenstein,[b] Stojan Stavber,[a] Marko Zupan[a,c] and Jernej Iskra*[a]

Various alkenes (internal, terminal, aryl and alkyl substituted) and 1,2-diphenylethyne were efficiently and selectively dibrominated using 2 equivalents of 48% aqueous hydrobromic acid, with air as an oxidant and sodium nitrite as a catalyst. Despite the presence of water, only *trans* dibromination occurred producing *anti*-1,2-dibromoalkanes and (*E*)-1,2-dibromo-1,2-diphenylethene. A comparison of resource demand, waste production and environmental, health and safety issues of the $NaNO_2$ catalyzed aerobic bromination with molecular bromine and other oxidative bromination methods revealed that the proposed method is not only selective and effective but has a better environmental profile.

Introduction

Bromination of alkenes and alkynes has garnered a significant amount of attention among those studying bromination reactions. Dibrominated derivatives are useful precursors for organometallic reagents and are widely applicable as intermediates in synthetic organic chemistry.[1,2] However, the use of molecular bromine in chlorinated solvents remains the preferred choice in the dibromination of organic molecules in spite of its toxic and corrosive nature. Moreover, the reactive nature of bromine results in highly exothermic reactions that makes performing bromination in a selective manner difficult and leads to its substitution by different pyridinium and quarternary ammonium tribromides[3] or *N*-bromosuccinimide in combination with lithium bromide.[4] The negative impact of such brominating protocols on the environment includes the use of environmentally unfriendly solvents, significant waste production and the need to remove residual reagents.[5] Nevertheless, bromine is still needed to prepare the reagents and when compared to alternative protocols, this classical approach of using molecular bromine remains resource efficient.[5b] Alternatively, nature has developed a molecular halogen-free strategy for halogenation using hydrogen peroxide (*haloperoxidase*) or oxygen (flavin dependent *halogenase*) and X⁻ to produce "X⁺" at the enzyme's active site.[6] The oxidative halogenation with the *in situ* formation of an active brominating species *via* the oxidation of bromide in

a more suitable solvent could be a promising way of overcoming the current drawbacks, especially when either hydrogen peroxide or oxygen, as the most environmentally benign of the oxidants, are involved.[7–10]

Alkenes are useful substrates for investigating the nature of active halogenating agents[11] and are used many times in biomimetic studies of haloperoxidation, mainly with a metal catalyst.[12] Research has focused on the selectivity of bromohydrin and dibromide formation in a vanadium(V) or molybdenium(VI) catalyzed oxybromination of alkenes using potassium bromide and hydrogen peroxide. Performing these reactions in water gave bromohydrin as the main product, despite a large excess of bromide ions.[13] In a two-phase system using either H_2O-$CHCl_3$[9d,12c,d,13] or H_2O-CH_2Cl_2,[12d,e] more dibrominated product together with bromohydrin was formed. Only when tetrabutylammonium bromide together with H_2O_2 and catalytic V_2O_5 in H_2O-CH_3CN was used as a tribromide precursor was the formation of dibromides from cyclohexene and styrene observed.[9c] A non-catalyzed oxidative bromination with H_2O_2/HBr in a two-phase system with either CCl_4 or an ionic liquid also gave dibromides selectively.[8a,14]

In contrast with hydrogen peroxide, oxygen has seldom been used for oxidative halogenation despite it being the most abundant, cheapest and atom economical oxidant. Only a few examples of aerobic oxybrominations of aromatic compounds catalyzed by various metal catalysts are reported.[10b,f,g] Zhang *et al.* describe a metal-free catalyzed oxidative bromination of aromatic compounds and aryl ketones utilizing a combination of aqueous hydrobromic acid, molecular oxygen and sodium nitrite as the catalyst.[10c] A similar system was also used for aerobic iodination.[10d] To the best of our knowledge, there are only two examples of aerobic oxidative halogenation that includes the oxidative halogenation of alkenes using a metal species as a catalyst. Bromination of 1-octene[10g] and chlorination of cyclododecene and *trans*-5-decene[15] resulted in the non-stereoselective formation of dihaloalkanes accompanied by products of addition of hydrohalic acid to the double bond.

[a] Laboratory of Organic and Bioorganic Chemistry, "Jožef Stefan" Institute, Jamova 39, 1000, Ljubljana, Slovenia.
E-mail: jernej.iskra@ijs.si; Fax: +386 1 4773 822; Tel: +386 1 4773 631
[b] Gymnasium Ganderkesee, Am Steinacker 12, 27777, Ganderkesee, Germany
*[c] Faculty of Chemistry and Chemical Technology, University of Ljubljana, Aškerčeva 5, 1000, Ljubljana, Slovenia*

† Electronic supplementary information (ESI) available: NMR spectra of (2,3-dibromo-1,1,1-trifluoropropan-2-yl)benzene **20**, Environmental factor E of different bromination methods, UV-vis spectra of Br_2 in CH_3CN and UV-vis spectra of NOBr. See DOI: 10.1039/b814989e

This report presents a study on the selective and stereoselective aerobic dibromination of alkenes and alkynes using air at near ambient pressure as the oxidant, an equimolar amount of aqueous hydrogen bromide and sodium nitrite as a catalyst. Environmental aspects, such as resource demands and waste production together with health and safety issues, will be evaluated in comparison to Br_2 addition and other oxidative bromination. Furthermore, the effect of the slow generation of the "active brominating agent" on the selectivity of bromination is discussed.

Results and discussion

To define optimum reaction conditions for oxidative bromination of alkenes in an HBr/air/NaNO$_2$(cat.) system we initially studied the reaction of styrene (**1**) in different solvents (acetonitrile, ethyl acetate, dichloromethane, hexane, methanol and water). Styrene (**1**) makes an excellent test substrate since its transformation is particularly sensitive to reaction conditions, *eg.* polymerization, incorporation of various nucleophiles from the milieu into the first-formed carbocation. First, 1 mmol of styrene (**1**) was dissolved in 10 mL of MeCN, then 2 mmol of 48% aqueous HBr (226 µL) and 5 mol% of NaNO$_2$ were added. The flask was immediately covered with an air filled balloon and stirred at 22 °C for 5 hours. On completion, ethyl acetate was added. The organic phase was discoloured by adding a few drops of 37% aq. NaHSO$_3$, neutralized by NaHCO$_3$ and dried over anhydrous Na$_2$SO$_4$. After removing the solvent, the 1,2-dibromo-1-phenylethane (**2**) was obtained. The role of solvent on functionalization of **1** is shown on Scheme 1. The best yield of **2** is obtained in acetonitrile, where only a trace amount of bromohydrin **3** was observed in the crude reaction product. Also, no excess hydrogen bromide was necessary for the complete conversion of styrene (**1**) into dibromide **2**. Interestingly, although 10 equivalents of water were present in the reaction mixture from using an aqueous solution of HBr, it did not interfere in the bromination process by forming bromohydrin **3**. In ethyl acetate, 78% of the dibrominated product **2** was formed non-selectively, the reaction in hexane gave a complex mixture of products, while in dichloromethane only a trace amount of **2** was obtained. Moreover, the use of either methanol or water as a reaction medium completely suppressed the oxidative bromination of styrene (**1**).
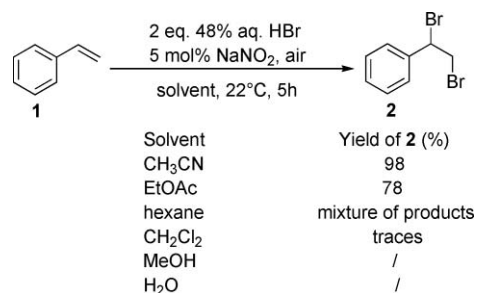
Scheme 1

Next, the effect of the mode of addition of sodium nitrite on conversion was investigated. Five mol% of solid NaNO$_2$ was added in one portion (Method A), in three portions every

Table 1 The effect of the mode of addition of NaNO$_2$ on aerobic oxidative bromination of styrene (**1**) with hydrobromic acid

Entry	Method[a]	Distribution (%)[b]						
		1	:	**2**	:	**3**	:	**4**
1	A	/	:	94	:	6	:	/
2	B	/	:	95	:	5	:	/
3	C	/	:	98	:	2	:	/
4	C, without addition of NaNO$_2$	66	:	/	:	/	:	34
5	C, without an air balloon	18	:	34	:	/	:	48

[a] Method A: 5 mol% of solid NaNO$_2$ was added in a single portion, Method B: 5 mol% of solid NaNO$_2$ was added in three portions every 2 hours, Method C: 20 µL of 2.5 M aq. NaNO$_2$ was added; [b] Determined by ^{1}H NMR spectroscopy.

2 hours (Method B) and as a 20 µL aqueous solution of 2.5 M NaNO$_2$ (Method C). Table 1 shows that there is no significant difference when sodium nitrite is added either all at once or in three discrete portions. However, a slightly higher yield of dibrominated product **2** was obtained when sodium nitrite was added as a 2.5 M aqueous solution, possibly because the sodium nitrite was uniformly distributed in the reaction mixture. Interestingly, although additional water was present in the system less bromohydrin was formed. Therefore, in all subsequent experiments an aqueous solution of sodium nitrite was added.

To highlight the role of sodium nitrite and the presence of air on the course of oxidative bromination of styrene (**1**), blank experiments both without sodium nitrite and air were performed. In the absence of sodium nitrite, the addition of HBr to styrene (**1**) is the sole reaction with 34% of (1-bromo-ethyl)-benzene (**4**) being formed (Table 1). In the absence of air only 34% of the dibrominated product **2** was formed and the addition of HBr on the double bond was the main reaction resulting in the formation of **4** in a 48% yield. From this we can conclude that catalytic amounts of sodium nitrite under aerobic conditions prevent the addition of hydrobromic acid to the alkene, while air as an oxidant enables the "*in situ*" formation of the brominating species and therefore the dibromination of the alkene.

To evaluate the scope of this catalytic system, optimum reaction conditions: 1 mmol of substrate, 2 mmol of 48% aqueous solution of HBr, 20 µL of 2.5 M aq. NaNO$_2$ (5 mol%) and 10 mL of acetonitrile, were used to oxidatively brominate various internal and terminal aryl and alkyl substituted alkenes and 1,2-diphenylethyne. The results are represented in Schemes 2–5. Yields were determined by ^{1}H NMR spectroscopy and are based on the starting compound, while the yields given in parentheses refer to isolated yields. Using this method, β-substituted styrenes were quantitatively and diastereoselectively converted to dibrominated products (Scheme 2). Bromination of *trans*-stilbene (**8**), ethyl *trans*-cinnamate (**9**) and acenaphthylene (**11**) gave *anti*-brominated products diastereo-specifically. *cis*-Stilbene (**5**) was also *trans* brominated under the above conditions yielding *syn*-1,2-dibromo-1,2-diphenylethane (**6**) accompanied by 5% of the *anti* isomer **7**.

The introduction of a second substituent in the α position in styrene (**1**) modifies the stability of the carbocation

Scheme 2

2 eq. 48% aq. HBr,
5 mol% NaNO$_2$, air
CH$_3$CN, 22°C, 5-24h

1 R^1=R^2=H
5 R^1=H, R^2=Ph
8 R^1=Ph, R^2=H
9 R^1=COOEt, R^2=H

2 98% (90%)
6 95% (90%) 7 5%
7 100% (95%)
10 100% (93%)

11

12 100% (96%)
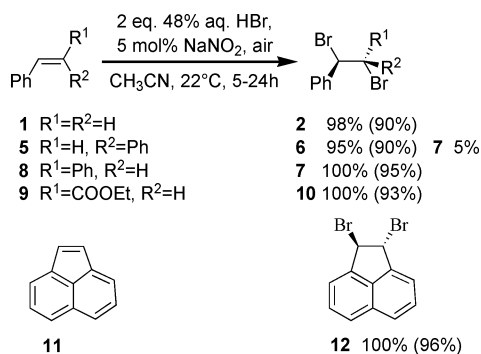
intermediate so that besides the competitive addition of a nucleophile, deprotonation resulting in an addition–elimination process could become an important reaction channel. With α-methylstyrene (13), only an addition reaction occurred with the competitive formation of the dibromide 14 and the bromohydrin 15 in a ratio of 44/56. (Scheme 3). α-(Trifluoromethyl)styrene (16), that forms a more deactivated bromocarbonium ion, was brominated in a lower yield, nevertheless dibromoalkane 17 was the main product. Bromination of 1,1-diphenylethene (18) follows an addition-elimination mechanism to give 2-bromo-1,1-diphenylethene (20) and 35% of the addition product 19.

2 eq. 48% aq. HBr
5 mol% NaNO$_2$, air
CH$_3$CN, 22°C, 24h

13 R=CH$_3$
16 R=CF$_3$
18 R=Ph

14 44% (35%)
17 82% (70%)
19 35%

15 56% (40%)
5%

20 65% (55%)
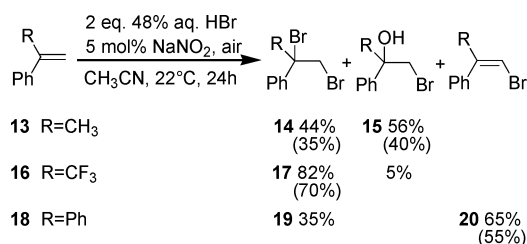
Scheme 3

The aliphatic terminal alkene 21 and internal alkene 23 were quantitatively and selectively brominated to give 1,2-dibromooctane (22) and anti-4,5-dibromooctane (24), respectively (Scheme 4).

2 eq. 48% aq. HBr
5 mol% NaNO$_2$, air
CH$_3$CN, 22°C, 24h

21 R^1=C$_6$H$_{13}$, R^2=H
23 R^1=R^2=C$_3$H$_7$

22 100% (92%)
24 100% (93%)

Scheme 4

On completion, aerobic oxidative bromination was tested for bromination of the alkyne 25. Similarly to reactions with alkenes, 25 was also trans-brominated to (E)-1,2-dibromo-1,2-diphenylethene (26) stereospecifically with an isolated yield of 93% (Scheme 5).

2 eq. 48% aq. HBr
5 mol% NaNO$_2$, air
CH$_3$CN, 22°C, 24h

Ph—≡—Ph
25

26 100% (93%)
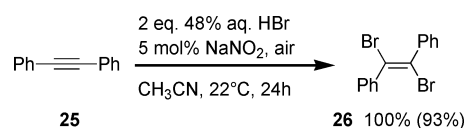
Scheme 5

In a small scale experiment, extraction or dilution with an appropriate organic solvent has to be applied in a work-up procedure. This method has the potential of producing a simpler work-up procedure due to the absence of any organic by-products and residues. On a larger scale, 5-times less MeCN is required for the reaction and a different work-up procedure, depending on the aggregate state of the formed product, was employed. Oxidative bromination of trans-stilbene (8) and trans-4-octene (23) were performed on a 5 mmol scale (5 mmol of alkene, 10 mmol of 48% aq. HBr, 70 µL of 3.6 M aq. NaNO$_2$, 10 mL of CH$_3$CN). After stirring the reaction mixture for either 16 h or 24 h at room temperature, the acetonitrile was distilled off and regenerated. In the case of the solid product 7, the crude reaction mixture was poured into water and the resultant white precipitate was filtered off, and after drying 95% of meso-1,2-dibromo-1,2-diphenylethane (7) was obtained.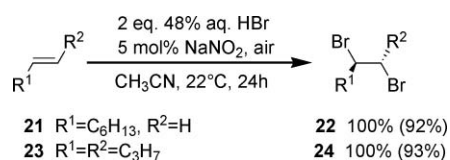 In the case of the liquid product 24, a minimum quantity of EtOAc was added, the resultant organic phase was dried over Na$_2$SO$_4$ and the solvent was evaporated. The result was anti-4,5-dibromooctane (24) in a 94% yield.

When comparing alternative protocols, the relevant environmental, health and safety aspects must also be taken into consideration. Regarding resource efficiency, the conventional procedure using molecular bromine[16] (Scheme 6a) or hydrobromic acid and hydrogen peroxide[8a] (Scheme 6b) compare favourably to the twenty-four procedures examined.[5b] These procedures had been chosen to be juxtaposed to the larger-scale procedure for aerobic oxidative dibromination of trans-stilbene (8) with HBr/air/NaNO$_2$(cat.) system (Scheme 6c).

a) + Br$_2$ → 95%

b) + 2 HBr + H$_2$O$_2$ → + 2 H$_2$O 99%

c) + 2 HBr + ½O$_2$ → + H$_2$O 95%
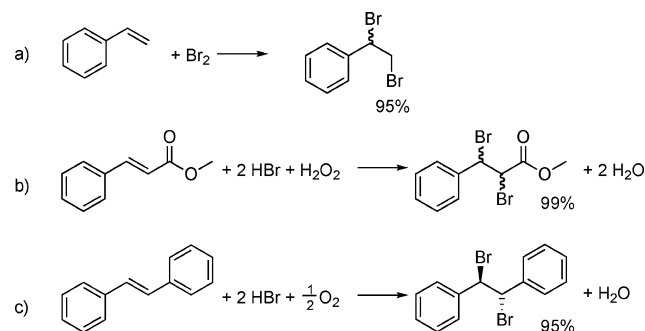
Scheme 6 Bromination methods using (a) molecular bromine,[16] (b) hydrobromic acid and hydrogen peroxide,[8a] and (c) hydrobromic acid and oxygen.

The protocols are from the laboratory stage. Against this background, the environmental factors E = $\sum$ Waste [kg]/Product [kg] given in Fig. 1 demonstrate that there is no significant difference regarding waste production and solvent demand between this method and other bromination methods[5b] with much higher E factors. Protocol (a) has the advantage that no water is used so waste water treatment is unnecessary.

Contrary to the quantitative results, the nature of the reagents used distinguishes themselves notably. Both, molecular bromine and an aqueous solution of hydrobromic acid have corrosive properties. Additionally, hydrogen peroxide is not only corrosive but can decompose in a runaway scenario.[18] However, bromine is much more volatile and has a higher risk potential than hydrobromic acid. Another important issue is the use of toxic

Table 2 Break down of environmental factor E shown in Fig. 1

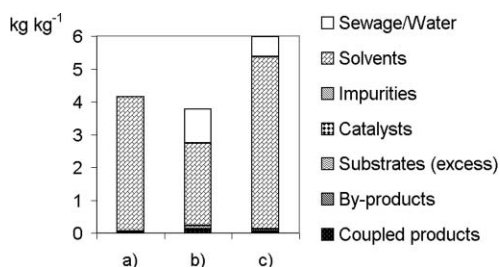|	(a)	(b)	(c)
Coupled products		0.1119	0.057
By-products	0.0526	0.0112	0.0556
Substrates (excess)		0.1066	
Catalysts			0.0115
Impurities	0.0042		
Solvents	4.1054	2.5002	5.2359
Sewage/Water		1.0478	0.6305
Sum	4.1622	3.7777	5.9905

Fig. 1 Environmental factor E of different bromination methods shown in Scheme 6 using the software EATOS.[17] For details see Table 2. Work-up procedures have not been described in detail[8a,16] and, thus, were not considered here: (a) recrystallization; (b) washing with water, brine and drying over sodium sulfate; (c) pouring into 10 mL of water.

and environmentally problematic substances such as chloroform (solvent of protocol (a)) or tetrachloromethane (solvent of protocol (b)). Evidence, although limited, suggests that CCl_4 is a carcinogen. Moreover it can have long-term adverse effects on the aquatic environment, is ozone depleting and a greenhouse gas. The authors of protocol (b) suggest dioxane as an alternative solvent, but dioxane is an irritant, highly flammable, can form explosive peroxides and potentially carcinogenic. Obviously, the advantage of substituting bromine with hydrobromic acid in protocol (b) becomes revoked because technology equipment has to avert the potential risk associated with the use of halogenated solvent or dioxane. In this regard, the application of acetonitrile, albeit highly flammable but merely harmful instead of toxic in protocol (c) respresents a significant progress and, furthermore, air is used instead of hydrogen peroxide.

The actual mechanism of aerobic oxidative bromination using hydrobromic acid and sodium nitrite as a catalyst is yet to be investigated. However, bromine was proposed as a reactive brominating species for the bromination of aromatic compounds and aryl ketones.[10c] Alkenes are convenient substrates to study the mechanism of halogenation and the nature of halogenating reagents. We performed a study on the effect of a brominating reagent's structure and the mode of its addition on the course of bromination of styrene (**1**) and observed some interesting results. Classical bromination of **1** with bromine in acetonitrile follows a different pathway to that of an $HBr/air/NaNO_2$(cat.) system; only 60% of 1,2-dibromo-1-phenylethane (**2**) was formed, with the remainder being acetamide **27** and oxazole **28** formed by the incorporation of acetonitrile into the carbocation intermediate (Table 3, entry 2). An analogous reaction with an additional 10 equivalents of water, as is present when using aqueous HBr in aerobic oxidative bromination, yielded a similar amount of dibromide **2** (entry 3). Also, significant differences were notice-

Table 3 Bromination of styrene (**1**) with various brominating reagents

| | | | Distribution (%)[a] | | | |
Entry	Reagent	Time (h)	**2**	**3**	**27**	**28**
1	HBr (2eq.), $NaNO_2$ (0.05 eq.), air	5	98	2	/	/
2	Br_2 (1eq.)[b,c]	3	60	/	20	20
3	Br_2 (1eq.), H_2O (10 eq.)[b]	3	61	23	11	5
4	Br_2 (1eq.)[d]	24	96	4	/	/
5	HBr_3 (1eq.)[e]	3	98	2	/	/
6	BrOH/NaBr (1eq.), H_2O (10 eq.)[f]	3	84	14	1	1
7	H_2O_2 (1eq.), HBr (2 eq.)[g]	24	90	10	/	/

[a] Determined by ^1H NMR spectroscopy. [b] Styrene (1 mmol) was added to the solution of Br_2 (1 mmol) (and H_2O (10 mmol)) in CH_3CN (10 mL). [c] A similar reactivity was observed to that reported in ref. 19. [d] Bromine vapours were added by diffusion from the gaseous phase[20] to the solution of styrene (1 mmol) in CH_3CN (10 mL). [e] Br_2 (1 mmol) and HBr (1 mmol) were mixed together in CH_3CN (10 mL) followed by the addition of styrene (1 mmol). [f] Br_2 (1 mmol) and NaOH (1 mmol) were mixed together and then the solution of styrene (1 mmol) in CH_3CN (10 mL) and H_2O (10 mmol) was added. [g] 30% aq. H_2O_2 (1 mmol) and 48% aq. HBr (2 mmol) were added to the solution of styrene (1 mmol) in CH_3CN (10 mL).

able when molecular bromine was added slowly to a solution of styrene (**1**) in acetonitrile by its diffusion *via* the gaseous phase. In this case similar results to aerobic oxidative bromination were obtained, with the selective formation of the dibrominated product **2** (entry 4), thus pointing to the importance of the slow formation of the brominating species during the course of the oxidative bromination. A similar result was observed when HBr_3 was formed as a brominating agent prior to the addition of **1**; less bromohydrine **3** was formed despite aqueous HBr being used (entry 5). When using BrOH/NaBr for bromination (entry 6) and when the brominating agent is formed *in situ via* haloperoxidase-like oxidation of HBr with hydrogen peroxide (entry 7), the formation of bromohydrin **3** is more expressed. It appears that the slow generation of bromine could be the key for the selective formation of *vic*-dibromides with the possibility of forming HBr_3 due to an excess of HBr at the early stages of the reaction.

Also, what is noteworthy is the selective formation of *trans*-addition products in aerobic bromination. This result is different to bromination with bromine in chlorinated solvents, where *cis*-addition was also observed in the bromination of acenaphthy-lene (**11**, *trans* : *cis* 70 : 30),[21] *trans*-stilbene (**8**, *trans* : *cis* 84 : 16)[22] and diphenylethyne (**25**, *trans* : *cis* 60 : 40).[23] Alternatively, when H_2O_2/HBr was used for bromination in a biphasic system with CCl_4 or an ionic liquid only *trans*-bromination takes place in the bromination of methyl *trans*-cinnamate.[8a,24] A similar effect was observed in bromination with pyridinium tribromide, where a reaction with *trans*-stilbene (**8**) in CH_2Cl_2 produces an 86 : 14 mixture of *trans* : *cis*-adducts, while the reaction in a water suspension yields only the *trans*-adduct.[22]

Nitrogen oxides were suggested to be the catalyst in this reaction due to a well known decomposition of nitrite under

acidic conditions into a mixture of nitrogen oxides. By mixing $NaNO_2$ with a strong acid ($HClO_4$) in MeCN, colorless bubbles immediately start to evolve and solution remained colorless even after a prolonged period of time in air. When HBr is used as an acid, dark yellow bubbles appear and the solution gradually becomes yellow-orange which, together with the fact that a solution of bromine in MeCN is red-brown, suggests the formation of a different decomposition product of $NaNO_2$ with HBr. A review of available literature suggests that the formation of a nitrosyl bromide could explain the yellow-orange colour of the solution (Scheme 7A). NOBr reportedly decomposes at room temperature into nitric oxide and bromine (Scheme 7B).[25a] We turned to UV-vis spectroscopy to determine the presence of NOBr as a product of the decomposition of $NaNO_2$ with HBr in acetonitrile. In the spectra obtained for a solution of Br_2 in MeCN, two peaks at 269 (s) and 390 (br) nm are observed, whereas for a degassed suspension of $NaNO_2$ in MeCN treated with HBr, a spectra is obtained with peaks at 269 (br) and 330 (br) nm. According to the literature data, NOBr has a peak at 225 nm that is in our case overlapped by the strong signal of Br_2,[25b,c] while a broad band at 330 nm corresponds with the literature one.[25b] However, after 30 min only absorption signals for Br_2 are observed. Our conclusion is that during $NaNO_2$ catalyzed aerobic dibromination of alkenes, nitrite is first transformed into NOBr, which then decomposes to bromine and nitric oxide (Scheme 7). Thus, a small amount of bromine is already formed in this pre-catalytic phase and is rapidly consumed by the alkene. This shifts the equilibrium towards complete decomposition of NOBr.
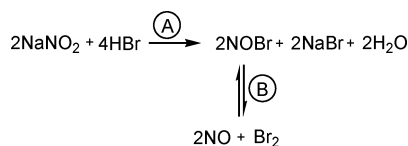
Scheme 7

At which point, nitric oxide enters into the catalytic cycle of aerobic bromination, where it is oxidized into NO_2 by air. This in turn oxidizes HBr into Br_2 (Scheme 8). It appears that the slow generation of bromine is crucial for selective *trans*-dibromination of alkenes, while the presence of unreacted HBr in the reaction mixture makes the formation of HBr_3 possible and its role in selective dibromination can not be precluded (Table 3, entries 4, 5).
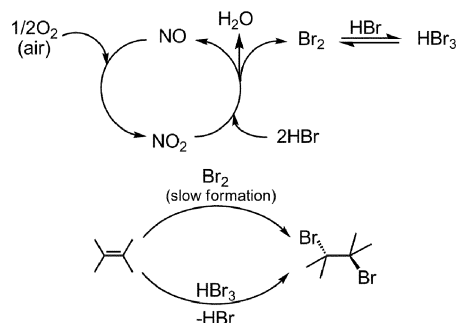
Scheme 8

Conclusion

Reported herein is a mild and simple method for the efficient and selective bromination of alkenes, in which aqueous HBr is used as a source of bromine, air at near ambient pressure as the oxidant and $NaNO_2$ as a low-cost catalyst. This procedure performed in acetonitrile provides a practical alternative to other procedures by avoiding the use of volatile bromine and problematic halogenated solvents. Furthermore, the isolation procedure is straightforward requiring only the separation of the organic product from the inorganic salts. It was established that NOBr is first formed from the catalyst and HBr and its decomposition leads to the generation of NO that acts as the true catalyst in aerobic oxidative bromination. In the bromination step, the formation of different active brominating agents is possible, however it seems that the selectivity of bromination is governed by the slow formation of bromine through aerobic oxidation, while its conversion into HBr_3 with residual HBr could also play an important role.

Both, environmental and health and safety aspects were also considered and compared with alternative protocols and aerobic dibromination. The obtained E-factors show that this aerobic protocol is similar to bromination using Br_2 and an H_2O_2/HBr system in chlorinated solvents. However, aerobic bromination with HBr/$NaNO_2$/air replaces Br_2 with the less volatile aqueous HBr and hydrogen peroxide with air, while chlorinated solvents are eliminated altogether. These and the good selectivity and yield makes this method a promising alternative to other dibromination protocols.

Experimental

General

All chemicals were obtained from commercial sources and were used without further purification. Acetonitrile was distilled before use. Column and thin layer chromatography were carried out using silica gel 60 (0.063–0.200 mm) and silica 60F-245 plates, respectively. ^{1}H and ^{13}C NMR spectra were recorded in $CDCl_3$ using a Varian Inova 300 MHz spectrometer. The chemical shifts (δ) are reported in ppm units relative to TMS as an internal standard for ^{1}H NMR and $CDCl_3$ for ^{13}C NMR spectra. Melting points were determined using a Büchi 535 melting point apparatus. Mass spectra were obtained using an Autospec Q mass spectrometer with electron impact ionization (EI, 70 eV).

Typical reaction procedure for aerobic oxidative dibromination of alkenes and 1,2-diphenylethyne with HBr/air/$NaNO_2$(cat.) system

In a typical experiment 1.0 mmol of substrate was dissolved in 10 mL of freshly distilled acetonitrile, then 2.0 mmol of 48% aqueous solution of HBr (226 µL) and 20 µL of 2.5 M aqueous solution of $NaNO_2$ (0.05 mol of $NaNO_2$) were added. The flask was immediately covered with an air filled balloon (1 L) and the solution stirred at room temperature for 5–24 h. The progress of the reaction was monitored by TLC. At the end of the reaction, 5 mL of ethylacetate was added. The organic phase was discoloured by adding a few drops of 37% aq. $NaHSO_3$, neutralized

by NaHCO$_3$ and finally dried over anhydrous Na$_2$SO$_4$. After the removal of solvent, the isolated reaction mixture was analyzed by ^{1}H NMR spectroscopy. Finally, products were isolated by flash or column chromatography (SiO$_2$, hexane–EtOAc) or purified by crystallization and their structures determined by comparison with the literature data.

(1,2-Dibromoethyl)benzene (2),[26] 5 h at r.t., 237 mg (90%). mp 70–72 °C (lit.[27] 73 °C), white crystals; δ$_H$ (300 MHz; CDCl$_3$; Me$_4$Si) 4.06 (t, J 10.4, 1H, CH$_2$Br), 4.08 (dd, J 10.4, 5.7, 1H, CH$_2$Br), 5.14 (dd, J 10.4, 5.7, 1H, CHBr), 7.32–7.42 (m, 5H, Ar-H); δ$_C$ (76 MHz; CDCl$_3$; Me$_4$Si) 35.0 (CH$_2$Br), 50.9 (CHBr), 127.6 (Ar-C), 128.8 (Ar-C), 129.2 (Ar-C), 138.6 (Ar-C); m/z (EI, 70 eV) 185 (60%), 183 (60%), 104 (100%).

rac-1,2-Dibromo-1,2-diphenylethane (6),[28] 8 h at r.t., 306 mg (90%). mp 105–107 °C (lit.[28] 112–113 °C), white crystals; δ$_H$ (300 MHz; CDCl$_3$; Me$_4$Si) 5.48 (s, 2H, CHBr), 7.16 (s, 10H, Ar-H); δ$_C$ (76 MHz; CDCl$_3$; Me$_4$Si) 59.1 (CHBr), 128.1 (Ar-C), 128.5 (Ar-C), 137.8 (Ar-C); m/z (EI, 70 eV) 342 (0.3%, M$^+$+4), 340 (0.6%, M$^+$+2), 338 (0.3%, M$^+$), 261 (47%), 259 (47%), 180 (100%), 171 (43%), 169 (43%).

meso-1,2-Dibromo-1,2-diphenylethane (7),[26] 12 h at r.t., 323 mg (95%). mp 249–250 °C (lit.[29] 242–243 °C), white crystals; δ$_H$ (300 MHz; CDCl$_3$; Me$_4$Si) 5.48 (s, 2H, CHBr), 7.34–7.45 (m, 6H, Ar-H), 7.50–7.54 (m, 4H, Ar-H); δ$_C$ (76 MHz; CDCl$_3$; Me$_4$Si) 56.1 (CHBr), 127.9 (Ar-C), 128.8 (Ar-C), 129.0 (Ar-C), 139.3 (Ar-C); m/z (EI, 70 eV) 342 (0.3%, M$^+$+4), 340 (0.6%, M$^+$+2), 338 (0.3%, M$^+$), 261 (57%), 259 (57%), 180 (100%), 171 (12%), 169 (12%).

anti-Ethyl 2,3-dibromo-3-phenylpropanoate (10),[30] 24 h at r.t., 312 mg (93%). mp 66–67 °C (lit.[30] 71–72 °C), white crystals; δ$_H$ (300 MHz; CDCl$_3$; Me$_4$Si) 1.38 (t, J 7.1, 3H, CH$_3$), 4.36 (q, J 7.1, 2H, CH$_2$), 4.83 (d, J 11.8, 1H, CHBr(COOEt)), 5.34 (d, J 11.8, 1H, CHBr(Ph)), 7.33–7.42 (m, 5H, Ar-H); δ$_C$ (76 MHz; CDCl$_3$; Me$_4$Si) 13.9 (CH$_3$), 47.0 (CHBr(Ph)), 50.7 (CHBr(COOEt)), 62.6 (CH$_2$), 128.0 (Ar-C), 128.9 (Ar-C), 129.3 (Ar-C), 137.6 (Ar-C), 167.8 (Ar-C); m/z (EI, 70 eV) 338 (0.5%, M$^+$+4), 336 (1.1%, M$^+$+2), 334 (0.5%, M$^+$), 293 (1%), 291 (2.5%), 289 (1%), 265 (1.7%), 263 (3.2%), 261 (1.7%), 257 (65%), 255 (65%), 185 (30%), 183 (30%), 131 (65%), 103 (100%), 91 (25%), 77 (55%).

trans-1,2-Dibromo-1,2-dihydroacenaphthylene (12),[31] 8 h at r.t., 300 mg (96%). mp 122 °C (lit.[32] 121–122 °C), brown crystals; δ$_H$ (300 MHz; CDCl$_3$; Me$_4$Si) 6.00 (s, 2H, CHBr), 7.58–7.64 (m, 4H, Ar-H), 7.78–7.84 (m, 2H, Ar-H); δ$_C$ (76 MHz; CDCl$_3$; Me$_4$Si) 54.9 (CHBr), 122.5 (Ar-C), 125.8 (Ar-C), 128.8 (Ar-C), 130.9 (Ar-C), 134.8 (Ar-C), 140.5 (Ar-C); m/z (EI, 70 eV) 314 (1%, M$^+$+4), 312 (3%, M$^+$+2), 310 (1%, M$^+$), 233 (23%), 231 (23%), 152 (100%).

(1,2-Dibromopropan-2-yl)benzene (14),[26] 24 h at r.t., 97 mg (35%). oil; δ$_H$ (300 MHz; CDCl$_3$; Me$_4$Si) 2.32 (s, 3H, CH$_3$), 4.13 (d, J 10.2, 1H, CHBr), 4.35 (d, J 10.2, 1H, CHBr), 7.28–7.40 (m, 3H, Ar-H), 7.53-7.57 (m, 2H, Ar-H). δ$_C$ (76 MHz; CDCl$_3$; Me$_4$Si) 29.9 (CH$_3$), 40.8 (CHBr), 43.5 (CBr), 126.5 (Ar-C), 128.5 (Ar-C), 128.6 (Ar-C), 141.8 (Ar-C); m/z (EI, 70 eV) 198 (34%), 196 (34%), 117 (100%) and

1-bromo-2-phenylpropan-2-ol (15),[26] 86 mg (40%). oil; δ$_H$ (300 MHz; CDCl$_3$; Me$_4$Si) 1.67 (s, 3H, CH$_3$), 3.68 (d, J 10.4, 1H), 3.75 (d, J 10.4, 1H), 7.23–7.30 (m, 1H, Ar-H), 7.33–7.39 (m, 2H, Ar-H), 7.43-7.47 (m, 2H, Ar-H); δ$_C$ (76 MHz; CDCl$_3$; Me$_4$Si) 28.0 (CH$_3$), 46.2 (CHBr), 73.1 (COH), 124.8 (Ar-C), 127.5 (Ar-C), 128.4 (Ar-C), 144.1 (Ar-C); m/z (EI, 70 eV) 198 (1%), 196 (1%), 121 (100%), 105 (15%), 77 (17%).

(2,3-Dibromo-1,1,1-trifluoropropan-2-yl)benzene (17), 24 h at r.t., 232 mg (70%). oil; δ$_H$ (300 MHz; CDCl$_3$; Me$_4$Si) 4.18 (d, J 11.9, 1H, CH$_2$Br), 4.38 (d, J 11.9, 1H, CH$_2$Br), 7.39–7.45 (m, 3H, Ar-H), 7.64–7.67 (m, 2H, Ar-H); δ$_C$ (76 MHz; CDCl$_3$; Me$_4$Si) 34.9 (CH$_2$Br), 65.7 (q, J 28.2, C), 123.6 (q, J 283, CF$_3$), 128.4 (Ar-C), 128.9 (Ar-C), 129.7 (Ar-C), 133.0 (Ar-C); m/z (EI, 70 eV) 334 (M$^+$+4, 0.2%), 332 (M$^+$+2, 1%), 330 (M$^+$, 0.2%), 253 (96%), 251 (96%), 172 (100%), 103 (65%), 77 (43%); Exact mass calculated for C$_9$H$_7$F$_3$Br$_2$ 329.886657, found 329.888000.

(2-Bromoethene-1,1-diyl)dibenzene (20),[33] 24 h at r.t., 143 mg (55%). mp 48–50 °C (lit.[34] 42–43 °C), white crystals; δ$_H$ (300 MHz; CDCl$_3$; Me$_4$Si) 6.76 (s, 1H, CHBr), 7.18–7.24 (m, 2H, Ar-H), 7.25–7.33 (m, 5H, Ar-H), 7.34–7.43 (m, 3H, Ar-H); m/z (EI, 70 eV) 260 (M$^+$+2, 60%), 258 (M$^+$, 60%), 179 (100%).

1,2-Dibromooctane (22),[35] 24 h at r.t., 250 mg (92%). oil; δ$_H$ (300 MHz; CDCl$_3$; Me$_4$Si) 0.87–0.92 (m, 3H, CH$_3$), 1.23–1.62 (m, 8H, (CH$_2$)$_4$), 1.72–1.84 (m, 1H, CH$_2$), 2.08–2.19 (m, 1H, CH$_2$), 3.63 (t, J 10.0, 1H, CH$_2$Br), 3.85 (dd, J 10.2, 4.4, 1H, CH$_2$Br), 4.13–4.21 (m, 1H, CHBr); δ$_C$ (76 MHz; CDCl$_3$; Me$_4$Si) 14.0, 22.5, 26.7, 28.5, 31.6, 36.0, 36.3, 53.1; m/z (EI, 70 eV) 193 (6.5%), 191 (6.5%), 151 (6%), 149 (7.3%), 137 (4.5%), 135 (6%), 121 (2%), 119 (3.7%), 111 (70%), 69 (100%).

anti-4,5-Dibromooctane (24),[35] 24 h at r.t., 252 mg (92%). oil; δ$_H$ (300 MHz; CDCl$_3$; Me$_4$Si) 0.95 (t, J 7.4, 6H, CH$_3$), 1.37–1.53 (m, 2H, CH$_2$), 1.58–1.74 (m, 2H, CH$_2$), 1.86–2.12 (m, 4H, CH$_2$), 4.13–4.21 (m, 2H, CHBr); δ$_C$ (76 MHz; CDCl$_3$; Me$_4$Si) 13.4 (CH$_3$), 20.3 (CH$_2$), 38.9 (CH$_2$), 59.8 (CHBr); m/z (EI, 70 eV) 193 (4%), 191 (4%), 111 (46%), 69 (100%).

(E)-1,2-Dibromo-1,2-diphenylethane (26),[36] 24 h at r.t., 314 mg (93%). mp 214–215 °C (lit.[36] 215–216 °C), white crystals; δ$_H$ (300 MHz; CDCl$_3$; Me$_4$Si) 7.34–7.46 (m, 6H, Ar-H), 7.51–7.55 (m, 4H, Ar-H); m/z (EI, 70 eV) 340 (M$^+$+4, 15%), 338 (M$^+$+2, 30%), 336 (M$^+$, 15%), 259 (12%), 257 (12%), 178 (100%).

Larger-scale procedure for aerobic oxidative dibromination of trans-stilbene (8) with HBr/air/NaNO$_2$(cat.) system

5.0 mmol (901 mg) of **8** was mixed with 10 mL of freshly distilled acetonitrile, then 10.0 mmol of a 48% aqueous solution of HBr (1.13 mL) and 70 µL of a 3.6 M aqueous solution of NaNO$_2$ (0.25 mol of NaNO$_2$) were added. The flask was immediately covered with an air filled balloon (1 L) and solution stirred at room temperature for 12 hours. The progress of the reaction was monitored by TLC. At the end of the reaction MeCN was evaporated under reduced pressure, crude reaction mixture was poured into 10 mL of water and white precipitate was filtered off. After drying, 1.615 g (4.75 mmol) of **7** was obtained as white crystaline product.

Larger-scale procedure for aerobic oxidative dibromination of *trans*-4-octene (23) with HBr/air/NaNO₂(cat.) system

5.0 mmol (561 mg) of **23** was mixed with 10 mL of freshly distilled acetonitrile, then 10.0 mmol of a 48% aqueous solution of HBr (1.13 mL) and 70 μL of a 3.6 M aqueous solution of NaNO₂ (0.25 mol of NaNO₂) were added. The flask was immediately covered with an air filled balloon (1 L) and solution stirred at room temperature for 24 hours. The progress of the reaction was monitored by TLC. At the end of the reaction MeCN was evaporated under reduced pressure. Crude reaction mixture was diluted with 6 mL of EtOAc, dried with 0.25 g of Na₂SO₄ and inorganic material filtered off. After evaporating the solvent 1.278 g (4.70 mmol) of **24** was obtained as oily product.

Acknowledgements

Notes and references

1 *The Chemistry of Functional Groups: Supplement D2, The Chemistry of Halides, Pseudo-Halides and Azides, Part 1 & 2*, ed. S. Patai and Z. Rappoport, Wiley, Chichester, 1995.
2 M. J. Dagani, H. J. Barda, T. J. Benya and D. C. Sanders, Bromine Compounds, in *Ullmann's Encyclopedia of Industrial Chemistry*, electronic edition, Wiley-VCH, Weinheim, 2005.
3 (*a*) K. Tanaka, R. Shiraishi and F. Toda, *J. Chem. Soc., Perkin Trans. 1*, 1999, 3069–3070; (*b*) J. Salazar and R. Dorta, *Synlett*, 2004, 1318–1320; (*c*) G. Bellucci, R. Bianchini, R. Ambrosetti and G. Ingrosso, *J. Org. Chem.*, 1985, **50**, 3313–3318; (*d*) R. Bianchini and C. Chiappe, *J. Org. Chem.*, 1992, **57**, 6474–6478; (*e*) V. Kavala, S. Naik and B. K. Patel, *J. Org. Chem.*, 2005, **70**, 4267–4271.
4 L.-X. Shao and M. Shi, *Synlett*, 2006, **8**, 1269–1271.
5 (*a*) P. T. Anastas and J. C. Warner, *Green Chemistry: Theory and Practice*, Oxford University Press Inc., New York, 1998; (*b*) M. Eissen and D. Lenoir, *Chem.–Eur. J.*, 2008, **14**, 9830–9841.
6 (*a*) F. H. Vaillancourt, E. Yeh, D. A. Vosburg, S. Garneau-Tsodikova and C. T. Walsh, *Chem. Rev.*, 2006, **106**, 3364–3378; (*b*) D. G. Fujimori and C. T. Walsh, *Curr. Opin. Chem. Biol.*, 2007, **11**, 553–560; (*c*) K. H. van Pee, C. J. Dong, S. Flecks, J. Naismith, E. P. Patallo and T. Wage, *Adv. Appl. Microbiol.*, 2006, **59**, 127–157.
7 (*a*) W. J. Jones, *Applications of Hydrogen Peroxide and Derivatives*, Royal Society of Chemistry, Cambridge, 1999; (*b*) D. Lenoir, *Angew. Chem., Int. Ed.*, 2006, **45**, 3206–3210.
8 (*a*) N. B. Barhate, A. S. Gajare, R. D. Wakharkar and A. V. Bedekar, *Tetrahedron*, 1999, **55**, 11127–11142; (*b*) A. Podgorsek, S. Stavber, M. Zupan and J. Iskra, *Green Chem.*, 2007, **9**, 1212–1218; (*c*) A. Podgorsek, S. Stavber, M. Zupan and J. Iskra, *Tetrahedron Lett.*, 2006, **47**, 7245–7247; (*d*) J. Iskra, S. Stavber and M. Zupan, *Synthesis*, 2004, 1869–1873; (*e*) J. Barluenga, M. Marco-Arias, F. Gonzalez-Bobes, A. Ballesteros and J. M. Gonzalez, *Chem.–Eur. J.*, 2004, **10**, 1677–1682; (*f*) R. Ben Daniel, S. P. de Visser, S. Shaik and R. Neumann, *J. Am. Chem. Soc.*, 2003, **125**, 12116–12117.
9 (*a*) B. Sels, D. De Vos, M. Buntinx, F. Pierard, A. Kirsch-De Mesmaeker and P. Jacobs, *Nature*, 1999, **400**, 855–857; (*b*) B. F. Sels, D. E. De Vos and P. A. Jacobs, *J. Am. Chem. Soc.*, 2001, **123**, 8350–8359; (*c*) U. Bora, G. Bose, M. K. Chaudhuri, S. K. Dhar, R. Gopinath, A. T. Khan and B. K. Patel, *Org. Lett.*, 2000, **2**, 247–249; (*d*) V. Conte, F. DiFuria and S. Moro, *Tetrahedron Lett.*, 1996, **37**, 8609–8612; (*e*) V. Conte, B. Floris, P. Galloni and A. Silvagni, *Adv. Synth. Catal.*, 2005, **347**, 1341–1344.
10 (*a*) O. V. Branytska and R. Neumann, *J. Org. Chem.*, 2003, **68**, 9510–9512; (*b*) L. Menini and E. V. Gusevskaya, *Chem. Commun.*, 2006, 209–211; (*c*) G. F. Zhang, R. H. Liu, Q. Xu, L. X. Ma and X. M. Liang, *Adv. Synth. Catal.*, 2006, **348**, 862–866; (*d*) J. Iskra, S. Stavber and M. Zupan, *Tetrahedron Lett.*, 2008, **49**, 893–895; (*e*) F. Radner, *J. Org. Chem.*, 1988, **53**, 3548–3553; (*f*) R. Raja and P. Ratnasamy, *J. Catal.*, 1997, **170**, 244–253; (*g*) R. Neumann and I. Assael, *J. Chem. Soc., Chem. Commun.*, 1988, 1285–1287.
11 D. Lenoir and C. Chiappe, *Chem.–Eur. J.*, 2003, **9**, 1037–1044.
12 (*a*) G. Rothenberg and J. H. Clark, *Green Chem.*, 2000, **2**, 248–251; (*b*) W. Adam, C. Mock-Knoblauch, C. R. Saha-Moller and M. Herderich, *J. Am. Chem. Soc.*, 2000, **122**, 9685–9691; (*c*) V. Conte, F. DiFuria and S. Moro, *Tetrahedron Lett.*, 1994, **35**, 7429–7432; (*d*) V. Conte, F. DiFuria, S. Moro and S. Rabbolini, *J. Mol. Catal. A: Chem.*, 1996, **113**, 175–184; (*e*) M. Andersson, V. Conte, F. DiFuria and S. Moro, *Tetrahedron Lett.*, 1995, **36**, 2675–2678.
13 T. Moriuchi, M. Yamaguchi, K. Kikushima and T. Hirao, *Tetrahedron Lett.*, 2007, **48**, 2667–2670.
14 T. K. Ying, W. L. Bao and Y. M. Zhang, *J. Chem. Res.*, 2004, 806–807.
15 C. Limberg and J. H. Teles, *Adv. Synth. Catal.*, 2001, **343**, 447–449.
16 H. G. O. Becker in *Organikum: Organisch-chemisches Grundprak-tikum*, Wiley-VCH, Weinheim, 21st edn, 2001, p. 299, (see ref. 5b for a translation).
17 M. Eissen and J. O. Metzger, *Chem.–Eur. J.*, 2002, **8**, 3580–3585.
18 M. Eissen, A. Zogg and K. Hungerbühler, *J. Loss Prev. Process Ind.*, 2003, **16**, 289–296.
19 G. Bellucci, R. Bianchini and C. Chiappe, *J. Org. Chem.*, 1991, **56**, 3067–3073.
20 A. Podgorsek, S. Stavber, M. Zupan and J. Iskra, *Eur. J. Org. Chem.*, 2006, 483–488.
21 G. Bellucci, C. Chiappe, R. Bianchini, P. Lemmen and D. Lenoir, *Tetrahedron*, 1997, **53**, 785–790.
22 K. Tanaka, R. Shiraishi and F. Toda, *J. Chem. Soc., Perkin Trans. 1*, 1999, 3069–3070.
23 R. Bianchini, C. Chiappe, G. Lo Moro, D. Lenoir, P. Lemmen and N. Goldberg, *Chem.–Eur. J.*, 1999, **5**, 1570–1580.
24 T. Ying, W. Bao and Y. Zhang, *J. Chem. Res.*, 2004, 806–807.
25 (*a*) C. T. Retcliffe and J. M. Shreeve, Nitrosyl Halides, in *Inorganic Syntheses*, ed. W. L. Jolly, McGraw-Hill Book Company, Inc., 1968, vol. XI, pp. 194–200; (*b*) H.-P. Loock and C. X. W. Qian, *J. Chem. Phys.*, 1998, **108**, 3178–3186; (*c*) G. Maier, H. P. Reisenauer and M. De Marco, *Chem.–Eur. J.*, 2000, **6**, 800–808.
26 C. F. Ye and J. M. Shreeve, *J. Org. Chem.*, 2004, **69**, 8561–8563.
27 S. Lin and W. H. Saunders, *J. Am. Chem. Soc.*, 1994, **116**, 6107–6110.
28 R. Maidan, Z. Goren, J. Y. Becker and I. Willner, *J. Am. Chem. Soc.*, 1984, **106**, 6217–6222.
29 K. Yates and R. S. Mcdonald, *J. Org. Chem.*, 1973, **38**, 2465–2478.
30 G. W. Kabalka, K. Yang, N. K. Reddy and C. Narayana, *Synth. Commun.*, 1998, **28**, 925–929.
31 S. Sternhel and P. W. Westerma, *J. Org. Chem.*, 1974, **39**, 3794–3796.
32 V. F. Anikin and T. I. Levandovskaya, *Zh. Org. Khim.*, 1988, **24**, 1064–1070.
33 A. Annunziata, C. Galli, P. Gentili, A. Guarnieri, M. Beit-Yannai and Z. Rappoport, *Eur. J. Org. Chem.*, 2002, 2136–2143.
34 W. M. Jones and R. Damico, *J. Am. Chem. Soc.*, 1963, **85**, 2273–2278.
35 D. Lexa, J. M. Saveant, H. J. Schafer, K. B. Su, B. Vering and D. L. Wang, *J. Am. Chem. Soc.*, 1990, **112**, 6162–6177.
36 J. H. Espenson, Z. L. Zhu and T. H. Zauche, *J. Org. Chem.*, 1999, **64**, 1191–1196.

Nanoparticle-supported and magnetically recoverable nickel catalyst: a robust and economic hydrogenation and transfer hydrogenation protocol

Vivek Polshettiwar,* Babita Baruwati and Rajender S. Varma*

A magnetic nanoparticle-supported leach-proof Ni catalyst was readily prepared from inexpensive starting materials which catalyzes various hydrogenation and transfer hydrogenation reactions; high catalytic activity and ease of recovery using an external magnetic field are additional eco-friendly attributes of this catalytic system.

Introduction

The metal-catalyzed hydrogenation of an alkyne and the transfer hydrogenation of ketones have received much interest in the past because of the immense number of opportunities that exist to prepare high-value products.[1] These reactions are featured in numerous multistep organic syntheses, which are generally catalyzed by precious metal catalysts.[2–5] However, the efficient separation and subsequent recycling of homogeneous transition metal catalysts remain scientific challenges of economical and ecological relevance. The practical use of the ever increasing number of tailor-made transition metal catalytic species is indeed connected with the problem of separation and reuse of the rather costly catalyst systems.[6] Several strategies for advanced catalyst recycling have been explored, including supported catalysts.[7–9] Unfortunately, in this research area, a single solution to the separation problem does not exist, and problems such as solubility of different components, catalyst instability, and metal leaching during the recycling procedure strongly limit the utility of some of these concepts.

Recently, functionalized magnetic nanoparticles have emerged as viable alternatives to conventional materials, as a robust, readily available, high-surface-area heterogeneous catalyst support.[10] They offer an added advantage of being magnetically separable, thereby eliminating the requirement of catalyst filtration after completion of the reaction. Also, there is an urgent need to develop less expensive and easily available, non-precious metal catalysts for the hydrogenation of alkynes.[11] Engaged in the development of greener and sustainable pathways for organic transformations[12] and nanomaterials,[13] herein, we report a simple and efficient synthesis of a nano-ferrite-supported, magnetically recyclable, and inexpensive Ni catalyst and its application in hydrogenation and transfer hydrogenation reactions. At the outset of this study, no example of a nanoparticle-supported Ni catalyst had been reported, despite the potential inherent stability and activity of such a material.

Sustainable Technology Division, National Risk Management Research Laboratory, U. S. Environmental Protection Agency, MS 443, Cincinnati, Ohio 45268, USA. E-mail: polshettiwar.vivek@epa.gov, varma.rajender@epa.gov; Fax: +1 513-569-7677; Tel: +1 513-487-2701

Results and discussion

The first step in the accomplishment of this goal was the synthesis and functionalization of magnetic nanoparticles (Scheme 1). The catalyst was prepared by sonicating nano-ferrites with dopamine in water for 2 h, followed by the addition of Ni chloride at a basic pH. Material with Ni nanoparticles on the amine-functionalized nano-ferrites was obtained in excellent yield.
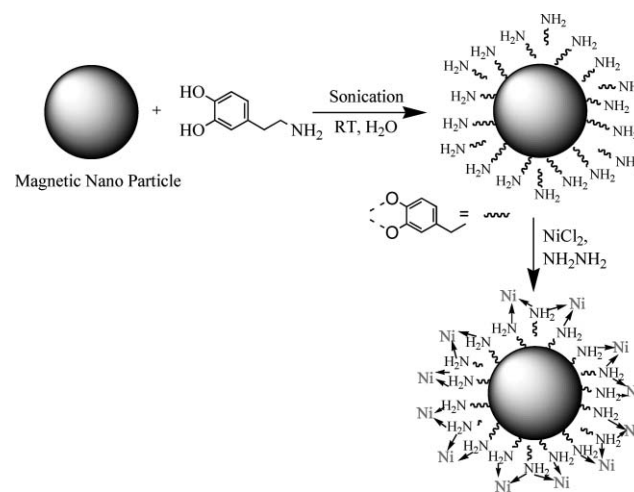
Scheme 1 Synthesis of functionalized nano-ferrite with Ni-coating.

Catalyst characterization by X-ray diffraction (XRD) (Fig. 1) and transmission electron microscopy (TEM) (Fig. 2) confirm the anchoring of Ni nanoparticles on amine-functionalized ferrite surfaces. The XRD pattern confirms the formation of single-phase Fe_3O_4 nanoparticles. The crystallite size, calculated from the Scherrer formula, was found to be 9.21 nm. XRD peaks at $2\theta = 15.1$ and 43.2 indicate the formation of an amine–nickel complex. TEM micrographs show the particles to be highly dispersed with spherical morphology and a size range of 10–13 nm, which is comparable with the crystallite size calculated from the X-ray spectrum. The weight percentage of Ni was found to be 8.3% by inductively coupled plasma-atomic emission spectroscopy (ICP-AES) analysis.
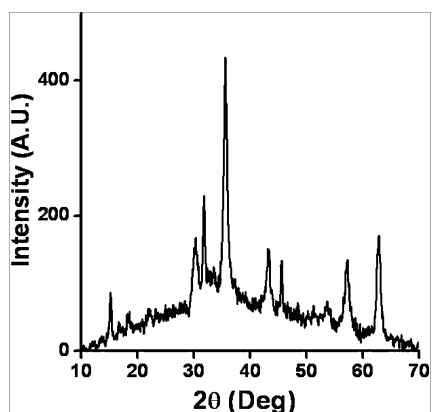
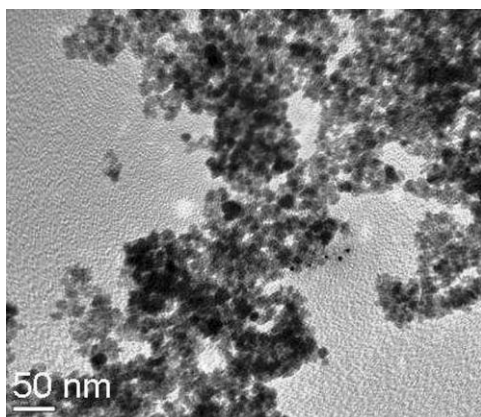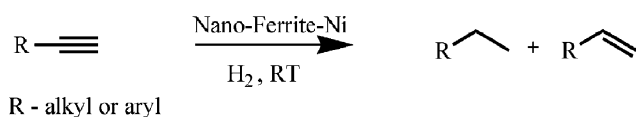**Fig. 1** XRD of functionalized nano-ferrite with Ni-coating.

Fig. 2 TEM of functionalized nano-ferrite with Ni-coating.

This Ni-coated nanomaterial was then explored as a heterogeneous catalyst for hydrogenation reactions of alkynes (Scheme 2).

R - alkyl or aryl

Scheme 2 Nano-ferrite–Ni catalyzed hydrogenation reactions.

Initially, experiments were performed to optimize reaction conditions for the hydrogenation of phenylacetylene as a substrate. Interestingly, we observed two products, *i.e.* alkene and alkane, depending on the solvent used and reaction time (Table 1). In methanol, hydrogenation of phenylacetylene yielded ethylbenzene as the major product; however, in dichloromethane, styrene was the major product.

Subsequently, this catalyst was explored for the hydrogenation of a variety of alkynes in methanol (Table 2) and dichloromethane (Table 3). Each of the reactions described proceeded smoothly at room temperature to give the desired products. Alkynes were hydrogenated in methanol to yield alkanes, with greater than or equal to 90% of product yield (Table 2, entries 1 through 8). However, heterocyclic alkyne (Table 2, entry 9) yielded a negligible amount of product and nitro groups were not hydrogenated (NR) under these conditions (Table 2, entries 10 and 11). Alkynes can also be hydrogenated

Table 1 Study of reaction solvent and reaction time for hydrogenation of phenylacetylene[a]

Entry	Solvent	Reaction time/h	Selectivity (%) Ethylbenzene	Styrene
1	Methanol	12	10	40
2	Methanol	24	80	20
3	Dichloromethane	12	00	40
4	Dichloromethane	24	00	80
5	Dichloromethane	48	10	90

[a] Reactions were carried out with 1 mmol of phenylacetylene, 50 mg of nano-ferrite–Ni catalyst, and 2 mL of solvent at room temperature, in an autoclave at 100 psi hydrogen pressure.

Table 2 Hydrogenation reaction of various alkynes using nano-ferrite–Ni catalyst in methanol[a]

Entry	Substrate	Product	Yield (%)
1			97
2			92
3			91
4			90
5			90
6			90
7	$CH_3(CH_2)_7CCH$	$CH_3(CH_2)_7CH_2CH_3$	98
8	$CH_3(CH_2)_9CCH$	$CH_3(CH_2)_9CH_2CH_3$	96
9			10
10	O_2N-	H_2N-	NR
11	O_2N-	H_2N-	NR

[a] Reactions were carried out with 1 mmol of alkyne, 50 mg of nano-ferrite–Ni, and 2 mL of methanol at room temperature, in an autoclave at 100 psi hydrogen pressure for 24 h.

in dichloromethane selectively to alkenes in good yield (Table 3, entries 1 through 8). The selectivity of the catalyst (based on reaction solvent) can be very useful in total synthesis of drug molecules, wherein it is possible to hydrogenate an alkyne to an alkene or alkane by simply changing the solvent.

Table 3 Hydrogenation reaction of various alkynes using nano-ferrite–Ni catalyst in dichloromethane[a]

Entry	Substrate	Product	Yield (%)
1			80
2			82
3			80
4			76
5			72
6			76
7	$CH_3(CH_2)_7CCH$	$CH_3(CH_2)_7CH=CH_2$	78
8	$CH_3(CH_2)_9CCH$	$CH_3(CH_2)_9CH=CH_2$	78
9			NR
10			NR
11			NR

[a] Reactions were carried out with 1 mmol of alkyne, 50 mg of nano-ferrite–Ni, and 2 mL of dichloromethane at room temperature, in an autoclave at 100 psi hydrogen pressure for 48 h.

Table 4 Transfer hydrogenation reaction of various ketones using nano-ferrite–Ni catalyst[a]

Entry	Substrate	Product	Yield (%)
1			98
2			98
3			95
4			98
5			80
6			80
7			5
8			5

[a] Reactions were carried out with 1 mmol of ketone, 50 mg of nano-ferrite–Ni, and 2 mL of isopropanol at 100 °C, under MW-irradiations for 45 min.

The reduction of carbonyl compounds to the corresponding alcohols is a synthetically important transformation and catalytic transfer hydrogenation is one of the best possible methods. In general, a precious metal such as Pd or Au is used for this protocol.[14] We decided to explore the inexpensive nano-ferrite–Ni catalyst for transfer hydrogenation of a variety of ketones (Scheme 3) under microwave (MW) irradiation conditions (Table 4).
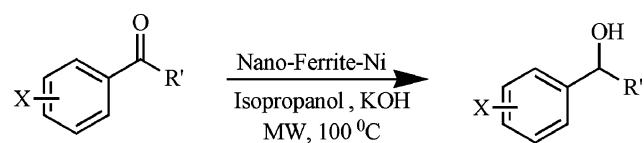
R' - Me, Ph
X - Cl, Br, NO₂, NH₂

Scheme 3 Nano-ferrite–Ni catalyzed transfer hydrogenation.

The scope of the catalyst was established for a wide range of ketones and in all cases the reaction was completed within 30–45 min with an excellent yield. Interestingly, in bromo-substituted ketones, debromination of the alcohol was observed (Table 4, entries 3, 4), while for nitro-substituted ketones (Table 4, entries 5, 6), reduction of nitro to amine predominates over hydrogenation of the carbonyl group. These are highly valuable chemoselective transformations that can be useful in multistep organic synthesis. However, our attempt for the transfer hydrogenation of amino-substituted ketones (Table 4, entries 7, 8) produced desired alcohols in low yield, which is due to the cyclization of amino-ketones to yield heterocyclic by-products.

For practical applications of heterogeneous systems, the lifetime of the catalyst and its level of reusability are very important factors. To clarify this issue, we established a set of experiments using the recycled catalyst for the hydrogenation reaction of phenylacetylene (Fig. 3). The reactions were carried out under similar conditions in methanol. After the completion of the first reaction to afford the corresponding ethylbenzene in 97% yield, the catalyst was recovered magnetically, washed with methanol and finally dried at 60 °C for 30 min. A new reaction was then performed with fresh solvent and reactants under the
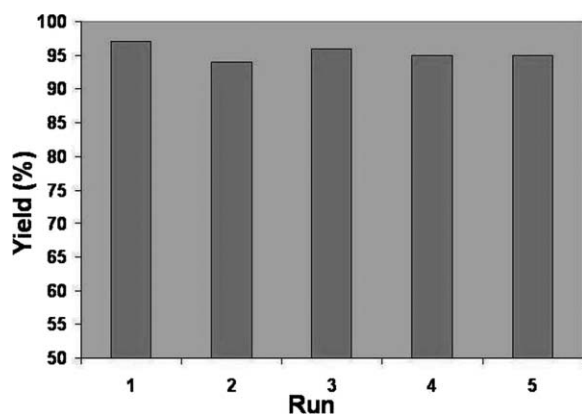
Fig. 3 Recyclability and reusability of nano-ferrite–Ni catalyst.

same conditions. To our satisfaction, nano-ferrite-supported Ni catalyst could be used at least five times without any change in activity.

Metal leaching was studied by ICP-AES analysis of the catalyst before and after the reaction. The Ni concentration was found to be 8.3% before the reaction and 8.21% after the reaction, which confirmed negligible Ni leaching. Also, no Ni-metal was detected in the final hydrogenated product. In fact, to date there is no 100% leach-proof metal catalyst; hence, the most important criterion in choosing the catalyst is metal recovery. It would be more preferable to use a more accessible, lower cost Ni-catalyst, provided that the process works at high turn over numbers and turn over frequencies and that the catalyst leaves no remnants of metal in the end product, since metal contamination is highly regulated by the pharmaceutical industry. All the above conditions are well satisfied by our recyclable nano-ferrite-supported Ni catalyst.

Conclusions

In summary, we have developed a convenient synthesis of a nano-ferrite-supported Ni catalyst which was readily prepared from inexpensive starting materials in water. Nano-ferrites were then functionalized and coated with inexpensive Ni-metal which then catalyzed the hydrogenation of alkynes and transfer hydrogenation of ketones with high yields. Also, being magnetically separable eliminated the requirement of catalyst filtration after completion of the reaction, which is an additional eco-friendly attribute of this synthetic protocol.

Experimental

The phase of the as-synthesized nanoparticles was determined by XRD in an MMS X-ray diffractometer with a Cu Kα source in the 2θ range 10 to 70. The data were collected with a step of 0.5 deg min^{-1}. TEM micrographs were recorded on a JEOL JSM-1200 II microscope at an operating voltage of 120 kV. The particles were dispersed in ethanol by ultrasonication, loaded on a carbon-coated copper grid, and then allowed to dry at room temperature before recording the micrographs. Elemental analyses of the catalyst before as well as after the reactions were performed on a Perkin Elmer Optima 3300 DV ICP-AES. Five mg of each sample was dissolved in 2.5 mL

of concentrated aqua regia and the volume was adjusted to 50 mL in a volumetric flask. This solution was then used for the elemental analysis. Gas chromatography–mass spectrometry (GC–MS) spectra were collected on a HP 6890 series GC system coupled with a 5973 Mass Selective Detector.

Synthesis of magnetic nano-ferrites

FeSO$_4$·7H$_2$O (13.9 g) and Fe$_2$(SO$_4$)$_3$ (20 g) were dissolved in 500 mL of water in a 1000 mL beaker. Ammonium hydroxide (25%) was added slowly to adjust the pH of the solution to 10. The reaction mixture was then continually stirred for 1 h at 60 °C. The precipitated nanoparticles were separated magnetically, washed with water until the pH reached 7, and then dried under a vacuum at 60 °C for 2 h. This magnetic nano-ferrite (Fe$_3$O$_4$) was then used for further chemical modification.

Surface modification of nano-ferrites

Nano-Fe$_3$O$_4$ (2 g) was dispersed in 25 mL of water by sonication for 30 min. Dopamine hydrochloride (2 g) dissolved in 5 mL of water was added to this solution and again sonicated for 2 h. The amine-functionalized nanomaterial was then precipitated using acetone, isolated by centrifugation, and dried under vacuum at 60 °C for 2 h.

Synthesis of nano-ferrite–Ni catalyst

Amine-functionalized nano-Fe$_3$O$_4$ (1 g) was dispersed in water and nickel chloride solution in water was added to the mixture to get 10 wt% of Ni. Hydrazine monohydrate solution in water was added drop-wise to bring the pH of this mixture to 9, followed by the addition of 0.1 g of NaBH$_4$. The reaction mixture was then stirred for 24 h at room temperature. The product was allowed to settle, washed several times with water and acetone, and dried under vacuum at 60 °C for 2 h. The weight percentage of Ni in the catalyst was found to be 8.3% by ICP-AES analysis.

Hydrogenation of alkyne using nano-ferrite–Ni catalyst

To a solution of alkynes (1 mmol) in 2 mL methanol–dichloromethane, 50 mg of nano-ferrite–Ni catalyst was added. The reaction vessel was purged three times with hydrogen and charged to 100 psi, and then closed off to the source of hydrogen. The reaction was stirred at room temperature and, after completion of the reaction, the product was isolated by removing the catalyst magnetically from the reaction mixture. All the products are known in the literature and were identified by the ^{1}H NMR of representative compounds and by comparing the GC–MS spectra of the products with a standard Wiley mass spectral library.

Transfer hydrogenation of ketone using nano-ferrite–Ni catalyst

In a typical reaction, 1 mmol of the ketone was taken in 2 mL of isopropyl alcohol in a 10 mL glass tube, to which 50 g of catalyst and 0.1 mmol of potassium hydroxide were added. The reaction mixture was then subjected to MW irradiation in a CEM Discover microwave system at 100 °C for 30–45 min. After completion of the reaction, the product was isolated by removing the catalyst magnetically from the reaction mixture. All products

are known in the literature and were identified by comparing the GC–MS spectra of the products with a standard Wiley mass spectral library.

Acknowledgements

References

1 (*a*) D. Teschner, E. Vass, M. Hävecker, S. Zafeiratos, P. Schnörch, H. Sauer, A. Knop-Gericke, R. Schlögl, M. Chamam, A. Wootsch, A. S. Canning, J. J. Gamman, S. D. Jackson, J. McGregor and L. F. Gladden, *J. Catal.*, 2006, **242**, 26; (*b*) G. W. Kabalka and R. S. Varma, *Comprehensive Organic Synthesis*, ed. B. M. Trost and I. Fleming, Pergamon Press, Oxford, 1991, vol. 8, p. 363; (*c*) T. Ikariya and A. J. Blacker, *Acc. Chem. Res.*, 2007, **40**, 1300.

2 A. Dedieu, S. Humbel, C. Elsevier and C. Grauffel, *Theor. Chem. Acc.*, 2004, **112**, 305.

3 A. M. Kluwer, T. S. Koblenz, T. Jonischkeit, K. Woelk and C. J. Elsevier, *J. Am. Chem. Soc.*, 2005, **127**, 15470.

4 M. W. van Laren, M. A. Duin, C. Klerk, M. Naglia, D. Rogolino, P. Pelagatti, A. Bacchi, C. Pelizzi and C. J. Elsevier, *Organometallics*, 2002, **21**, 1546.

5 J. López-Serrano, S. B. Duckett, S. Aiken, K. Q. A. Leñero, E. Drent, J. P. Dunne, D. Konya and A. C. Whitwood, *J. Am. Chem. Soc.*, 2007, **129**, 6513.

6 B. Chen, U. Dingerdissen, J. G. E. Krauter, H. G. J. Lansink Rotgerink, K. Möbus, D. J. Ostgard, P. Panster, T. H. Riermeier, S. Seebald, T. Tacke and H. Trauthwein, *Appl. Catal., A*, 2005, **280**, 17.

7 S. D. Jackson and A. Monaghan, *Catal. Today*, 2007, **128**, 47.

8 A. Papp, Á. Molnár and Á. Mastalir, *Appl. Catal., A*, 2005, **289**, 256.

9 N. Marín-Astorga, G. Pecchi, T. J. Pinnavaia, G. Alvez-Manoli and P. Reyes, *J. Mol. Catal. A: Chem.*, 2006, **247**, 145.

10 (*a*) A. Hu, G. T. Yee and W. Lin, *J. Am. Chem. Soc.*, 2005, **127**, 12486; (*b*) R. Abu-Reziq, H. Alper, D. Wang and M. L. Post, *J. Am. Chem. Soc.*, 2006, **128**, 5279; (*c*) C. O. Dalaigh, S. A. Corr, Y. Gunko and S. J. Connon, *Angew. Chem., Int. Ed.*, 2007, **46**, 4329; (*d*) T. Hara, T. Kaneta, K. Mori, T. Mitsudome, T. Mizugaki, K. Ebitanic and K. Kaneda, *Green Chem.*, 2007, **9**, 1246; (*e*) A. H. Latham and M. E. Williams, *Acc. Chem. Res.*, 2008, **41**, 411.

11 F. Studt, F. Abild-Pedersen, T. Bligaard, R. Z. Sørensen, C. H. Christensen and J. K. Nørskov, *Science*, 2008, **320**, 1320.

12 (*a*) V. Polshettiwar and R. S. Varma, *Chem. Soc. Rev.*, 2008, **37**, 1546; (*b*) V. Polshettiwar and R. S. Varma, *Acc. Chem. Res.*, 2008, **41**, 629; (*c*) V. Polshettiwar and R. S. Varma, *Curr. Opin. Drug Discovery Dev.*, 2007, **10**, 723; (*d*) V. Polshettiwar and R. S. Varma, *J. Org. Chem.*, 2008, **73**, 7417; (*e*) V. Polshettiwar and R. S. Varma, *J. Org. Chem.*, 2007, **72**, 7420.

13 (*a*) V. Polshettiwar, M. N. Nadagouda and R. S. Varma, *Chem. Commun.*, 2008, DOI: 10.1039/b814715a; (*b*) M. N. Nadagouda and R. S. Varma, *Cryst. Growth Des.*, 2008, **8**, 291; (*c*) M. N. Nadagouda and R. S. Varma, *Cryst. Growth Des.*, 2007, **7**, 686; (*d*) M. N. Nadagouda and R. S. Varma, *Cryst. Growth Des.*, 2007, **7**, 2582; (*e*) H. Choi, Y. J. Kim, R. S. Varma and D. D. Dionysiou, *Chem. Mater.*, 2006, **18**, 5377; (*f*) V. Polshettiwar and R. S. Varma, *Org. Biomol. Chem.*, 2008, DOI: 10.1039/b817669h; (*g*) B. Baruwati, M. N. Nadagouda and R. S. Varma, *J. Phys. Chem. C*, 2008, DOI: 10.1021/jp807245g.

14 F.-Z. Su, L. He, J. Ni, Y. Cao, H.-Y. He and K.-N. Fan, *Chem. Commun.*, 2008, 3531.

Direct analysis of cryptotanshinone and tanshinone IIA in biological samples and herbal medicinal preparations by a green technique of micellar liquid chromatography

Li Zhu,[a] Li Ding,[a] Qianli Zhang,[a] Lin Wang,[a] Fei Tang,[a] Qian Liu[a] and Shouzhuo Yao*[a,b]

Nowadays, chromatographic methods are widely applied in contemporary chemistry, *e.g.* HPLC, HPLC–MS, *etc*. However, organic solvents are required here, sometimes even in large quantities, including toxic acetonitrile, methanol, *etc*. Hence, chemical methods with less or no use of organic solvents, the so-called green chemistry methods are attracting great interest. In this paper, a green micellar liquid chromatography (MLC) method is proposed, and the use of a micellar mobile phase to give a more sensitive and rapid separation than in conventional high-performance liquid chromatography (HPLC). As an example, the method was successfully applied to the analysis of cryptotanshinone (CT) and tanshinone IIA (TS), which are usually used as the bioactive markers in biological samples or herbal medicinal preparations. No extraction step is required. A C_{18} column and a micellar mobile phase of 0.15 M sodium dodecyl sulfate (SDS) and 6.4% *n*-butanol were used. No interferences were caused by proteins or endogenous compounds in the urine, serum samples and herbal medicinal preparations. The limits of detection (LODs) for CT and TS were 12.5 and 15 ng mL^{-1} in micellar solutions, 18 and 25 ng mL^{-1} in urine samples and 20 and 30 ng mL^{-1} in serum samples, respectively. Compared with conventional reversed-phase chromatography where methanol–water (75 : 25, v/v) is used as the mobile phase, the proposed MLC method is more sensitive and time-saving.

Introduction

At present, chromatographic methods are widely applied in chemical analysis.[1] The liquid chromatography methods are rapid with high-resolution and are rather sensitive. With these advantages, liquid chromatography methods are being applied in many fields, such as biochemistry,[2] environmental analysis,[3] food analysis,[4] *etc*. Chromatographic coupling techniques are also an important trend, *e.g.*, HPLC–FLD,[5] HPLC–MS,[6] *etc*. However, these methods usually need a mass of organic, toxic or inflammable solvents (such as acetonitrile and methanol) as the mobile phase. Here, a green and sensitive micellar liquid chromatography (MLC) method has been proposed. Sodium dodecyl sulfate (SDS) is used to prepare the micellar mobile phase, which is non-toxic, non-flammable and relatively inexpensive. Moreover, as an application example, this method was successfully applied to the analysis of two hydrophobic bioactive compounds, cryptotanshinone (CT) and tanshinone IIA (TS), in biological samples and herbal medicinal preparations.

CT and TS are the major active diterpenoid tanshinones contained in *Radix Salvia miltiorrhiza* (Danshen). They have attracted much attention due to their powerful and wide

pharmacological activities including anticancer,[7] antioxidant[8] and treating cell apoptosis in the HL60 human premyelocytic leukemia cell line.[9] In quality control of the herbal medicinal preparations, they are usually used as the bioactive markers. Many methods have been reported for their determination including HPLC with UV detection[10] and non-aqueous capillary electrophoresis.[11] Recently, quantitative determination of biomarkers in biological samples such as plasma, urine or tissue homogenates has attracted much attention. Mass spectrometry detection methods have been developed for their determination.[12] However, tandem mass spectrometry detection is rather expensive for common labs, and a great amount of organic and toxic solvent is used as the HPLC mobile phase. In addition, drugs may be strongly bound to proteins and numerous endogenous compounds in a complex matrix thus interfering with the analysis and contaminating the source of the mass spectrometer. So the precipitation of proteins and the extraction of drugs with an organic solvent must be performed before the analysis. The sample preparation is time-consuming and laborious.

In this work, to overcome such problems, the direct determination of chemical compounds in biological samples and herbal medicinal preparations by green MLC is proposed. The micellar mobile phase is environmentally friendly compared with the organic solvents used in conventional liquid chromatography. And the biological samples are analyzed without laborious separation of proteins and other interfering substances, as the micelles can bind proteins competitively, thereby releasing

[a]College of Chemistry and Chemical Engineering, Hunan University, Changsha, 410082, China. E-mail: szyao@hnu.cn, aily8521845@163.com; Fax: +86 731-8821848; Tel: +86 731-8821968
[b]Key Laboratory of Chemical Biology and Traditional Chinese Medicine Research, Hunan Normal University, 410081, China

protein-bound drugs and proteins, rather than precipitating onto the column. In this way, direct analysis with no need for use of toxic or inflammable organic solvents is achieved and the cost and analysis time is greatly reduced and the separation efficiency significantly improved.

Experimental

The liquid chromatographic system (Shimadzu, Kyoto, Japan) consisted of two LC-20AT pumps, a CTO-10AS VP column oven and an SPD-M20A DAD system. These apparatus were connected *via* a communication bus module (Model CBM-20A) and controlled by a Shimadzu LC Solution workstation. A column of Ultimate™ XB-C$_{18}$ (4.6 mm × 150 mm, 5 μm, Welch Materials Inc., USA) was utilized. A mobile phase consisting of 0.15 M SDS–6.4% (m/m) *n*-butanol fixed at pH 5 with hydrochloric acid was used, which was filtered though an 0.45 μm membrane before use. The flow rate was 1 mL min^{-1} and the injection volume was 20 μL. The chromatographic runs were carried out at 30 °C. DAD detection was monitored in the range of 210–600 nm. The detection wavelengths were 265 and 270 nm for CT and TS, respectively. The structures of CT (MW = 296) and TS (MW = 294) are shown in Fig. 1. A mixed stock solution containing CT (50 μg mL^{-1}) and TS (50 μg mL^{-1}) was prepared in methanol. Dilution was then performed using the selected micellar mobile phase. A series of standard working solutions was obtained in the range of 0.05–10 μg mL^{-1} for both CT and TS, respectively. The standard solutions were stored in the refrigerator and protected against light before use. The micellar mobile phase was prepared by dissolving appropriate amounts of SDS in ultra-pure water and after filtration *n*-butanol or *n*-propanol was added to achieve the desired concentration (m/m). The solution was adjusted to pH 5 with HCl.
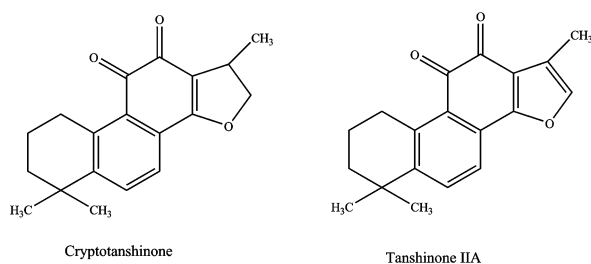

Fig. 1 The chemical structures of cryptotanshinone and tanshinone IIA.

Blank serum and urine samples were collected from volunteers in the Hospital of Hunan University (Changsha, China) and stored at 4 °C. Appropriate milliliters of stock solution of CT and TS were added to the blank urine and human serum solutions. The obtained samples were diluted by the micellar mobile phase and the final content of serum and urine in the solution was 10% (v/v). The biological samples were obtained in the range of 0.05–10 μg mL^{-1} for CT and TS, respectively. The solutions were then stored in the refrigerator and protected against light before use.

The Danshen medicinal preparations were presented in the form of pills and capsules. Ten pills or capsules, after removing the sugar-coat or capsule shell, were ground to a homogeneous powder in a mortar. 0.1 g samples were weighed out, and were extracted with 90% methanol aqueous solution (10 mL) under sonication for 30 min, and then centrifuged at 4024 × g for 5 min. The residue was extracted again with 5 mL of 90% methanol aqueous solution and centrifuged. The supernatants were combined, diluted ten times with the micellar mobile phase, and filtered through a 0.45 μm membrane prior to injection.

Results and discussion

Optimization of the mobile phase

In conventional chemical separations, organic solvents are widely used, *e.g.* in HPLC and HPLC–MS acetonitrile and methanol are used as the mobile phase, sometimes in large quantities, causing serious environmental problems. In this work, a green mobile phase, which was the solution of SDS with the addition of only very little organic-modifier, has been tested.

When the pure micellar mobile phase of SDS was used as the mobile phase with the conventional pore size HPLC stationary phases, due to their strong hydrophobicity and the weak eluting power of the micellar mobile phases,[13] analytes could only be detected after more than half an hour, and the retention times were 30.41 and 37.32 min for CT and TS, respectively. In order to reduce the retention time of the analytes, the short chain alcohol of *n*-propanol and *n*-butanol were considered to modify the mobile phase. When 8.0% *n*-propanol or 8.0% *n*-butanol was added to 0.15 M SDS, the retention times of the two compounds decreased significantly. The main effect of the addition of alcohol is to reduce the amount of adsorbed surfactant on the stationary phase (with 8% *n*-butanol, from 30.41 and 37.32 min to 8.06 and 12.98 min for CT and TS, respectively), as well as to improve the poor wetting of the stationary phase when only aqueous micellar mobile phases are employed.[14] Thereby the mass transfer of the analyte can be greatly improved, and the retention time is reduced significantly. The results are shown in Fig. 2. It is obvious that higher efficiency and better symmetry were obtained with the *n*-butanol and so *n*-butanol was chosen as the organic-modifier. Furthermore, the effect of the concentration of *n*-butanol in the micellar mobile phase was tested, and 1.6, 4.0,
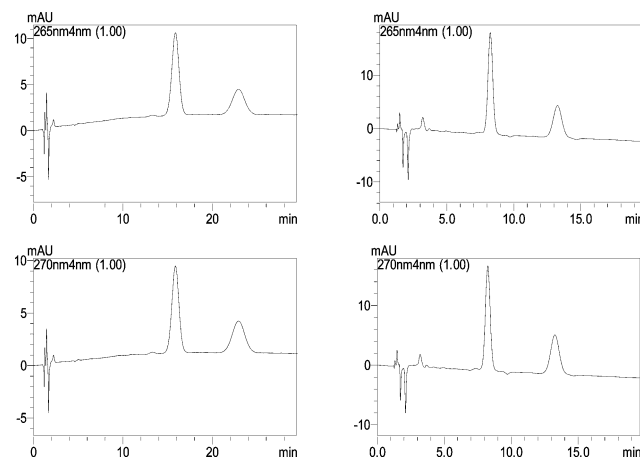

Fig. 2 The chromatograms of CT (265 nm) and TS (270 nm) with 8.0% *n*-propanol (left) and 8.0% *n*-butanol (right) added to the micellar mobile phase (pH = 3).

6.4 and 8.0% of *n*-butanol in the micellar mobile phase at pH 3 were compared. The relationship between the concentration of *n*-butanol and the retention factor *k'* value of the analytes is shown in Fig 3a. The retention factor *k'* is calculated by the following equation:

$$k' = \frac{t_R}{t_R - t_0} \quad (1)$$

where t_R is the retention time of the analyte, t_0 is the dead time of the column. It can be seen that the retention factor is decreased with increased concentration of *n*-butanol. When 6.4% *n*-butanol was used, higher and narrower peaks for both CT and TS were obtained. Moreover, the total analysis time (less than 16 min) was suitable for the analysis. When higher concentrations of *n*-butanol were employed, no further improvements in the peak shapes were observed and the baseline was less smooth than that of 6.4% *n*-butanol. So 6.4% *n*-butanol was selected as the organic-modifier in the micellar mobile phase.
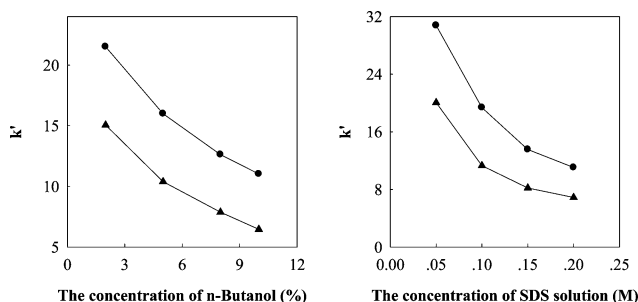

Fig. 3 Left: The influence of the concentration of *n*-butanol in the micellar mobile phase on the retention factor *k'* of CT (▲) and TS (●) (experiment conditions: 0.15 M SDS–*n*-butanol, pH 3). Right: The influence of the concentration of SDS on the *k'* of CT (▲) and TS (●) (experiment conditions: SDS–6.4% *n*-butanol, pH 3).

For further investigation, four different concentrations of 0.05, 0.10, 0.15 and 0.20 M of the SDS solutions, all modified by using 6.4% *n*-butanol and fixed at pH 3 and all above the critical micelle concentration of SDS were discussed. The relationship between the concentration of SDS and the retention factor *k'* value of the analytes is shown in Fig. 3b. It was found that the retention factor *k'* of the analytes was reduced by increasing the concentration of the SDS solution. When the middle concentration of 0.15 M was used, narrow peaks, good symmetry and smooth baselines were obtained.

The influence of pH was investigated in detail. In our preliminary study, we found that CT and TS could not be detected when the mobile phase pH was above 7. When the mobile phase was fixed at 3, 5 and 7, the peaks of the analytes were detected. This phenomenon may be related to the existing state of CT and TS under different pH. The positively charged forms of CT and TS are predominant from pH 3 to 7. The interaction of the protonated tanshinones at pH < 7 with the hydrophilic layer formed by the sulfate head groups of SDS reduces the penetration depth of the compounds into the bonded phase. Thus the retention time of the tanshinones is shortened. Better peak shapes were observed at pH 5. So pH 5 was chosen to carry out the experiments.

When adjusting the pH of the mobile phase, the ability of hydrochloric acid and 0.1 M phosphate buffer solution were compared. No significant differences between the peak shapes and retention times were observed in both cases, therefore, hydrochloric acid was selected for its convenience.

Based on the above results, 0.15 M SDS–6.4% *n*-butanol fixed at pH 5 was selected as the best mobile phase. Fig. 4 shows a typical chromatogram of the tanshinones under the optimized chromatographic conditions.
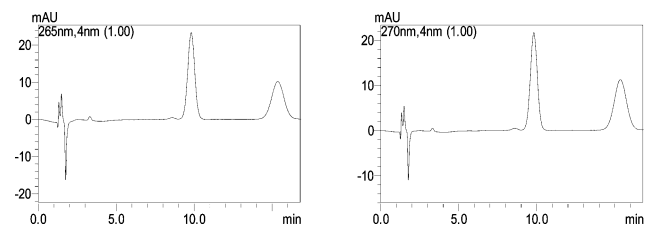

Fig. 4 A typical chromatogram of CT (265 nm, left) and TS (270 nm, right) under optimized chromatographic conditions.

The peaks are baseline separated and the shapes are symmetrical. The micellar mobile phase is compatible with a fluorescence detector. But in this work, the excited wavelength and emission wavelength of the selected mobile phase is similar to the analytes, which interfere in the detection sensitivity of the analyte. So a photodiode array detector was used instead in this work. By using the photodiode array detector (DAD), the maximum absorption wavelengths (λ_{max}) of the target peaks were measured. The optimal wavelengths for the simultaneous analysis of CT and TS were set at 265 and 270 nm, respectively.

Method validation

The linearities of the analytes were studied in three different matrices: micellar solution, serum and urine, respectively. Limits of detection (LODs) of the analytes were measured with a signal-to-noise ratio of 3 set as the criterion. The results of slopes, intercepts, correlation coefficients (r^2) and LODs are listed in Table 1. The results show good linearity ($r^2 > 0.998$) of the calibration curves. No significant differences were found between the three different kinds of samples. The LODs of CT and TS were 12.5 and 15 ng mL^{-1} in micellar solutions, 20 and 30 ng mL^{-1} in serum samples and 18 and 25 ng mL^{-1} in urine samples, respectively.

Under the optimized chromatography conditions, the intra-day and inter-day precision and accuracy of the method were evaluated by assaying five replicate spiked serum, urine samples and micellar media samples at three different concentration levels (low, mid and high quantification concentrations) of the tanshinones on the same day and on two consecutive days, respectively. The relative standard deviations (R.S.D.) of the intra-day and inter-day precision and accuracy values for spiked biological samples and micellar media samples are summarized in Table 2. The R.S.D. of the intra-day and inter-day precision were less than 2.7 and 3.5% for CT and TS, respectively. These results indicate that the present method has good accuracy and precision and it is suitable for analyzing the biological samples.

The recovery of the method was studied using the standard addition method. The reference standards were added at three

Table 1 Linear ranges, slopes, intercepts, correlation coefficients (r^2) and limits of detection (LODs) of the compounds

	Compound and matrix ($n = 6$)	Linear range/ng mL^{-1}	Slope	Intercept	r^2	LOD/ng mL^{-1}
CT	Micellar media	50–10 000	1.483×10^2	-0.728×10^4	0.9994	12.5
	Serum		1.443×10^2	-1.086×10^4	0.9980	20
	Urine		1.476×10^2	-0.887×10^4	0.9989	18
TS	Micellar media	50–10 000	1.263×10^2	-1.457×10^4	0.9988	15
	Serum		1.274×10^2	-1.862×10^4	0.9980	30
	Urine		1.278×10^2	-1.552×10^4	0.9984	25

Table 2 The mean accuracy and R.S.D. of precision for CT and TS detection in micellar media, serum and urine samples

		CT		TS	
Nominal conc./ng mL^{-1}		Mean accuracy (%)	R.S.D. of precision (%)	Mean accuracy (%)	R.S.D. of precision (%)
Intra-day ($n = 6$)					
Micellar media	100	96.32	2.05	95.67	2.19
	500	98.65	2.36	97.56	2.42
	5000	96.13	2.68	96.12	1.78
Serum	100	95.88	1.97	97.45	2.69
	500	97.74	2.64	96.53	2.01
	5000	97.69	2.03	97.24	1.56
Urine	100	96.85	2.69	95.29	2.49
	500	96.56	1.97	95.36	2.42
	5000	97.17	2.05	96.47	1.93
Inter-day ($n = 6$)					
Micellar media	100	94.25	3.12	95.52	2.43
	500	96.17	3.09	95.27	2.20
	5000	95.61	2.15	96.91	2.13
Serum	100	95.26	2.29	96.43	2.49
	500	96.35	3.04	95.15	2.98
	5000	95.90	3.16	96.27	3.16
Urine	100	95.46	2.95	95.39	2.86
	500	96.54	3.16	96.82	2.71
	5000	95.71	3.46	94.38	3.01

different concentration levels (low, mid and high concentrations of the matrix) with five parallels at each level. The recoveries of CT and TS in micellar solution, serum and urine matrices are shown in Table 3.

It can be seen that satisfactory recovery was obtained using the proposed method. A comparison with the reported hydro-organic HPLC method[15] for the analysis of CT and TS is shown in Table 4. Wider linear ranges, shorter sample pretreatment times and higher recoveries were obtained for CT and TS, which are superior to the hydro-organic HPLC method.

Since a large quantity of serum or urine injected may damage the packing materials and shorten the life of the column, dilution of the sample prior to its injection was necessary to benefit the column, which can reduce the width of the protein band too. In this work, the blank and spiked drug serum and urine samples were diluted ten times before injection. Fig. 5A and C shows the representative chromatograms of blank serum and urine samples, respectively. Fig. 5B and D shows the chromatograms of the spiked serum and urine samples. No interference from the proteins and endogenous components of the urine and serum

Table 3 Recovery for CT and TS from blank mobile phase, serum and urine samples^a

		CT		TS	
Nominal conc./ng mL^{-1}		Mean recovery (%)	R.S.D. (%)	Mean recovery (%)	R.S.D. (%)
Micellar media	100	97.38	1.86	97.26	2.81
	500	98.63	2.34	102.94	2.24
	5000	101.43	2.51	99.18	1.90
Serum	100	97.48	2.01	98.92	2.03
	500	97.56	2.36	97.48	2.69
	5000	99.23	2.19	102.14	1.97
Urine	100	96.97	2.43	101.06	2.18
	500	101.86	2.57	97.86	2.97
	5000	99.45	2.90	98.35	3.04

^{a} $n = 5$.

Table 4 Comparison of the reported work with present work[a]

Instrumentation	Pretreatment time/min	CT		TS		Recovery (%)
		Linear range/ng mL^{-1}	LOD/ng mL^{-1}	Linear range/ng mL^{-1}	LOD/ng mL^{-1}	
HPLC-UV[15]	>120	800–12 500	400	800–12 500	400	86–102
This work	<5	50–10 000	18	50–10 000	25	97–103

[a] In urine samples.

A$_1$ A$_2$

B$_1$ B$_2$

C$_1$ C$_2$

D$_1$ D$_2$

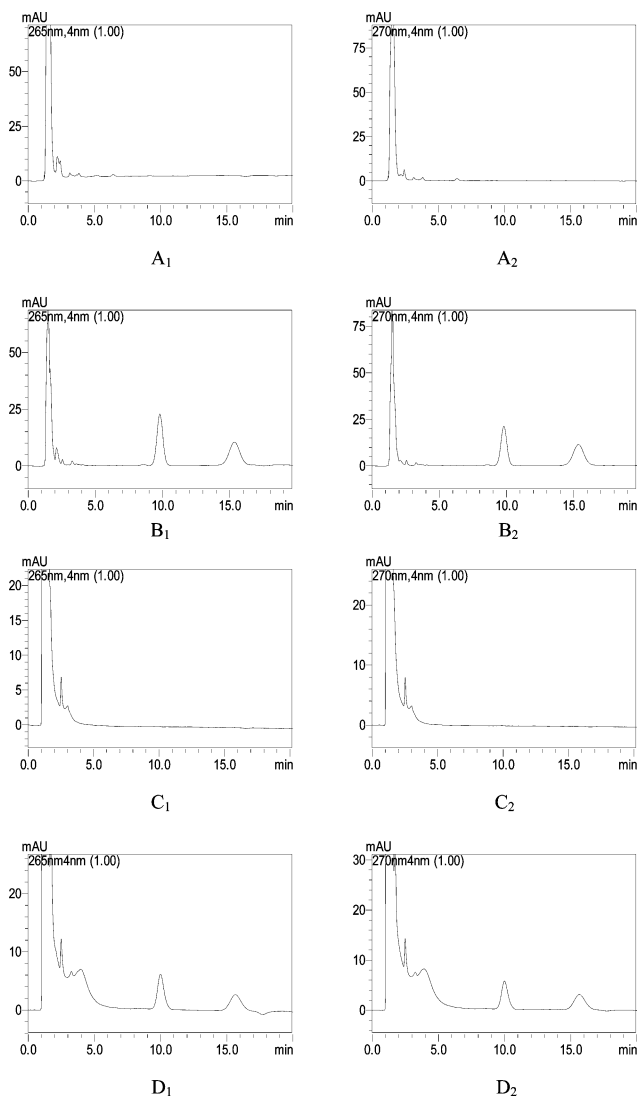**Fig. 5** (A) The chromatogram of a blank urine sample at 265 and 270 nm. (B) The chromatogram of a spiked urine sample at 265 and 270 nm. CT (left) and TS (right) (5 μg mL^{-1}). (C) The chromatogram of a blank serum sample at 265 and 270 nm. (D) The chromatogram of a spiked serum sample at 265 and 270 nm. CT (left) and TS (right) (2 μg mL^{-1}).

samples were observed, which shows the excellent specificity of the method for the determination of CT and TS with direct injection of the biological (serum and urine) samples.

The proposed method was also applied to the analysis of the three Danshen medicinal preparations samples (Fu-Fang-Dan-Shen-Pian manufactured by two different companies and Guan-Xin-Shu-Tong-Jiao-Nang). Fig. 6 shows the chromatograms of
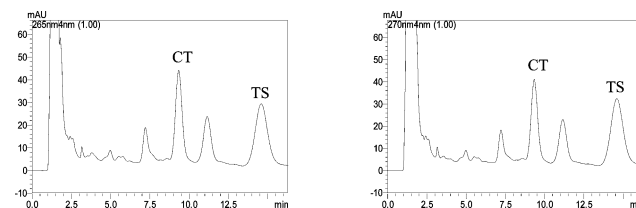

Fig. 6 Chromatograms of the Danshen medicinal preparations at 265 and 270 nm.

the extracts of the preparations. The tanshinones contained in the samples were identified by the retention times of the standard tanshinones. No interference was found from other drugs accompanying the assayed drugs in the medicinal preparations. The contents of tanshinones were determined by the established regression equation. The results are listed in Table 5. The contents of CT and TS are quite different in different medicinal preparations, therefore, it is necessary to quality control the medicinal preparations. The developed MLC method can be used as a quality control and a detecting method for the tanshinones.

Comparison of MLC with conventional reversed-phase liquid chromatography

In this work, the analysis ability of this MLC method was compared with conventional reversed-phase liquid chromatography, where methanol–water (75 : 25, v/v) or even acetonitrile is used as the mobile phase, while in this technique, only a micellar mobile phase (0.15 M SDS–6.4% n-butanol) is used. Hence, the use of hazardous substances is greatly decreased.

In addition, the proposed method with a micellar mobile phase has the advantage of direct injection of the samples, avoiding complicated sample pretreatment and extraction procedures. In conventional aqueous–organic HPLC, the precipitation of protein is needed when analyzing biological samples, with methanol added into the spiked serum or urine samples (methanol 80%, v/v). The whole separation process is

Table 5 The determination of the two tanshinones in herbal medicinal preparations

Samples[b]	Contents determined/mg g^{-1}[a]	
	CT	TS
Herbal preparation1#	0.299 ± 0.024	0.583 ± 0.020
Herbal preparation2#	0.459 ± 0.018	0.822 ± 0.015
Herbal preparation3#	0.293 ± 0.026	0.500 ± 0.023

[a] Mean ± standard deviation. [b] Herbal preparation1#: Guan-Xin-Shu-Tong-Jiao-Nang, 2#: Bai-Yun-Shan-Fu-Fang-Dan-Shen-Pian and 3#: Li-Li-Xin-Fu-Fang-Dan-Shen-Pian.

time-consuming: after vortex-mixing for 1 min, the solution is centrifuged at 3000 rpm for 10 min, the supernatant is evaporated to dryness under nitrogen flow at 30 °C, then the residue is reconstituted. However, no such complicated separation is needed in this work, an aliquot sample was simply injected into the LC system. Fig. 7 illustrates the chromatograms of the urine sample in MLC micellar mobile phase (left) and aqueous–organic HPLC (right). The analytes show that the retention times by MLC are only 9.68 and 15.01 min for CT and TS, respectively, while for the conventional hydro-organic HPLC, 11.68 and 18.73 min, respectively. Nevertheless, higher recoveries were obtained, which are superior to the hydro-organic HPLC method.
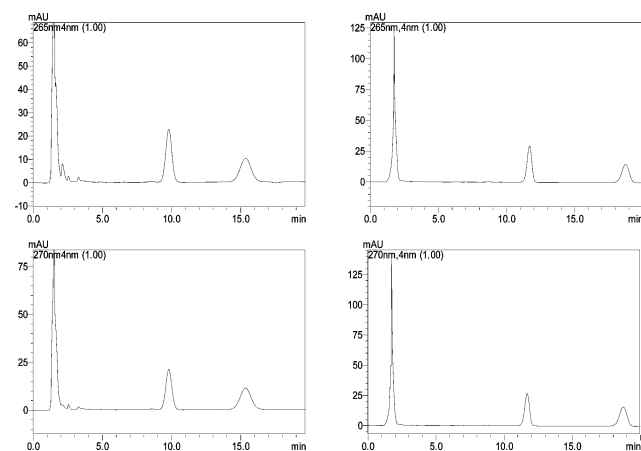

Fig. 7 The chromatograms of the urine sample in the micellar mobile phase (left) and the hydro-organic mobile phase (right) at 265 and 270 nm for CT and TS, respectively.

Conclusion

In this paper, a green MLC method is proposed. Here, instead of using toxic acetonitrile or flammable methanol, SDS with a small amount of *n*-butanol is proposed as a media for the analysis of biological samples and herbal medicinal preparations by MLC. The method was successfully applied to the analysis of bioactive compounds, CT and TS, in biological samples and herbal medicinal preparations. In comparison with the conventional HPLC method, this method is advantageous not only in it being "green" and less-toxic to living things and the environment, but also yielding a more rapid and sensitive separation than the conventional HPLC method. Hopefully, the new MLC method can also be used to separate the other classes of compounds.

Acknowledgements

References

1 (*a*) B. J. Prazen, K. J. Johnson, A. Weber and R. E. Synovec, *Anal. Chem.*, 2001, **73**, 5677; (*b*) A. Lienau, T. Glaser, M. Krucker, D. Zeeb, F. Ley, F. Curro and K. Albert, *Anal. Chem.*, 2002, **74**, 5192; (*c*) G. E. Taylor, M. Gosling and A. Pearce, *J. Chromatogr., A*, 2006, **1119**, 231.
2 G. Suresh Kumar, S. M. Musser, J. Cummings and M. J. Tomasz, *J. Am. Chem. Soc.*, 1996, **118**, 9209.
3 R. M. Sara, J. L. A. Maria and B. Damià, *Talanta*, 2006, **69**, 377.
4 R. J. Pawlosky and V. P. Flanagan, *J. Agric. Food Chem.*, 2001, **49**, 1282.
5 T. Okuda, D. Naoi, M. Tenmoku, S. Tanaka, K. B. He, Y. L. Ma, F. M. Yang, Y. Lei, Y. T. Jia and D. H. Zhang, *Chemosphere*, 2006, **65**, 427.
6 (*a*) S. Strohschein, C. Rentel, T. Lacker, E. Bayer and K. Albert, *Anal. Chem.*, 1999, **71**, 1780; (*b*) S. L. Yuan, X. J. Wang and Y. Q. Wei, *Ai Zheng*, 2003, **22**, 1363 (Article in Chinese).
7 X. Wang, Y. Wei, S. Yuan, G. Liu, Y. Lu, J. Zhang and W. Wang, *Int. J. Cancer*, 2005, **116**, 799.
8 E. H. Cao, X. Q. Liu and J. F. Li, *Acta Biophys. Sin.*, 1996, **12**, 339.
9 Y. Yoon, Y. O. Kim, W. K. Jeon, H. J. Park and H. J. Sung, *J. Ethnopharmacol.*, 1998, **68**, 121.
10 A. Chen, C. Li, W. Gao, Z. Hu and X. Chen, *J. Pharm. Biomed. Anal.*, 2005, **37**, 811.
11 A. J. Che, J. Y. Zhang, C. H. Li, X. F. Chen, Z. D. Hu and X. G. Chen, *J. Sep. Sci.*, 2004, **27**, 569.
12 (*a*) J. Li, G. J. Wang, P. Li and H. P. Hao, *J. Chromatogr., B: Anal. Technol. Biomed. Life Sci.*, 2005, **826**, 26; (*b*) H. P. Hao, G. J. Wang, P. Li, J. Li and Z. Q. Ding, *J. Pharm. Biomed. Anal.*, 2006, **40**, 382; (*c*) P. Li, G. J. Wang, J. Li, H. P. Hao and C. N. Zheng, *J. Chromatogr., A*, 2006, **1104**, 366.
13 A. S. Kord and M. G. Khaledi, *Anal. Chem.*, 1992, **64**, 1894.
14 D. P. Thomas and J. P. Foley, *J. Chromatogr., A*, 2007, **1149**, 282.
15 M. Xue, Y. Cu, H. Q. Wang, Z. Y. Hu and B. Zhang, *J. Pharm. Biomed. Anal.*, 1999, **21**, 207.

Natural Product Reports (NPR)
Current developments in natural products chemistry

NPR

Natural Product Reports

Current developments in natural products chemistry

www.rsc.org/npr

Volume 25 | Number 1 | February 2008 | Pages 1–204

ISSN 0265-0568

REVIEW
Elfie Stocker-Wörgötter
Metabolic diversity of lichen-forming ascomycetous fungi

Chemical Biology
In this issue...

RSC Publishing

0265-0568(2008)25;1:1-S

Now published monthly

Natural Product Reports (NPR) is doubling in frequency to 12 issues per year, so you can now get hold of the most topical reviews in key areas even faster, including: bioorganic chemistry, chemical biology, natural product synthesis, chemical ecology and carbohydrates

● Impact factor 7.66* (2007 Thomson Scientific (ISI) Citation Reports)

● High visibility – indexed in MEDLINE

● Themed issues published on key topics

...go online to find out more

2009

JANUARY FEBRUARY MARCH APRIL

MAY JUNE JULY AUGUST

SEPTEMBER OCTOBER NOVEMBER DECEMBER

RSCPublishing

www.rsc.org/npr

Registered Charity Number 207890

Now published

Free access to current issue

Integrative Biology is a new journal focusing on quantitative multi-scale biology using enabling technologies and tools to exploit the convergence of biology with physics, chemistry, engineering, imaging and informatics. The current issue is freely available online. (Online institutional access to all 2009 and 2010 content is available on registration.)

Forthcoming articles include:

The migration of charged species in photo-patterned SAM supported lipid membranes in electric fields
Stephen Evans *et al, University of Leeds, UK*

The evolution of chemotaxis assays from static models to physiologically relevant platforms
S. Toetsch *et al, Trinity Centre for Health Sciences, Ireland*

Models of protein linear molecular motors for dynamic nanodevices
D. Nicolaou *et al, University of Liverpool, UK*

From the Cellular Perspective: Exploring differences in the cellular baseline in macroscale and microfluidic cultures
David Beebe *et al, University of Widconsin, USA*

Mina Bissell, *Editorial Board chair*

"I am convinced that finally the time is right to launch a truly unique and multidisciplinary journal that strives to introduce novel technologies to answer significant questions in biology."
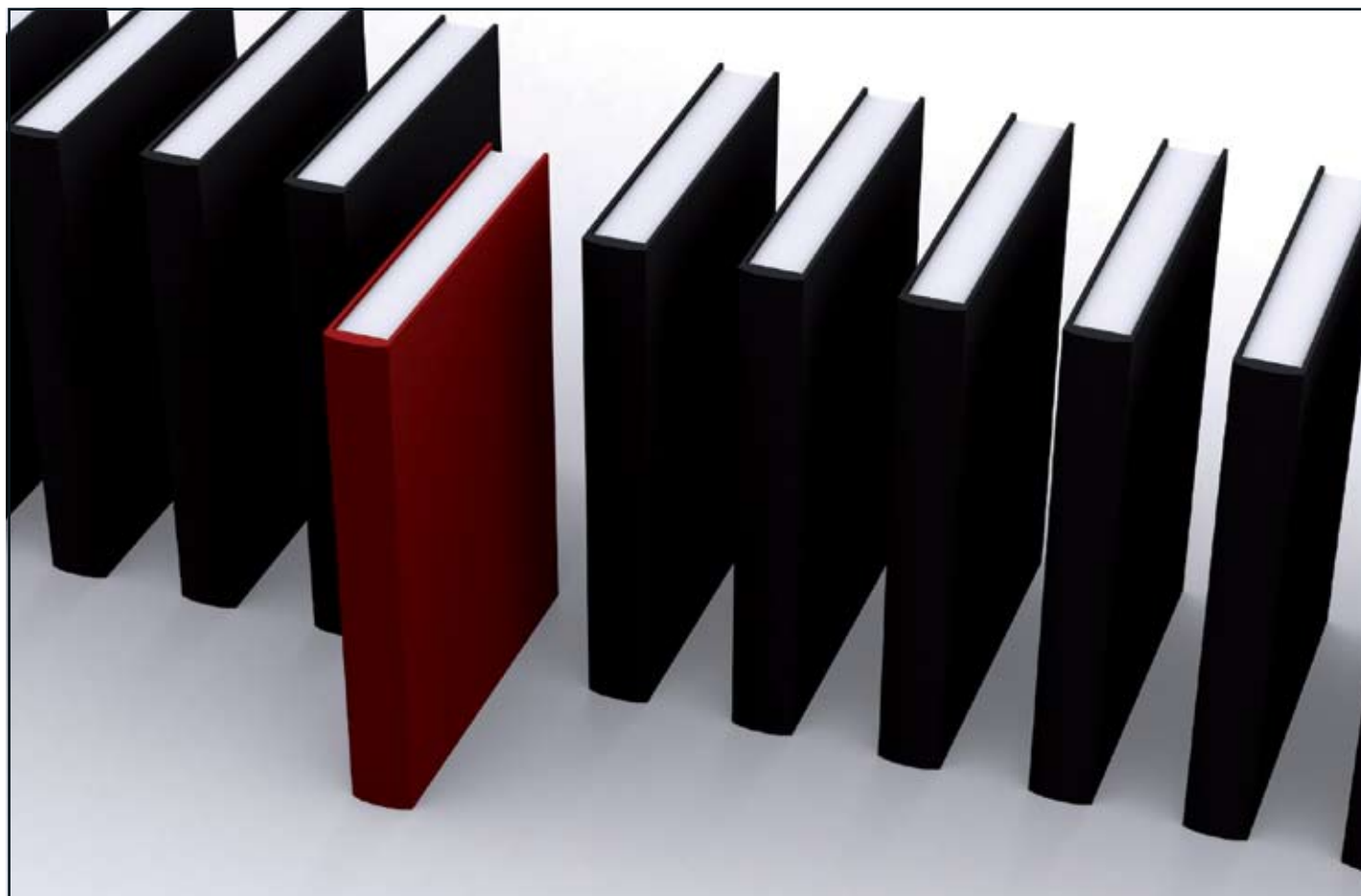
110850

Go online today!

RSC Publishing

www.rsc.org/ibiology

'Green Chemistry book of choice'

Why not take advantage of free book chapters from the RSC? Through our 'Green Chemistry book of choice' scheme Green Chemistry will regularly highlight a book from the RSC eBook Collection relevant to your research interests. Read the latest chapter today by visiting the Green Chemistry website.

The RSC eBook Collection offers:

- Over 900 new and existing books
- Fully searchable
- Unlimited access

Why not take a look today? Go online to find out more!

RSC Publishing

www.rsc.org/greenchem

Registered Charity Number 207890